Functional study of waist-hip ratio associated loci and the *WARS2* gene as modulators of fat distribution.

Milan Mušo
DPhil Candidate

Professor Roger Cox
Dr Rebecca Dumbell
Supervisors

Department of Biochemistry
Wolfson College, University of Oxford

Genetics of Type 2 Diabetes,
MRC Mammalian Genetics Unit, Harwell

Trinity 2019

MRC Harwell Institute

DEPARTMENT OF BIOCHEMISTRY
UNIVERSITY OF OXFORD

Functional study of waist-hip ratio associated loci and the *WARS2* gene as modulators of fat distribution.

Milan Mušo
Department of Biochemistry, Wolfson College, University of Oxford
Geneticcs of Type 2 Diabetes, MRC Mammalian Genetics Unit, Harwell
A thesis presented for the degree of Doctor of Philosophy, Trinity Term, 2019

Abstract

Waist-hip ratio (WHR) is a risk factor for diabetes and cardiovascular disease. Genome-wide association studies identified 346 loci linked to increased WHR adjusted for Body Mass Index (WHRadjBMI) (Shungin *et al.*, 2015; Pulit *et al.*, 2018). To elucidate the genetic underpinning of WHRadjBMI, I aimed to identify causal SNPs in 4 of these loci and test the tryptophanyl-tRNA synthetase 2 (*WARS2*) gene, previously shown to severely affect adipose mass, as modulators of fat distribution and browning.

To prioritise real signals, with colleagues, I selected 3 SNPs in *EMILIN2*, *VEGFA*, *C5orf67* loci with posterior probability analysis (PPA) scores > 0.95 for functional analysis. In the more complex *TBX15-WARS2* locus, we filtered 61 SNPs and selected 5 SNPs with a PPA score > 0.2 and further 8 top-scoring SNPs according to the epi-Phylogenetic Module Complexity Analysis (epi-PMCA). Using electrophoretic mobility shift assays (EMSAs) and luciferase assays in a differentiating human white adipose cell line, I showed that rs3936510 in the *C5orf67* locus and rs3810068 in the *EMILIN2* affected DNA-protein binding and identified enhancer/promoter activities in these loci. I demonstrated that rs3810068 altered the binding of CCAAT/enhancer-binding protein beta (CEBP/β). In the *TBX15-WARS2* locus, I used luciferase assays, RNA degradation analysis and allele-specific qPCR to show that the rs2645294, lead SNP in the 3'UTR of *WARS2*, did not impact RNA stability.

Wars2 (Wars2$^{V117L/V117L}$*)* mice showed previously progressive tissue-specific pathologies including reduced adiposity and browning of white adipose tissue (GTEx-Consortium, 2013; Civelek *et al.*, 2017; Agnew *et al.*, 2018). I show that whilst heterozygous female mice *(Wars2*$^{+/V117L}$ and *Wars2*$^{+/-}$*)* were unaffected, *Wars2*$^{V117L/V117L}$ mice failed to gain fat mass on a high-fat diet (HFD) in both sexes, had increased visceral:subcutaneous adipose ratio specifically in males on HFD and showed lower food intake in males. In both sexes, brown adipose tissue (BAT) showed loss of browning markers and mitochondrial dysfunction. In white adipose tissue (WAT), browning markers were upregulated, with a greater difference in the subcutaneous inguinal WAT compared to visceral gonadal WAT. In differentiated primary preadipocytes no difference in browning was observed. Plasma showed elevated levels of Fibroblast growth factor-21 (FGF21) and Growth/differentiation factor 15 (GDF15) In summary, a hypomorphic mutation in the mitochondrial gene *WARS2* reduced fat mass irrespective of diet and altered fat distribution in a diet and sex-specific manner, likely due to differences in depot-specific browning and elevation of mitokines FGF21 and GDF15 from other affected tissues.

Word Count: ~ 42, 000

Acknowledgements

This PhD has been an exciting journey into the world of science. With all its ups and downs, I have learned a number of lessons; perhaps most importantly, the invaluable role of working together with others.

Thus, first and foremost, I would like to thank Professor Roger Cox for his mentorship, insightful scientific discussions and the ever-present reminder "*What's the hypothesis*?" I am very grateful for Roger's encouragement to apply to multiple courses, conferences and the opportunity to present at the Keystone Diabetes meeting in Canada. I would also like to extend my thanks to my co-supervisor Dr Rebecca Dumbell, especially for her help with experimental planning, statistical analysis and for helping me set realistic goals for the project, thesis submission and future career. I also greatly appreciate the invaluable help of Dr Liz Bentley with setting up my phenotyping cohorts, planning experiments and critical reading of this thesis. A special thanks goes to Dr Rajesh Pandey, who has become a great friend and mentor to me, advising me both on science and life choices. I am also grateful to Dr Ying Bai, Dr Yixing Wu and Ms Louisa Zolkiewski for their useful advice, friendship, jokes and creating a very warm and enjoyable atmosphere to work in. Thank You, also to Dr Thomas Agnew who has given me an exciting introduction to the lab during my rotation and to Dr Dragoș Leordean and Dr Dominic Norris for giving me strong foundations in molecular biology and bacterial cloning.

I owe a debt of gratitude to all the MRC Harwell Institute staff that contributed to this work, especially Lucie Vizor and the Ward 4 staff in the Mary Lyon Centre, Dr Marianne Yonn, Emily File, Lynn Beresford from the Pathology Team and Debbie Williams.

Much of this work would not be possible without our collaborators Dr Samantha Laber and Nasa Sinnott-Armstrong from the Melina Claussnitzer lab at the Broad Institute, US and Sara Pulit from the Cecilia Lindgren group at the Big Data Institute in Oxford. I am also grateful to Dr Alfredo Castello at The Biochemistry Department, Oxford for advice on RNA stability experiments.

Finally, I want to express great gratitude to Ms Oana Kubinyecz and my friends Panos Pandis, Dominik Schreier, David Pavlíček, Daniel Jahn and Enrique Tong for their inspiration and being there for me at all times.

I would like to dedicate this thesis to my parents Zuzana and Ivan, my brother Ivan and my grandfather Milan Žuffa. Without their love, support and guidance, I would not be where I am today.

Table of Contents

Table of Figures

Table of Tables

Abbreviations

18S	18S ribosomal RNA
3'UTR	3' untranslated region
3T3-L1	A murine fibroblast/pre-adipocyte cell line
4SU	4-thio-uridine
ACC	Acetyl-CoA Carboxylase
ACTB	Beta actin
ActD	Actinomycin D
Adrb3	β3 adrenergic receptor
AGTRAP	Type-1 angiotensin II receptor-associated protein
AMPK	AMP-activated protein kinase
ANOVA	Analysis of variance
APCs	Adipose progenitor cells
AR	Adrenergic receptor
ARID5B	AT-Rich Interaction Domain 5B
ASAT	Abdominal subcutaneous adipose tissue
ASE	Allele-specific expression
asWAT	Anterior subcutaneous WAT
ATAC-seq	Assay for transposase-accessible chromatin using sequencing
Atf4	Activating transcription factor 4
ATGL	Adipose triglyceride lipase
ATP	Adenosine triphosphate
ATP5A	ATP synthase subunit 5 alpha
BAT	Brown adipose tissue
BMI	Body Mass Index
BMP-2	bone morphogenetic protein-2
BMP-4	bone morphogenetic protein-4
BSA	Bovine serum albumin
C/EBPα	CCAAT/enhancer-binding protein alpha
C5orf67	Chromosome 5 open reading frame 67
Canx	Calnexin
Cas9	CRISPR associated protein 9
CDKN2B	Cyclin-dependent kinase 4 inhibitor B
CEBP/β	CCAAT/enhancer-binding protein beta
CELF1-4	UGBP Elav-like family member 1-4
CF	Coronary flow
CGL	Congenital generalised lipodystrophy
ChIP-Seq	Chromatin Immunoprecipitation Sequencing
Cidea	Cell death-inducing DFFA-like effector a
CL	Chemiluminescence

CNS	central nervous system
COPD	Chronic obstructive pulmonary disorder
Cox5b	Cytochrome c oxidase subunit 5B, mitochondrial
Cox7a1	Cytochrome c oxidase polypeptide 7A1, mitochondrial
Cox8b	Cytochrome c oxidase subunit 8B, mitochondrial
COXI	Cytochrome c oxidase subunit-1
CPC	Central pair complex
CRE	Cis-regulatory element
CRISPR	Clustered regularly interspaced short palindromic repeats
Ct	Cycle threshold (qPCR)
CT	Computerized tomography
CTCF	CCCTC-binding factor
cWAT	Cardiac WAT
DAPI	4′,6-diamidino-2-phenylindole
DARS2	Aspartyl-tRNA synthetase 2, mitochondrial
DEXA	Dual-X ray absorptiometry
DHS	DNase hypersensitivity sites
Dio2	Type II iodothyronine deiodinase
DMSO	Dimethyl sulfoxide
DNA	Deoxyribonucleic acid
DNaseI	Deoxyribonuclease I
DNase-Seq	DNase I hypersensitive sites sequencing
Dot1l	Disruptor of telomeric silencing 1-like
DPBS	Dulbecco's phosphate-buffered saline
dsDNA	Double-stranded DNA
DTT	Dithiothreitol
ECAR	Extracellular acidification rate
ECL	Enhanced chemiluminescence
ECM	Extracellular matrix
EDTA	Ethylenediaminetetraacetic acid
eIF2α	Eukaryotic initiation factor 2 α
EIF4B	Eukaryotic translation initiation factor 4B
ELISA	Enzyme-linked immunosorbent assay
EMILIN2	Elastin Microfibril Interfacer 2
EMSA	Electrophoretic mobility shift assay
En1	Engrailed-1
ENU	N-ethyl-N-nitrosourea
epi-PMCA	Epigenetic phylogenetic module complexity analysis
eQTL	Expression quantitative trait locus
ERK	Extracellular signal-regulated kinase
ETC	Electron transport chain
FAM	Fluorescein
FAS	Fatty acid synthase
FBS	Fetal bovine serum

FCCP	Carbonyl cyanide-4-(trifluoromethoxy)phenylhydrazone
FDG-PET	Fluorodeoxyglucose positron emission tomography
FFAs	Free fatty acids
FGF21	Fibroblast growth factor-21
FGF21	Fibroblast growth factor-21
FISH	Fluorescence in situ hybridization
FPLD	Familial partial lipodystrophy
FTO	Fat mass and obesity-associated protein
FUS	Fused in Sarcoma/Translocated in Sarcoma protein
FW	Forward (primer)
Gapdh	Glyceraldehyde 3-phosphate dehydrogenase
GDF15	Growth/Differentiation factor 15
gDNA	Genomic DNA
GDP	Gross domestic product (Economics)
GFP	Green fluorescent protein
GIANT	Genetic Investigation of ANthropometric Traits
GRAFL	GDNF family receptor α–like
GSAT	Gluteofemoral subcutaneous adipsoe tissue
GTEx	Genotype-Tissue Expression project
GWAS	Genome-wide association study
gWAT	Gonadal WAT
H&E stain	Hematoxylin and eosin stain
HAART	Highly active anti-retroviral therapy
HAO2	Hydroxyacid oxidase 2
HDAC1	Histone deacetylase 1
HEK293T	Human Embryonic Kidney 293T cells
HET	Heterozygous
HFD	High-fat diet
Hi-C	Genome-wide chromatin conformation capture
HIV	Human immunodeficiency virus
HOM	Homozygous
HOX	Homeobox (transcription factors)
HR	Hazard ratio
HSL	Hormone sensitive lipase
hWAT	Human white adipose cell line
iBAT	Interscapular BAT
IBMX	3-isobutyl-1-methylxanthine
IL-6	Interleukin-6
IMR90	Human lung fibroblast cell line
IRX3	Iroquois-class homeodomain protein 3
IRX5	Iroquois-class homeodomain protein 5
ISE	Intron Splicing Enhancer
ISR	Integrated Stress Response
iWAT	inguinal WAT

JNK1	c-Jun N-terminal kinase 1
KALRN	Kalirin
Kcnj2	Kir2.1 inward-rectifier potassium ion channel
KD	Knock-down
Kl	β-klotho
KOMP	Knockout Mouse Project
LBSL	Leukoencephalopathy with brainstem and spinal cord involvement and lactate elevation
LD	Linkage disequilibrium
LFD	Low-fat diet
LMNA/C	Lamin A/C
lncRNA	Long non-coding RNA
LPIN2	Lipin 2
LPL	Lipoprotein lipase
LY86	Lymphocyte antigen 86
LYPLA1	Lysophospholipase 1
Mc4r	Melanocortin 4 receptor
MDM2	Mouse double minute 2 homolog
MED1	Mediator subunit 1
Meox1	Mesenchyme Homeobox 1
METSIM	Metabolic Syndrome in Men study
MFN2	Mitofusin 2
MGL	Monoglyceride lipase
MHO	Metabolically-healthy obese
MI	Myocardial infarction
miRNA	MicroRNA
MLASA	Myopathy, lactic acidosis and sideroblastic anemia
MPRA	Massively parallel reporter assay
MRI	Magnetic resonance imaging
MS	Metabolic syndrome
MSL	Multiple symmetrical lipomatosis
mt-aaRS	Mitochondrial aminoacyl synthesases
MT-ATP6	Mitochondrially encoded ATP synthase membrane subunit 6
MTCO1	Mitochondrially encoded cytochrome c oxidase I
mtDNA	Mitochondrial DNA
mt-Nd1	Mitochondrially encoded NADH:Ubiquinone oxidoreductase core subunit 1
MT-ND6	Mitochondrially encoded NADH dehydrogenase 6
mWAT	Mesenteric WAT
MYC	Myelocytomatosis oncogene
Myf5	Myogenic factor 5
Myf5	Myogenic factor 5
MyoD1	Myogenic differentiation 1
NAFLD	Non-alcoholic fatty liver disease
NDUFB8	NADH:Ubiquinone oxidoreductase subunit B8

NIH	National Institutes of Health, USA
NMR	Nuclear magnetic resonance
OCR	Oxygen consumption rate
PAI-1	Plasminogen-activated inhibitor-1
Pax3	Paired box protein 3
Pax7	Paired box protein 7
Pgc1a	Peroxisome proliferator-activated receptor gamma coactivator 1-alpha
PKB	Protein kinase B
PLC-γ1	Phospholipase C-γ1
Plin1	Perilipin 1
PLOD1	Procollagen-Lysine,2-Oxoglutarate 5-Dioxygenase 1)
PLPM	Posterior lateral plate mesoderm
PMCA	Phylogenetic module complexity analysis
PolyA-	Non-polyadenylated RNA
PolyA+	Polyadenylated RNA
PPA	Posterior probability analysis
Pparα	Peroxisome proliferator-activated receptor alpha
PPARγ	Peroxisome proliferator-activated receptor gamma
prBAT	Perirenal BAT
Prdm16	PR domain containing 16
prWAT	perirenal WAT
PVDF	Polyvinylidene fluoride or polyvinylidene difluoride
qPCR	quantitative polymerase chain reaction
qRT-PCR	Real-time qPCR
QTL	Quantitative trait locus
RBP	RNA-binding protein
RET	Rearranged during transfection tyrosine kinase
RIN	RNA Integrity value
RNA	Ribonucleic acid
Rpl13a	Ribosomal protein L13a
rtpWAT	Retroperitoneal WAT
RV	Reverse (primer)
SAT	Subcutaneous adipose tissue
SD	Standard deviation
SDHB	Succinate dehydrogenase [ubiquinone] iron-sulfur subunit, mitochndrial
Shox2	Short stature homeobox 2
Sim1	Single-minded homolog 1
siRNA	Silencing RNA
SIRT1	Sirutin 1
SMCHD1	Structural maintenance of chromosomes flexible hinge domain-containing protein 1
SNP	Single nucleotide polymorphism
SOX9	SRY-Box 9
Sp1	Specificity protein 1

SPAG17	Sperm-associated antigen-17
sQTL	Splicing QTL
subscBAT	Subcapular BAT
SVF	Stromal vascular fraction
$t^{1/2}$	Half-life
T2D	Type 2 diabetes
T3	3,3′,5-Triiodo-L-thyronine
TAD	topologically associated domain
TBE	Tris-borate EDTA
TBST	Tris-buffered saline Tween 20
TBX15	T-box 15
TCF7L2	Transcription factor 7-like 2
TF	Transcription factor
TFBS	TF binding site
TG	Triacylglycerol
TIMP1	Tissue specific inhibitor of metalloproteinase-1
TNFα	Tumour necrosis factor α
TRIB2	Tribbles pseudokinase 2
TZD	Thiazolidinedione
UCP1	Uncoupling protein 1
UKBB	UK Biobank
UPRmt	Mitochondrial unfolded protein response
UQCR2	Cytochrome b-c1 complex subunit 2, mitochondrial
UTR	Untranslated region
VAT	Visceral adipose tissue
VDAC1	Voltage-dependent anion-selective channel 1
VEGFA	Vascular Endothelial Growth Factor A
VIC	2′-chloro-7′phenyl-1,4-dichloro-6-carboxy-fluorescein
WARS2	Tryptophanyl(W)-tRNA synthetase 2, mitochondrial
WAT	White adiopse tissue
WC	Waist circumference
WHO	World Health Organisation
WHR	Waist-Hip ratio
WHRadjBMI	WHR adjusted for BMI
WT	Wild type
Wt1	Wilms Tumor 1
YARS2	Tyrosyl-RNA synthetase 2, mitochondrial
Ywhaz	14-3-3 protein zeta/delta

1. Introduction

1.1. Obesity and fat distribution

1.1.1. The Obesity epidemic

We live in the midst of a global syndemic of obesity, undernutrition and climate change (Swinburn et al., 2019). Almost 2 billion people are either overweight or obese whilst 815 million people are chronically undernourished. The closely linked effects of planetary health threaten to further worsen the situation (Habicht, 2008; Afshin *et al.*, 2017). We are thus in pressing need for both a systemic change and better understanding of malnutrition-associated health problems.

The "obesity epidemic" has an impact that costs the health system ~$2 trillion (2.8% of the global GDP) worldwide which is comparable to the impact of smoking or armed conflict (Dobbs *et al.*, 2014). In 2015, excess bodyweight was estimated to account for ~4 million deaths and 120 million disability-adjusted years (Afshin *et al.*, 2017). Over two thirds of BMI-related deaths could be explained by cardiovascular disease, diabetes contributed to a further 15% of deaths (Afshin *et al.*, 2017). Furthermore, a recent report by Cancer Research UK has shown that being overweight or obese surpassed smoking as a risk factor for bowel, kidney, ovarian and liver cancers, contributing to 6% of all cancer-related deaths (Brown *et al.*, 2018; Cancer Research UK, 2019). Obesity is also linked to obstructive sleep apnea, gallbladder disease, non-alcoholic fatty liver disease (NAFLD), osteoarthritis of the knee and depression (Must *et al.*, 1999; Xavier Pi-Sunyer, 2009; Luppino *et al.*, 2010). Indeed, reducing fat mass either through bariatric surgery or weight loss was shown to reduce the cardiovascular and diabetes risk factors, respectively (Colditz *et al.*, 1995; Ryden and Torgerson, 2006).

1.1.2. Metabolic syndrome and expandable fat hypothesis

The Metabolic syndrome (MS), originally known as Syndrome X, is a combination of obesity, insulin resistance, dyslipidaemia and hypertension that predisposes towards diabetes and other metabolic complications (Reaven, 1993; Virtue and Vidal-Puig, 2010). The well-established adipose expandability hypothesis states that rather than obesity itself, it is the oversaturation of adipocytes and ectopic lipid deposition in liver, muscle, heart and pancreas that leads to insulin resistance and starts the cascade of damaging effects of MS (Unger and Scherer, 2010). Rather than a disease, obesity may thus be a protective response of adipocytes against the lipotoxic threat to other tissues (Zhou and Grill, 1994; Lee *et al.*, 2004). Indeed, a proportion of the population has been described as insulin-sensitive or metabolically-healthy obese (MHO) (van Vliet-Ostaptchouk *et al.*, 2014). MHO individuals show smaller adipocyte size suggesting that despite their obesity adipocytes are still able to contain the caloric excess sparing other tissues (Kloting *et al.*, 2010). In agreement with this hypothesis, lipodystrophies, characterised by complete or partial loss of metabolically active adipose tissue that often originate from a genetic defect, can also cause early onset MS (Figure 1.1).

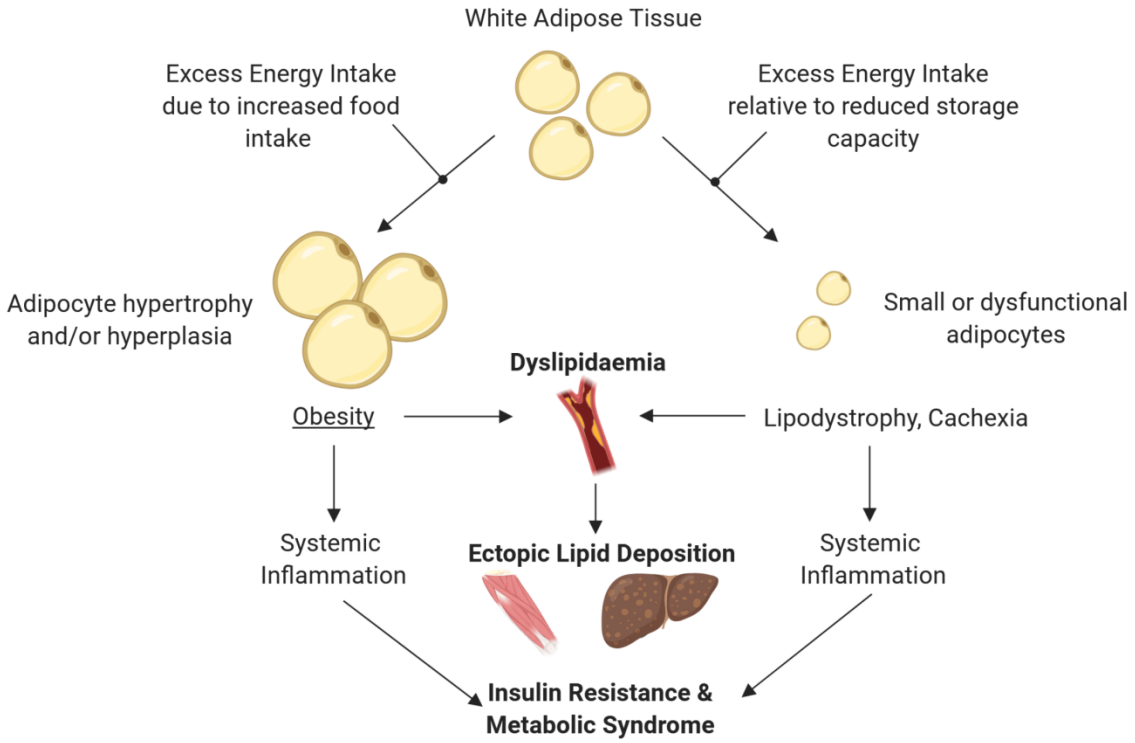

Figure 1.1 | The adipose tissue expandability hypothesis. Both obesity and lipodystrophy can lead to saturation of adipose tissue expandability. Excess lipid and inflammation interfere with adipose insulin sensitivity leading to ectopic lipid deposition, systemic insulin resistance – the hallmarks of metabolic syndrome. Adapted from (Vegiopoulos, Rohm and Herzig, 2017). Created in BioRender.com.

1.1.3. Fat mass, distribution and disease

Body mass index (BMI) is used to classify people as either overweight (BMI > 25) or obese (BMI >30) and is defined as the person's weight in kilograms divided by the square of height in metres (kg/m^2). BMI is only a crude measure of adiposity and fails to detect many people with excess fat as obese and can misclassify others, such as those with high muscle mass (i.e. bodybuilders), as overweight or obese (Romero-Corral *et al.*, 2008; Dulloo *et al.*, 2010). Other methods such as bioelectrical impedance analysis, dual energy X-ray absorptiometry (DEXA) and magnetic resonance imaging (MRI) are thus used to provide more accurate measures of adiposity (Lee and Gallagher, 2008).

Since the 1950s, it's been known that fat distribution, rather than just total fat amount, affects the risk of disease (Vague, 1956). Depot-specific fat accumulation, especially in the central abdomen, presents a risk independent of BMI (Wang *et al.*, 2005). In large population studies, body fat distribution can be easily assessed by waist-hip ratio (WHR), the ratio of waist circumference to hip circumference. Higher WHR, suggesting greater visceral fat accumulation, is associated with increased mortality and risk of coronary heart disease, myocardial infarction and type 2 diabetes (T2D) (Figure 1.2) (Snijder *et al.*, 2003; Wang *et al.*, 2005; Yusuf *et al.*, 2005; Canoy, 2008). The World Health Organisation (WHO) defines abdominal obesity (android or visceral), if WHR is above 0.90 for males and above 0.85 for females (WHO, 2011). Lower WHR, indicative of higher gluteal or subcutaneous fat accumulation, is protective for T2D and mortality (Snijder *et al.*, 2004; Mason, Craig and Katzmarzyk, 2008). WHR has been shown to outperform BMI as a predictor of T2D in men and a recent study of the UK Biobank (UKBB) also showed it is a better predictor for myocardial infarction (MI) in both sexes (Table 1.1, Figure 1.3) (Wang *et al.*, 2005; Peters, Bots and Woodward, 2018).

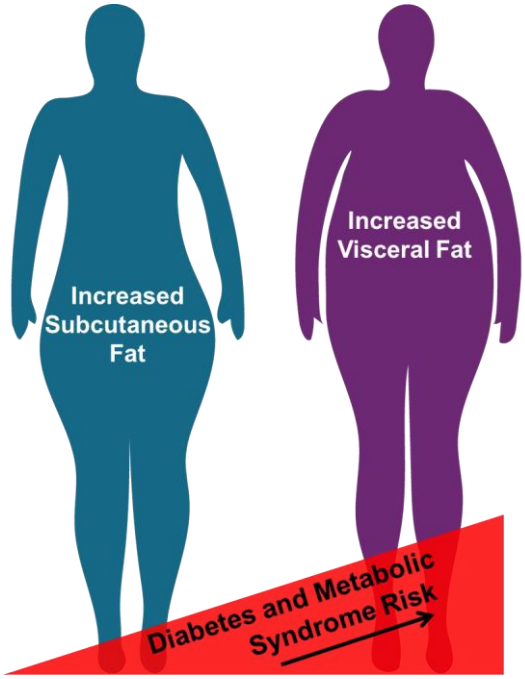

Figure 1.2 | The health risks associated with fat distribution. 'Android' body shape characterised by increased abdominal obesity shows increased risks of diabetes and metabolic syndrome onset compared to people with 'gynoid' shape where more fat is stored in the gluteofemoral regions.

Studies in twins have estimated the variation in individual WHR to be 36%-61% heritable after adjustment for BMI (Rose *et al.*, 1998; Mills *et al.*, 2004). This broad range, common to all heritability studies, may be in part due to small sample sizes of the studies, incorrect assumptions about shared environment and differences in sample group selection (Tenesa and Haley, 2013). A more recent study which included thousands of people with broad age range and multiple types of familial interactions estimated the narrow heritability (additive genetic effects) of WHR to be ~31% (van Dongen *et al.*, 2013). Multiple genome-wide association studies (GWAS) followed and most recently elucidated over 300 different genetic loci associated with WHR (Heid *et al.*, 2010; Shungin *et al.*, 2015; Pulit *et al.*, 2018). One key finding of these studies is that unlike genes in BMI-associated loci that are largely expressed in the brain and hypothalamus, genes in WHR-associated loci are predominantly expressed in adipocytes suggesting that whereas obesity is primarily

regulated through food intake and appetite, fat distribution is determined by modulating adipocyte biology (Locke *et al.*, 2015; Shungin *et al.*, 2015).

Table 1.1 | Age-adjusted relative risks of Type 2 Diabetes in men associated with waist circumference (WC), waist-to-hip ratio (WHR) and body mass index (BMI). Data from a cohort study (Health Professionals Follow-Up Study) of 27 270 men, normalised to the 1st quintile (Wang et al., 2005).

Quintile:	1st	2nd	3rd	4th	5th
WC	1.0	2.0	2.7	5.0	12.0
WHR	1.0	2.1	2.7	3.6	6.9
BMI	1.0	1.1	1.8	2.9	7.9

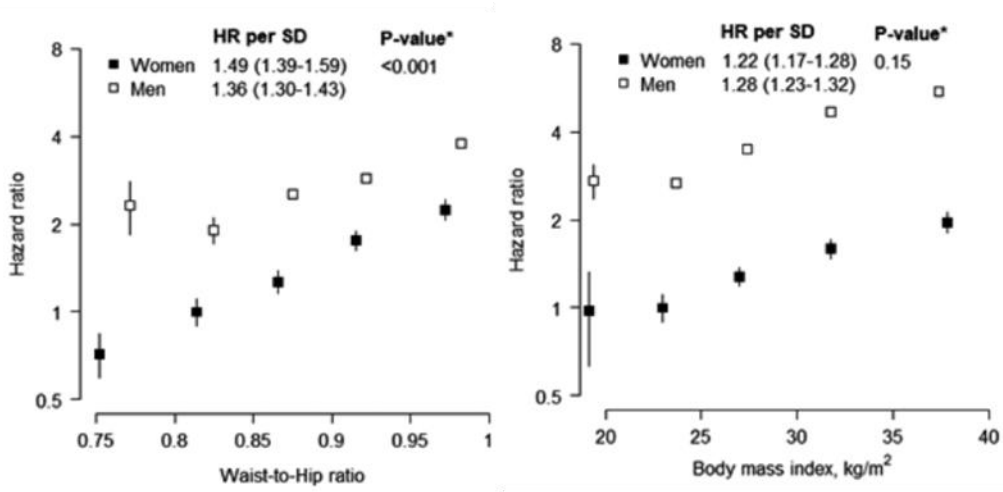

Figure 1.3 | Adjusted Hazard Ratio (HR) for myocardial infarction associated with waist-to-hip ratio and body mass index. Adjusted for age, Townsend deprivation index, and smoking status. Data from ~0.5 million people of the UK Biobank. HRs are shown for fifths of the respective measures, with the second fifth as the reference group. 95% confidence intervals are show for each data point. Shown above are HRs for a 1-SD higher value for each sex. *P-value for interaction by sex for the continuous analysis. Figure from (Peters, Bots and Woodward, 2018).

1.1.4. Other measures of fat distribution

More accurate non-invasive methods for assessing fat distribution are computerised tomography (CT) and whole body magnetic resonance imaging (MRI) scan. The Dual X-ray absorptiometry (DEXA) scan, although effective for quantifying fat mass and lean mass, provides no information on fat volume and distribution. (Marzola *et al.,* 2016). Another technique termed fluorodeoxyglucose positron emission tomography (FDG-PET) detects gamma rays emitted from injected radiotracers in live bodies and can be used for defining highly-metabolising tissues, such as the brown adipose tissue (BAT), discussed later in this chapter (Nedergaard *et al*, 2007).

MRI uses strong magnetic fields to detect the differences in resonance frequency shifts of water and fat protons and can thus detect distribution of adipose depots, their functional state, but also presence of ectopic fat such as intermuscular fat depots (Gallagher *et al.*, 2005). The CT scan employs computer-processed combinations of X-ray measurements from different angles to compile a series of virtual tomographic sections through the body. X-rays are differently absorbed by different materials and since fat has higher carbon to hydrogen ratios, it can be distinguished from other soft tissues such as bone and muscle. The generated images are then used to extrapolate the volume and attenuation of subcutaneous (SAT) and visceral fat tissues (VATs) (Maurovich-Horvat *et al.,* 2007). Similar to the links with increased WHR, the CT-derived measure of increased SAT:VAT ratio was associated with most risk factors for cardiometabolic disease such as higher triacylglycerol (TG), blood pressure, fasting glucose and higher prevalence of diabetes and metabolic syndrome in the Framingham Heart Study (Kaess *et al.*, 2012). In line with the adipose expandability hypothesis, lower CT attenuation, which is indicative of higher lipid content, was associated with disease risk in both SAT and VAT, independently of depot size (Rosenquist *et al.*, 2013, 2015; Abraham *et al.,* 2015). The complementarity of the

VAT:SAT and WHR ratio was further highlighted by a GWAS study that identified 2 previously WHRadjBMI loci, *LY86* and *LYPLA1*, to be also associated with VAT:SAT ratio (Chu *et al.*, 2017). Furthermore, the alleles associated with higher WHRadjBMI were collectively associated with higher VAT:SAT ratio and higher measures of pericardial and visceral fat depots (Pulit *et al.*, 2018). However, unique genetic loci and specific regulatory mechanisms can exist for specific depots. For example, the *TRIB2* locus is only associated with pericardial fat volume, but not visceral fat, BMI or WHR (Fox *et al.*, 2012; Locke *et al.*, 2015; Shungin *et al.*, 2015).

1.1.5. Sexual dimorphism of fat distribution

Body shape and fat distribution are established to be highly sexually dimorphic in humans and other species (Pulit, Karaderi and Lindgren, 2017). Females generally have more SAT and men relatively more VAT (Fox *et al.*, 2007). It is postulated that much of the dimorphism can be explained by sexual hormones. In agreement with this, pregnancy causes women to gain more SAT in thigh areas whilst menopause will lead to women gaining more fat viscerally (Sidebottom, Brown and Jacobs, 2001; Lovejoy *et al.*, 2008). Adipose intrinsic mechanisms may contribute too. The activity of lipoprotein lipase (LPL), a primary regulator of lipid uptake in adipose, with different depot-specific activity, was shown to be inhibited by testosterone in men (Arner *et al.*, 1991; Pouliot *et al.*, 1991; Ramirez *et al.*, 1997). The dimorphism may also stem from the different gene expression profiles observed in the same fat depots between sexes (Grove *et al.*, 2010). In line with this, the heritability of fat distribution itself is dimorphic - higher in women than men (van Dongen *et al.*, 2013). Of the 49 associated loci discovered in the 2015 WHRadjBMI GWAS meta-analysis, 20 were classified as significant for sexual heterogeneity (Shungin *et al.*, 2015). It is interesting to speculate whether preferential gluteofemoral fat deposition

in women contributes to the greater prevalence of metabolically-healthy obesity in women than men.

1.1.6. Lessons from lipodystrophies

Both excess and lack of adipose tissue are associated with adverse health consequences (Vegiopoulos, Rohm and Herzig, 2017). Lipodystrophies are characterised by complete or partial loss of metabolically active adipose tissue and can originate from a genetic defect or be acquired, as in HIV-infected patients receiving highly active anti-retroviral therapy (HAART) (Garg, 2004; Grinspoon and Carr, 2005).

Congenital generalised lipodystrophy (CGL) is caused by mutations of genes involved in phospholipid, TG and lipid droplet synthesis and is characterised by nearly complete loss of body fat (Patni and Garg, 2015). Interestingly, all mechanical fat, such as in the joints, orbits and palms is spared (Garg *et al.*, 1992). CGL patients develop signs of MS such as dyslipidaemia, ectopic fat accumulation, hyperinsulinemia and T2D (Van Maldergem *et al.*, 2002). The situation is further exacerbated by reduced levels of leptin, the satiety-signalling adipokine, resulting in increased appetite (McDuffie *et al.*, 2004). These findings are in line with the "expandability hypothesis" and show that adipose tissue is essential for metabolic health (Unger and Scherer, 2010; Virtue and Vidal-Puig, 2010).

Concerning the importance of specific fat depots, partial lipodystrophies are especially informative. Patients with familial partial lipodystrophy (FPLD) Dunningan-type have mutations in the nuclear lamina Lamin A/C (LMNA) gene or the key adipocyte differentiation regulator peroxisome proliferator-activated receptor γ (PPARγ) and lose predominantly subcutaneous fat of their legs and arms, whereas the size of most visceral depots is unaffected or increased (Garg, Peshock and Fleckenstein, 1999). They develop severe insulin resistance, dyslipidaemia and early-onset hypertension (Schmidt *et al.*,

2001; Savage *et al.*, 2003). Although not a lipodystrophy, the subcutaneous to visceral fat redistribution observed in Cushing's syndrome is associated with similar adverse outcomes to FPLD (Arnaldi *et al.*, 2010). Conversely, patients with Barraquer-Simon's syndrome, who progressively lose subcutaneous fat from their upper body but maintain their gluteofemoral adipose show lower incidence of diabetes and moderate insulin resistance compared to other forms of lipodystrophy (Misra et al., 2004). These findings further demonstrate that specifically gluteofemoral subcutaneous adipose tissue is important as the "metabolic sink" for excess energy (Ibrahim, 2010).

1.2. White, brown and beige adipocytes

The adipose depot is a heterogeneous tissue with multiple cell types including the lipid-filled mature adipocytes and the cells of the stromal vascular fraction (SVF), composed of endothelial cells, pericytes, smooth muscle cells, immune cells and preadipocytes (Miettinen, Sarkanen and Ashammakhi, 2008; Tchkonia *et al.*, 2013). The adipocytes themselves can be split into 3 major types – the white, brown and beige (Figure 1.4).

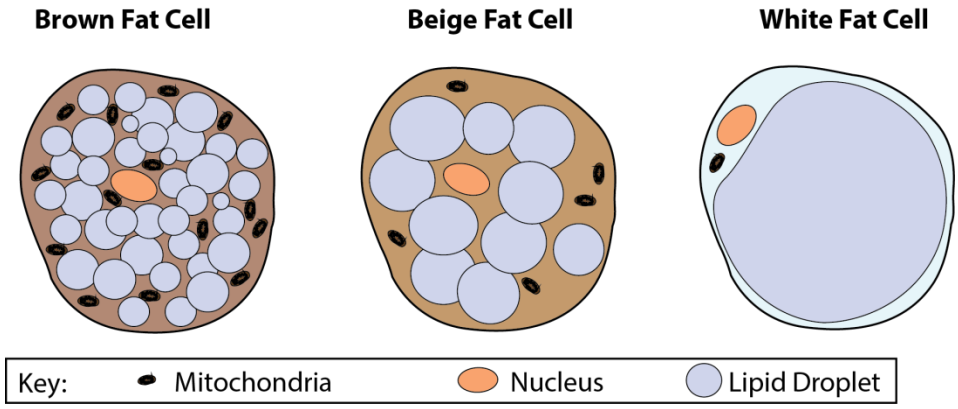

Figure 1.4 | The 3 main adipocyte cell types differ in function. The primary role of the white adipocyte is energy storage and release. The multilocular brown adipocytes contain many mitochondria and express high levels of UCP1 to generate heat. Beige fat cell is normally indistinguishable from the white fat cell, but upon β-adrenergic stimulation, it upregulates mitochondria, UCP1 and becomes multilocular.

The primary role of the human white adipocyte is energy storage. The cell is characterised by a large lipid droplet, with a single phospholipid layer filled with triglycerides. In the postprandial state, the fat cell takes up lipids in the form of gut-derived chylomicrons or lipoprotein particles and stores them as triglycerides (Nelson and Cox, 2005). White adipocytes can also directly uptake glucose and synthesise fatty acids (FAs) via Acetyl-CoA Carboxylase (ACC) and Fatty Acid Synthase (FAS) through de-novo lipogenesis, a process normally occurring in the liver (Abel *et al.*, 2001; Mao *et al.*, 2009). In response to conditions of low glucose, increased physical activity and β-adrenergic stimulation, the white adipocyte will activate lipolysis, the breakdown of triglycerides into free fatty acids

(FFAs) and glycerol through the action of adipose triglyceride lipase (ATGL), hormone-sensitive lipase (HSL) and monoglyceride lipase (MGL) (Figure 1.5). FFAs are released into the circulation and metabolised in the mitochondria of other tissues through β-oxidation (Nelson and Cox, 2005). As discussed later, adipocytes also have an equally important endocrine role whereby they can regulate food intake and systemic energy homeostasis through the release of adipokines such as leptin and adiponectin.

A different purpose is served by the brown adipose tissue (BAT). BAT has been long known to be present in small mammals and human infants (Rothwell and Stock, 1997). After a long controversy, its existence has been confirmed also in adult humans by FDG-PET analyses of glucose uptake (Saito *et al.*, 2009; Virtanen *et al.*, 2009). In humans, the amount of BAT is inversely correlated with BMI and diabetes incidence, suggesting that BAT activation could be a potential therapy to treat obesity and metabolic disorders (Ouellet *et al.*, 2011). Since BAT is highly vascularised and brown adipocytes are multilocular (multiple lipid droplets) with large numbers of mitochondria (containing cytochrome enzymes with iron as a cofactor), it has a characteristic dark red appearance (Lee, Swarbrick and Ho, 2013). From the perspective of gene expression, brown preadipocytes express many myogenic markers including *Myf5* and are also capable of differentiating into myoblasts (Seale *et al.*, 2008). The primary role of BAT is to generate heat by non-shivering thermogenesis in response to cold, β-adrenergic stimulation and also food intake (Li *et al.*, 2018). BAT can achieve this primarily through the activation of uncoupling protein 1 (UCP1) which uncouples the proton gradient in the inter-membrane space of mitochondria allowing the acceleration of electron transport chain (ETC) reactions thus generating heat at the cost of lower ATP output through ATP synthase (Complex V) (Cannon and Nedergaard, 2004). Even in normal fibroblasts, mitochondria were recently shown to generate temperatures up to 50°C (Chrétien *et al.*,

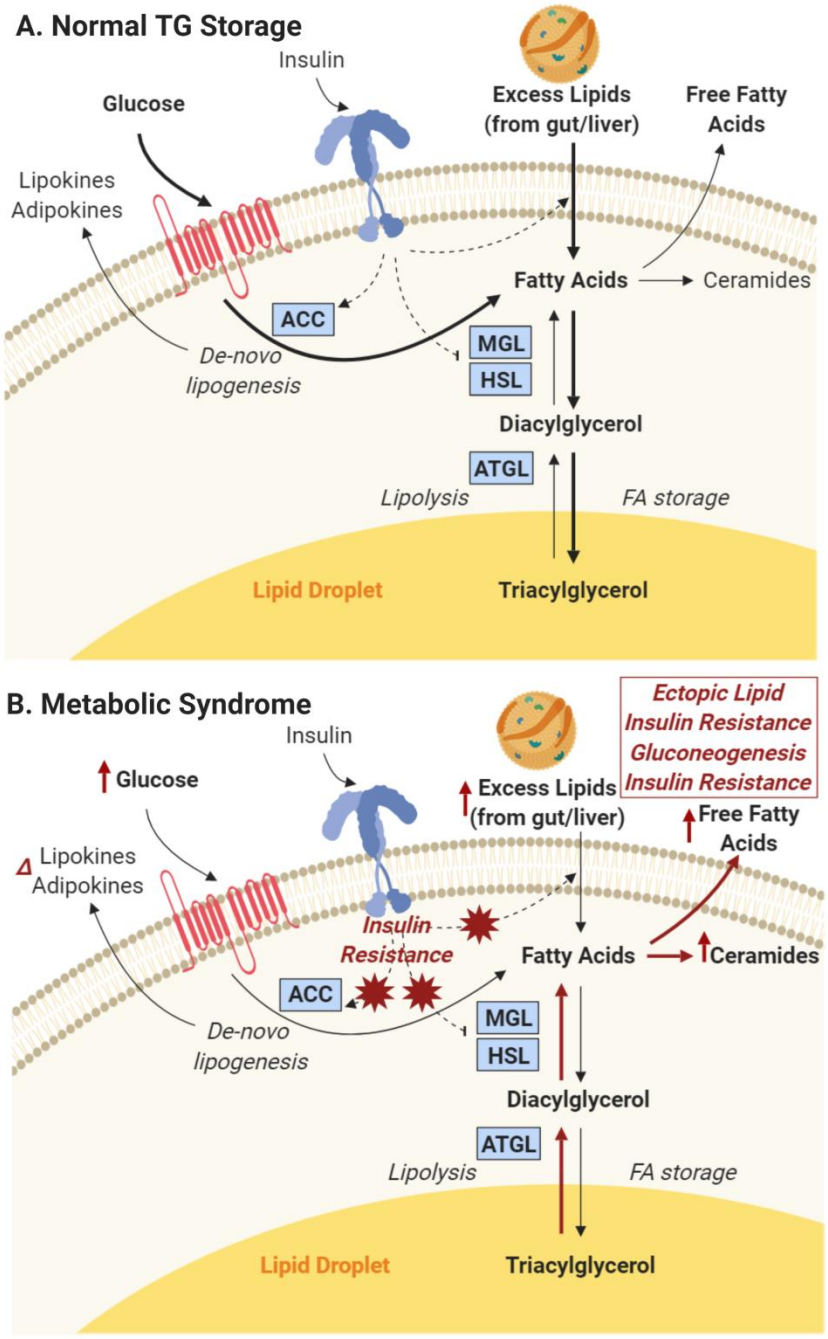

Figure 1.5 | Lipolysis and fatty acid storage in health and disease.
Under normal conditions (A), postprandial state activates insulin signalling which triggers uptake of lipids and glucose. Fatty acids get stored as triglycerides in the lipid droplets. In metabolic syndrome (B), insulin resistance in overloaded adipocytes interferes with the inhibition of lipolysis, activation of lipogenesis and glucose uptake. In effect constitutive fatty acid mobilisation contributes to elevated plasma and lipid levels as well as production of lipotoxic diacylglycerol and ceramides and altered lipokine and adipokine secretion. Together, these effects result in ectopic lipid deposition and insulin resistance in other tissues. Adapted from Vegiopoulos et al., 2017.

2018). It is thus not surprising that BAT, with multiple copies of these organelles in a hyper-activated state, is one of the most metabolically active tissues in the body (Rothwell and Stock, 1983; Astrup *et al.*, 1985). In unstimulated brown adipocytes, UCP1 is thought to be inactive, at least in part due to inhibitory effects of ATP and GDP (Nicholls, 2006; Sluse *et al.*, 2006). Stimulation of lipolysis leads to elevated levels of free fatty acids that bind and activate UCP1 (Fedorenko, Lishko and Kirichok, 2012). Importantly, *Ucp1*$^{-/-}$ mice can withstand cold temperatures if applied gradually (Meyer *et al.*, 2010). This suggests that UCP1 deficiency can be compensated for by other mechanisms of non-shivering thermogenesis including calcium and creatine cycling in white adipose tissue (WAT) or sarcolipin-mediated calcium cycling in skeletal muscle (Kazak *et al.*, 2015; Rowland *et al.*, 2015; Ikeda *et al.*, 2017).

The existence of a third type of adipocyte - the brown-in-white (brite) or beige adipocyte in some adipose depots has been well described (Bartelt and Heeren, 2014). When unstimulated, brite fat cells are unilocular and similar to white adipocytes. Browning, the appearance of UCP1-expressing multilocular cells within white adipose depots occurs upon chronic cold exposure or β_3-adrenoceptor stimulation (Cousin *et al.*, 1992; Sidossis *et al.*, 2015). Although still a controversial topic, it appears that brite adipocytes can be generated both by de-novo differentiation from preadipocytes and trans-differentiation from pre-existing white adipocytes (Barbatelli *et al.*, 2010; Y.-H. Lee *et al.*, 2015). Another hypothesis suggests that a pre-determined brite adipocyte lineage might give rise to a white adipocyte-like cell indistinguishable from non-thermogenic white adipocytes until an appropriate stimulus is received (Sidossis *et al.*, 2015; Sanchez-Gurmaches, Hung and Guertin, 2016). Interestingly, browning can be also induced by exercise, cancer cachexia and burn injuries (De Matteis *et al.*, 2013; Petruzzelli *et al.*, 2014; Sidossis *et al.*, 2015). Apart from a pure thermogenesis role, browning might thus serve as a stress

response to the altered metabolic profile when increased sympathetic signalling upregulates lipolysis and imposes stress on the relatively sparse WAT mitochondria (Sanchez-Gurmaches, Hung and Guertin, 2016).

1.3. Heterogeneity of adipose depots

The main adipose depots in humans are intra-abdominal VAT (omental and mesenteric), upper-body subcutaneous and lower-body subcutaneous (gluteal, subcutaneous leg fat and intramuscular fat). In an attempt to explain the increased disease risks associated with increased WHR, I will assess differences between VAT, abdominal subcutaneous adipose tissue (ASAT) and gluteofemoral subcutaneous adipose tissue (GSAT) (Tchkonia *et al.*, 2013). At the end of this subchapter, I will also compare the browning capacity between humans and mice and elucidate the developmental origins of different fat depots.

1.3.1. Lipid metabolism in human adipose

Firstly, adipose depots differ in the rates of fatty acid storage and lipolysis. [^{3}H]-triolein studies showed that storage of diet-derived fatty acids is more efficient in omental and mesenteric VAT, less efficient in ASAT and even less in GSAT (Jensen *et al.*, 2003). Visceral and subcutaneous upper body fat together took up 74% of dietary lipids that were not oxidised. Similarly to FA storage, VAT and ASAT in comparison to GSAT were found to be more lipolytic, more responsive to lipolytic stimuli and resistant to insulin-mediated inhibition of lipolysis (Caserta *et al.*, 2001; Tchkonia *et al.*, 2013). For example, isolated ASAT adipocytes treated with noradrenaline upregulated lipolysis up to 5-fold more compared to GSAT adipocytes (Wahrenberg, Lonnqvist and Arner, 1989). Higher expression of β-adrenoceptors and activity of the rate-determining enzyme of lipolysis the hormone-sensitive lipase (HSL) in the ASAT depot could contribute to this result (Arner *et al.*, 1990; Tan *et al.*, 2004). Furthermore, human studies have shown that ASAT elicited a stronger lipolytic response than GSAT in response to fasting and adrenaline stimulation (Horowitz and Klein, 2000; Gjedsted *et al.*, 2007). Similarly, in the postprandial state, the upper body fat is more lipolytic and a major source of FFAs (Guo *et al.*, 1999). This could be explained by marked insulin sensitivity of leg fat combined with resistance of VAT to

the antilipolytic effects of insulin (Meek, Nair and Jensen, 1999). In summary, the visceral adipose is more flexible and responsive depot adapted for short-term buffering of lipid metabolism, whereas the less-responsive subcutaneous depot with its slow lipid release may act as a long term "metabolic sink."

1.3.2. Endocrine function

Apart from its role in lipid metabolism, adipose tissue can also secrete hormones to induce systemic effects. These hormones, termed adipokines, can be produced either by the adipocyte (e.g. leptin, adiponectin) or by resident macrophages (e.g. interleukins). Leptin, the regulator of appetite and lipid partitioning is positively correlated with fat mass and is expressed more strongly in SAT than VAT (Fontana *et al.*, 2007; Wiest *et al.*, 2010). Indeed, leg fat was shown to be the net producer of leptin (Jensen *et al.*, 1999). Another adipokine, the insulin-sensitizing, anti-apoptotic, anti-inflammatory and proangiogenic hormone adiponectin is negatively correlated with WHR and visceral fat mass (Arita *et al.*, 1999; Park *et al.*, 2004). In agreement with this, *in vivo* studies have showed lower adiponectin and its receptor expression in visceral fat mass (Fisher *et al.*, 2002; Rasmussen *et al.*, 2006). In one study, this was only true for lean individuals since obesity was associated with reduced adiponectin levels in SAT but no effect on VAT (Kovacova *et al.*, 2012). Other studies either did not find a difference or found higher adiponectin expression in VAT as opposed to SAT (Fontana *et al.*, 2007; Wiest *et al.*, 2010). On the other hand, cytokines tumour necrosis factor α (TNFα) and interleukin 6 (IL-6) are generally associated with inflammatory states and obesity and levels of IL-6 are elevated in VAT compared to subcutaneous depots (Zahorska-Markiewicz *et al.*, 2000; Fain *et al.*, 2004; Fontana *et al.*, 2007). However, not all studies found differences in cytokine expression between fat depots (Rakotoarivelo *et al.*, 2018). Despite this, visceral fat venous blood flow is drained through the portal vein directly into the liver and it is thus possible that

visceral-derived FFAs and adipokines have a direct effect on liver metabolism. Other adipokines, such as plasminogen-activated inhibitor 1 (PAI-1), vaspin or asprosin, may further contribute to depot-specific disease association (Tchkonia *et al.*, 2013; Romere *et al.*, 2016).

Since secretion profiles of preadipocytes and immune cells differ from those of fat cells, it is possible that any depot-specific differences in cytokine secretion might be due to differences in preadipocyte or macrophage proportions (Tchkonia *et al.*, 2013). Indeed, preadipocyte proportions in the adipose SVF can vary between 50 to 85% between depots and macrophage infiltration was found to be 4 times higher in omental VAT compared to ASAT (Zhang *et al.*, 2009; Gupta *et al.*, 2012; Raajendiran *et al.*, 2019).

1.3.3. Replicative potential and differentiation

Fat depots differ in their propensity to expand by hyperplasia or hypertrophy and this may be linked to inflammation and insulin sensitivity (Tchoukalova *et al.*, 2010; Laurencikiene *et al.*, 2011). Mature adipocytes are post-mitotic, with around 8% of adipocytes being turned over each year to match the rate of apoptosis (Spalding *et al.*, 2008). Thus, it is the replicative and differentiation potential of preadipocytes that determines the capacity for hyperplasia. Colonies of preadipocytes isolated from human ASAT show more extensive replication than those from omental VAT, with mesenteric VAT being intermediate (Tchkonia *et al.*, 2006). Differentiation potential was also higher in ASAT preadipocytes compared to omental VAT cells (Figure 1.6) (Tchkonia *et al.*, 2002). Part of the reason for this could be enrichment of SAT for a particular preadipocyte subtype, that is more prone to replication, differentiation and less prone to apoptosis (Tchkonia *et al.*, 2005). In agreement with this, administration of thiazolidinediones is associated with greater fat gain in SAT as opposed to VAT (Mori *et al.*, 1999). Furthermore, the expression of the key adipogenic transcription factors PPARγ and C/EBPα are higher in ASAT compared to

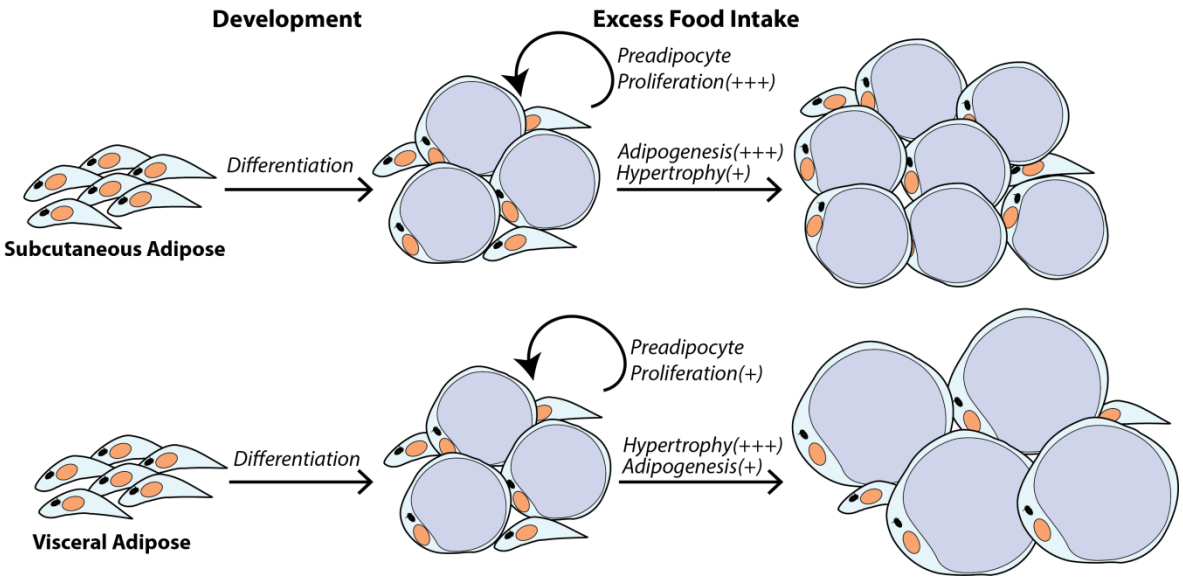

Figure 1.6 | Different mechanisms of adipose expansion during obesity in subcutaneous and visceral adipose.
Both human and mouse studies have shown that subcutaneous fat, such as gluteofemoral adipose in humans and inguinal WAT in mice, expands primarily by increase in cell number (A). Visceral depots, including omental depot in humans and gonadal WAT in mice, expand primarily by hypertrophy. These differences can be linked to the underlying SVF capacities to differentiate and proliferate. Adapted from Tchkonia et al., 2013.

omental VAT differentiating preadipocytes (Tchkonia *et al.*, 2002). Later studies have shown that differences in key lipid metabolism and developmental genes are present between depots already at the level of undifferentiated preadipocytes. These genes included the homeobox (HOX) transcription factors, the upstream developmental regulators of specialization of segments along the anteroposterior axis (Tchkonia *et al.*, 2007). The differences in differentiation and proliferative capacity persisted even in telomerase-immortalised cells after 40 population doublings, suggesting that they can be explained by inherent differences in the properties of fat cell progenitors rather than their environment (Tchkonia *et al.*, 2006). In line with Tchkonia et al. 2005, a recent study also identified different preadipocyte subtypes, forming mature cells with differences in potential for lipolysis, FA storage and browning (Raajendiran *et al.*, 2019). However, there was no difference in subtype proportions between the depots suggesting that the major

determinant of expansion by hyperplasia or hypertrophy could be the depot-specific differences in total preadipocyte to mature adipocyte proportions (Raajendiran *et al.*, 2019). Differences in cell-surface markers used to define the "preadipocyte" population could also explain this disagreement.

1.3.4. Extracellular matrix and angiogenesis

The microenvironment of specific depots can also influence adipocyte replicative and differentiation potential. For adipose tissue to expand, the extracellular matrix (ECM) must remodel and create enough space for larger adipocytes and new blood vessels which will prevent hypoxia (Sun, Kusminski and Scherer, 2011). Importantly, the exact composition of ECM differs between depots. In an analysis of the secretomes of fat tissue from obese people, VAT showed specific expression of collagen VI (α1, α2, α3) and SAT specifically expressed collagen I and metalloproteinase inhibitor 1 (TIMP1) (Roca-Rivada *et al.*, 2015). These differences could contribute to the reduced differentiation potential of VAT SVF cells. In line with this, plating VAT SVF cells on de-cellularized ECM from SAT improved VAT SVF differentiation capacity (Grandl *et al.*, 2016).

Apart from supplying oxygen, blood vessels are also an important source of adipose progenitors. The most important pro-angiogenic signal is mediated by the vascular endothelial growth factor (VEGF) which activates quiescent endothelial cells (ECs) to form new vessels and in effect causes adipose browning and improved metabolic profile (Park *et al.*, 2017). Importantly, SAT appears to have a greater capacity to upregulate angiogenesis compared to VAT, but this difference diminishes with increasing obesity (Tang *et al.*, 2008). Further differences between depots exist also at the level of neurite innervations. Using a 3D imaging approach, Chi et al have shown that compared to VAT, SAT was well structurally organised with dense nerve bundles and neurite projections. This difference is in part regulated by endocrine signals from adipocytes (Chi *et al.*, 2018).

1.3.5. Fat distribution in mouse models

Despite 89 million years of evolutionary divergence, animal models are frequently used for the study of adipose and obesity (Kumar *et al.*, 2017). Like in humans, adipose tissue in mice is a multi-depot organ, but the specific anatomy differs (Figure 1.7). While humans

have two main subcutaneous depots around the gluteofemoral and abdominal areas, the two major subcutaneous depots in mice are located anteriorly between the scapulae and posteriorly spreading from dorsolumbar region to gluteal region. The location of the latter, the inguinal WAT (iWAT) is thus similar to GSAT in humans (Chusyd *et al.*, 2016).

The main rodent visceral depots are the gonadal WAT (gWAT) surrounding the gonads, perirenal WAT (prWAT) or retroperitoneal WAT (rtpWAT) covering the kidneys and the mesenteric WAT (mWAT) alongside the intestinal tract (Chusyd *et al.*, 2016). Of these depots, mWAT is the most analogous to humans visceral adipose by its location and also it's drainage to the portal vein (Cinti, 2005). However, poor surgical access of mWAT and its infiltration with blood vessels have made gWAT the preferred representative tissue of visceral fat in mice, although this depot seems absent in humans. Another major human VAT depot, the omental fat, is present in mice too, but in lower quantities (Frontini and Cinti, 2010).

Importantly, the different health consequences associated with visceral and subcutaneous fat seen in humans seem to be conserved in mice. Removal of gWAT in mice improved insulin action and longevity and reduced tumorigenesis in mice (Gabriely *et al.*, 2002; Lu *et al.*, 2012). Furthermore, transplanting subcutaneous, but not visceral fat, improved glucose metabolism in mice, especially when placed in the viscera (Tran *et al.*, 2008). The lack of similar effect of human omentectomy, the removal of omental fat, during gastric bypass operations in humans is likely to be due to the very small total VAT removed in humans (<10%) compared to mice (~75%) (Fabbrini *et al.*, 2010; Herrera *et al.*, 2010). Importantly, in both aging mice and humans, subcutaneous fat depots are depleted, contributing to accumulation of visceral and ectopic fat stores in liver, pancreas, bone, and skeletal muscle (Kuk *et al.*, 2009; Tchoukalova *et al.*, 2010)**.**

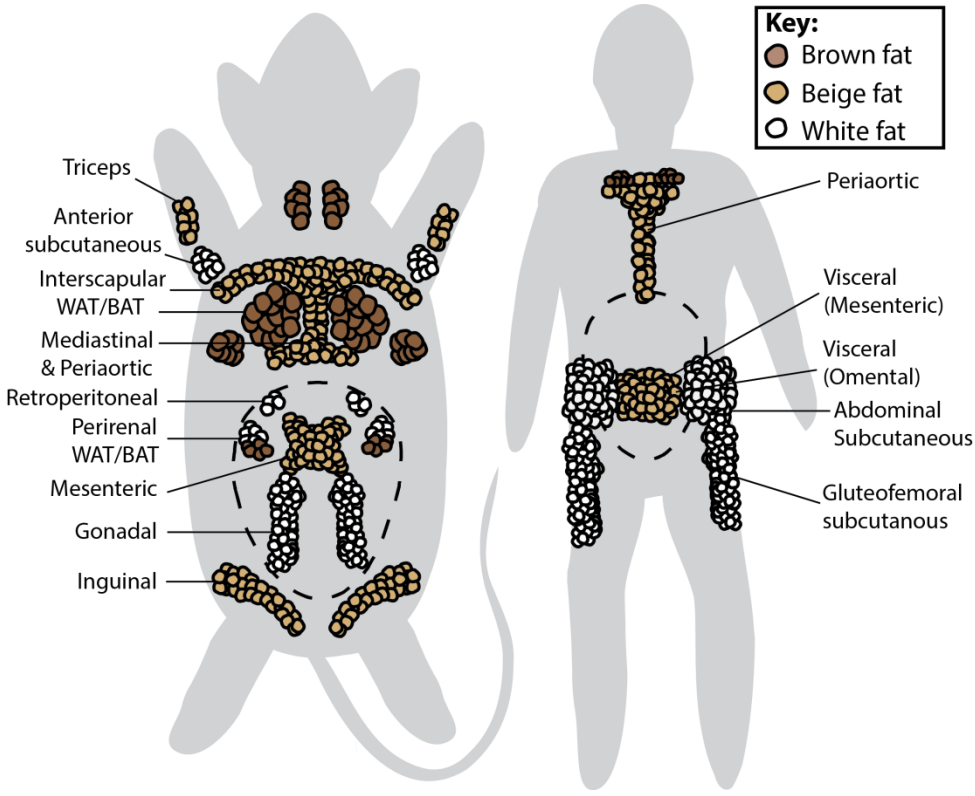

Figure 1.7 | Major fat depots in human and mice. Two main subcutaneous depots of the mouse are the inguinal and interscapular depots. In humans, subcutaneous adipose is found both in the gluteofemoral and abdominal region. Several visceral depots exist in both human and mice with the mesenteric depots being comparable between human and mice, but gonadal depot being largely absent in humans. Both human and mice have beige adipose tissue with high browning propensity in the periarotic and mediastinal regions. Unlike human gluteofemoral subcutaneous tissue, mouse inguinal adipose has also a high browning capacity. Brown adipose is more prominent in mice in the interscapular region. Based on reviews by Chusyd et al. 2016, Giordano et al. 2016 and de Jong et al. 2015.

In humans, VAT is more lipolytically active than subcutaneous adipose and is preferentially decreased during weight loss compared to SAT (Goodpaster *et al.*, 1999). Similar dynamics during fasting exist in mice where mesenteric and gonadal VAT depots are preferentially reduced compared to inguinal and anterior subcutaneous WAT (asWAT) in response to weight loss (Ding *et al.*, 2016; Tang *et al.*, 2017). Elaborate mouse studies have shown that differentially expressed genes, such as Short stature homeobox 2 (*Shox2*) which modulates β3 adrenergic receptor (*Adrb3*) expression, contribute to the differences in rate of lipolysis (Lee *et al.*, 2013). However, differences between mice and humans also

exist. For example, the ratio of β-adrenergic receptors (AR) and α2-ARs, which stimulate and inhibit lipolysis, respectively, differs markedly between humans and rodents (Castan *et al.*, 1994). Genetically shifting this ratio closer to the human situation promotes obesity in mice (Valet *et al.*, 2000). Human and mouse show also cell-intrinsic depot similarities. Similar to humans, the mouse subcutaneous pre-adipocytes, derived from inguinal WAT (iWAT), differentiate much better than visceral pre-adipocytes, from gonadal WAT (gWAT). Interestingly, this difference can be rescued by treatment with the bone morphogenetic protein (BMP)-2 or BMP-4 (Macotela *et al.*, 2012). Endocrine profiles of the fat depots may differ between the two species. For example, whilst leptin is expressed predominantly by the subcutaneous depot in humans, mouse expression is higher in either depot based on sex, diet and due to pregnancy (Trayhurn *et al.*, 1995; Schlitt and Schulz, 2012).

In summary, the health associations of visceral and subcutaneous fat translate between mice and humans. However, the proportion of specific depots, adipokine release and lipolysis regulation differs under certain conditions.

1.3.6. Brown fat and browning in mice and humans

Activation of BAT increases energy expenditure, reduces adiposity, prevents diet-induced obesity and thus holds a promise for a potential obesity therapy (Bachman *et al.*, 2002; Feldmann *et al.*, 2009). The murine dorsal-cervical (interscapular, subscapular and cervical) BAT is a sizeable depot, whereas the adult supraclavicular BAT in thermoneutral humans is markedly smaller and its contribution to metabolism is probably minor (Figure 1.7) (Giordano, Frontini and Cinti, 2016). Furthermore human BAT size is inversely associated with age and obesity and thus the much larger white fat depots with a potential for browning (beige depots) are potentially better therapeutic targets for treatment of obesity (Saito *et al.*, 2009; Virtanen *et al.*, 2009; Vijgen *et al.*, 2011).

PET analyses of "brownable" or beige adipose in humans exposed to β-adrenergic agonist revealed substantial browning of adipose surrounding the thoracic and abdominal aorta and its branches (Cypess *et al.*, 2015). This physical proximity to the aorta allows for rapid transport of heat around the whole body. In half of the adipose samples from pheochromocytoma patients, visceral depots distant from the aorta such as the omental depot were also susceptible to browning (Frontini *et al.*, 2013). In line with this, a recent study showed that human omental fat is more prone to browning than the subcutaneous depots (Zuriaga *et al.*, 2017).

In mice, it is widely accepted that subcutaneous depots such as the iWAT are more susceptible to browning compared to gWAT and that this may contribute to their opposing health benefit associations (Zuriaga *et al.*, 2017). For example, ablation of the beige-adipocyte regulator *Prdm16* caused subcutaneous iWAT to gain many properties of visceral gWAT and prevented the health benefits associated with iWAT transplantation (Cohen *et al.*, 2014). The unique browning of murine subcutaneous depots, which is not

observed in humans, could be an effective strategy of heat dispersion for smaller mammals with high body surface : volume ratio (Giordano, Frontini and Cinti, 2016). On the other hand, recent evidence suggests that mice housed at thermoneutrality are more similar to humans. In this case, iWAT is almost resistant to browning and instead the classical murine iBAT shows more similar gene expression and browning capacity to human BAT (de Jong *et al.*, 2019). Despite browning-resistance of gWAT, other visceral depots, especially those in contact with the aorta and its main branches, show browning upon cold induction in mice (Vitali *et al.*, 2012). In line with this, the visceral mediastinal depot that surrounds the aortic and thoracic aorta contains the highest density of noradrenergic fibres and shows one of the strongest browning responses observed in mice (Murano *et al.*, 2009; Vitali *et al.*, 2012).

Thus in summary, both murine and human visceral depots, especially those proximal to the aorta, are highly susceptible to browning. However, differences exist. The mouse gWAT is highly resistant to browning whilst its subcutaneous depots are highly prone to browning. It is likely that at least some of these inter-species differences arise from mice being housed below thermoneutrality.

1.3.7. Adipocyte lineages across depots

Classification of adipocytes into brown, beige and white is helpful to describe the key characteristics of adipose, but does not inform us about the function and origins of different depots. To do this, a number of primarily mouse studies have tried to define the progeniors of different depots, as summarised in this review (Sebo and Rodeheffer, 2019). For over 100 years, it has been known that adipose originates primarily from the mesoderm (Flemming, 1871). Modern lineage tracing studies have confirmed this finding, although evidence for ectodermal neural crest origin of salivary gland WAT was also found (Billon *et al.*, 2007). Especially the cell-membrane localised reporter mTmG system has been invaluable for studying adipocytes which are labelled poorly using traditional soluable reporters such as XGal and YFP (Muzumdar *et al.*, 2007).

Following gastrulation, the mesoderm is divided into somites, intermediate mesoderm and posterior lateral plate mesoderm (PLPM). The somites can be further subdivided into the myotome, sclerotome and dermomyotome. The dermomyotome is composed of the dorsomedial lip, central and ventrolateral lip parts (Figure 1.8). *MyoD1*-Cre:mTmG reporter mice clearly showed that the myotome does not contribute to any adipose tissue (Sanchez-Gurmaches and Guertin, 2014). Instead, the majority of adipocytes appear to originate from the somite dermomyotome and PLPM. Studies of central dermomyotome specific markers *En1*, *Pax7* showed labelling of interscapular BAT (iBAT) and interscapular WAT (isWAT) (Atit *et al.*, 2006; Lepper and Fan, 2010). Tracing the myogenic marker *Myf5*-expressing cells has shown the dorsomedial lip of dermomyotome also contribute to iBAT (Seale *et al.*, 2008). Thus BAT and muscle share a common progenitor which is in line with previous findings where BAT preadipocytes express some myogenic markers, not present in WAT preadipocytes (Timmons *et al.*, 2007). However, more recent studies demonstrated that *Myf5*$^{+}$ cells contribute also to dorsal anterior

subcutaneous WAT (asWAT) and retroperitoneal WAT (rtpWAT) (Sanchez-Gurmaches and Guertin, 2014). Interestingly, compared to the *Myf5*-Cre line, the neural crest and whole dermomyotome-specific *Pax3*-driven Cre showed staining of additional adipocytes in perirenal BAT (prBAT) and a subset of male, but not female gWAT, compared to the *Myf5*-line (Sanchez-Gurmaches and Guertin, 2014). This suggests that either the neural crest or the ventrolateral lip of the dermomyotome generate these additional cells. Since the pan-somite *Meox1*-Cre staining mirrored that of the *Pax3*-Cre, the adipocytes of perirenal BAT and male gWAT must therefore originate from the ventrolateral lip of the dermomyotome (Sebo *et al.*, 2018).

The PLPM is also an important contributer to adipose tissue. Studies of the *Wt1*-driven Cre, expressed in the splanchnic PLPM and intermediate mesoderm, and the *Prx1*-Cre, expressed in the limb-bud mesenchyme, revealed that the splachnic PLPM contributes to visceral depots, such as mWAT and female gWAT, but not subcutaneous depots (Chau *et al.*, 2014; Sanchez-Gurmaches, Hsiao and Guertin, 2015). On the other hand, the pan-PLPM expressed *HoxB6*-Cre stained both visceral and subcutaneous depots, suggesting that somatic PLPM gives rise to subcutanous depots, such as iWAT (Sebo *et al.*, 2018).

Thus in summary, adipose depots show a complex developmental fate map with different depots originating from different progenitors and some depots, such as iBAT, made up adipocytes from different progenitors. Importantly, rather than specific gene expression, as for the case of *Myf5*$^{+}$ cells, specific anatomical location might be crucial in determing the fate of an adipocyte precursor. The cexample of gWAT shows that some depots may have sex-dependent differences in developmental origins.

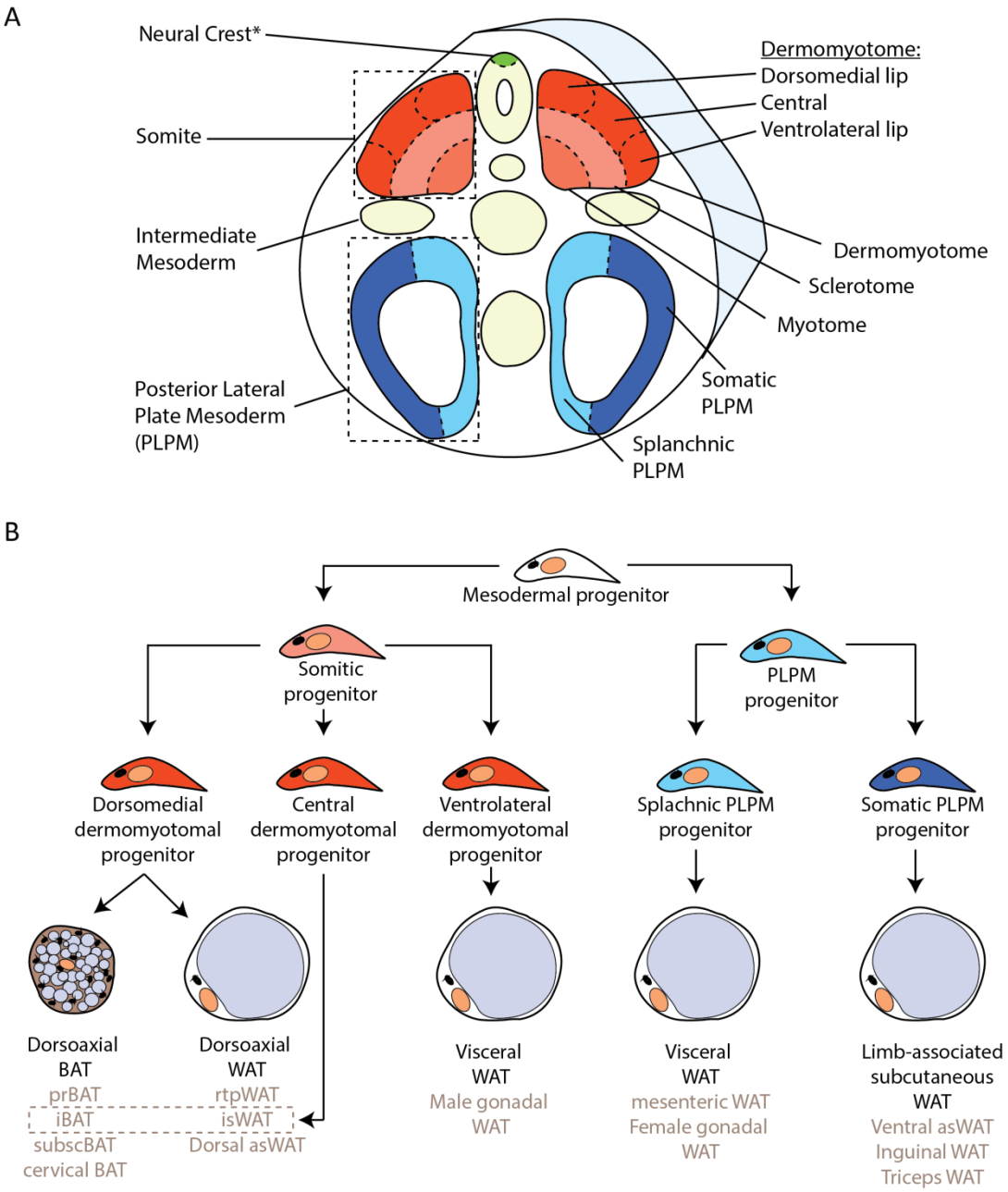

Figure 1.8 | Fate map diagram for different adipose depots. Majority of brown and white adipocytes originates either from the dermomyotome layer of the somites or from the Posterior lateral plate mesoderm (PLPM). Also neural crest cells can give rise to adipocytes in salivary gland WAT (A). The fate map of adipose progenitors towards different white and brown adipose depots. Triceps WAT is an internal supramuscular depot. prBAT, perirenal BAT; iBAT, interscapular BAT; subscBAT, subscapular BAT; rtpWAT, retroperitoneal WAT; isWAT, interscapular WAT; asWAT, anterior subcutaneous WAT. Adapted from (Sebo and Rodeheffer, 2019).

1.4. Deciphering GWAS loci

1.4.1. From GWAS to understanding fat distribution regulation

Since the completion of the human genome sequence in 2003, genome-wide association studies (GWAS) have been deployed to understand the genetic contribution to disease risk and complex traits. In the most recent GWASs , 941 BMI associations were discovered in 536 loci and 463 WHRadjBMI associations in 346 genomic loci (Pulit *et al.*, 2018; Yengo *et al.*, 2018). Since up to 94% of GWAS SNPs lie in non-coding regions, it remains a challenge to identity the effector genes in each locus (Matthew T Maurano *et al.*, 2012). Furthermore, as shown in Figure 1.9, SNPs are often closely linked with other SNPs in a haplotype by linkage disequilibrium (LD), which complicates the search for causal SNPs and suggests that in some loci, there might be multiple interacting polymorphisms (Nicolae *et al.*, 2010; Schaub *et al.*, 2012).

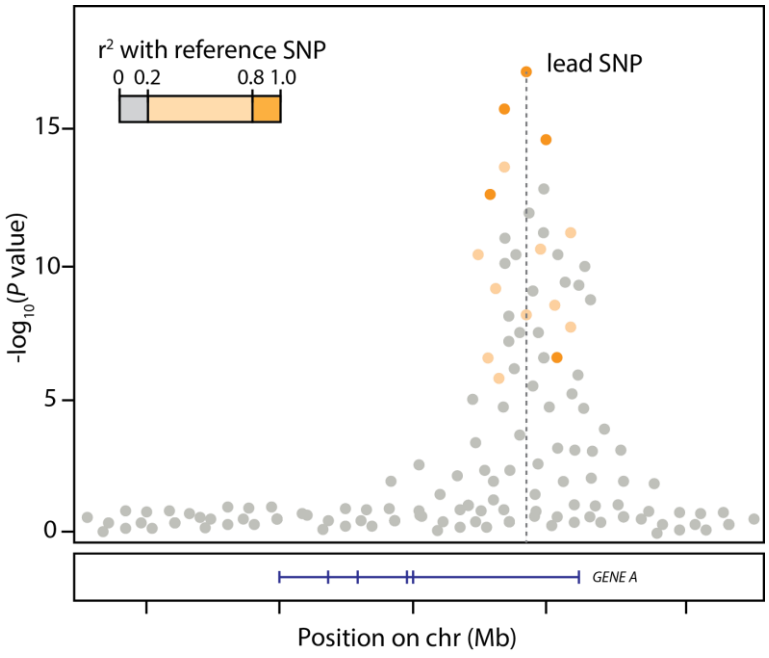

Figure 1.9 | The challenge of deciphering GWAS loci. Apart from the lead SNP (lowest association p-value in the region) multiple other SNPs often show significant associations for a given trait in each locus. Since most of SNPs associated with complex diseases and traits are non-coding, identifying functional SNPs and genes is challenging. Selecting only SNPs in close linkage disequilibrium ($r^2 \geq 0.8$) with the lead SNP is often the first step in SNP filtering.

1.4.2. Variation in the non-coding genome

How could a SNP in the non-coding region affect expression of a distant gene? For many years, the non-coding genome was believed to be largely inactive. We now know it contains many functional elements that may regulate gene expression and processing or packaging of DNA into chromatin (Figure 1.10) (Ward and Kellis, 2012).

The expression of each gene is driven primarily at the level of its promoter and indeed GWA SNPs within promoters may affect gene expression. For example, a SNP in the *MDM2* promoter increases the DNA-binding of the transcriptional activator Sp1 leading to higher levels of MDM2 expression and accelerated tumour formation (Bond *et al.*, 2004). Chromatin is highly organised in the cell nucleus and multiple genes and enhancers are often linked in a single topologically associated domain (TAD), as shown for the *TBX15-WARS2* locus (Figure 1.11) (Dixon *et al.*, 2012). Enhancers can further influence gene expression within these domains; it is estimated that in any given tissue there are three active enhancers per gene (Hait *et al.*, 2018). Similarly, a single enhancer can regulate multiple genes. For example, in the BMI-associated *FTO* locus, rs1421085 disrupts a motif for the ARID5B repressor leading to derepression of a preadipocyte enhancer and doubling of *IRX3* and *IRX5* expression during adipocyte differentiation (Claussnitzer *et al.*, 2015). Due to the tissue-specific activation of enhancers, genetic variation of these elements can affect only some tissues and not others, thus affecting the risk of specific traits or diseases associated with that tissue (Matharu *et al.*, 2019).

Gene expression and function can be also regulated at the level of splicing and RNA processing. SNPs in consensus splicing donor and acceptor splice sites may result in inclusion or exclusion of additional introns/exons. For example, the causal SNP rs10201872 in the *SP140* locus associated with multiple sclerosis has been shown to act by causing exon skipping and thus leading to reduction of SP140 protein expression

(Matesanz *et al.*, 2015). Splicing is also regulated at the level of splicing enhancers and inhibitor sequences interspaced throughout introns and exons (Fu and Ares, 2014). SNPs associated with splicing of a close gene, termed splicing quantitative trait loci (sQTLs), can be identified and are listed in databases, such as the Genotype-Tissue Expression (GTEx) project (Mele *et al.*, 2015). Post-transcriptional regulation is also strongly influenced by the 3' untranslated regions (3'UTR). Compared to simpler eukaryotes, such as yeast, human 3'UTR are ~10 fold longer and contain complex RNA-structural elements, miRNA and RNA-binding protein (RBP) binding sites and can thus affect the localisation, translation or degradation of RNAs (Mayr, 2017).

Other functional elements in the genome could also be potential targets of disease-risk SNPs. For example, the binding of CCCTC-binding factor (CTCF) and Cohesin defines the insulators and boundaries of TADs. Study of the *Sox9–Kcnj2* locus showed that although disruption of these binding sites results in the fusion of TADs, there is no major effect on gene expression (Despang *et al.*, 2019). However, generation of new boundary elements was shown to cause rewiring of enhancer-promoter contacts and gene expression (Despang *et al.*, 2019).

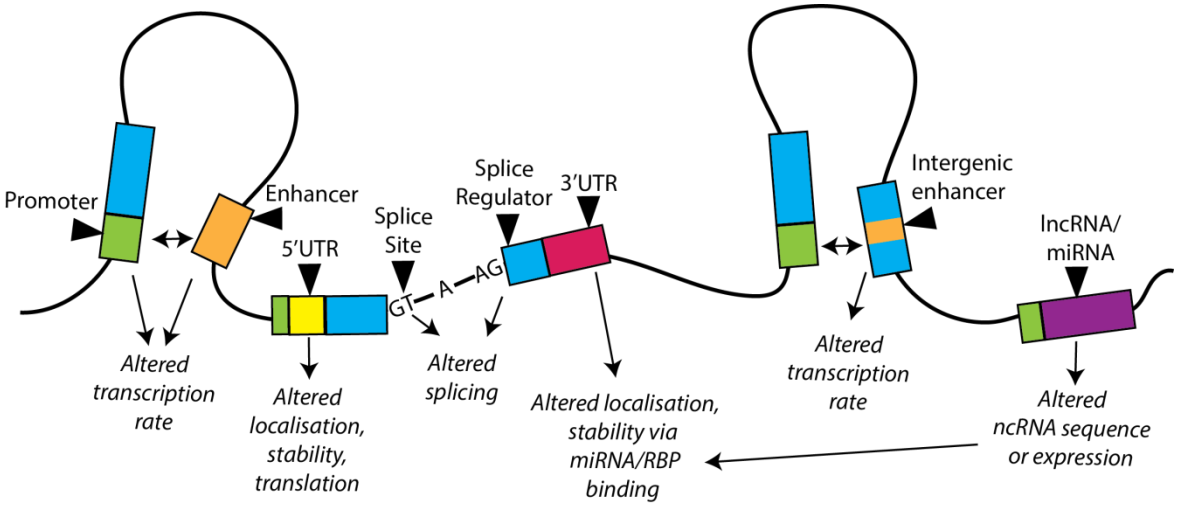

Figure 1.10 | Potential effects of non-coding polymorphisms. SNPs in promoters and enhancers can directly affect gene transcription rates. On the other hand, SNPs in 5' and 3'UTRs can interfere with post-transcriptional regulation through altering RNA binding protein (RBP) or miRNA binding. Variations in long non-coding RNAs (lncRNAs) and miRNAs can impact both transcription rates and post-transcriptional regulation. Interrupting canonical splicing signals, splicing enhancers or inhibitors can result in altered transcript structure or isoform proportions.

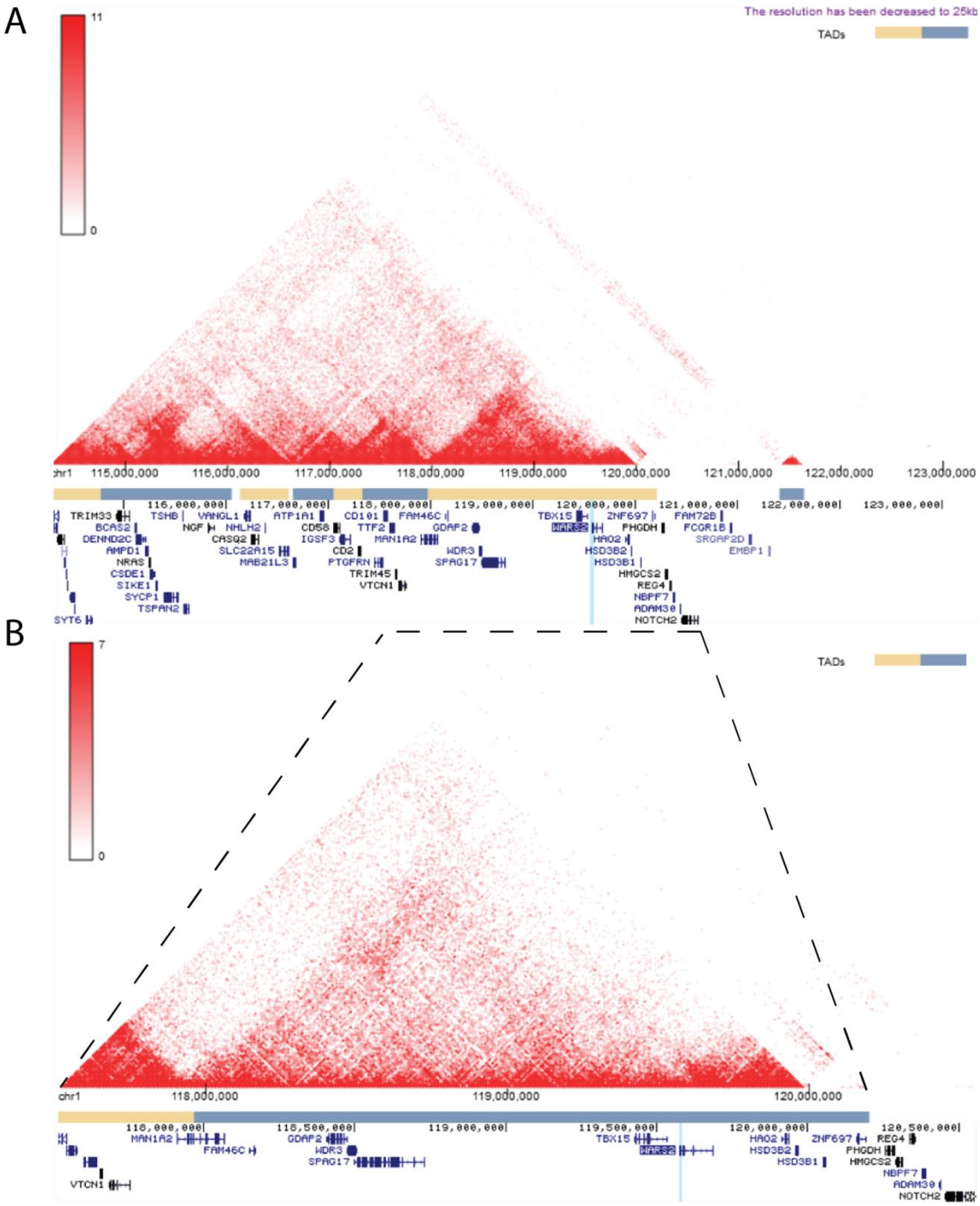

Figure 1.11 | Hi-C interaction map surrounding the *TBX15-WARS2* locus. 3D Genome Browser (http://promoter.bx.psu.edu/hi-c/) image of the Hi-C interactions at the 3'end of chromosome 1 in IMR90 fibroblasts (A) and a closer view of the Topologically Associated Domain (TAD), containing *TBX15-WARS2* locus, shown under the blue bar (B). Apart from *TBX15* and *WARS2*, the topologically-associated domain (TAD) contains several other genes including *SPAG17* and *HAO2* (Rao *et al.*, 2014; Y. Wang *et al.*, 2018).

1.4.3. The dynamic chromatin – adipose differentiation

Enhancers and their chromatin states are not only tissue-specific, but differ also between different developmental stages. It is thus possible that a SNP might have an effect on a particular stage of adipocyte differentiation, but might be undetectable in mature cells or vice versa.

Adipogenesis is one example of extensive chromatin remodelling during differentiation and has been studied the most in mouse 3T3-L1 preadipocytes (Siersbaek *et al.*, 2011). Differentiation of these cells can be induced after growth arrest using an adipogenic cocktail containing high levels of insulin, dexamethasone and 3-isobutyl-1-methylxanthine (IBMX) (Student et al., 1980). DNaseI-hypersensitive site sequencing (DNase-Seq) showed that already after 4 hours of treatment with the differentiation media, the number of accessible sites increases 3-fold compared to the preadipocyte (Siersbaek *et al.*, 2011). This is due to the expression of early adipogenic transcription factors, such as CCAAT-enhancer binding protein β (CEBPβ), which form transcription factor (TF) hotspots and recruit coactivators, chromatin-re-modellers thus activating a cascade of gene expression

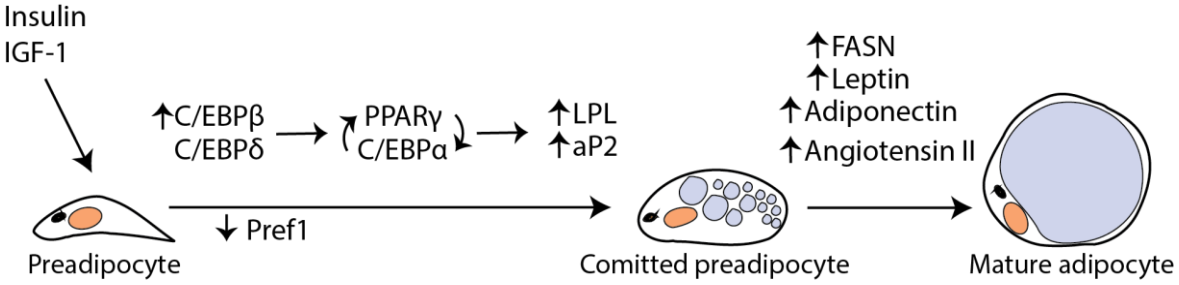

Figure 1.12 | An overview of adipocyte differentiation.
Preadipocyte differentiation is activated by hormones and growth factors such as Insulin and IGF-1, leading to elevation of C/EBPβ which together with C/EBPδ induces C/EBPα and PPARγ expression, which also further transcriptionally upregulate each other. C/EBPα and PPARγ then upregulate intermediate-phase genes such as aP2 and LPL, causing formation of first lipid droplets, and eventually terminal-phase genes such as FASN, Leptin, Adiponectin and Angiotensin II. Pref-1, preadipocyte factor-1; C/EBP, CCAAT/enhancer binding protein; PPARγ, peroxisome proliferator-activated receptor-γ; LPL, lipoprotein lipase. Based on (Miettinen, Sarkanen and Ashammakhi, 2008).

(Figure 1.12). The TF hotspots are especially enriched in super-enhancers, several kilobase long regions containing clusters of TF binding sites with high levels of Mediator subunit 1 (MED1) binding (Siersbaek *et al.*, 2014). Studies using chromatin capture methods such as Promoter Catpure Hi-C (PCHi-C) showed that although TADs remain stable during 3T3-L1 differentiation, many promoter-enhancer loops gain strength which is associated with increased gene expression. Rather than forming new enhancers, many poised preadipocyte enhancers are activated (Siersbæk *et al.*, 2017). Eventually, in mature adipocytes, the number of DNase-Seq peaks reduces again and is similar to preadipocytes, but including many novel mature-specific regions (Siersbaek *et al.*, 2011).

1.4.4. Prioritising functional SNPs

Multiple different methods have been developed to identify likely functional SNPs in GWAS loci. Firstly, fine-mapping studies which incorporate GWAS data from other ethnic populations with different LD structure can markedly reduce the list of candidates (Liu *et al.*, 2014). Second, Bayesian statistical methods such as the posterior probability analysis (PPA) can be used to reanalyse GWAS to assess how much of the trait-association signal can each SNP explain (Maller *et al.*, 2012). This method identified single SNPs which explained the entire association signals in each of the *TCF7L2* and *CDKN2B* T2D-associated loci. GWAS signals can also be co-localised with eQTL signals to implicate the most likely functional genes within a locus (Hormozdiari *et al.*, 2016a). Since each regulatory element could affect multiple genes, this method allows identifying only those genes which correlate with an effect on a given trait.

For functionally-informed approaches, all SNPs in close LD ($r^2 > 0.8$) with the lead SNP are first selected for further analysis. Large epigenomic datasets of multiple cell lines and tissues, such as gathered by The Roadmap Epigenomics Consortium, can predict the biological function of regions overlapping the associated SNPs (Kundaje *et al.*, 2015). For example, promoter regions can be distinguished by H3K4me3 chromatin immunoprecipitation sequencing (ChIP-Seq) signals, whereas active enhancers are enriched for a high H3Kme1:H3Kme3 ratio and H3K27ac signal. Heterochromatin or inactive DNA is generally marked by H3K9me3 (Calo and Wysocka, 2013). These chromatin marks were integrated by ChromHMM , an automated computational system for learning chromatin states, to assign regulatory annotations genome-wide (Ernst and Kellis, 2012). Furthermore, overlapping GWAS SNPs with annotated elements across a range of tissues can identify the most likely target tissue of effect for the trait (Ernst *et al.*, 2011).

Prioritised SNPs overlapping functional regulatory elements can be tested in a single locus level through luciferase assays, electrophoretic mobility shift assays (EMSAs) and CRISPR-Cas9 mutagenesis (Claussnitzer *et al.*, 2015). On a genome-wide scale, massively-parallel reporter assays (MPRAs) that can be performed using luciferase or green fluorescent protein (GFP) to identify functional SNPs, are more suitable (Buckley *et al.*, 2016; Rabani *et al.*, 2017; X. Wang *et al.*, 2018). However, reporter assays implemented from episomes are believed to lack physiological chromatin and any findings thus have to be validated by endogenous mutagenesis (Inoue *et al.*, 2017).

Other methods such as Sasquatch or phylogenetic module complexity analysis (PMCA) can reduce the need for experimental screening. In Sasquatch, sequence motifs of GWA SNPs overlapping DNase-Seq peaks in the cell-type of interest are extracted and tested genome-wide for a SNP-effect on DNaseI footprints, an indirect measure of protein binding (Schwessinger *et al.*, 2017). Thus variation of the open chromatin in the single cell

line of interest is used to directly test the effect of the SNP and can even predict an effect on binding of specific TFs.

PMCA works on the assumption that important regulatory elements often contain conserved co-occurring binding sites for multiple transcription factors, so called transcription factor binding modules (Claussnitzer *et al.*, 2014). The method extracts sequences surrounding the SNPs and assesses them for multiple factors such as number of TFs in TF modules conserved across species, number of TFs in total, and number of TF modules in total in order to predict the likelihood of a SNP to affect gene expression. Using the method, Claussnitzer et al. have identified rs1421085 as an effector of *IRX3* and *IRX5* expression and adipose tissue browning. An improved version of this method is employed in this work.

1.5. The *TBX15-WARS2* locus

1.5.1. Trait and gene expression associations

A major part of this work focuses on the *TBX15-WARS2* locus that has consistently been associated with WHRadjBMI in all the major GWA meta-analyses (Heid *et al.*, 2010; Shungin *et al.*, 2015; Pulit *et al.*, 2018). A haplotype of the locus has introgressed from Denisovans to Greenland Inuits in which it is under positive selection, thus suggesting a potential protective function in cold climates (Racimo *et al.*, 2017). Analysis of the UK Biobank data showed further associations with Hip Circumference alone and Body Electrical Impedance further confirming a putative role of this locus in adipose tissue regulation (Figure 1.13).

To identify functional genes and SNPs in the WHR GWAS meta-analysis by Heid et al., a fine-mapping study, with additional data from over 20,000 African ancestry individuals, was performed, narrowing the WHRadjBMI association of the locus to just 1591bps within intron 1 of *TBX15* (Liu *et al.*, 2014). However, a more recent and better-powered GWAS (67,326 additional European ancestry individuals) identified up to four potentially independent associations signals (Risk Blocks A, B, C and D) across Sperm-associated antigen-17 (*SPAG17),* T-box 15 (*TBX15)* and Tryptophanyl(W)-tRNA synthetase 2, mitochondrial (*WARS2)* genes (Shungin *et al.*, 2015). This suggests that the previous fine-mapping study narrowed only on one of these association signals.

From the perspective of expression quantitative trait loci (eQTLs), the WHR-increasing alleles in the Risk Block A of *TBX15-WARS2* locus were previously associated with increased *TBX15* expression in omental VAT fat (Heid *et al.*, 2010). eQTL in the same direction exists in the GTEx database for both SAT and VAT (Figure 1.14) (GTEx-Consortium, 2013). On the other hand, Risk Blocks A, B and C in the *TBX15-WARS2* locus were all associated with reduced *WARS2* expression in almost all assessed tissues

(Figure 1.15). No eQTLs were discovered for *SPAG17* (Heid *et al.*, 2010; GTEx-Consortium, 2013). In the Metabolic Syndrome in Men (METSIM) study of over 10,100 Finnish men, both *TBX15* and *WARS2* male SAT expression were associated with metabolic traits (Civelek *et al.*, 2017). *TBX15* expression was associated with WHR (effect size = -0.203, $p = 1.3 \times 10^{-8}$), BMI (effect size = -0.331, $p = 2.82^{-18}$) and 11 other metabolic traits including Insulin, FFA and TGs levels ($p = 4.3 \times 10^{-21}$ to 2.6×10^{-4}). *WARS2* expression correlated with BMI (effect size = -0.211, $p = 3.49^{-9}$) and Matsuda Insulin Sensitivity Index (effect size = 0.129 , $p = 3.41^{-4}$) (Civelek *et al.*, 2017). A smaller study (222 participants) revealed strong negative correlation of *WARS2* expression in both ASAT and abdominal VAT with BMI, SAT and VAT areas, whilst *TBX15* showed only weak correlation with VAT area. In this study, expression of neither of the two genes correlated with WHR (Schleinitz *et al.*, 2014). In summary, the *TBX15*-*WARS2* locus harbours multiple WHRadjBMI association signals that are linked to the expression of both *TBX15* and *WARS2*. The locus may thus act through different SNPs and genes. I will now summarise the literature for the three genes overlapping the WHRadjBMI signal.

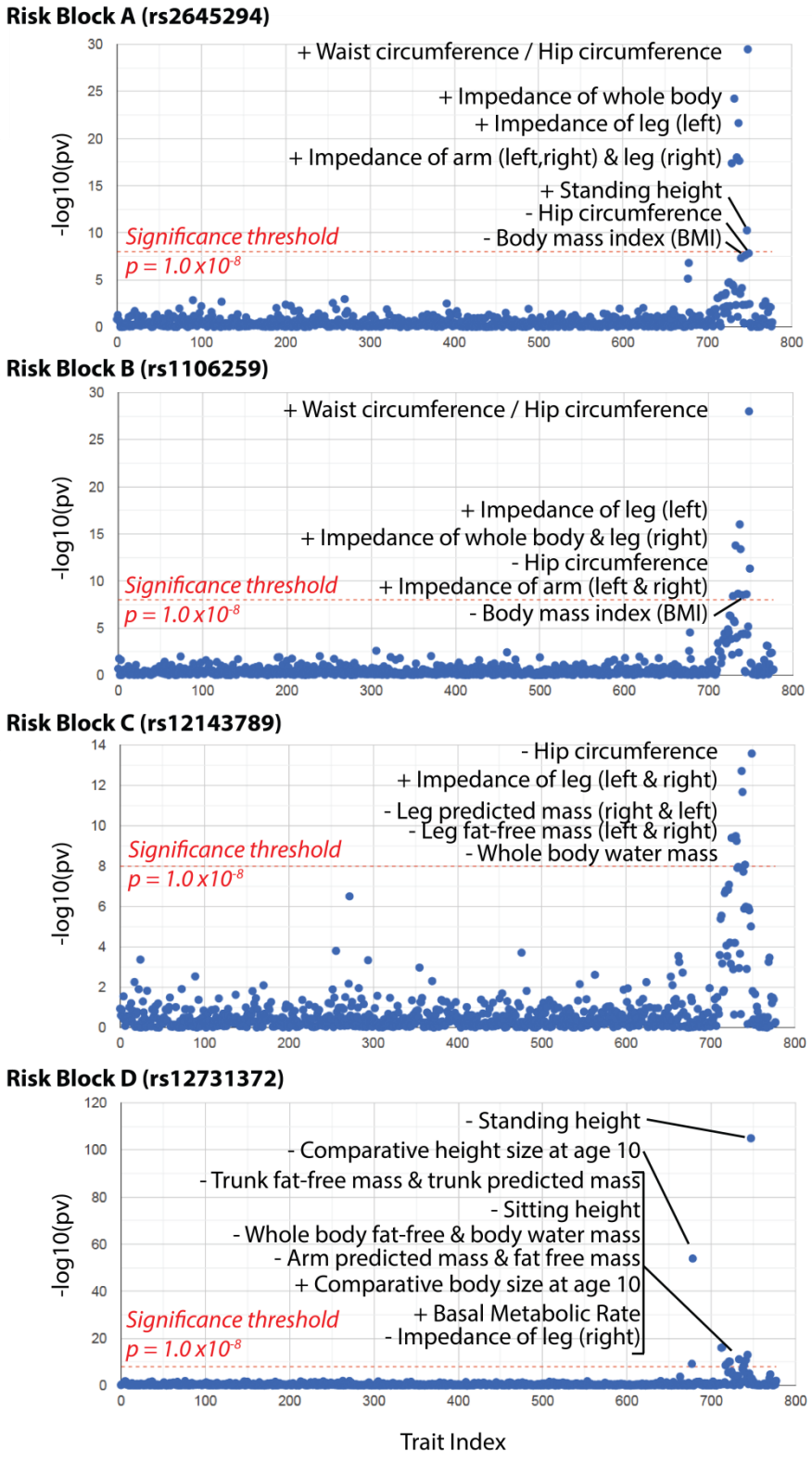

Figure 1.13 | Associations of the *TBX15-WARS2* locus beyond WHR. Four independent Risk Blocks (A, B, C, D) were associated with WHRadjBMI in this locus (Shungin *et al.*, 2015). This figure shows significant associations of the lead SNPs of each risk block across the 700+ traits assessed by the UK Biobank (Canela-Xandri, Rawlik and Tenesa, 2018). The direction of the effect of the WHRadjBMI-increasing allele is indicated with either + (increasing) or – (decreasing) sign.

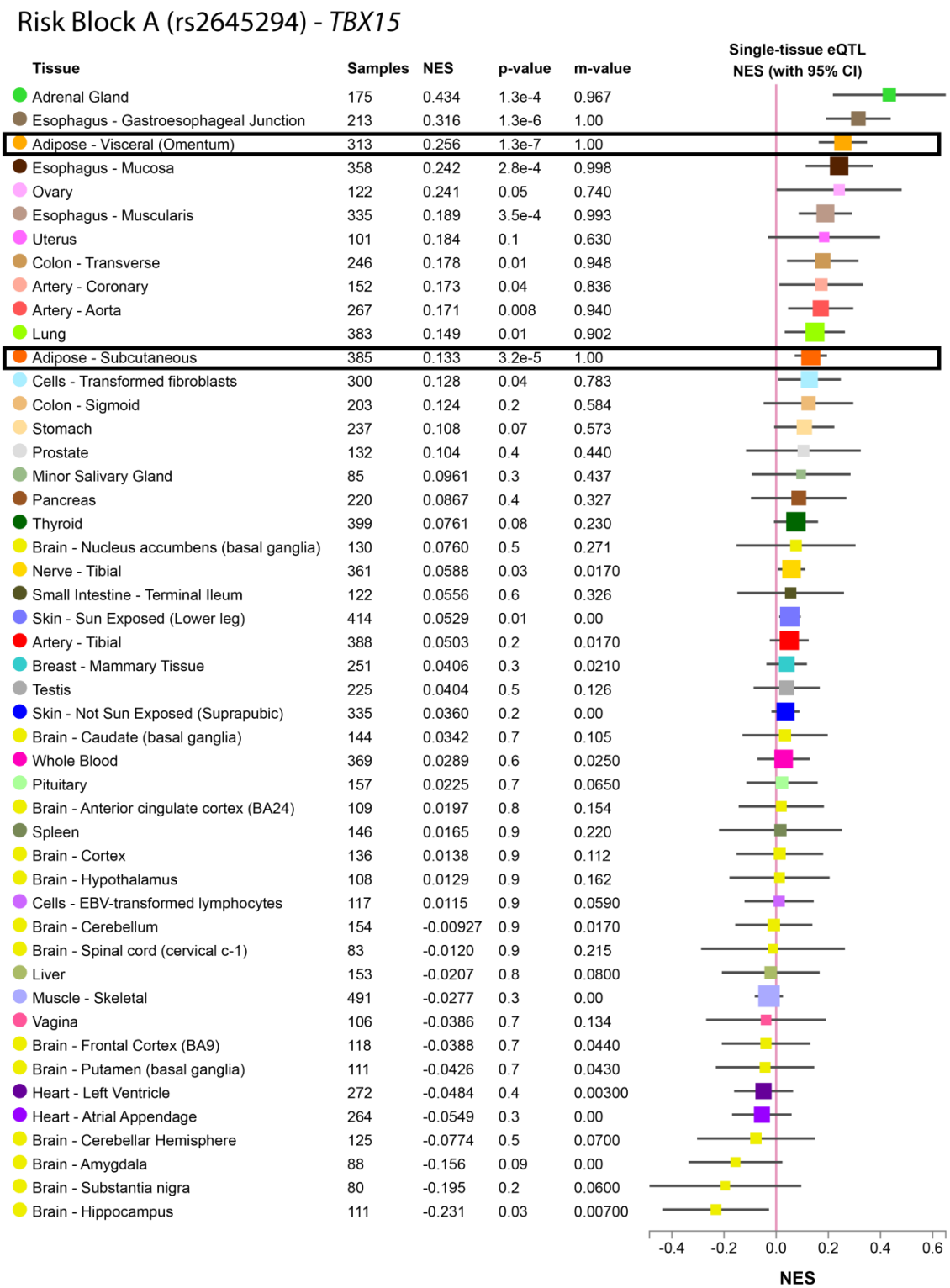

Figure 1.14 | Association of rs2645294 (Risk Block A) with *TBX15* across different tissues in the GTEx database. No other Risk Blocks showed eQTLs with *TBX15* expression (GTEx-Consortium, 2013). NES, Normalised effect size. m-value, posterior probability that an eQTL exists in each tissue tested in cross-tissue meta-analysis (ranges from 0 to 1). CI, confidence intervals.

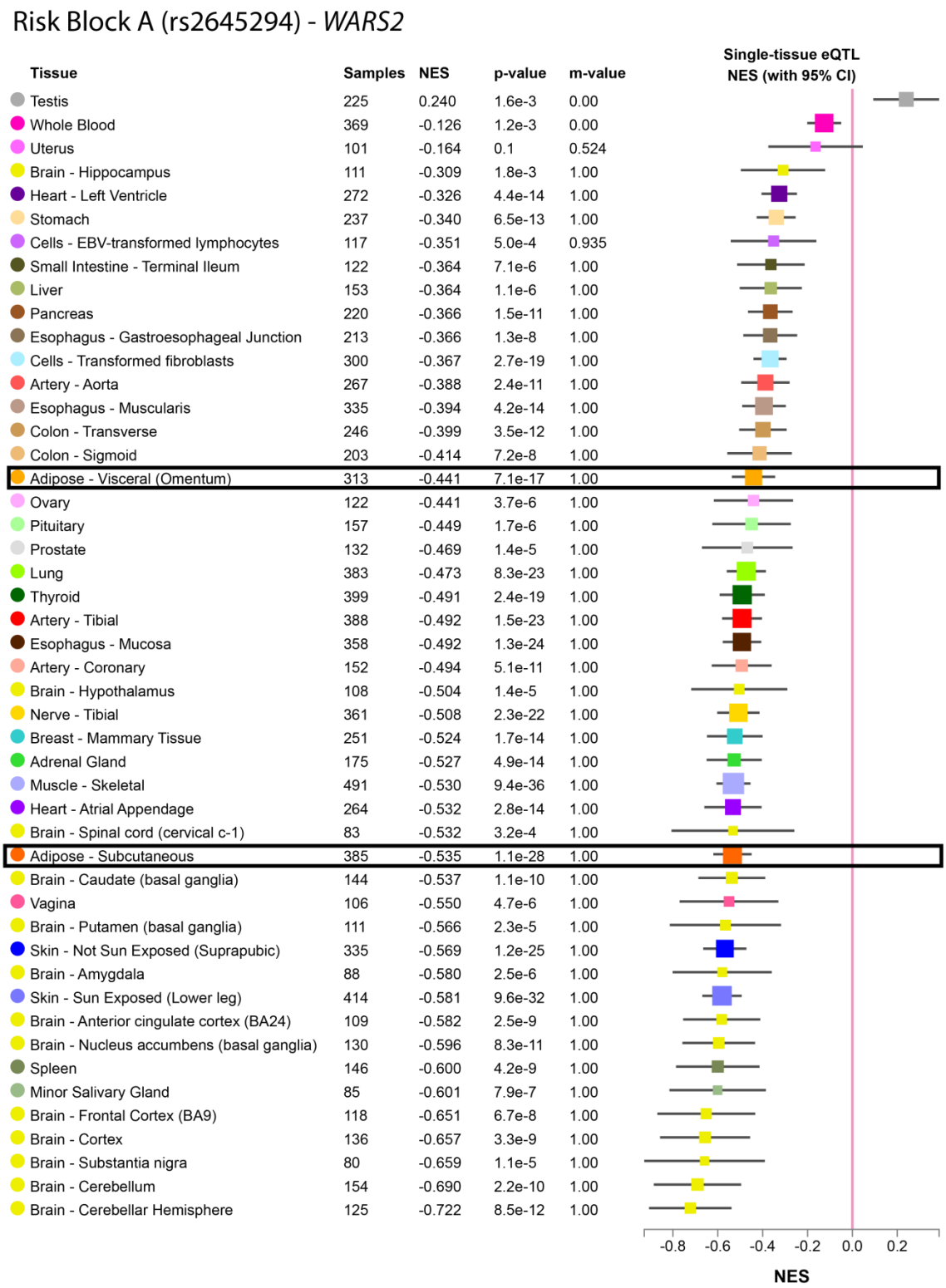

Figure 1.15 | Association of rs2645294 (Risk Block A) with *WARS2* across different tissues in the GTEx database. Also Risk Blocks B and C showed eQTLs with *WARS2* expression (GTEx-Consortium, 2013). NES, Normalised effect size. m-value, posterior probability that an eQTL exists in each tissue tested in cross-tissue meta-analysis (ranges from 0 to 1). CI, confidence intervals.

1.5.2. SPAG17

Sperm-associated antigen-17 (SPAG17) encodes a large 250kDa protein of the axoneme central pair complex (CPC) of motile cilia and flagella. The orthologue of SPAG17 in the green algae *Chlamydomonas reinhardtii,* PF6, was identified first and shown to be important for flagellar motility and assembly of the CPC (Goduti and Smith, 2012). In humans, the full-length SPAG17 is primarily expressed in testis and tissues with motile cilia, but other splice variants and cleavage fragments have been described (Silina *et al.*, 2011).

Homozygous missense mutations in *SPAG17* protein were recently identified in twins with severe asthenozoospermia, a common cause of male infertility due to reduction in sperm motility (Xu *et al.*, 2018). In line with the human data, *Spag17*$^{-/-}$ mice showed skeletal malformations and infertility due to reduced spermatogenesis (Teves *et al.*, 2015; Kazarian *et al.*, 2018). The mice demonstrated severely dysfunctional motile cilia with primary effects in the brain and trachea and the resulting respiratory distress caused these mice to die within 12 hours of birth (Teves *et al.*, 2013).

Primary cilia are present in almost all vertebrate cells, including adipose progenitor cells (APCs) in adipose tissue, and have a role in transducing extracellular signals. In obese patients, primary cilia of APCs are shorter and dysfunctional, compromising APC differentiation potential (Malicki and Johnson, 2017; Ritter *et al.*, 2018). Based on the GTEx data, *SPAG17* is expressed in human adipose, especially SAT, but to my best knowledge, no direct characterisation of its role in adipose tissue exists to date (GTEx-Consortium, 2013).

The lead SNP rs12731372 of one of the WHRadjBMI signals (Risk Block D) in the *TBX15-WARS2* locus resides in the intragenic region, just downstream of *SPAG17* and

apart from WHR and body impedance, rs12731372 is also associated with BMI, Standing Height and Comparative Height Size at Age 10 (Figure 1.13) (Denny *et al.*, 2013). Other independent non-coding SNPs in *SPAG17* locus were associated with idiopathic short stature in Korean population (Kim *et al.*, 2010). These height associations are in agreement with the phenotype of the *Spag17*$^{-/-}$ mice and suggest *SPAG17* could be a gene affected by the Risk Block D.

1.5.3 TBX15

T-box 15 (TBX15) is a member of the large family of 18 transcription factors characterised by their T-box DNA-binding domain. T-box genes are crucial for developmental processes, such as mesoderm specification and skeletal development (Naiche *et al.*, 2005; Sheeba and Logan, 2017). *Tbx15* can act both as a transcriptional activator, or as a repressor, via its interaction with Groucho co-repressors (Farin *et al.*, 2007). In humans, homozygous nonsense mutations of *TBX15* have been shown to cause Cousin syndrome, a condition of short stature, craniofacial and skeletal abnormalities (Lausch *et al.*, 2008; Dikoglu *et al.*, 2013). Similarly, the mouse mutant *droopy-ear* of *Tbx15*, as described already in 1959, shows a widespread reduction in bone size and altered body shape (Curry, 1959; Singh *et al.*, 2005). The effect on adipose tissue was not assessed in this model.

In the mouse coat, *Tbx15* shows dorso-ventral patterning mirroring the expression of the agouti protein and its disruption in the *droopy ear* mouse alters coat patterning (Candille *et al.*, 2004). In line with the role of developmental pathways regulating fat distribution, *Tbx15* showed differential expression between different fat depots. *Tbx15* was highly expressed in murine BAT and almost 39-fold more expressed in iWAT than gWAT (Gesta *et al.*, 2011; Gburcik *et al.*, 2012). This difference was more pronounced in the SVF and in isolated preadipocytes from these two WAT depots (Gesta *et al.*, 2006). Differential

expression was reported also in humans, although results did not always agree. Lean humans showed 27-39-fold higher *TBX15* expression in VAT compared to ASAT and in a study of 99 women and 99 men, a major drop in TBX15 VAT expression was observed with increased BMI levels, resulting in a strong negative correlation between BMI and VAT *TBX15* levels ($R = 0.706\text{-}0.852$, $p < 0.0001$). VAT *TBX15* expression was also strongly correlated with WHR ($R = 0.604\text{-}0.817$, $p < 0.0001$) but ASAT did not show any strong correlations (Gesta *et al.*, 2006). A study focusing on overweight/obese 222 people with a mean BMI of 41.6 ± 13.7 kg m^{-2} found *TBX15* to be 3-fold higher expressed in ASAT compared to abdominal VAT with no major differences between lean, overweight and obese people (Schleinitz *et al.*, 2014). This agrees with the previous findings in mice and a study of Australian child cohort where *TBX15* ASAT levels were 28-fold higher compared to abdominal VAT (Tam *et al.*, 2011). The only conflicting results from Gesta et al., 2006, might thus be an artefact of the small cohort of lean individuals.

Mechanistically, TBX15 was shown to affect metabolism, differentiation and browning of adipocytes. Within a single iWAT tissue, both adipocytes and preadipocytes partition into *Tbx15*-high (*Tbx15*^{Hi}) and *Tbx15*-low expressing cells (*Tbx15*^{Low}). *Tbx15*^{Hi} cells expressed lower levels of oxidative metabolism markers (*Pgc1a*, *Cox5b*, and *Cox8b*), higher levels of glycolytic metabolism genes (*K2* and *Gapdh)* and showed a trend toward decreased levels of BAT markers. In agreement with previous expression studies, *Tbx15*^{Hi} cells were absent in the gonadal depot (Lee *et al.*, 2017). A similar role for *Tbx15* was discovered in muscle, where *Tbx15*^{Hi} cells were found exclusively in glycolytic fast-twitch fibres and were absent in the oxidative-slow twitch fibres (K. Y. Lee *et al.*, 2015). *Tbx15*$^{-/-}$ muscles showed altered fibre-type proportions and increased whole-body oxygen consumption suggesting *Tbx15* may play a key role in regulating glycolytic cell type identity in different tissues.

Tbx15 overexpression in 3T3-L1 cells was shown to impair preadipocyte differentiation, to lower mitochondrial mass, reduce basal respiration, reduce triglyceride content and increase adipocyte lipolysis:lipogenesis ratios (Gesta *et al.*, 2011). In line with this finding, in isolated ASAT adipocytes from 114 women, *TBX15* expression correlated with catecholamine-induced lipolysis and negatively with insulin-stimulated lipogenesis (Dahlman *et al.*, 2016). Interestingly, *Tbx15* knockdown in murine preadipocytes had a similar effect to the overexpression in 3T3-L1. The *Tbx15*-KD cells from iWAT and BAT exhibited impaired differentiation and lower expression of browning markers (Gburcik *et al.*, 2012). Recently, adipose-tissue specific *Tbx15*-KO mice demonstrated reduced browning of iWAT and BAT in response to cold and β adrenergic stimulation, reduced energy expenditure and increased fat mass, including both iWAT and gWAT. The authors suggested that *Tbx15* may regulate browning through activation of the *Prdm16* promoter (Sun *et al.*, 2019). The positively-selected introgressed allele in Greenland Inuits is associated with reduced *TBX15* promoter methylation and increased *TBX15* expression. Thus increased *TBX15* expression in Greenland Inuits could stimulate browning and thus provide an evolutionary advantage in extreme cold conditions (Racimo *et al.*, 2017).

In summary, *Tbx15* shows differential expression in subcutaneous and visceral fat depots in both humans and mice, implicating it as a strong candidate for WHR regulation. Knockdown and overexpression studies in preadipocytes suggest it plays an important role in regulating adipocyte differentiation, browning and lipolysis. The discovery of glycolytic $Tbx15^{Hi}$ cells suggests that in addition to its developmental role, *Tbx15* could be directly affecting white preadipocyte and adipocyte metabolism. The *droopy ear* mouse model and human coding mutations suggest that *TBX15* could also affect body shape through effects on bone growth and morphology.

1.5.4. WARS2 and mitochondrial aminoacyl synthesases

WARS2 is a mitochondrial tryptophanyl-tRNA synthetase, a ubiquitously expressed enzyme essential for mitochondrial translation. The mitochondria are comprised of more than 1500 proteins with 13 of these being components of the electron transport chain (ETC) transcribed from the mitochondrial DNA (mtDNA) and thus requiring local translational machinery (Schmidt, Pfanner and Meisinger, 2010). Due to shared function in mitochondrial translation, mutations in the 19 mitochondrial aminoacyl synthesases (mt-aaRS) would be expected to show similar pathologies. Indeed, mt-aaRS mutations frequently result in ETC protein deficiencies and the most commonly affected tissues are of a high energy demand, such as the central nervous system (CNS), which is affected by mutations in 17 of the 19 mtAARs and all of the respective mt-tRNAs (Lott *et al.*, 2013; Moulinier *et al.*, 2017). However, effects on other tissues show marked pleiotropy. For example, mutations in aspartyl-tRNA synthetase 2 (*DARS2*) cause Leukoencephalopathy with brainstem and spinal cord involvement and lactate elevation (LBSL), an autosomal recessive disorder of brain white matter (Scheper *et al.*, 2007). On the other hand, mutations in tyrosyl-RNA synthetase 2 (YARS2) result in myopathy, lactic acidosis and sideroblastic anemia (MLASA) (Riley *et al.*, 2010).

The pahthology of mutations in mt-aaRSs and the respective tRNAs also markedly differ. Unlike LBSL-causing *DARS2* mutations, mutations in mt-tRNA^{Asp} lead to mitochondrial myopathy, sporadic bilateral optic neuropathy, myoclonic epilepsy and psychomotor regression (Chimnaronk *et al.*, 2005; Gotz *et al.*, 2011; Sasarman *et al.*, 2012). Clinical, genetic and structural data for all described human mt-aaRSs mutations are available in the MiSynPat repository (http://misynpat.org) (Moulinier *et al.*, 2017). These complex phenotypes and pleiotropies show that apart from their role in translation, mt-aaRS might have additional functions and specific roles in the cross-talk with the cell such as through

mitochondrial unfolded protein response (UPR^{mt}) (Sissler, Gonzalez-Serrano and Westhof, 2017).

1.5.5. *WARS2* – candidate for fat distribution regulation

Mutations in *WARS2* resulted primarily in neurological phenotypes, such as ataxia, aggressive behaviours, intellectual disability, parkinsonism and leukoencephalopathy. In some but not all cases, patients also showed growth retardation, cardiomyopathy, muscle weakness, lactic acidosis and severe hepatopathy (Burke *et al.*, 2017; Musante *et al.*, 2017; Theisen *et al.*, 2017; Vantroys *et al.*, 2018; Maffezzini *et al.*, 2019; Virdee *et al.*, 2019). None of these studies have assessed the effect on adipose tissue, but depot-specific differences were revealed in the general population with *WARS2* expression slightly elevated in VAT compared to ASAT (Heid *et al.*, 2010; Schleinitz *et al.*, 2014).

Two studies in rats have revealed potential additional functions of *Wars2* beyond its canonical role in mitochondrial translation. A genome-wide genotyping study in a genetic cross of Brown Norway and Spontaneously Hypertensive Rats investigating coronary flow (CF), an indirect measure of cardiac capillary density, identified *Wars2* as a determinant of angiogenesis. Its low activity allele *Wars2*-L53F could explain the reduced CF in rats and WARS2 inhibition in endothelial cells reduced their angiogenic potential. Inhibition of *Wars2* in zebrafish showed an effect on angiogenesis both in and outside the heart (Wang *et al.*, 2016). A study from the same inbred strain identified the same *Wars2*-L53F variant to be associated with glucose oxidation and glucose incorporation into BAT lipids (Pravenec *et al.*, 2017). A rescue of the mutant allele with WT *Wars2* resulted in increased glucose oxidation and incorporation in the BAT which was correlated with reduced bodyweight and gWAT weight. Fibroblasts from these mice demonstrated increased oxygen consumption and mitochondrial proteosynthesis in fibroblasts. Interestingly, no

effect on BAT angiogenesis was observed. Thus, *Wars2* has been independently implicated as a regulator of angiogenesis and BAT function.

In previous work from our laboratory, a hypomorphic allele of *Wars2*$^{V117L/V117L}$ was identified in a *N*-ethyl-*N*-nitrosourea (ENU) mutagenesis screen for hearing loss and reduced bodyweight (Agnew *et al.*, 2018). These mice showed a failure to gain fat mass, hypertrophic cardiomyopathy, failure to thermoregulate upon cold exposure, reduced energy expenditure and upregulated ketogenesis. iWAT of these mice showed histological and molecular signs of browning, whilst the BAT downregulated browning markers, UCP1 and had more of a white fat appearance. These changes were hypothesised to be driven primarily by ETC Complex deficiency, observed in many, but not all tissues. Especially, the heart showed ETC Complex deficiencies as early as 3 months and contributed to elevated Fibroblast growth factor-21 (FGF21) levels in these mice. This study thus showed that *Wars2* dysfunction can have severe effects on both WAT and BAT, although it is not clear whether this is a direct adipose or systemic effect.

1.6. Thesis hypotheses

- Chapter 3 – Prioritised WHRadjBMI-associated SNPs rs998584, rs3936510, rs3810068 affect gene expression in adipose by interfering with transcription factor binding and changing the activity of adipose promoters/enhancers and thus impacting on fat distribution.

- Chapter 4 - Risk Block A of the *TBX15-WARS2* locus alters fat distribution by reducing *WARS2* levels.

- Chapter 4 – The 3'UTR SNP rs26452954 regulates *WARS2* post-transcriptionally.

- Chapter 5 - *Wars2* deficiency in mice will increase visceral to subcutaneous adipose ratio.

- Chapter 5 – *Wars2* deficiency will cause fat depot-specific mitochondrial complex deficiencies and subsequent responses including subcutaneous-specific adipose tissue browning leading to increased energy consumption and weight loss predominantly in the subcutaneous compared to visceral depots.

1.7. Thesis aims

- Chapter 3 – To test rs998584, rs3936510, rs3810068 for an effect on DNA-protein binding and gene expression. To functionally assess an overlap with an active promoter/enhancer in a human adipose cell line.

- Chapter 4 – To identify potentially functional SNP/s in the risk block A of the *TBX15-WARS2* locus.

- Chapter 4 – To test rs2645294 for an effect on *WARS2* mRNA stability.

- Chapter 5 – To assess bodyweight, body composition and fat distribution in *Wars2*$^{+/-}$, *Wars2*$^{+/V117L}$ and *Wars2*$^{V117L/V117L}$ mice on low-fat and high-fat diet.

- Chapter 5 – To test for mitochondrial complex level changes and activation of browning in visceral (gWAT) compared to subcutaneous (iWAT) and brown (iBAT) adipose tissue of 4-month old *Wars2*$^{V117L/V117L}$ mice.

- Chapter 5 – To distinguish adipose-intrinsic from systemic effects on WAT in *Wars2*$^{V117L/V117L}$ mice. Directly by assessing oxygen consumption in primary adipocyte cultures and indirectly by assessing the levels of mitokines and food intake.

2. Materials and methods

2.1. Cell culture techniques

2.1.1. hWAT culture and differentiation

Primary stromal vascular fraction (SVF) cells were provided by Prof Yu-Hua Tseng, PhD at Harvard Medical School, Joslin Diabetes Center, Boston, MA 02215. The cells were previously isolated from the white fat in the neck of a female, aged 56 with a BMI of 30.8, and immortalised using telomerase reverse transcriptase (TERT)-expressing plasmid. The differentiation capacity of these cells was tested using the previously described protocol (Xue *et al.*, 2015). Briefly, the hWAT preadipocytes were cultured at 37°C, 5% CO_2 in DMEM GlutaMAX (# 10569010 DMEM, high glucose, GlutaMAX™ supplement, pyruvate) with 10% Fetal Bovine Serum (FBS), (Gibco 10082-147) and 1% Penicillin-Streptomycin (5,000U/ml , Gibco, 15070063). When cells reached 80-90% confluency, they were split 1:2 or 1:3 using 0.25% trypsin-EDTA (Gibco, with 25200056). Passages between P17 and P23 were used. For differentiation in T75 flasks, 2-days post-confluent cells were induced using a freshly prepared Induction Medium (ingredients are listed below). The media was replaced every three days for 20-24 days, until fully differentiated or until day 4 for the purposes of the luciferase and EMSA assays. The stock reagents were prepared as shown:

- Biotin: 0.08g in a final volume of 10ml 0.1N NaOH (30 mM)
- Insulin: 10 mg/ml (Sigma, I9278)
- Pantothenate (Sigma, P5155): 8.5mM in H2O (500x)
- Dexamethasone: 0.002g (Sigma, D1756-25MG) in 1ml EtOH (2mg/ml; 5 mM)

- Isobutyl methylxanthine (IBMX, Sigma, **I5879)**: 50 mM stock in 0.1 M KOH
- 3,3′,5-Triiodo-L-thyronine (T_3) (Sigma, T6397): add 1.0ml of 1.0 N NaOH to 1 mg, gently swirl to dissolve the powder and add 152.6ml of sterile DMEM GlutaMAX (# 10569010) (10 μM)
- Indomethacin: Dissolve 447.25 mg Indomethacin (Sigma, 17378) in 10ml EtOH (0.125 M). Heat to 75°C.

The Induction Medium was prepared as shown below. FBS and Human Insulin were added last, after the filter sterilisation step using a 0.22μm low-affinity binding filter (MILLEX, SLGP033RB) .

Components	Volume	Final concentration
DMEM, 1% P/S	48.5ml	
Biotin	50ul	33 μM
Indomethacin	12.5ul	30 μM
Pantothenate	100μl	17 μM
Dexamethasone	1μl	0.1 μM
T3	10μl	2 nM
IBMX	500ul	500 μM
FBS	1ml	2%
Human Insulin	15ul	0.5 μM

2.1.2. HEK293T cell culture

HEK293T cells were purchased from Public Health England ECACC General Cell Collection (ECACC 12022001, lot 16G020, Sigma-Aldrich). The cells were maintained at 37°C, 5% CO_2 in DMEM GlutaMAX (# 10569010 DMEM, high glucose, GlutaMAX™ supplement, pyruvate) with 10% Fetal Bovine Serum (FBS, Gibco 10082-147) and 1% Penicillin-Streptomycin (5,000U/ml, Gibco, 15070063). Sub-confluent cultures (70-80%) were split 1:5 approximately every 3 days using Trypsin-EDTA (ThermoFisher, # 25300054). Cells were used between passages P14 and P17.

2.1.3. Forward siRNA transfection in hWAT cells

For forward transfection, hWATs were differentiated in T75 flasks to day 4 and then plated at 120K cells/well to reach ~80% confluence next day. The cells were transfected with Lipofectamine RNAiMAX (ThermoFisher #13778075) using the standard protocol. Briefly, Lipofectamine RNAiMAX and the siRNA were separately diluted in Opti-MEM medium, mixed and incubated for 10 minutes. Meanwhile, the cells were washed with PBS and new antibiotic-free media was added. The transfection complex was then applied to the cells to reach final concentrations of 2.3µl RNAiMAX/ml and 18.2 nM siRNA, as shown below. All silencing experiments were performed with 2-3 technical replicates. Table 2.1 and Figure 2.1 show the siRNAs used and the setup for *CEBPβ* knockdown using FlexiTube GeneSolution GS1051 (Qiagen, # 1027416) to determine the optimal efficiency using Western Blot.

6 well plate	**Volume /well**	**Volume of complex /well**	**Ab-free Medium**	**Final volume**	**Final conc**
OptiMEM	98 ul	200 ul	2 ml	2.2 ml	18.2nM
siRNA oligo (20µM)	2 ul				
RNAiMAX	5 ul				

Table 2.1 | List of FlexiTube GeneSolution siRNAs used for *CEBPβ* knockdown in hWAT cells.

Product name	Cat. no.	Target Sequence	% GC	Lot number	Validated cell line	% KD
Hs_CEBPB_5	SI02777292	CGGGCCCTGAGTAATCGCTTA	57	20150901501	HeLa	85
Hs_CEBPB_7	SI03058062	CACCCTGCGGAACTTGTTCAA	52	20150604538		
Hs_CEBPB_6	SI03022341	TTCCGTTTCAAGCATTAAGAA	33	20160205504		
Hs_CEBPB_4	SI00073640	CCCGTGGTGTTATTTAAAGAA	38	20151103569		

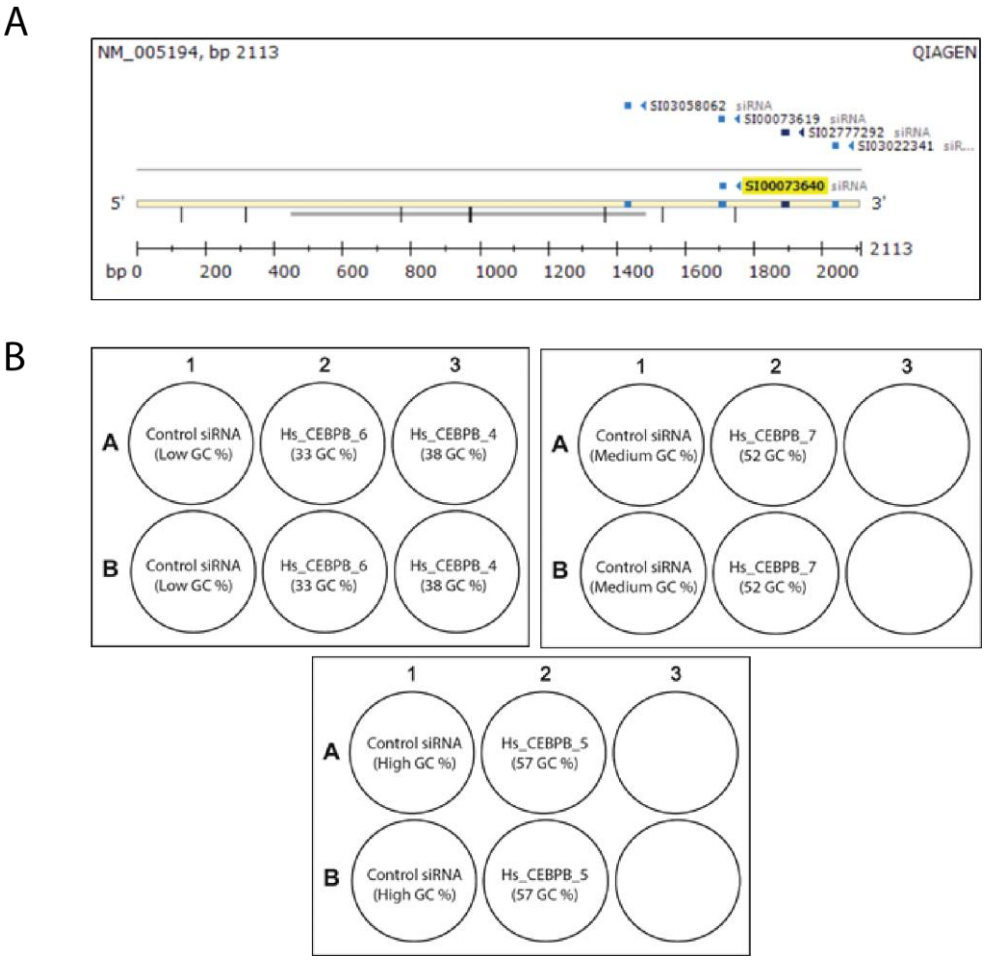

Figure 2.1 | *CEBPβ* KD experiment. The location of the siRNA targeting sequences in the NM_005194 *CEBPβ* transcript (A). The plate setup for the experiment including nonsense siRNA controls with matching GC% (B).

2.1.4. Preadipocyte isolation, culture and differentiation

Mouse primary preadipocytes were isolated according to the previously described protocol (Church, Berry and Rodeheffer, 2014). Briefly, mouse inguinal and gonadal WAT depots were dissected from 6-8 week old C3H/Pde mice and placed in PBS at room temperature. Tissues were finely minced, digested in 5ml/depot of filter-sterilised digestion buffer - Hank's Balanced Salt Solution (HBSS) (Gibco, H8264), 0.8mg/ml collagenase type 2 (Worthington Biochemical Corporation, LS004174), 3% cell-culture grade bovine serum albumin (BSA, A9418) for 60min, with shaking by hand every 10 minutes, until most tissue clumps were not visible. Cells were then centrifuged at 300G for 3min in order to separate the pelleted SVF, which contains preadipocytes, from the floating mature adipocytes. The supernatant was carefully removed and the cell pellet resuspended in pre-warmed growth media: DMEM GlutaMAX (# 10569010 DMEM, high glucose, GlutaMAX™ supplement, pyruvate) with 10% Fetal Bovine Serum (FBS, Gibco 10082-147), 1% Penicillin-Streptomycin (5,000U/ml, Gibco, 15070063). To remove cell clumps, the suspension was subsequently filtered through a 40µm nylon mesh (ThermoFisher, 352 340) onto a 10cm dish and grown at 37°C, 5% CO_2. Next day, the cells were washed twice with PBS and fresh media applied. The cells were grown another 2-3 days to reach 80% confluence.

For differentiation studies, the pre-adipocytes were detached using TrypLE™ Express Enzyme (1X) (Gibco 12605-010) and counted using the Countess II Automated Cell Counter (Invitrogen). 100K cell/ml were plated in 6-well (2ml/well) or Seahorse XF96 well plates (80µl/well) and grown to confluence. At two days of post-confluence, differentiation was induced as described in section "2.1.1. hWAT culture and

differentiation" with one difference. In this case, a final concentration of 1μM Dexamethasone was used for mouse primary cell differentiation.

2.1.5. Seahorse

Oxygen Consumption Rate (OCR) & Extracellular Acidification Rate (ECAR) was assessed using the MitoStress Kit (Agilent, # 103015-100) and the Seahorse XFe96 Analyzer (Agilent). The protocol was adapted from (Bugge, Dib and Collins, 2014). Primary preadipocytes were differentiated in Seahorse XF96 plates as described in "*2.1.4. Preadipocyte isolation, culture and differentiation.*" Bright-field images of each well in the Seahorse 96 were taken by the Cytation 1 Cell Imaging Reader (BioTek) and could be used to distinguish the dark-appearing lipid-filled mature adipocytes. The evening before the assay, the XFe96 cartridge was incubated with the Seahorse XF Calibrant (Agilent, # 100840-000) in a CO_2-free incubator at 37°C overnight. Next day, the cells old media was replaced with 180μl of minimal medium prepared by supplementing Seahorse XF DMEM Medium pH 7.4 (48.5 ml) (Agilent, # 103575-100) with glucose, glutamine and pyruvate, as shown below.

	Volume to add	**Final Conc.**
Seahorse XF DMEM medium	48.5ml	~100%
1.0M glucose (Agilent, # 103577-100)	0.5ml	10 mM
100 mM pyruvate (Agilent, # 103578-100)	0.5ml	1 mM
200 mM glutamine (Agilent, # 103579-100).	0.5ml	2 mM

The cells were then placed at 37°C in a CO_2-free Cytation 1 Cell Imaging Reader (BioTek) to obtain bright-field images of each well. The assay should not be started until the cells

have had at least 45-60mins to equilibrate in the CO_2-free environment to let the CO_2 diffuse out of solution. According to the manufacturer's protocol, the MitoStress Kit compound vials were then dissolved in the minimal medium to create the stock solutions:

	Volume of medium	**Final Stock conc.**
Oligomycin *Complex 5 inhibitor*	630ul	100uM
FCCP *Mitochondrial uncoupler*	720ul	100uM
Rotenone/Antimycin A *Complex I and III inhibitors*	540ul	50uM

The stock solutions were then diluted and loaded into the XFe96 cartridge as shown below. Hoechst 33342 Solution (20mM) (ThermoFisher, # 62249) was added to the final Rotenone/Antimycin A solution to allow for subsequent quantification of cell number.

	Final well conc.	**Stock volume**	**Media volume**	**10X conc. (in Port)**	**Add to port**
Port A Oligomycin	1.0 µM	300 µl	2700 µl	10 µM	20 uL
Port B FCCP	2.0 µM	600 µl	2400 µl	20 µM	22 uL
Port C Rotenone / Antimycin A + Hoechst Stain	0.5 µM	300 µl + 3 µl Hoechst stain	2700 µl	5 µM	25 uL

The cartridge was calibrated and the assay ran according to the default "*XF Cell Mito Stress Test*" settings. To study the effect of β-adrenergic stimulation, half of the technical

replicates were stimulated by 1μmol/l Isoprotrenolol (Sigma, I6504) instead of oligomycin. After the completion of the assay, the plate was moved back to the Cytation 1 Cell Imaging Reader and fluorescent images of each well taken using the Seahorse XF Imaging system (Agilent) which automatically calculates stained cells and exports the numbers to the Wave (Agilent) software for normalisation. Wells with unfocused images were excluded in the analysis and the remaining normalised datasets were exported into a MS Excel report file with OCR, ECAR time course and calculated ATP turnover, proton leak, and spare mitochondrial capacity values for each condition.

2.2. Gene expression analysis

2.2.1. RNA isolation

Total RNA from cells and tissues (brown and white adipose) was extracted using the TRIzol reagent (ThermoFisher, #15596026). For tissues, 500µl TRIzol was added to ~50mg (brown adipose) or ~100mg (white adipose) and homogenised using the CK14 ceramic beads (Precellys) and a Precellys-24 automated homogeniser (Bertin Instruments). Cells grown in 6-well or Seahorse XFe96 well plates were treated with 400µl and 50µl TRIzol, respectively. Cells were washed off the wells, transferred to a clean eppendorf tube and incubated for 5 minutes at room temperature. Equal volume of 96-100% EtOH was then added to the TRIzol-lysate suspension in a 1:1 ratio and RNA extracted following the Direct-zol^{TM} RNA MiniPrep Plus kit protocol (Zymo research, #R2071). As a part of the protocol, RNA was treated with DNase I and eluted in 25 µl RNase-free water.

2.2.2. Nucleic acid quantification and RNA integrity assessment

The quantity of DNA and RNA was assessed using the Epoch Microplate Spectrophotometer (BioTek) and nucleic acid concentrations automatically calculated using the Beer Lambert Law from the 260nm/280nm ratio. Samples with ratio between ~1.8 and ~2.0 were accepted as `pure` DNA or RNA. If samples fell beneath this range, the nucleic acid was re-extracted where possible.

The purity of RNA was additionally assessed using the 260nm/230nm ratio, with values between ~2.0 and ~ 2.2 considered pure. The integrity of RNA was assessed using the Agilent 2100 Bioanalyzer System and the Agilent RNA 6000 Nano Kit (Agilent, # 5067-1511) according to the manufacturer's protocol. Samples with RNA Integrity (RIN) values > 7 were used for qPCR analysis.

2.2.3. cDNA Synthesis

RNA was reverse-transcribed to cDNA using the SuperScript™ III Reverse Transcriptase Kit (ThermoFisher, # 18080-044). Briefly, all RNA samples were diluted to 100 or 200ng/µl and then re-quantified. Using the newly derived concentrations, 2 µg of RNA was reverse transcribed in a 20µl reaction, as shown below. To control for cDNA and gDNA contamination, samples with "no cDNA" (water only) and "no reverse transcriptase" (RT-) were included for 1 or 2 samples in each experiment.

Component	**Volume**
Random primer (200ng/µl)	1 µl
dNTP mix (10mM)	1 µl
RNA	2 µg
Nuclease-free water	up to 14 µl

** Heat to 65°C for 5mins – chill on ice for at least 1min.*

5x First Strand buffer	4 µl
0.1M DTT	1 µl
Superscript III RT (200U/µl)	1 µl

Each reaction mixed thoroughly and thermal cycler programmed as shown below:

Step	**Temperature**	**Time**
1. Primer Annealing	25°C	5 mins
2. Reverse Transcription	50°C	60 mins
3. Inactivation	70°C	15 mins

2.2.4. qRT-PCR

Gene expression in tissues and cells was analysed using quantitative real-time PCR (qRT-PCR) detection by fluorescence. The reactions were set-up using the TaqMan™ Universal PCR Master Mix (ThermoFisher, # 4304437) and FAM-labelled probes (ThermoFisher, listed below). In a 20 µl reaction, 10 µl of Mastermix, 1 µl of probe, 4 µl of nuclease-free water and 5µl of cDNA (4ng/µl) were mixed and run on the ABIPRISM 7500 Fast Realt-Time PCR System (Applied Biosystems) using the „Fast" protocol with 40 cycles and quantitation – comparative C_T ($\Delta\Delta C_T$) analysis. First, a stable house-keeping gene was selected using the human or mouse GeNORM analysis kit (PrimerDesing, #ge-DD-12) for 6-8 genes. All white and brown adipose tissue data were normalised to the geometric mean of *Canx* and *Ywhaz*. All 3T3-L1 data were normalised to the geometric mean of *Canx* and *Rpl13a*. hWAT data were normalised to β-actin.

Targeted gene	**TaqMAN assay ID**
Canx	Mm00500330_m1
Rpl13a	Mm01612986_gH
Wars2	Mm04208965_m1
Ywhaz	Mm01722325_m1
Cidea	Mm0042554_m1
Cox7a1	Mm00438297_g1
Dio2	Mm00515664_m1
Ucp1	Mm01244861_m1
Fgf21	Mm00840165_g1
β-klotho	Mm00502002_m1
Pgc1α	Mm01208835_m1

Pparα	Mm00440939_m1
Pparγ	Mm01184322_m1
Prdm16	Mm00712556_m1

2.2.5. Statistical analysis

The C_T values of the technical replicates were averaged and the mean normalised to the geometric mean of the two houskeeping genes for each sample. The data was analysed using the comparative comparative $2^{-\Delta\Delta CT}$ methods by Applied Biosystems comparing the fold change of gene expression in samples with control group, as shown below.

ΔC_T = C_T(target gene) - C_T(geometric mean of house-keeping genes)

$\Delta\Delta C_T = \Delta C_T$ (treated sample) - ΔC_T (control sample)

Relative expression = $2^{-\Delta\Delta CT}$

Unless otherwise stated, all data was log-transformed and shown as mean ± standard deviation (SD) for visualisation and statistical analysis. Differences were analysed by unpaired Student's t-test, Welch's t-test or Mann-Whitney test according to the distribution and variance of the data. Statistical significance was indicated by using: * $p<0.05$, ** $p<0.01$, *** $p<0.001$.

2.3. DNA

2.3.1. Mitochondrial DNA copy number assay

Mitochondrial content in adipose tissue was assessed using the ratio of mitochondrial DNA (mtDNA) to genomic DNA (gDNA) as assessed using qRT-PCR. Previously, primers to amplify both the mouse genomic gene *Glyceraldehyde 3-phosphate dehydrogenase* (*Gapdh)* and mouse mitochondrial gene *Mitochondrially encoded NADH:Ubiquinone oxidoreductase core subunit 1 (mt-Nd1)* were designed and optimal concentrations determined. The sequences and concentrations are shown below. Total DNA, which contains both gDNA and mtDNA, was extracted from adipose tissue using the Dneasy Blood and Tissue Kit (Qiagen, # 69504) following the manufacturer's protocol. qRT-PCR was performed using the Fast SYBR Green System on a ABIPRISM 7500 Fast Real-Time PCR Machine (Applied Biosystems) using the default program for SYBR Green reagents. All samples were run in technical triplicates.

Primer	**Sequence 5' to 3'**
mt-Nd1 Forward	CCCATTCGCGTTATTCTT
mt-Nd1 Reverse	AAGTTGATCGTAACGGAAGC
Gapdh Forward	CAAGGAGTAAGAAACCCTGGACC
Gapdh Reverse	CGAGTTGGGATAGGGCCTCT

Mitochondrial assay reagents	**Volume (µl)**
Fast SYBR® Green Master Mix	10
mt-Nd1 Forward primer (5µM)	1.2
mt-Nd1 Reverse primer (5µM)	1.2
DNA (5ng/ µl)	2

Nuclease-free H_2O	5.6
Total	20
Mitochondrial assay reagents	**Volume (µl)**
Fast SYBR® Green Master Mix	10
mt-Nd1 Forward primer (5µM)	1.2
mt-Nd1 Reverse primer (5µM)	1.2
DNA (5ng/ µl)	2
Nuclease-free H_2O	5.6
Total	20

2.4. Protein analysis

2.4.1. ELISA

Plasma fibroblast growth factor-21 (FGF21) levels were measured using Quantikine ELISA Mouse / Rat FGF21 Immunoassay (Quantikine, # MF2100) according to the manufacturer's protocol. Briefly, the plasma from C3H/Pde mice was diluted 1:5 in Calibrator Diluent RD6Z. 50µl of the Assay Diluent RD1-41 was pipetted then into each well of the plate followed by 50µl of the diluted samples. The plate was incubated for 2 hours at room temperature to allow for FGF21-antibody binding. The wells were washed 5 times with the Wash Buffer and then incubated with Mouse / Rat FGF21 Conjugate and covered for 2 hours at room temperature. The plate was washed 5 times and 100 µl of Substrate solution added to each well for 30 mins. The reaction was stopped with 100 µL of Stop Solution and optical density measured using a microplate reader set to 450 nm. The samples were quantified using the included FGF21 standard curve, ranging from 20,000 pg/ml to 31.3 pg/ml.

2.4.2. Total protein extraction

Upon dissection, all tissues were snap-frozen in liquid nitrogen and stored at -80°C. The lysis buffer was prepared by adding 1 tablet of cOmplete™ Protease Inhibitor (Sigma) and 1 tablet of PhosSTOP™ Inhibitor (Sigma) to 10 ml of CelLytic™ MT Mammalian Tissue Extraction Reagent (Sigma). For tissue homogenisation, 0.5ml of the lysis buffer was dispensed in ice-chilled 2 ml tubes with ceramic beads (Precellys) before placing in 50-200mg of the tissue. For soft tissues (e.g. adipose) and harder tissues (e.g. heart) Precelly CK14 tubes or Precelly CK28 tubes were used, respectively. Tissues were homogenised using a Precellys-24 automated homogeniser (Bertin Instruments) in the mode of 5000 rpm for 20 seconds twice. To pellet cell debris, lysates were then transferred to 1.5 ml

eppendorf tubes and centrifuged at 13,000 rpm for 30 mins at 4°C. The supernatant was transferred to a new 1.5 ml eppendorf tube. For adipose samples, the floating lipid layer was carefully pierced with a P200 pipette tip, the supernatant transferred to a new eppendorf tube and samples spun again 1-2 more times until all lipid was removed.

Adherenet hWAT, 3T3-L1 cells and HEK293T cells were washed with DPBS (ThermoFisher) and then lysed directly in the well on ice using M-PER™ Mammalian Protein Extraction Reagent (ThermoFisher, # 78501) , supplemented with proteases and phosphatase inhibitors as listed above. 50µl of the lysis buffer was used per confluent 6-well plate well. Cells were scraped off using a plastic cell scraper and the suspension transferred into a pre-cooled 1.5 ml eppendorf tube. Samples were left shaking on ice for 30min for complete lysis. Samples were then centrifuged at 13,000 rpm for 30 mins at 4°C and the supernatant transferred into a new 1.5 ml eppendorf tube.

2.4.3. Protein quantification

Protein in the cell and tissue lysates was quantified using the DC™ Protein Assay (BioRad). The reaction is similar to the well-documented Lowry assay, but has been modified to save time. First, a standard curve with serial dilutions between 1 mg/ml - 15.625 µg/ml was prepared using the BSA Protein standard (Sigma Aldrich, # 82516). To achieve an absorbance within the linear range of the standard curve, samples were diluted 1:20 in ddH_2O. 5 µl of the diluted sample was pipetted on a flat-bottom 96-well optical plate in triplicates. Diluted buffer was included as a background control. 20 µl of Reagent S (BioRad, #500-0115) was added per 1ml of Reagent A (BioRad, #500-0113). 25 µl of the mixed A+ S reagent pipetted in each well, followed by 200 µl of Reagent B (BioRad, #500-0114). The plate was covered in aluminium foil and left to shake at 300rpm for 20 minutes. Absorbance was measured at 750 nm using an Epoch Microplate

Spectrophotometer (BioTek). Protein concentrations were determined using the standard curve, accounting for the 1:20 dilution and subtracting the background value of the diluted lysis buffer.

2.4.4. Western blot and analysis

Protein electrophoresis and immunoblotting was carried out using the Mini Gel Tank and Blot Module Set (ThermoFisher, NW2000) and NuPAGE MOPS (ThermoFisher, NP0001) and Transfer buffers (ThermoFisher, NP0006). Protein samples were diluted to 1.11 ng/µl as follows:

Component	**Volume**
NuPAGE LDS Sample Buffer (4X)	4.5 µl
NuPAGE Reducing Agent (10X)	1.8 µl
Protein	to 20 µg
ddH_2O	Add for a final volume of 18 µl

The samples were heated to 70°C for 10 minutes to denature the proteins, placed on ice, then briefly vortexed and centrifuged. Samples used for the Total OXPHOS Rodent WB Antibody Cocktail (Abcam, # ab110413) were only incubated at RT for 5 minutes, rather than 70°C, since the hydrophobic Cytochrome c oxidase subunit-1 (COXI) protein is highly sensitive to heating. Gel electrophoresis was performed using the linear gradient NuPAGE™ 4-12% Bis-Tris Protein Gels, 1.0 mm, 12-well (ThermoFisher, NP0322BOX) with 1X NuPAGE™ MOPS SDS Running Buffer in the Mini Gel Tank (ThermoFisher, A25977). The inner and outer chambers were filled with the 1X MOPS running buffer and the inner chamber supplemented with 0.5ml of NuPAGE™ Antioxidant (ThermoFisher, NP0005) to maintain reduced state of proteins during electrophoresis. 18 µl of protein

samples or 8 µl of SeeBlue™ Plus2 Pre-stained Protein Standard (ThermoFisher, LC5925) were loaded per well and samples run at 200V for 50 minutes. Gels to be used for mitochondrial complex visualization were only run for 45 minutes to avoid the risk of the Complex I subunit *NADH:Ubiquinone oxidoreductase subunit B8 (*NDUFB8) migrating out of the gel. The experimental and control groups (e.g. WT vs HOM) were always arranged in an alternating order to avoid local transfer biases.

Proteins were then wet-transferred to a PVDF membrane (Hybond – P, GE Healthcare Amersham, MU60103A) using the Mini Blot Module Set (ThermoFisher) in 1X NuPAGE™ Transfer Buffer (ThermoFisher) containing 10% methanol, run for 1 hr. Before the assembly, the PVDF membranes were charged for 1 min in 100% methanol. After transfer, membranes were incubated for 5 minutes in Ponceau S solution (Sigma, #P7170) to confirm complete and even transfer. Membranes were then washed twice in ddH_2O for 5 mins and blocked in 5% skimmed milk TBST or 5% BSA TBST (for p-eIF-2α antibody) for 1 hr at room temperature. Primary antibodies were then applied to the membranes in optimised dilutions in TBST-milk (or TBST-BSA) and incubated overnight at 4°C. The following day, membranes were washed 5 x 5mins in TBST followed by incubation with a respective species-specific secondary antibody conjugated to horseradish peroxidase (HRP) in TBST-milk for 1 hr at room temperature. Then, membranes were washed 5 x 5 mins in TBST at room temperature.

The chemiluminescent reaction was carried out using the Pierce™ ECL Plus Western Blotting Substrate (ThermoFisher, # 32132) for 5mins in dark, according to manufacturer's protocol. Excess reagent was removed, membranes wrapped in cling film. Membranes were then exposed to CL-Xposure™ Film (ThermoFisher, 34090) for an optimised length of time. Before probing with an antibody for a house-keeping gene, membranes were first

stripped using the Restore PLUS Western Blot Stripping Buffer (ThermoFisher, 46430) for 5 mins, briefly washed in TBST and blocked in TBST-milk for 30 mins. Protein bands were quantified using Image J and normalised to the respective house-keeping gene. All data was shown as mean ± SD. Differences were analysed by unpaired Student's t-test, Welch's t-test or Mann-Whitney test, according to the distribution of the data. Statistical significance was indicated by using: * $p<0.05$, ** $p<0.01$, *** $p<0.001$.

Target protein	**1° Antibody**	**Dilution**	**2° Antibody***	**Dilution**
Subunits of CI-CV	ab110413 (Abcam)	1:1000	α-mouse	1:3000
UCP1	ab23841 (Abcam)	1:1000	α-rabbit	1:5000
eIF2α	5324S (NEB)	1:1000	α-rabbit	1:3000
P(S51)-eIF2α	ab32157 (Abcam)	1:1000	α-rabbit	1:3000
VDAC1	ab15895 (Abcam)	1:2000	α-rabbit	1:5000
C/EBPβ	SC-7962(Santa Cruz)	1:100	α-mouse	1:2000
WARS2	In house	1:500	α-rabbit	1:3000
tubulin	2144(Cell Signalling)	1:10,000	α-mouse	1:10,000
GAPDH	ab8245 (Abcam)	1:10,000	α-mouse	1:10,000

* 2°: Goat anti-rabbit IgG-HRP conjugate (Bio-Rad, 170-6515)

* 2°: Goat anti-mouse IgG (H+L)–HRP (Bio-Rad, 170-6516)

2.5. Mouse methods

2.5.1. Animal husbandry

All mice used in this study were housed in the Mary Lyon Centre at MRC Harwell. Mouse studies were carried out under the Home Office Licenses 30/3146 and 19/0002, in accordance with the UK Animals (Scientific Procedures) Act (1986). Procedures were approved by the MRC Harwell Animal Welfare and Ethical Review Board (AWERB). Mice were housed in alignment with the UK Home Office welfare standards under controlled light (light 7am–7pm, dark 7pm–7am) at a temperature of 21°C ± 2 °C and humidity of 55 ± 10%. Mice had free access to water (25 ppm chlorine) and were fed ad libitum. As shown in Table 2.2, the D12492 and D12450J diets were chosen to represent the high-fat (HFD) and low-fat diets (LFD), respectively, because apart from the differences in lard (fat) and corn starch (carbohydrate), the ingredient composition (protein, mineral, vitamins) is identical. The mice used for primary pre-adipocyte isolations and mice of the 4-month *Wars2*$^{V117L/V117L}$ cohort were fed SDS maintenance chow (SDS Rat and Mouse No. 3 Breeding diet, RM3, 3.6 kcal/g) which is also the standard diet used for the International Mouse Phenotyping Consortium (Dickinson *et al.*, 2016).

Table 2.2 | Macronutrient composition and ingredients of the high and low fat diets used in this study.

	HFD (D12492)		**LFD** (D12450J)	
Component	**gm %**	**kcal %**	**gm %**	**kcal %**
Protein	26.2	20	19.2	20
Carbohydrate	26.3	20	67.3	70
Fat	34.9	60	4.3	10
Total kcal/gm	*5.24*		*3.85*	
Ingredient	**gm**	**kcal**	**gm**	**kcal**
Casein, 80 Mesh	200	800	200	800
L-Cystine	3	12	3	12
Cornstarch	0	0	506.2	2024.8
Maltodextrin 10	125	500	125	500
Sucrose	68.8	275.2	68.8	275.2
Cellulose, BW200	50	0	50	0
Soybean Oil	25	225	25	225
Lard*	245	2205	20	180
Mineral Mix, S10026	10	0	10	0
DiCalcium Phosphate	13	0	13	0
Calcium Carbonate	5.5	0	5.5	0
Potassium Citrate,1 H_2O	16.5	0	16.5	0
Vitamin Mix, V10001	10	40	10	40
Choline Bitartrate	2		2	
FD&C Blue Dye #1	0.05	0	0.01	0
FD&C Yellow Dye #5	0	0	0.04	0
Total	*773.85*	*4057*	*1055.05*	*4057*

2.5.2. Generation of genetic mouse models

Wars2$^{V117L/V117L}$ mice were generated by backcrossing the mutagenized C57BL/6J MPC-151 pedigree mice, originally from the The Harwell Aging ENU-mutagenesis Screen, to C3H/Pde mice, as documented previously (Potter *et al.*, 2016; Agnew *et al.*, 2018).

Two cohorts (58 mice in total, each) of *Wars2-V117L* male and female mice were generated from *Wars2*$^{+/V117L}$ x *Wars2*$^{+/V117L}$ matings and aged to 4 months for molecular studies (qPCR, Western Blot, mtDNA content, FGF21 levels). For longitudinal body composition-based phenotyping tests and fat depot weighing, three cohorts of both males and females were generated and aged to 6-months (185 mice in total). One additional cohort of males and females was generated for the study of food intake (30 mice in total).

The *Wars2*$^{+/-}$ mice were imported into our laboratory previously (Agnew *et al.*, 2018). Briefly, the NIH KOMP *Wars2*-KO allele (*Wars2*$^{tm1(KOMP)Vlcg}$) targeting construct was integrated into the C57BL/6N ES cell genome by homologous recombination, deleting 46632bp, including segments of both exon1 and exon2 of *Wars2* and producing a frameshift and a premature stop codon. *Wars2*$^{tm1(KOMP)Vlcg}$ ES cells were micro-injected into C57BL/6N blastocysts generating mosaic offspring. Germ-line transmission of the construct was tested by genotyping the C57BL/6N-*Wars2*$^{tm1(KOMP)Vlcg}$ x C57BL/6N offspring for the neomycin selection cassette. For longitudinal body composition-based phenotyping tests and fat depot weighing, a cohort of female *Wars2*$^{+/-}$ was generated on either HFD or LFD, totalling to 32 mice.

2.5.3. Genotyping strategy – *Wars2*$^{V117L/V117L}$

The *Wars2*$^{V117L/\ V117L}$ mouse cohorts were genotyped using the The Idaho Technology LightScanner (Idaho Technology Inc, Utah, USA), in accordance with the manufacturer's standard protocol. Briefly, PCR was performed in the presence double-stranded

DNA(dsDNA) binding dye LCGreen. PCR samples were then heated on the LightScanner and the fluorescence emitted by bound LCGreen monitored. As the dsDNA melts, the fluorescence decreases until no LCGreen remains bound. To distinguish the alleles, a 3' blocked unlabelled oligonucleotide (lunaProbe) was designed to directly overlap the mutation and run in an exhaustive PCR with uneven primer concentrations. This generates two products – the full length PCR product and the shorter lunaProbe-containing amplicon. Due to different binding affinities, the lunaProbe amplicon from mutant and wild-type alleles melt at different temperatures and can thus distinguish the genotype of a given mouse.

Primers/Probe sets 5' to 3'

Wars2V117L-LSF1	TCAGCCTATCCCTGTTGTCTA
Wars2V117L-LSR1	TGGTGTAAATGCTGCAATCG
Wars2V117L-PrF1	CCTTCCTTTTAGTTGTCTGAACACACTCAG

PCR mix

HotShot master mix	5µl
LCGreen	1µl
Wars2V117L-LSF1 (20ng/µl)	0.1µl
Wars2V117L-LSR1 (20ng/µl)	0.5µl
Wars2V117L-PrF1 (20ng/µl)	0.5µl
DNA (1/10 dil ABI)	2µl
ddH2O	0.9µl

PCR program

1) 95°C for 2 min	
2) 95°C for 30 sec	
3) 60°C for 30 sec	PCR cycle
4) 72°C for 30 sec	
5) Cycle from step 2, 55 times	
6) 95°C for 30 sec	
7) 25°C for 30 sec	Hybridisation
8) 15°C for 30 sec	

2.5.4. Genotyping strategy – *Wars2*$^{+/-}$

The *Wars2*-KO allele (*Wars2*$^{tm1(KOMP)Vlcg}$) was created by insertion of a *LacZ* cassette causing the deletion of wild-type sequence. Genotypes could thus be distinguished using standard TaqMAN FAM dye-labelled probes targeting either the lacZ or wild-type sequence in a qRT-PCR copy number assay. A VIC-labelled internal control *Dot1l* was also included. In these assays, amplification of targeted sequences releases quencher molecules from the fluorophore, resulting in increased fluorescence. The primer and probe sequences and PCR conditions are listed below.

Primer	**Sequence (5' to 3')**
Wars2-WT FW	GCCCAGCACTTGGGATGT
Wars2-WT RV	GCAGCCAGCTCACCAATG
Wars2-WT Probe (FAM)	TCCCTTCACTTTCCTGTCTCCGTTTC
Wars2-LacZ FW	CTCGCCACTTCAACATCAAC
Wars2-LacZ RV	TTATCAGCCGGAAAACCTACC

Wars2-LacZ Probe (FAM)	TCGCCATTTGACCACTACCATCAATCC
Dot1l FW	GCCCCAGCACGACCATT
Dot1l RV	TAGTTGGCATCCTTATGCTTCATC
Dot1l Probe (VIC)	CCAGCTCTCAAGTCG

Component	**Volume (µl)**
ABI GTX TaqMAN Master Mix	5
Dot1l Forward (20µM)	0.225
Dot1l Reverse (20µM)	0.225
Dot1l Probe (5µM)	0.2
FAM assay (probe 5µM & primers 15µM each)	0.2
ddH_20	1.55
DNA (5ng/µl)	2.5
Total	10

2.5.5. Retro-orbital bleed

Unfasted mice were euthanized by intra-peritoneal injection of an over-dose of anaesthetic, 0.2ml of pentobarbitone in alignment with the Home Office standards. Once fully anaesthetised, but still with a beating heart, a glass capillary was inserted into the anterior corner of the mouse eye to perforate the membrane of the retro-orbital sinus. The blood was then collected into Lithium-Heparin microvette tubes (CB300, Sarstedt, Numbrecht, Germany). After blood collection, cervical dislocation was performed, animals dissected and tissues taken for RNA/protein expression analysis.

2.5.6. Body composition analysis

Total body mass was measured every two weeks from 4 weeks of age on a scale calibrated to 0.01g. Body composition of the mice was measured every two weeks using an Echo-MRI (Echo-MRI-100, Echo-MRI, Texas, USA). Echo-MRI uses nuclear magnetic resonance (NMR) relaxometry to create contrast between soft tissues by measuring relaxations times of hydrogen spins and density in live, non-anaesthetised mice. The readings were total fat mass (g) and total lean mass (g).

2.5.7. Tissue collection and fat depot weighing

Mice aged between 3-12 months were sacrificed by cervical dislocation and following confirmation of death, multiple tissues were dissected. These included kidney, liver, heart, gastrocnemius skeletal muscle, soleus skeletal muscle, inguinal white adipose tissue, gonadal white adipose tissue, mesenteric white adipose tissue, perirenal white adipose, epicardial white adipose tissue and brown adipose tissue. Skin from the abdomen and skin from the back of the mouse were also taken, as shown in Figure 2.2, to assess subcutaneous fat thickness. The fur of relevant skin portions was trimmed, prior to dissections. Adipose tissues were placed on a scale and the weight recorded. Adipose depots and skin were then separately placed into 10% formalin pots (Leica, 3800840) for hematoxylin and eosin (H&E) staining and histology analysis. Separate cohorts were used for histology and expression studies, respectively, to avoid RNA and protein degradation.

2.5.8. Histology

Fixed tissues were paraffin embedded and 6 μm sections were stained with H&E according to standard protocols (Histology Department, MRC Harwell Institute). Stained sections were imaged using the Hamatsu NaoZoomer slide scanner and NDP2 program used for exporting the images.

Figure 2.2 | Skin Dissection. Ventral skin was cut diagonally to capture adipose tissue surrounding mammary glands (A). Dorsal skin was dissected from under the shoulder blades (B). Images by Dr Marianne Yonn.

2.5.9. Food intake study

4-week old mice were administered the RM3 diet, pair-housed by genotype and food was weighed twice a week and topped up to 200g each time, until 16 weeks of age. The two food intake values each week were used to calculate the weekly average food intake per mouse. Lean mass measurements, taken every 2 weeks, were used to normalise the food intake data to "grams of food intake per gram of lean weight".

2.5.10. Statistical analysis of body composition, fat depot weights and food intake

All bodyweight and body composition results are shown as mean ± SD. Statistical analysis was performed using Graph Pad Prism 7. Data were assessed for equal distribution using D'Agostino-Pearson normality test. Later time points of the body composition of the *Wars2-V117L* Cohorts 1 and 2 showed unequal distribution, but upon consultation with statistician Dr George Nicholson, I concluded that this is due to the groupings - $Wars2^{V117L/V117L}$ homozygous mice showed a severe reduction of fat mass compared to the other two genotypes. I thus proceeded using standard 2-way ANOVA with Bonferroni post-hoc test at each time-point with diet and genotype as independent factors. Male and females were analysed separately. I used standard significance thresholds depicted as: * $p<0.05$, ** $p<0.01$, *** $p<0.001$, unless otherwise stated.

Similarly, some fat depot weights were also not normally distributed. Such data were first transformed using log(Y), $(Y)^2$, 1/Y or exp(Y) before comparison by 2-way ANOVA. Normally distributed data were analysed by 2-way ANOVA directly. A Bonferroni post-hoc test compared each tested group with all other groups in the *Wars2-V117L* cohorts. Significant effects of diet, genotype, interaction and post-hoc tests were denoted by using * $p<0.05$, ** $p<0.01$, *** $p<0.001$.

D'Agostino-Pearson normality test showed normal distribution for the male food intake data. These were subsequently analysed using one-way ANOVA with Tukey's multiple comparisons test: * $p<0.05$, ** $p<0.01$, *** $p<0.001$. Numbers in females were too low for statistical comparison (n=2).

3. The functional study of candidate SNPs in three waist-to-hip ratio associated loci

3.1. Introduction

For 60 years it has been known that body fat distribution, not solely fat content, can modify the risk of disease and metabolic complications associated with obesity (Vague, 1956). Body fat distribution can be most easily assessed by WHR, the ratio of waist circumference to hip circumference, whilst other methods such as computed tomography (CT) and magnetic resonance imaging (MRI) provide more precise measures of visceral and subcutaneous adipose depots (Kaess *et al.*, 2012; Klopfenstein *et al.*, 2012). Increased WHR is associated with increased mortality and risk of coronary heart disease, myocardial infarction and T2D (Snijder *et al.*, 2003; Wang *et al.*, 2005; Canoy, 2008; Mason, Craig and Katzmarzyk, 2008; Peters, Bots and Woodward, 2018) Lower WHR, indicative of higher gluteal or subcutaneous fat accumulation, is protective for T2D and mortality (Snijder *et al.*, 2004; Mason, Craig and Katzmarzyk, 2008). Further evidence of this association arises from cases of lipodystrophies, such as Dunningan-type familial partial lipodystrophy, where the loss of subcutaneous adipose depots is accompanied by insulin resistance, hypertension and abnormal glucose levels (Peters *et al.*, 1998; Akinci, Meral and Oral, 2018). Deciphering the underlying genetics of fat distribution might thus lead to better understanding of disease etiology and the discovery of therapeutic or preventive targets.

Early twin studies of waist circumference (WC) and WHR suggested a strong heritability of these traits (Rose *et al.*, 1998). A number of GWAS have studied the genetic underpinning of WHR with the most recent meta-analysis identifying 346 different loci associated with WHRadjBMI (Pulit *et al.*, 2018). Importantly, the WHR-increasing alleles

in these loci also inversely correlate with subcutaneous:visceral adipose mass ratio as measured by MRI and CT scan imaging (Chu *et al.*, 2017; Pulit *et al.*, 2018). Since the majority of SNPs (~94%) associated with traits and common diseases overlap the non-coding part of the genome, effector genes in the majority of the loci remain to be identified (M T Maurano *et al.*, 2012). Furthermore, each locus often includes dozens of SNPs in close linkage disequilibrium (LD) and any of these SNPs could be causal or act through a combinatorial effect. To understand the underlying genetics and individual variation of fat distribution it will be important to identify the causative SNPs and functional genes in the WHR-associated loci.

To date, a plethora of diverse methods to prioritse the most likely functional variants using different assumptions have been developed (e.g. Claussnitzer *et al.*, 2014; Schwessinger *et al.*, 2017). Real association signals can be distinguished by Bayesian posterior probability analysis (PPA) of the GWAS data (Maller *et al.*, 2012). Furthermore, many of trait-associated variants are proposed to modulate gene expression by interfering with transcription factor binding in cis-regulatory elements (CREs), such as enhancers and promoters, and WHR-associated SNPs were specifically enriched in adipose-specific CREs (Pasquali *et al.*, 2014; Shungin *et al.*, 2015).

To identify the most likely functional SNPs in the WHR-associated loci, Dr Sara Pulit used posterior-probability analysis (PPA) to analyse the Genetic Investigation of ANthropometric Traits (GIANT) and UK Biobank data, which together contain genetic and anthropometric measures on close to 700,000 individuals. Since the expression of candidate WHRadjBMI-associated genes is enriched in adipocytes and multiple fat depots, the SNPs scoring highly in the PPA were filtered by overlap with putative CREs, as predicted by adipose open chromatin and epigenetic modifications data (Shungin *et al.*, 2015). Three loci, *VEGFA*, *C5orf67* and *EMILIN2*, in which a single SNP (rs998584,

rs3936510, rs3810068, respectively) explained over 95% of the WHRadjBMI association in each locus were prioritised by the Lindgren group for further functional analysis as described in this chapter (Figure 3.1).

3.1.1. Chapter hypothesis

We hypothesised that rs998584, rs3936510, rs3810068 affect gene expression during adipose tissue homeostasis or development by interfering with transcription factor binding and changing the activity of CREs, leading to altered adipocyte size or cell number.

3.1.2. Chapter aims

1. To test the effect of the SNPs on protein binding. In electrophoretic mobility shift assays (EMSAs), I incubated oligonucleotides with either allele of each SNP with nuclear protein from differentiating immortalised human white adipose tissue preadipocyte cells (hWAT). I chose the mid-stage differentiation in order to capture a time-point of chromatin remodelling and adipogenic transcription factor expression (Siersbaek *et al.*, 2011; Xue *et al.*, 2015).

2. To test the effect of the SNPs on gene expression. In collaboration with Dr Rebecca Dumbell, I used luciferase assays to study the effect on enhancer or promoter activity in the differentiating hWAT cells.

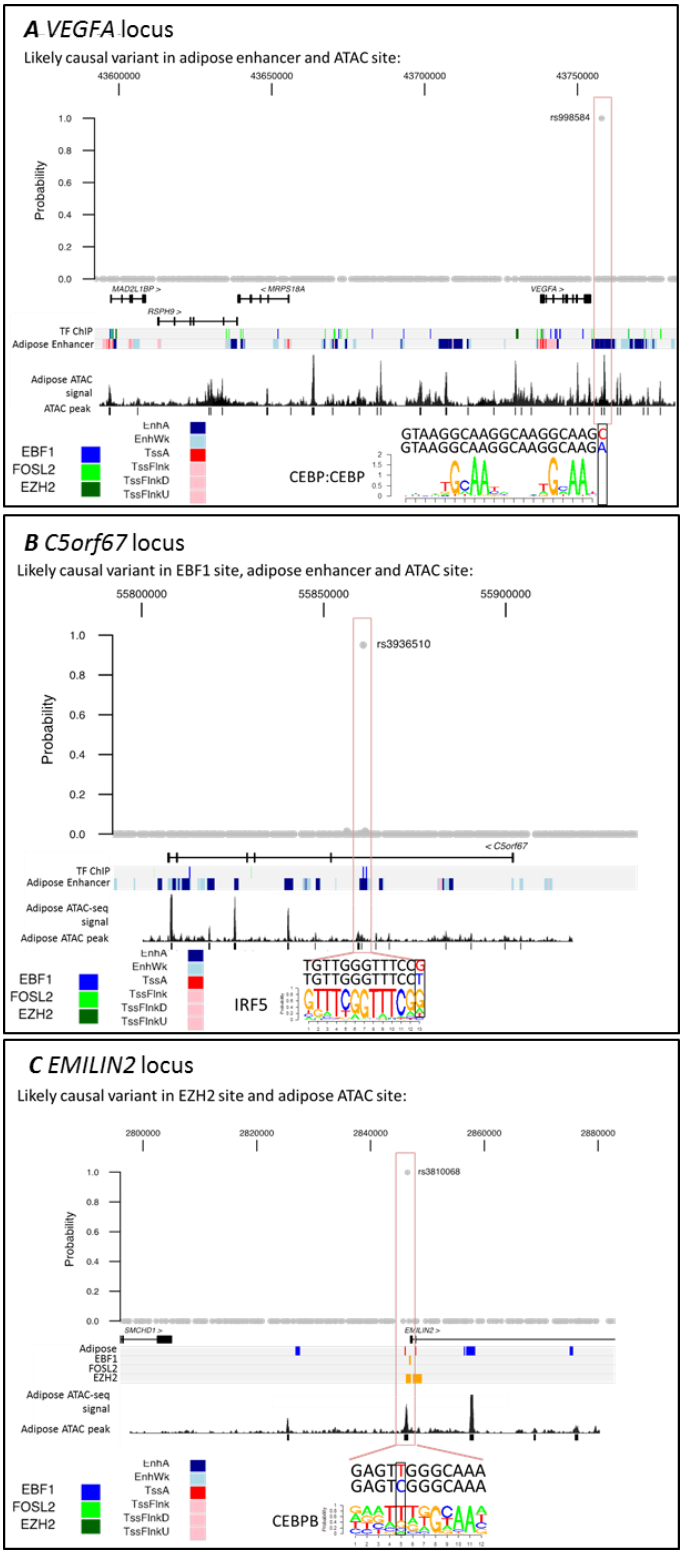

Figure 3.1 | Candidate SNPs in the three WHR-associated loci overlap adipose open chromatin regions. Posterior probability plots of rs998584, rs3936510, rs3810068 and linked SNPs (gray dots) in the *VEGFA* (A), *C5orf67* (B) and *EMILIN2* (C) loci, and their overlap with adipose open chromatin (ATAC-Seq), epigenetic annotations (adipose enhancer) and ChIP-Seq protein binding (TF ChIP). The consensus of the altered TF motifs based on JASPAR analysis (http://jaspar.genereg.net/) is shown for each locus below (Fornes *et al*., 2019). EnhA: enhancer; EnhWk: weak enhancer; TssA: active transcription start site; TssFlnk: flanking active transcription start site; TssFlnkD: flanking downstream active transcription;

3.2. Materials and methods

3.2.1. Adipocyte nuclear protein extraction

Nuclear protein was extracted from Day 4 differentiated hWAT adipocytes using the NE-PER™ Nuclear and Cytoplasmic Extraction Reagents (Thermo Fisher). The quantity of protein was measured with the DC™ Protein Assay (Biorad), as described in the main methods Chapter 2.

3.2.2. Oligonucleotide probe design and annealing

Oligonucleotide probes of 38 bases were designed to flank SNP sites for reference or alternate allele by 20 bases. 3'-biotinylated (Integrated DNA Technologies) and unlabelled (ThermoFisher) oligonucleotides in the forward (FW) orientation were annealed to unlabelled oligonucleotides (ThermoFisher) in the 3' to 5' reverse (RV) complement orientation according to the online ThermoFisher protocol (ThermoFisher, 2009). The sequences are shown in Table 3.1. Briefly, different combinations of the single-stranded probes were combined in the oligonucleotide annealing buffer (10mM Tris, 1mM EDTA, 50mM NaCl, pH 8.0) using recommended thermocycler conditions producing either biotinylated or unlabelled double stranded oligonucleotides, at a stock concentration of 2 pmol/µl. The reaction is outlined in

Table **3.2**.

Table 3.1 | **Nucleotide sequences that were used for the generation of the double stranded DNA.** Unlabelled DNA for competition experiments was generated by fusing unlabelled forward and reverse oligonucleotides. Labelled DNA was made by annealing 3'-biotin-labelled forward oligonucleotides with unlabelled reverse oligonucleotides.

SNP	**Forward oligonucleotides**
rs998584 Risk	GTAAGGCAAGGCAAGGCAAGAAAGAGATGTCTCCAGGGGCT
rs998584 Non-risk	GTAAGGCAAGGCAAGGCAAGCAAGAGATGTCTCCAGGGGCT
rs3936510 Risk	TTAGACATTGTTGGGTTTCCTTAATGCTGAGAAAATAGCAT
rs3936510 Non-risk	TTAGACATTGTTGGGTTTCCGTAATGCTGAGAAAATAGCAT
rs3810068 Risk	GATGGTGCCTAAGGCAGAGTTGGGCAAAGAAAGAACCAGCG
rs3810068 Non-risk	GATGGTGCCTAAGGCAGAGTCGGGCAAAGAAAGAACCAGCG

SNP	**Reverse oligonucleotides**
rs998584 Risk	AGCCCCTGGAGACATCTCTTTCTTGCCTTGCCTTGCCTTAC
rs998584 Non-risk	AGCCCCTGGAGACATCTCTTGCTTGCCTTGCCTTGCCTTAC
rs3936510 Risk	ATGCTATTTTCTCAGCATTAAGGAAACCCAACAATGTCTAA
rs3936510 Non-risk	ATGCTATTTTCTCAGCATTACGGAAACCCAACAATGTCTAA
rs3810068 Risk	CGCTGGTTCTTTCTTTGCCCAACTCTGCCTTAGGCACCATC
rs3810068 Non-risk	CGCTGGTTCTTTCTTTGCCCGACTCTGCCTTAGGCACCATC

Table 3.2 | **Annealing EMSA oligonucleotides.** In order to generate double-stranded biotin-labelled and unlabelled DNA at a stock concentration of 2 pmol/µl.

		Labelled Duplex (100pmol/µl)		**Unlabelled Duplex** (100pmol/µl)	
Oligonucleotides at 100pmol/µl:	**Genotype:**	Risk	Non-risk	Risk	Non-risk
Forward labelled	Risk	2µl			
	Non-risk		2µl		
Forward unlabelled	Risk			2µl	
	Non-risk				2µl
Reverse complement unlabelled	Risk	2µl		2µl	
	Non-risk		2µl		2µl
Oligonucleotide annealing buffer (10mM Tris, 1mM EDTA, 50mM NaCl, pH 8.0)		96µl	96µl	96µl	96µl

3.2.3. Electrophoretic mobility shift assay

The EMSA was performed according to the LightShift Chemiluminescent EMSA Kit protocol (ThermoFisher). The biotinylated double stranded probes (20fmol) of either allele were incubated with day 4-differentiated hWAT nuclear protein (4.5µg) in final concentration of 10mM Tris, 50mM KCl, 1mM DTT and 50ng/µl Poly (dI•dC) (ThermoFisher). For the competitor assays, an unlabelled oligonucleotide of the same sequence was included in 11, 33 or 100-fold excess. The reactions were incubated at room temperature for 20 minutes and resolved on a 6% DNA retardation gel (ThermoFisher, EC6365BOX) in 0.5M TBE buffer. The gel contents were transferred onto a nylon membrane, UV-crosslinked, then blocked and visualised using the Chemiluminescent Nucleic Acid Detection Module (ThermoFisher). For the supershift assays, in the case of the *EMILIN2* locus, an additional 1µg of anti-C/EBPß antibody (SantaCruz, sc 7962) was incubated with the protein before the addition of the biotinylated probes. 3-4 technical replicates were performed for each experiment.

3.2.4. siRNA knockdown

The hWAT cells were differentiated to day-4 as described in the main Materials & Methods chapter. Cells were trypsinised and plated at a density of 120,000 live cells/well on a 6-well plate, counted using Countess II automated cell counter (Invitrogen), to reach ~80% confluence next day. Cells were transfected with Hs_CEBPB_4 (Qiagen, shown below) using Lipofectamine® RNAiMAX (ThermoFisher) and harvested 48 hours later for nuclear protein extraction. The experiment was replicated 3 times.

siRNA:	**Catalog number**	**Target Sequence:**
Hs_CEBPB_4	SI00073640	CCCGTGGTGTTATTTAAAGAA

3.2.5. Molecular cloning of luciferase plasmids

Genomic sequences of ~1kb surrounding each of the SNPs were amplified using Q5® High-Fidelity DNA Polymerase (NEB) from either HEK293T DNA (*VEGFA* locus) or human DNA (1000Genomes ID: NA12045 (male), Coriell Biobank) (*C5orf67* and *EMILIN2* loci). The primers used and genomic co-ordinates of targeted sequences are shown in Table 3.3. The putative enhancer fragments of the *VEGFA* and *C5orf67* loci were cloned into pGL3-LRF (forward orientation, Addgene no. 66936) and/or pGL3-LRR (reverse orientation, Addgene no. 66937) using the Gateway LR Clonase II enzyme mix (Life Technologies) as described previously (Buckley *et al.*, 2016). Briefly, the forward and reverse primers for PCR amplification were synthesised with the Gateway attB1 and attB2 sequences, respectively. Since the pGL3-LRF and pGL3-LRR contain swapped recombination sequences "att L 1" and "att L 2", the PCR amplicons will be incorporated in forward and reverse direction, respectively. The promoter of *EMILIN2* was cloned using standard restriction enzyme cloning into the BglII and HindIII sites of the pGL3-Enhancer (Promega, cat. no. E1771) vector. The insertion was confirmed by sequencing and restriction enzyme digest. The plasmids were then mutated to generate the alternative alleles using the Q5® Site-Directed Mutagenesis Kit (NEB) and the inserts Sanger sequenced to ensure no additional mutations were present. I carried out the *C5orf67* fragment cloning, cloning for *VEGFA* and *EMILIN2* was done by Dr R Dumbell.

Table 3.3 | Primers used for amplifying target sequences and mutagenizing luciferase vectors. Red bases indicate cloning overhangs added to amplification primers: Gateway recombination sequences in *VEGFA* and *C5orf67* primers, BglII and HindIII for *EMILIN2* primers. Genome co-ordinates are from hg19 annotation.

Cloning primers

VEGFA FW	CAGCTACGCGTCCAACTTTGTACAAAAAAGCAGGCT CCCCCTTTGTTTGTCTCCCC
VEGFA RV	CAGCTCTCGAGCCAACTTTGTACAAGAAAGCTGGGT TCATAAAGCCGGCCCAGATTCA
region amplified:	chr6: 43,757,223-43,758,514
size:	1,292 bp

C5orf67 FW	CAGCTACGCGTCCAACTTTGTACAAAAAAGCAGGCT TGGGAGATGTGGGGATATTG
C5orf67 RV	CAGCTCTCGAGCCAACTTTGTACAAGAAAGCTGGG TGGAAATGGGGCTTTTCTCTT
region amplified:	chr5: 55,860,363-55,861,431
size:	1,069 bp

EMILIN2 FW	cagctAGATCTGCTCACAGAGGCCACAGTTT
EMILIN2 RV	cagctAAGCTTCTCCGGCTTCTCGTTCCTAC
region amplified:	chr18:2,846,003-2,847,033
size:	1,031 bp

Mutagenesis primers

VEGFA, C->A, FW	GCAAGGCAAGaAAGAGATGTC
VEGFA, RV	CTTGCCTTACCACACTTG
C5orf67, G->T, FW	TTGGGTTTCCtTAATGCTGAG
C5orf67, RV	CAATGTCTAAACAGCTGAC
EMILIN2, T->C, FW	AAGGCAGAGTcGGGCAAAGAAA
EMILIN2, RV	AGGCACCATCTGACAGTT

3.2.6. Luciferase assays

Transfection conditions for luciferase assays in day 4-differentiating hWAT cells were first optimised using different cell densities, different concentrations of pEGFP_C1 (BD Biosciences Clontech, cat. no. 6084-1) and Lipofectamine® 3000 (ThermoFisher). The optimised conditions were as follows and as demonstrated in Figure 3.2. On Day 4 of differentiation, 4000 hWAT cells/well were plated into a white solid bottom 96-well Greiner Bio-One CELLSTAR plate. Eight technical replicates (wells) per sample were included. Twenty-four hours later, the cells were transfected with 0.2μg firefly plasmid, 10ng pRL-TK - *Renilla* luciferase internal control plasmid (Promega, cat. no. E2241) and 0.2μl Lipofectamine® 3000 per well according to the commercial protocol. In each experiment, empty vectors were included as negative controls (pGL3-Enhancer for *EMILIN2* vectors, and pGL3-LRF for *VEGFA* vectors and pGL3-LRR and pGL3-LRF for *C5orf67* vectors). SV40-driven pGL3-control vector (Promega, cat. no. E1741) was included as a positive control. Each experiment also included separate 8 wells transfected with pEGFP_C1 as a transfection control. After 24-hours, the transfection efficiency in the control wells was assessed using a fluorescent microscope. If ~10% transfection was observed, the cells were lysed and the luciferase activity assayed using the Dual Luciferase Assay Kit (Promega) and the Varioskan® Flash microplate reader (ThermoFisher). Firefly luciferase values were normalised to renilla luciferase readings. The results were accepted and analysed if the positive control pGL3-Control vector showed >5-fold normalised firefly higher activity compared to the empty vector.

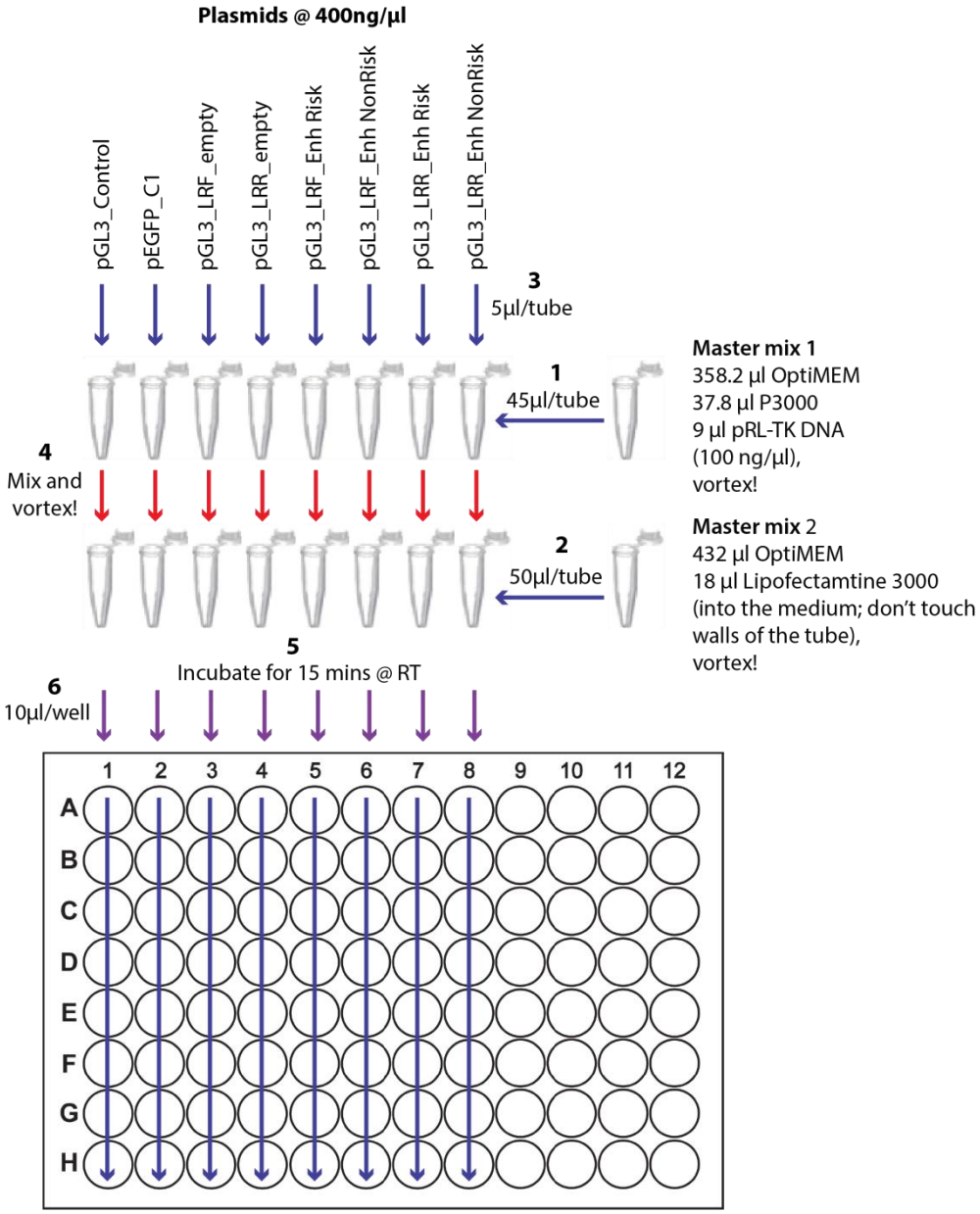

Figure 3.2 | Transfection of hWAT cells with luciferase plasmids. Day 4 differentiated hWAT cells were plated at 4000 cells /well. After 24 hours, they were transfected using the optimised concentrations of plasmids and Lipofectamine® 3000. 1kb putative enhancer regions with either Risk or Nonrisk alleles (Enh_Risk or Enh_Nonrisk) were cloned into SV40-driven firefly luciferase vector with recombination sites either in the forward (pGL3_LRF) or reverse (pGL3_LRR) direction respective to the firefly gene. pGL3_Control - SV40-driven firefly luciferase. pEGFP_C1 - GFP-containing vector. pRL_TK – Thymidine Kinase promoter-driven Renilla luciferase plasmid.

3.2.7. Statistical analysis

At least three indepedent experiments were carried out for each locus and technique. For luciferase assays, statistical comparison was by 1-way ANOVA or Kruskall-Wallis test between the fragment-containing vectors of either allele and the empty vector (repeated measures). For the *C5orf67* locus, the pGL3-LRR and pGL3-LRF vectors were analysed separately.

3.3. Results

3.3.1. Testing the effect of SNPs on transcription factor binding

To study the effect of the selected SNPs on protein binding in adipocytes, I used 38-bp biotinylated oligonucleotide double-stranded DNA (dsDNA) probes surrounding the different SNPs with either reference or alternative alleles. These probes were incubated with total nuclear protein from Day 4-differentiated hWAT and their protein binding compared using electrophoretic mobility shift assay (EMSA) (Figure 3.3). Increasing concentrations of competing unlabelled dsDNA of identical sequences were used to test the binding specificity.

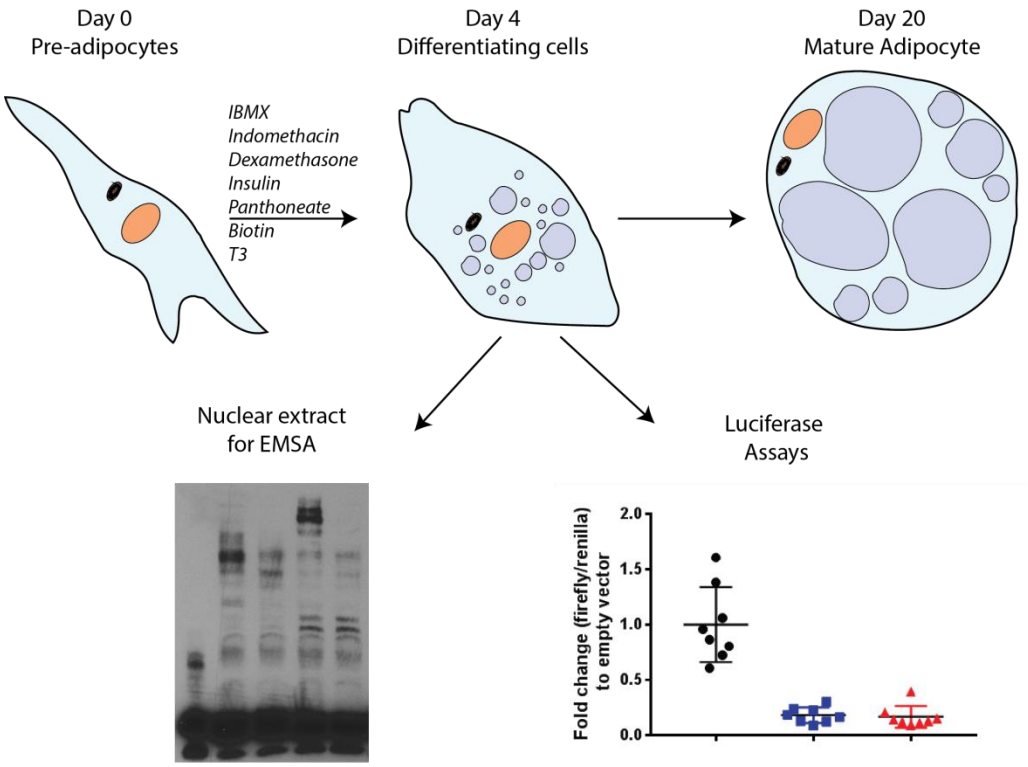

Figure 3.3 | SNP functional assays in day 4 differentiated hWAT cells. Differentiation of human white adipocyte cell line (hWAT) was initiated using 3-isobutyl-1-methylxanthine (IBMX), indomethacin, dexamethasone, insulin, panthoneate, biotin and triiodothyronine (T3). It took 20 days to reach the mature adipocyte stage, but an earlier time-point (Day 4) was selected to reach an expression of early adipogenic transcription factors and study the effect of SNPs on protein-DNA binding and reporter expression.

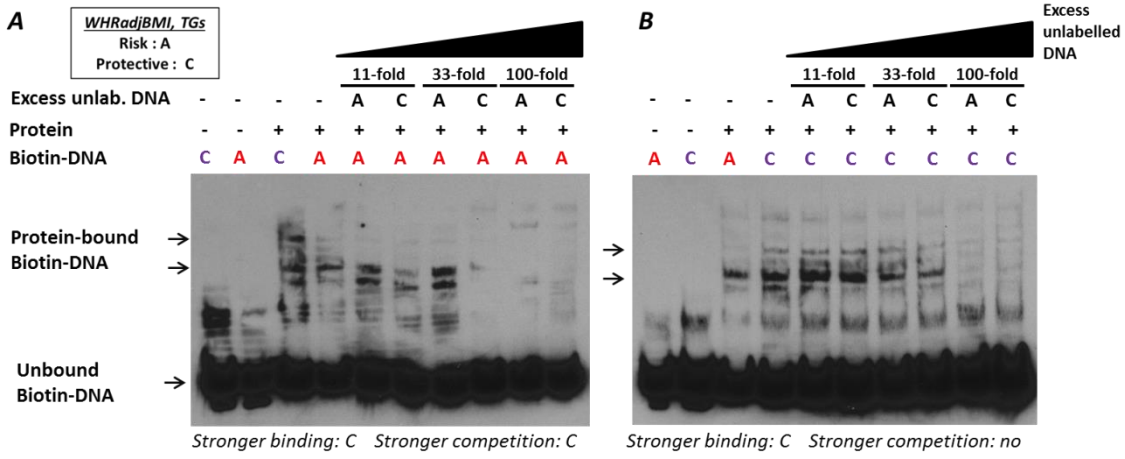

Figure 3.4 | The C allele at rs988584 shows stronger binding affinity, representative blots.

38bp biotin-labelled DNA probes surrounding rs998584 with either the A or C allele were incubated with nuclear protein from hWAT cells differentiated for 4 days. This resulted in shift of the biotin-DNA due to protein binding (shown with arrows). Excess unlabelled DNA of either allele were titrated against either the A (left blot) or C (right blot) allele to test specificity of protein binding. The C allele showed more intense or additional bands compared to the T allele. The titration experiments did not show consistent differences in the competition efficiency. Below, qualitative assessment of

which allele showed stronger binding or competed more effectively in titration assay.

3.3.2. *VEGFA* locus – Highly variable technical replicates show a trend for increased protein binding affinity for the C allele at rs998584

The A allele of the rs998584 SNP was associated with increased WHRadjBMI and triglyceride levels in the PheWAS portal (https://phewascatalog.org/) (Denny *et al.*, 2013). The A and C allele-containing oligonucleotides of the rs998584 SNP showed different intensities of the protein-bound bands (Figure 3.4A&B, lanes 3 and 4). As seen in Figure 3.5 and Figure 3.6**,** the allelic direction was not always replicated, but the majority of the technical replicates (6 out of 10 blots) discover stronger binding intensity or additional bands with the C allele. The A allele showed greater affinity in 3 blots. From the perspective of the competition assays (lanes 5 – 10), unlabelled C allele was a stronger competitor than the A allele in 3 out of 10 blots. For the remaining 7 blots, there was no difference. In summary, the effect of rs998584 on protein binding is highly variable across replicates, but differential binding was observed in the majority of replicates with a trend for stronger binding of the C allele.

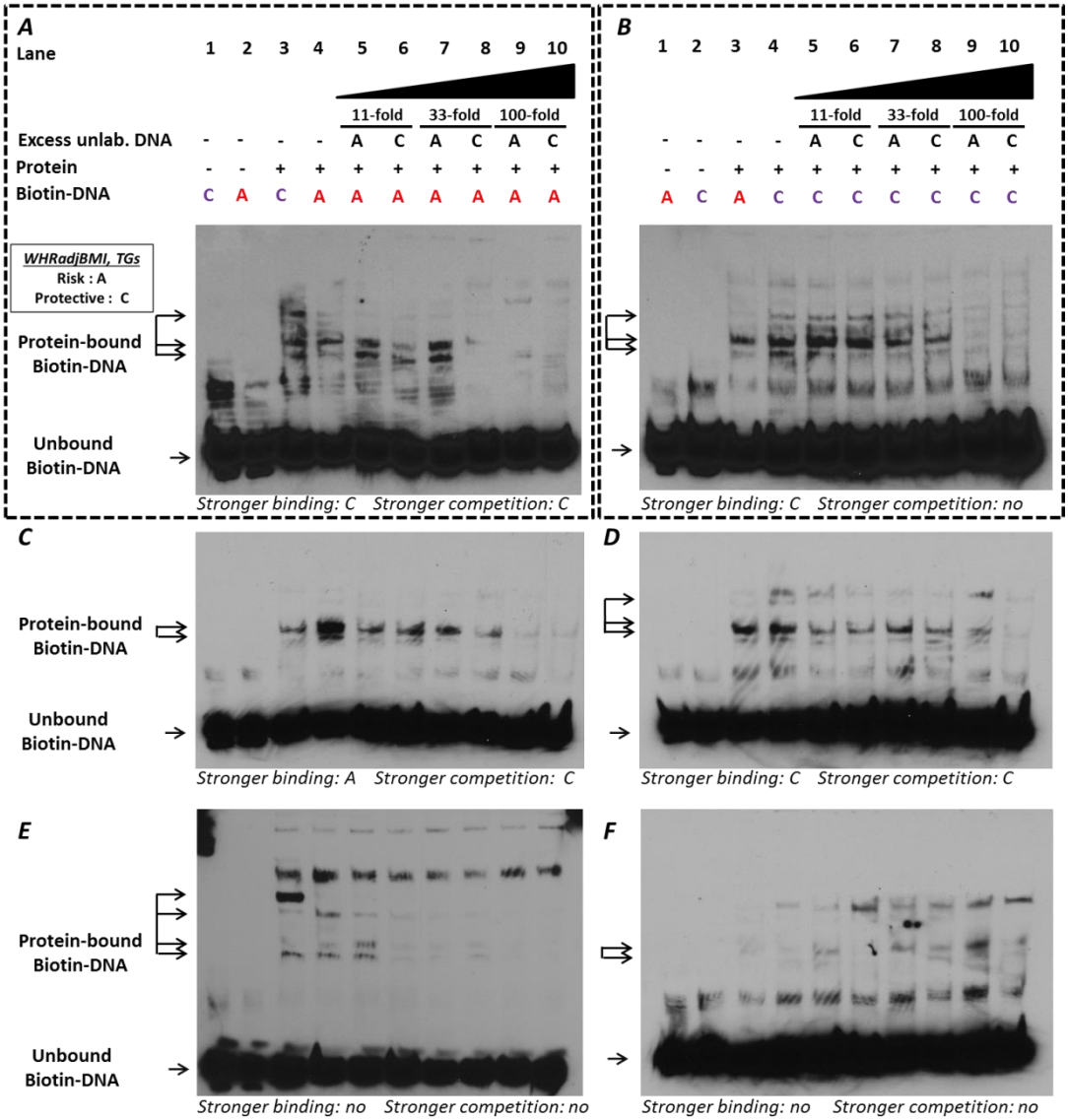

Figure 3.5 | rs998584 EMSA Replicates. The EMSA experiments showed high variability, but in most cases the protective C allele of rs998584 showed more intense or additional bands compared to the risk A allele (replicates A, C, D, E) and C was also the only allele to show stronger competition in the titration experiments (in blots A, C & D, the C allele showed a higher effectivity at removing the bands). Representative images used in Figure 3.4 are marked with a dotted line. Below, qualitative assessment of which allele showed stronger binding or competed more effectively in titration assay.

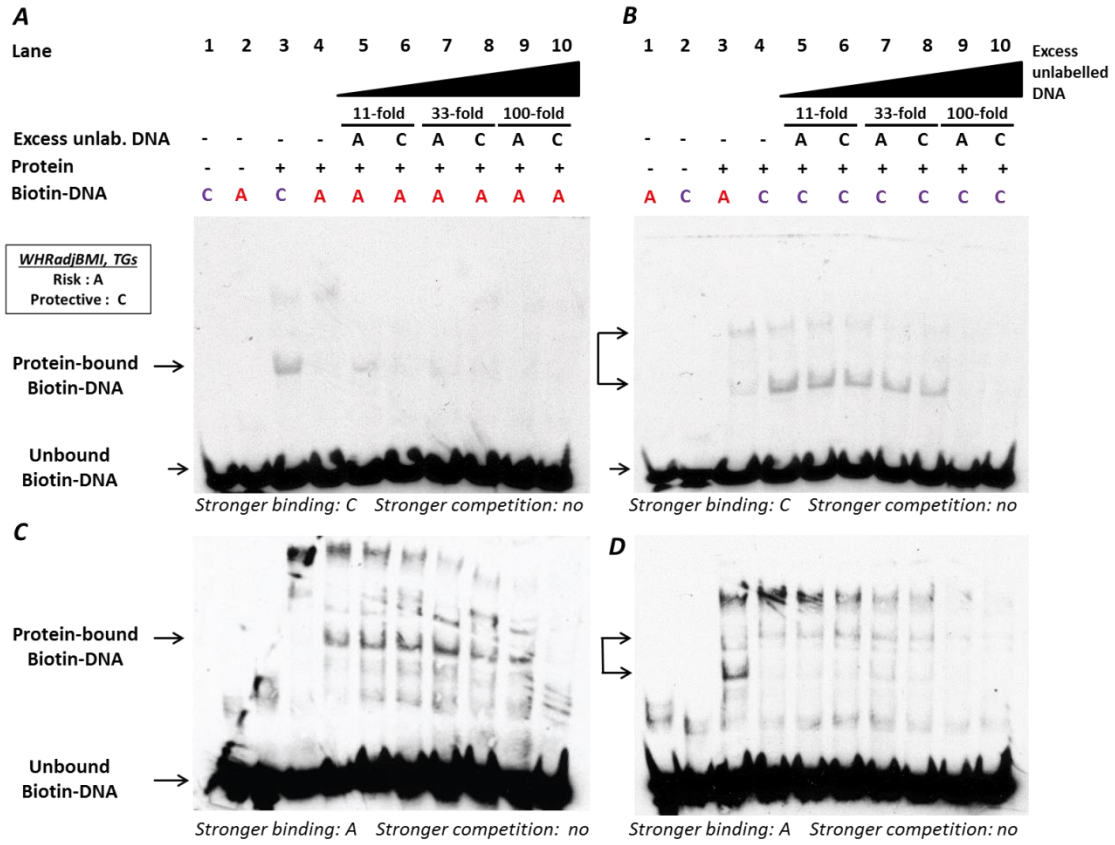

Figure 3.6 | Independent rs998584 EMSAs replicates. Two sets of repeats of representative EMSAs in Figure 3.4, performed by Dr Dumbell. For blots A & B, the C allele binds stronger/has a dark band in the middle of the membrane. In blots C & D, A allele shows stronger binding at the lower band than the C allele. There is no indication of a difference in competitive binding for either the unlabelled C or A oligonucleotides in any case. These blots are performed with independently annealed oligonucleotides. Below, qualitative assessment of which allele showed stronger binding or competed more effectively in titration assay.

3.3.3. *C5orf67* locus: G allele at rs3936510 enhances protein binding

The T allele of the rs3936510 SNP was previously associated with increased WHRadjBMI. The binding effect of rs3936519 of the *C5orf67* locus was tested as described above for the *VEGFA* locus. Upon incubation with the hWAT nuclear protein, the G-containing oligonucleotide showed multiple strong bands that were much fainter for the T allele (Figure 3.7, lanes 3 and 4). In agreement with this finding, the titration of excess unlabelled oligonucleotide (lanes 5 - 10) clearly showed that G allele is more effective at out-competing the biotin-DNA and thus has a greater affinity to the binding protein/s. The same difference was observed across all the replicates (Figure 3.7, Figure 3.8 and Figure 3.9).

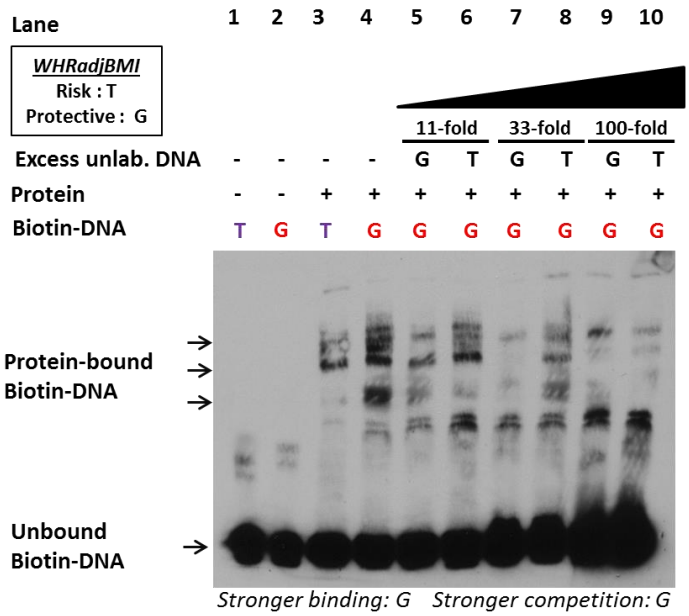

Figure 3.7 | The G allele at rs3936510 shows stronger binding affinity, representative blot. 38bp biotin-labelled DNA probes surrounding rs3936510 with either the T or G allele were incubated with nuclear protein from hWAT cells differentiated for 4 days. This resulted in shift of the biotin-DNA due to protein binding (shown with arrows). The G allele showed consistently more intense bands than the T allele, suggesting higher binding affinity of this sequence. This was supported by the titration of the unlabelled DNA of identical sequence – the unlabelled G allele sequence competed with the biotin-labelled DNA better than the T allele and resulted in fainter bands. The blot was repeated 3 times. Below, qualitative assessment of which allele showed stronger binding or competed more effectively in titration assay.

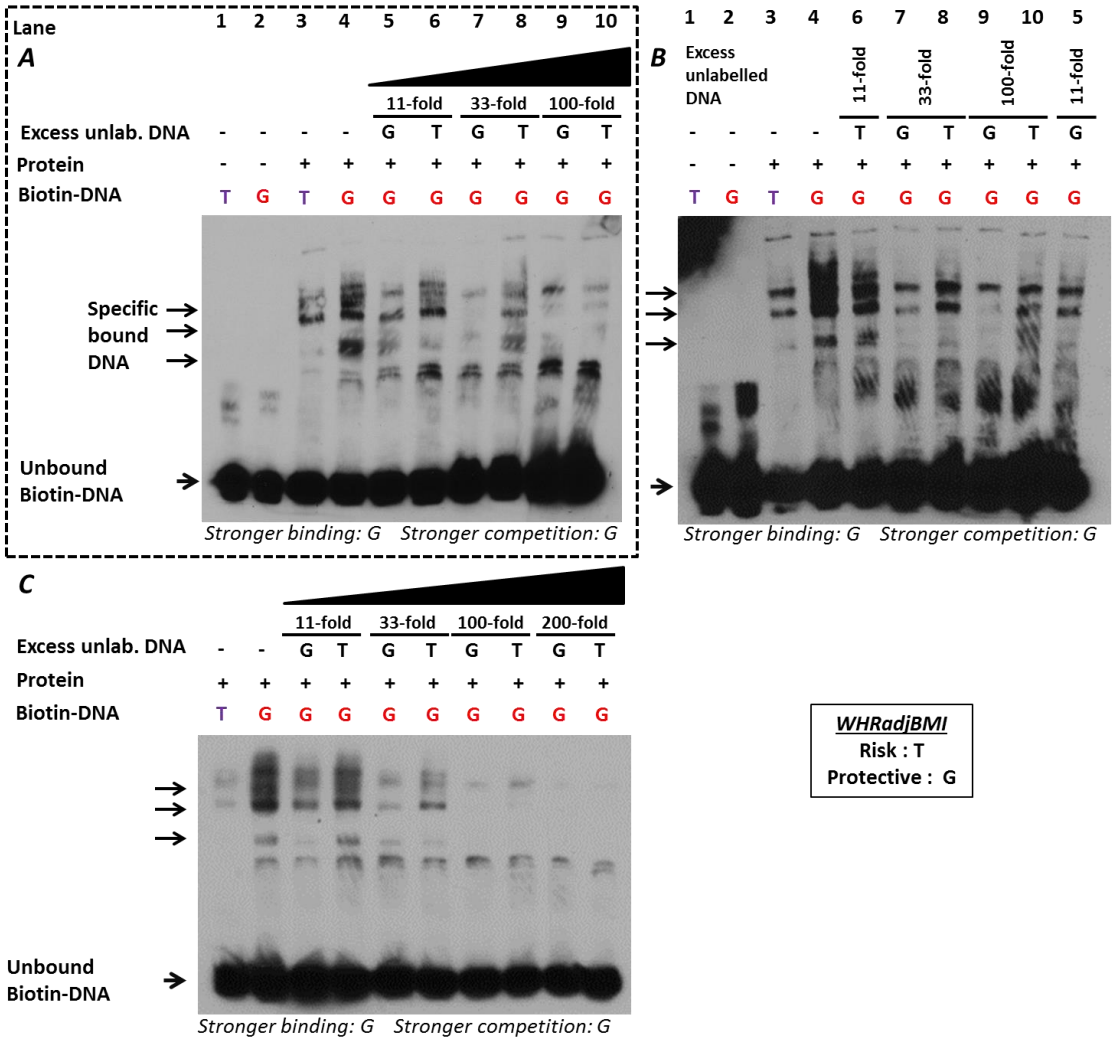

Figure 3.8 | rs3936510 EMSA replicates. In all the experiments, the G-containing oligonucleotide showed consistently stronger binding compared to the T allele. In the competition experiments the unlabelled G allele competed better than the unlabelled T allele. Representative image shown in Figure 3.7 is marked with dotted line (A). Below, qualitative assessment of which allele showed stronger binding or competed more effectively in titration assay.

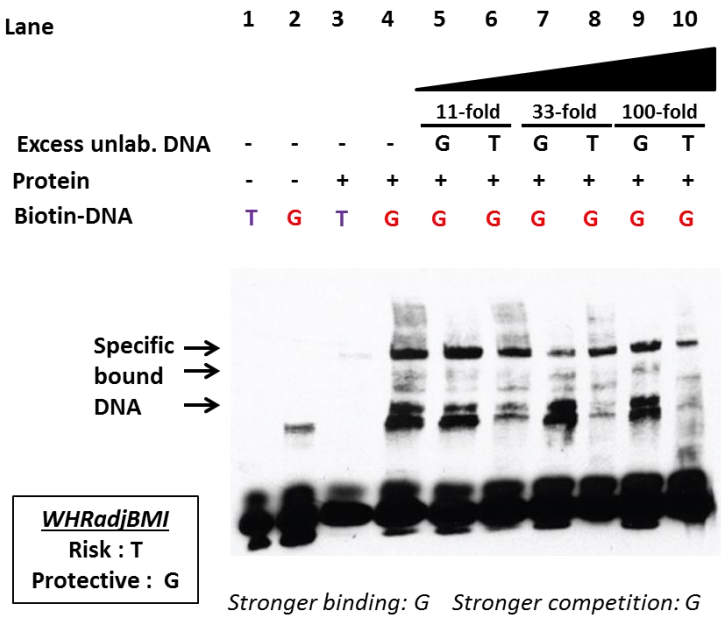

Figure 3.9 | Independent repeat of rs3936510 EMSA. Carried out by Dr Dumbell using independently annealed oligonucleotides. The blot replicates previous results with stronger binding and additional bands for the G allele. Below, qualitative assessment of which allele showed stronger binding or competed more effectively in titration assay.

3.3.4. T allele of rs3810068 introduces a new CEBPß binding site within the *EMILIN2* promoter

The binding profiles for the C and T allele-containing oligonucleotides of the rs3810068 were markedly different (Figure 3.10, lanes 2 and 7) with the T allele biding multiple additional bands. These bands were clearly specific as they were removed by excess unlabelled oligonucleotides (Figure 3.10, lanes 3-4 and 8-9). Based on JASPAR analysis (http://jaspar.genereg.net/) of the SNP-surrounding sequence, rs3810068 was predicted to alter a consensus binding site for CEBPß, a key transcriptional regulator (Fornes *et al.*, 2019) (Figure 3.1). I thus tested for its binding using an anti-CEBPß antibody (Rosen and MacDougald, 2006). Upon co-incubation of the antibody with hWAT nuclear protein and the T oligonucleotide, the T-specific bands disappeared and instead a new super-shifted band was observed (lane 5). Strikingly, no super-shift was detected with the C oligonucleotide (lane 10). This result was replicated multiple times (Figure 3.11, Figure

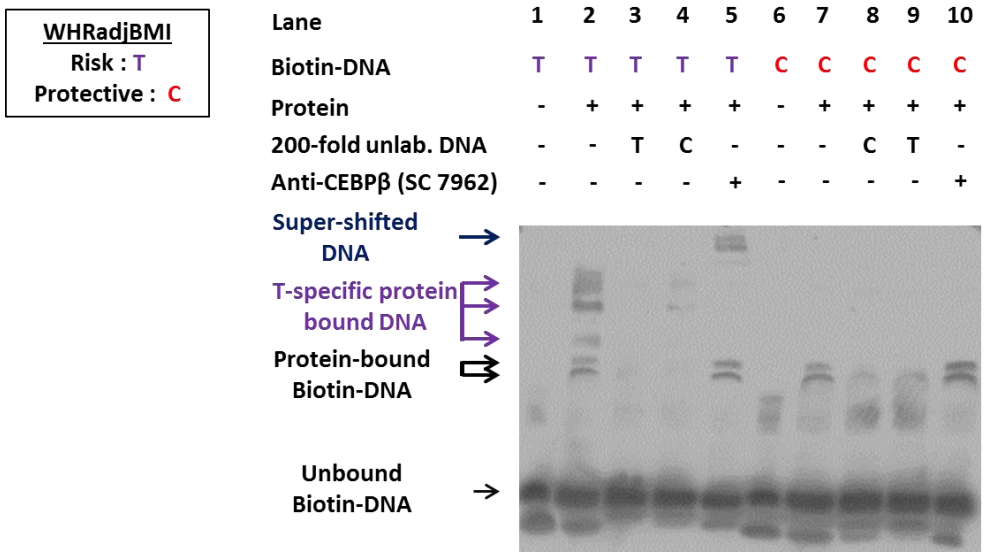

Figure 3.10 | Representative EMSA blot for rs3810068 at *EMILIN2* locus.

38bp biotinylated DNA probes surrounding rs3810068 with either the T or C allele were incubated with nuclear protein from hWAT cells differentiated for 4 days. This resulted in shift of the biotin-DNA due to protein binding (shown). These bands disappear upon incubation with the excess DNA of the same sequence suggesting that the interaction is sequence specific. There were additional bands seen exclusively with the T allele (shown). These bands were super-shifted (shown) upon incubation with the anti-CEBPβ antibody, but no difference was seen for the C allele.

3.12). Thus at least some of the T-specific bands observed in lane 2 involve binding of the oligonucleotide to CEBPß, which is interrupted with the C allele.

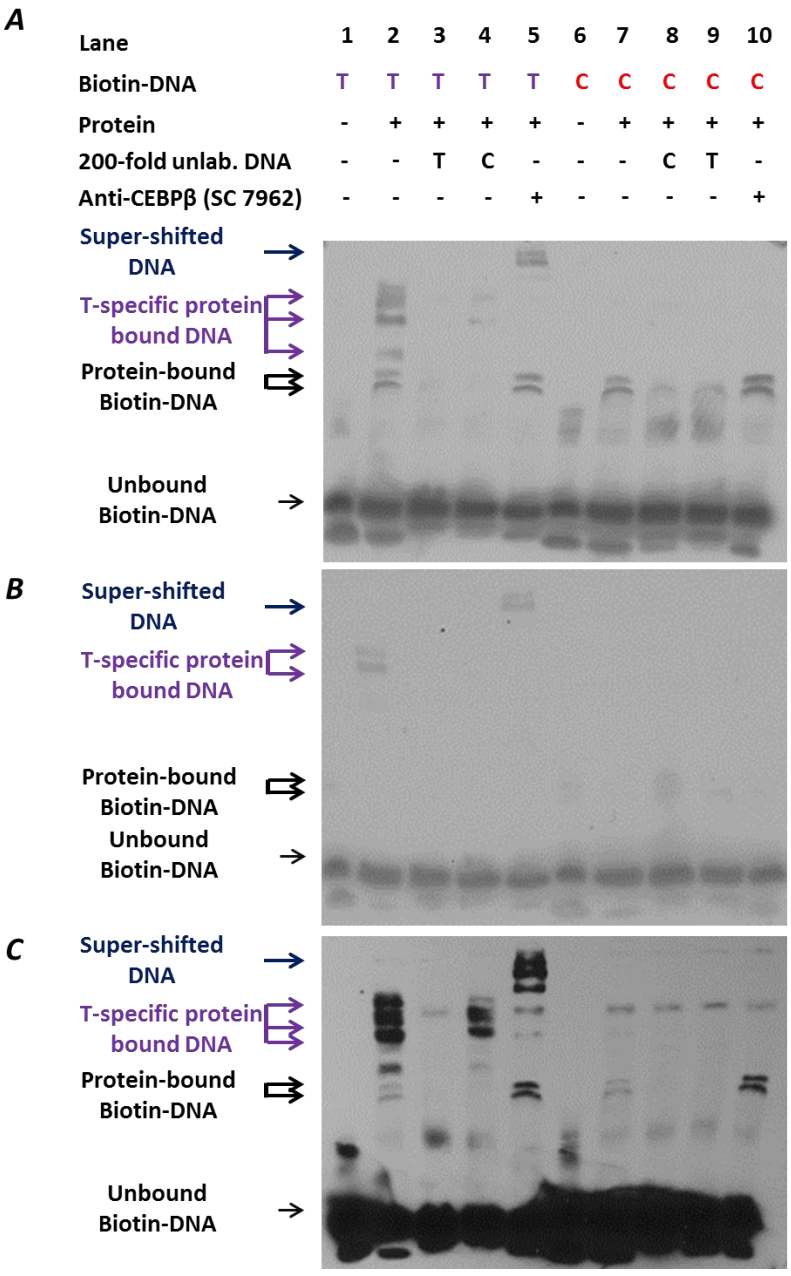

Figure 3.11 | Replication of representative *EMILIN2* EMSA.

The T-oligonucleotide consistently showed additional bands that were not seen with the C allele. Upon co-incubation with the CEBPβ antibody these bands were super-shifted indicating T-specific binding of the oligonucleotide to CEBPβ. (A) Showing the representative image from Figure 3.10. B and C are independent replicates.

To confirm this finding and the antibody specificity, I performed a *CEBPß* siRNA knockdown in Day 4-differentiated hWAT cells, extracted nuclear protein and showed a marked reduction in CEBPß level **(**Figure 3.13A). Incubation of *CEBPß*-KD nuclear protein with rs3810068 oligonucleotides resulted in reduced intensity of the T-specific bands compared to nonsense-KD protein (Figure 3.13B, lanes 2 and 3). More importantly, the T-specific super-shifted band (lane 4) completely disappeared upon KD (lane 5). There were no marked changes in the binding profile of the C-oligonucleotide due to *CEBPß* KD (lanes 7-8). These results were replicated 3 times (Figure 3.14, Figure 3.15). In summary, the T allele of rs3936510 establishes CEBPß binding in differentiating hWAT cells which is disrupted by the alternative C allele.

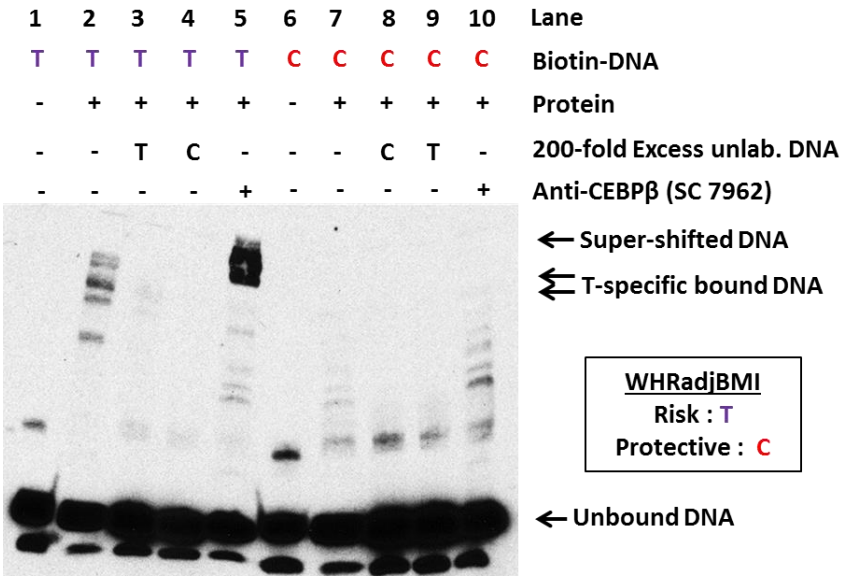

Figure 3.12 | Independent repeat of rs3810068 EMSA. Carried out by Dr Dumbell using independently annealed oligonucleotides. This blot clearly replicates previous results.

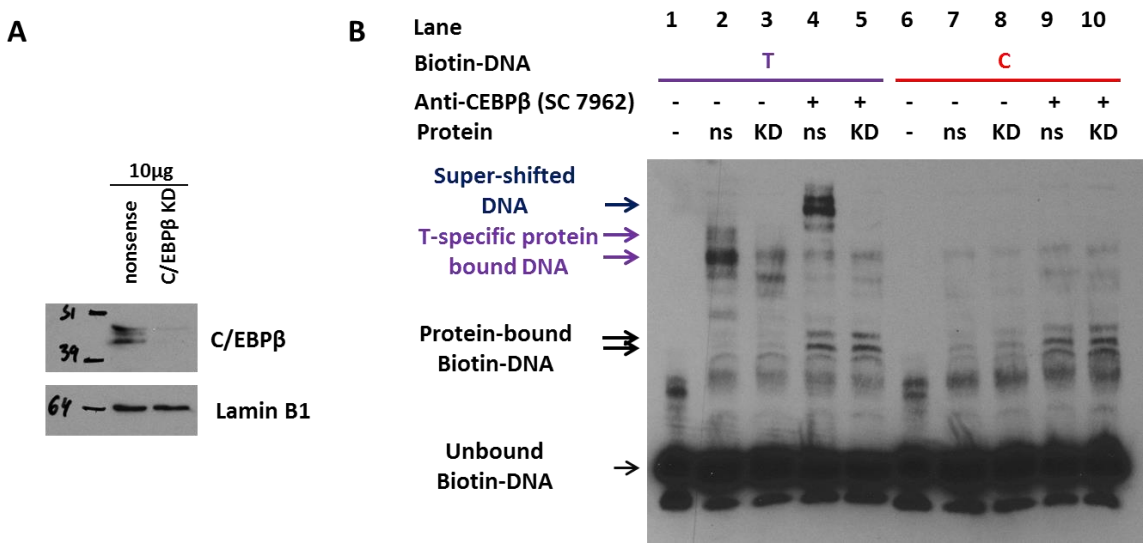

Figure 3.13 | Representative EMSA blot for rs3810068 at *EMILIN2* locus upon *CEBPβ* silencing. A. hWAT cells were differentiated for 4 days and then silenced with either nonsense or CEPBβ-silencing siRNA for 48 hours. The nuclear protein was extracted and knockdown was assessed and shown to be highly effective by Western Blot. **B.** 38bp biotin-labelled DNA probes surrounding rs3810068 with either the T or C allele were incubated with Day 4 differentiated hWAT cell nuclear protein, treated with nonsense (NS) or *CEPBβ*-silencing siRNA (KD). The T-allele super-shifted bands (shown) disappeared upon *CEPBβ* knockdown, but there is no change for the C allele suggesting that CEBPβ is specifically involved in the T-allele-protein interaction. The knockdown was repeated three times with 2 technical replicates per experiment.

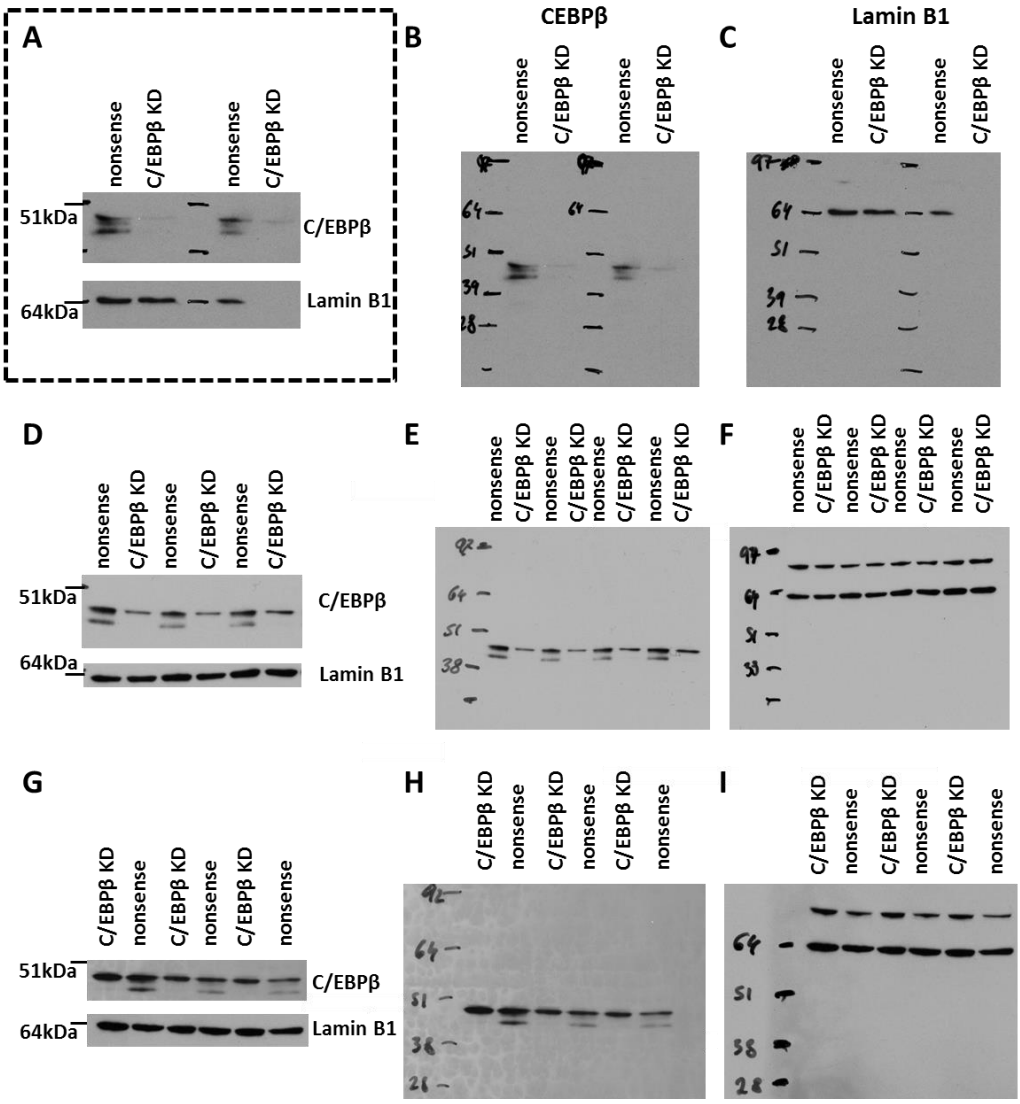

Figure 3.14 | *CEBPβ* knockdown Western Blot replicates. Three independent knockdown experiments were performed in Day 4 differentiated hWAT cells. All replicates showed consistent results with the lower band of CEBPβ at around 40 kDa losing intensity. In replicates A & D, the upper band is also markedly fainter. Each gel (A, D, G) shows 2-4 replicates of the same protein sample from a single experiment. Representative image shown in Figure 3.13 is marked with dotted line. B and C, E and F, H and I show the full blots of figures A, D and G, respectively.

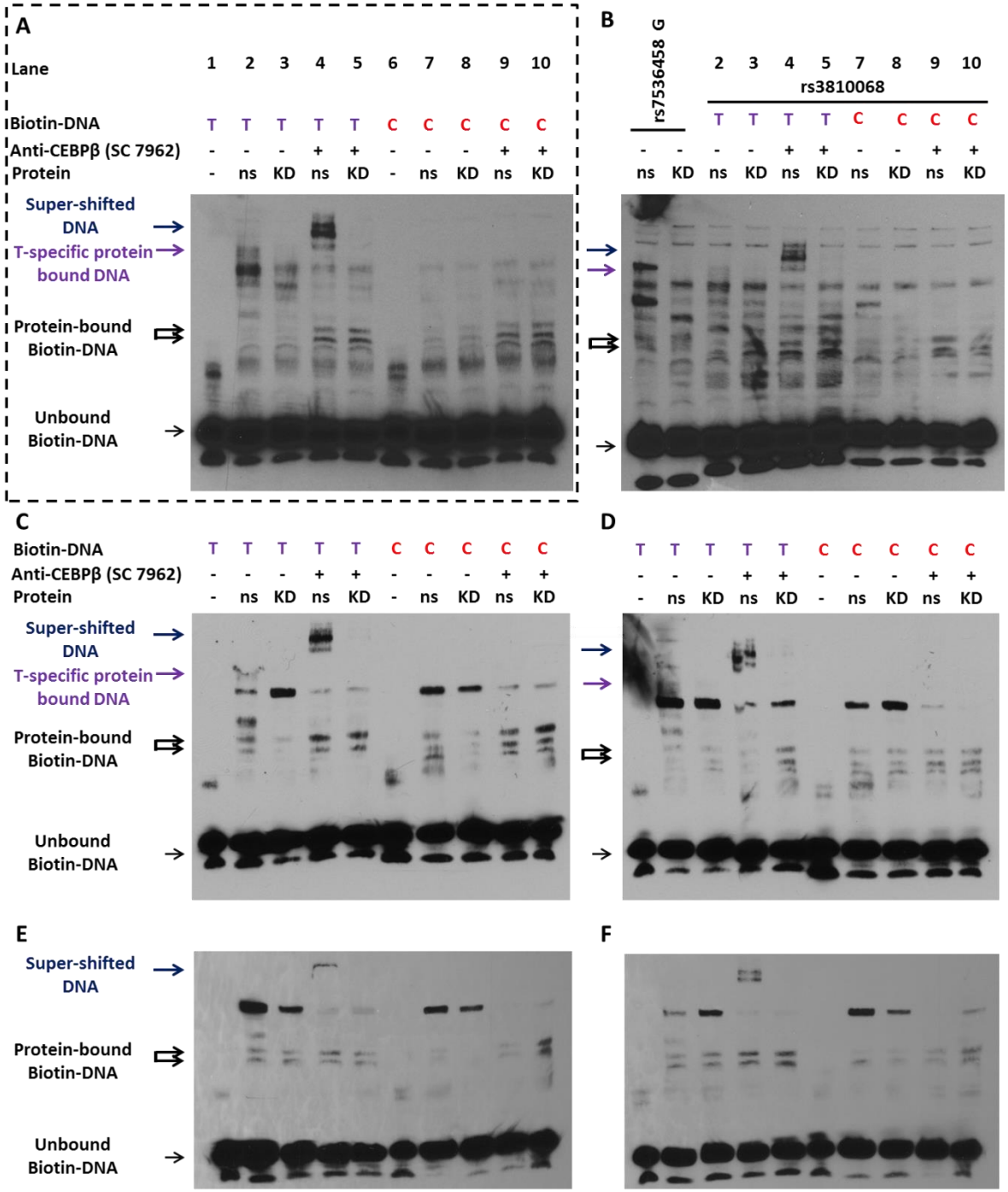

Figure 3.15 | *CEBPβ* knockdown EMSA replicates. Three independent knockdown experiments were performed in Day 4 differentiated hWAT cells with 2 technical replicates for each. In all replicates the T-allele specific super-shifted bands disappeared upon *CEBPβ* knockdown. The effect of *CEBPβ* knockdown on disappearance of T-specific bands without antibody co-incubation in (A) was not reproduced in blots E and F. Representative image (A) shown in Figure 3.13 is marked with dotted line. In the blot B, also an additional SNP rs7536458 for an unrelared experiment was included.

3.3.5. Transfection and luciferase assay in hWAT cells

To test the effect of the SNPs on gene expression, 1kb fragments centred on the SNPs with either allele were cloned into luciferase reporter vectors and transfected Day 4-differentiated hWAT cells. The putative enhancer fragments in the *VEGFA* and *C5orf67* loci were cloned upstream of a SV40 promoter to test for enhancer activity. The promoter region at *EMILIN2* was cloned upstream of a minimal promoter into an enhancer-containing vector to test for promoter activity. I first determined the optimal conditions for transfection of hWAT cells in the 96-well format with the maximum reaching 10% transfected cells (Figure 3.16). Based on these findings, I used 0.2µg plasmid, 0.3µl Lipofectamine 3000 per well in all the following experiments.

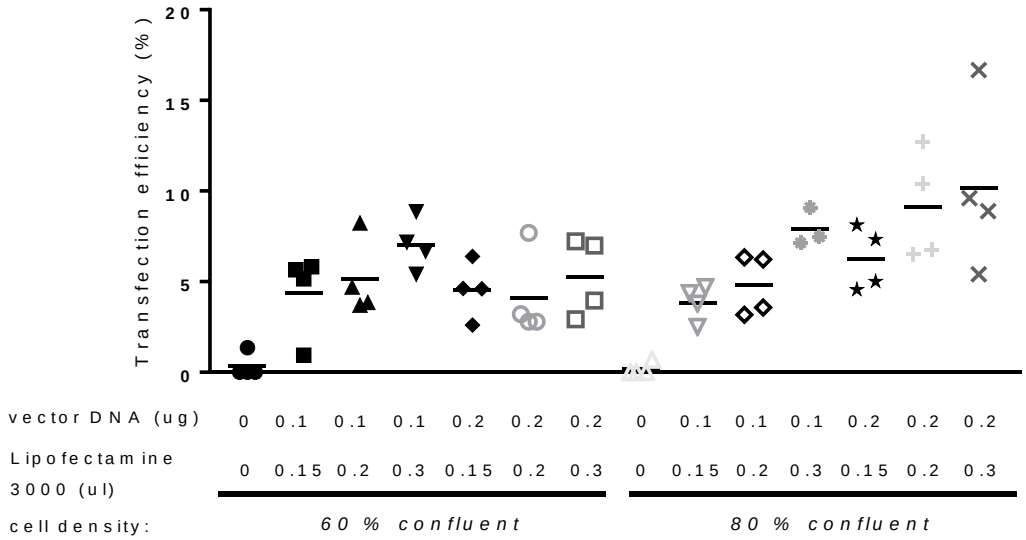

Figure 3.16 | Transfection efficiency optimisation. Day 4-differentiated adipocytes were plated in a 96-well plate to reach either 60% or 80% confluence the next day. Cells were transfected with a pEGFP_C1 using different plasmid and Lipofectamine 3000 concentrations. Transfection efficiency was calculated by dividing the number of GFP+ve cells by the total number of DAPI-stained nuclei.

3.3.6. Enhancer activity in the *VEGFA* locus shows high variability between replicates

The rs998584-containg fragment of the *VEGFA* locus showed significant enhancer activity with both the C (P=0.01) and A (P=0.037) alleles (Figure 3.17). However, as shown in Figure 3.18, the replicates for this locus showed high variability, with two replicates (C, D) not showing any enhancer activity and only the C allele showing significant activity in replicate A (P=0.009). Although most replicates of the positive control vector (CTRL) treated cells showed reporter activity ~50 higher than the empty vector, wide variability within the experiment was also observed in this case. This could be most likely explained by poor transfection efficiency in these replicates. No difference was observed between the 2 alleles in any of the replicates.

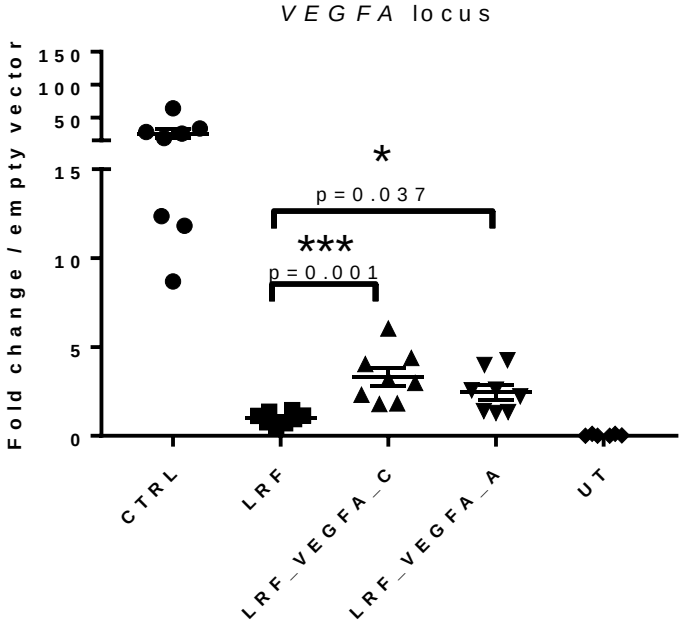

Figure 3.17 | Enhancer activity was detected at the *VEGFA* locus, representative figure.The 1kb region surrounding rs998584, with either the risk A allele (LRF_VEGFA_A) or protective C allele (LRF_VEGFA_C) allele, was cloned into the LRF vector in forward orientation and transfected into Day 4-differentiated hWAT cells. Significant difference from the empty vector (LRF) was detected for both alleles, but there was no difference between the alleles. Comparison is by one-way ANOVA with multiple comparisons (shown) between LRF (empty vector), LRF_VEGFA_A and LRF_VEGFA_C. CTRL: pGL3-Control, UT: untransfected. Carried out by Dr Dumbell.

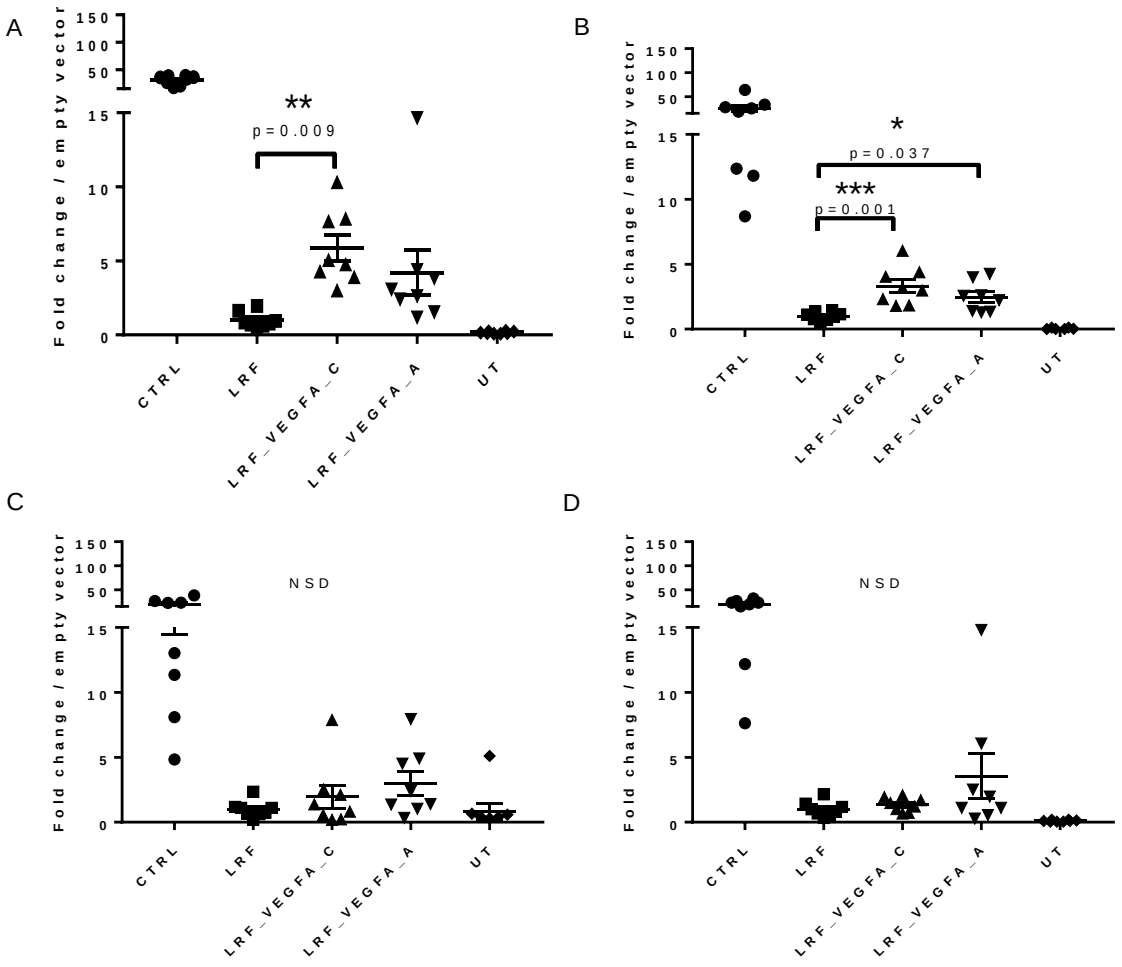

Figure 3.18 | *VEGFA* Enhancer Luciferase Assay Replicates. Enhancer activity was detected in LRF_VEGFA_C (A, B) and LRF_VEGFA_A (B) and no significant enhancer activity was detected in replicates C or D. Comparison is by one-way ANOVA (B, C) or Kruskall-Wallis test (A, D) with multiple comparisons between LRF (empty vector), LRF_VEGFA_A and LRF_VEGFA_C. CTRL: pGL3-Control, UT: untransfected, NSD: no significant difference. Replicate B was chosen as representative in Figure 3.17.

3.3.7. Enhancer activity is detected at the *C5orf67* locus

For the *C5orf67* locus, I cloned the rs3936510 containing fragment in either forward or reverse orientations with either allele. Enhancer fragments containing both alleles in both orientations were able to drive significantly higher luciferase expression relative to the respective empty vectors (Figure 3.19). 3 of the 4 replicates of this experiment detected enhancer activity in the region (Figure 3.20). No difference was detected between the alleles in either orientation in none of the replicates.

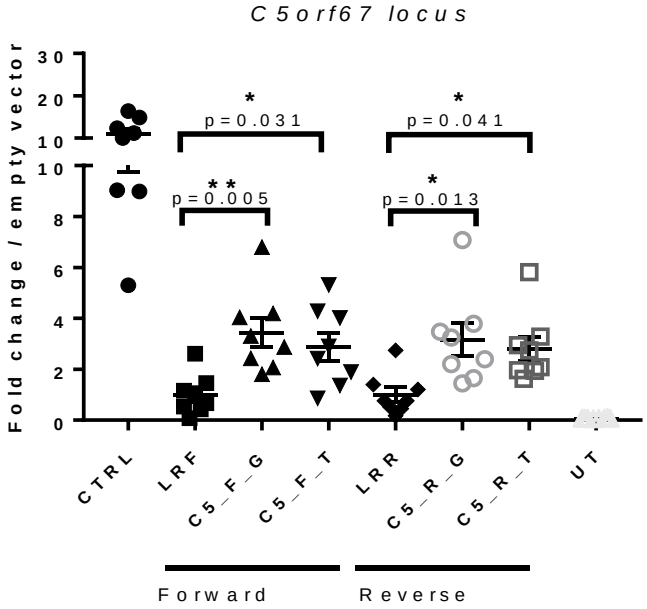

Figure 3.19 | Enhancer activity was detected at the *C5orf67 locus*, representative figure. The 1kb region surrounding rs998584 was cloned into either the forward or reverse orientation in LRF or LRR empty vectors, respectively, and transfected into Day 4-differentiated hWAT cells. This replicate was chosen to demonstrate that enhancer activity could be detected in all orientations and for both G and T SNP containing constructs. There was no significant difference between the alleles. Statistical comparison is within forward or reverse orientation vectors with one-way ANOVA, and multiple comparisons (shown). CTRL: pGL3-Control, UT: untransfected. LRF: empty vector forward, LRR: empty vector, reverse. Carried out by Dr Dumbell.

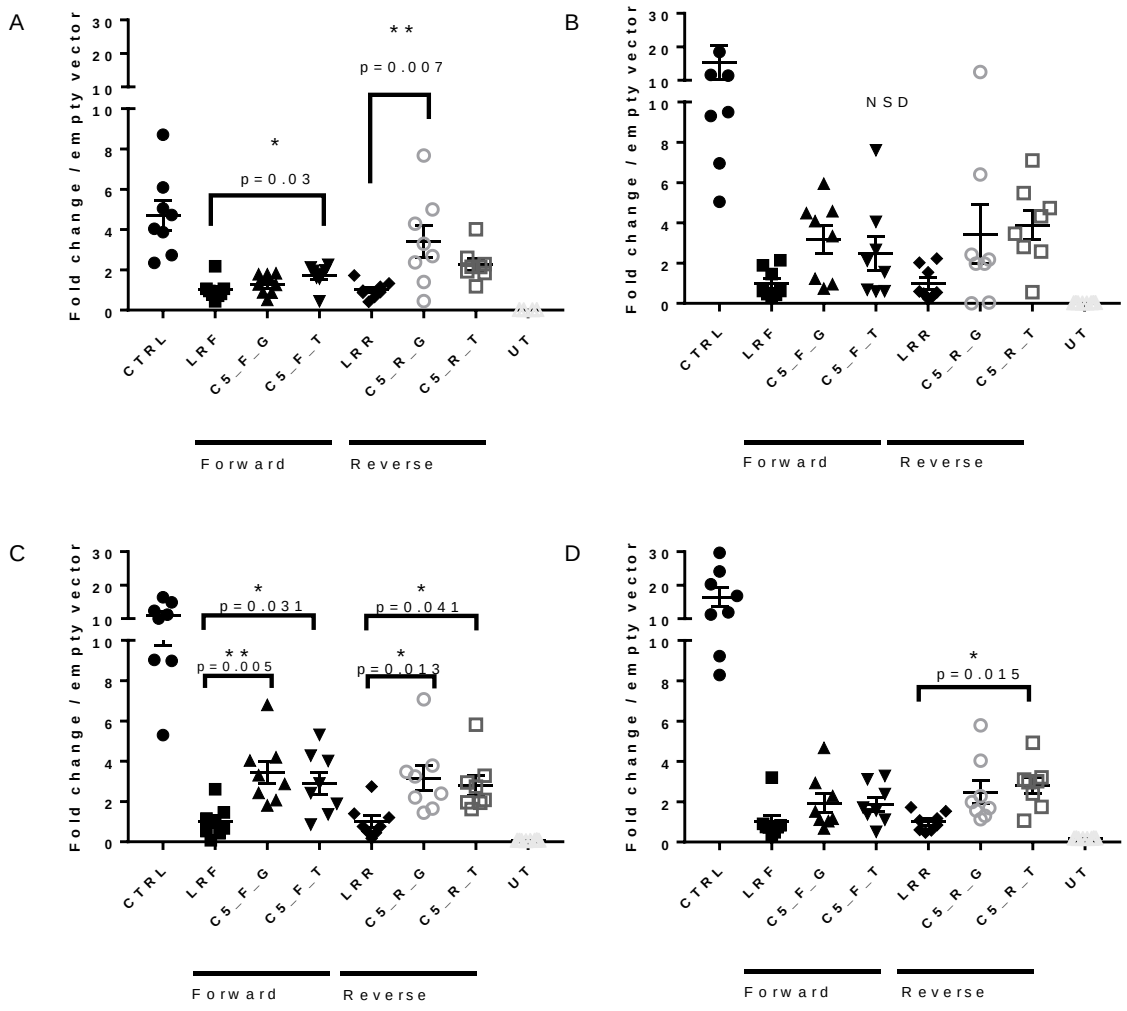

Figure 3.20 | *C5orf67* Enhancer Luciferase Assay Replicates. Enhancer activity for either the G or T allele in either the forward or reverse orientation was detected in all but one replicate (B). Statistical comparison is within forward or reverse orientation vectors with one-way ANOVA, and multiple comparisons (shown). Shown are multiple comparison statistics. CTRL: pGL3-Control, UT: untransfected, NSD: no significant difference. Replicate C was chosen as representative in Figure 3.19.

3.3.8. Promoter activity is detected in the region overlapping rs3936510

At the *EMILIN2* locus, both T and C-allele containing promoter regions drove significantly higher luciferase expression compared to the empty vector (Figure 3.21). In one of the replicates, only the T-allele containing fragment showed promoter activity (Figure 3.22). No significant difference was observed between the T and C allele-containing vectors.

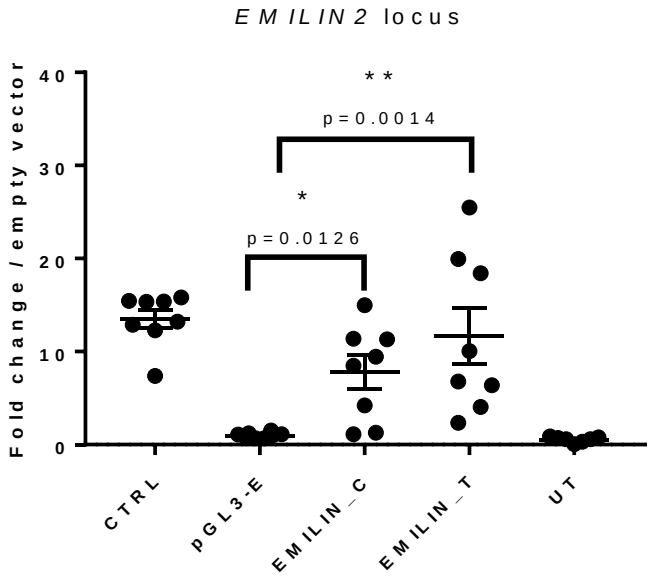

Figure 3.21 | *EMILIN2* promoter luciferase assay, representative figure. The 1kb region surrounding rs3810068, with either the risk T allele (pGL3_EMILIN_T) or protective C allele (pGL3_EMILIN_C) allele was cloned into the pGL3 Enhancer (pGL3_E) vector in forward orientation and transfected into Day 4-differentiated hWAT cells. Significant promoter activity was detected for both alleles, but no significant difference was observed between the alleles. Statistical comparison is Kruskal-Wallis test with multiple comparisons (shown). CTRL: pGL3-Control, UT: untransfected. Carried out by Dr Dumbell.

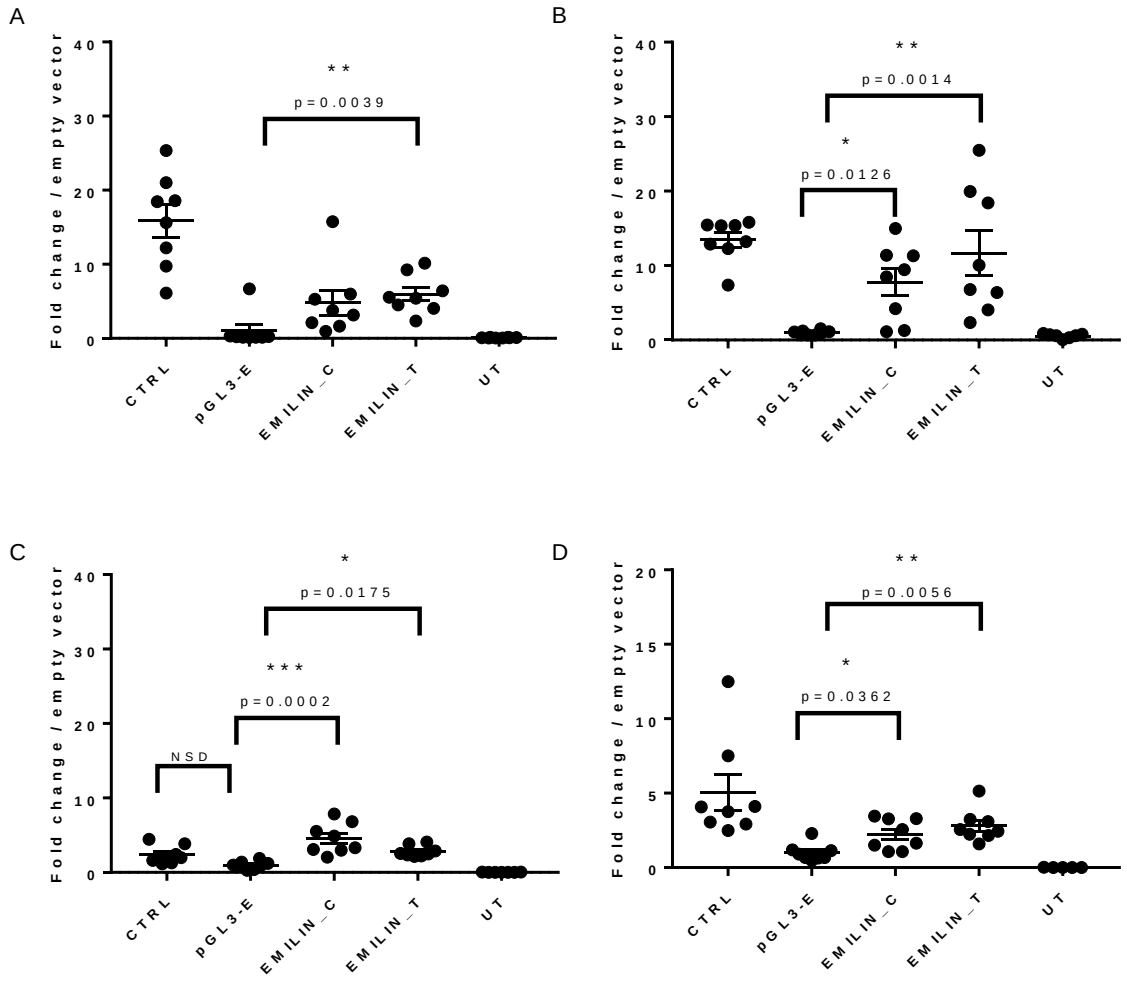

Figure 3.22 | *EMILIN* Luciferase Promotor Assay Replicates. B,D: Promotor activity can be detected in both alleles. A: Promoter activity detected only with the T construct. No significant differences (NSD) between constructs containing alternative alleles can be detected in either of the assay replicates. C: no significant difference between CTRL and empty vector (pGL3-E), this replicate should be discounted. D: Independent replicate carried out by me (Milan Mušo) using same plasmids as A-C. Comparisons are by Kruskal-Wallis test with multiple comparisons (shown). Replicate B was chosen as representative in Figure 3.21.

3.3.9. *EMILIN2* is a potential functional gene in the *EMILIN2* locus

Of the 3 SNPs studied, rs3810068 was the only one to show an eQTL signal, specifically for *EMILIN2* expression, in the GTEx database (GTEx-Consortium, 2013). This is in line with rs3810068 overlapping the *EMILIN2* promoter. However, it has been shown that promoters may act as enhancers also for more distant genes (Medina-Rivera *et al.*, 2018). Indeed, the TAD of this locus contains at least two other genes including Structural maintenance of chromosomes flexible hinge domain-containing protein 1 (*SMCHD1)* and Lipin 2 (*LPIN2)* (Figure 3.23). As *LPIN2* was previously associated with metabolic traits, I performed a GWAS-eQTL co-localisation to determine the most likely functional gene in the locus (Aulchenko *et al.*, 2007). The strongest correlation for rs3810068 was confirmed for *EMILIN2*, suggesting that *EMILIN2* is a potential novel regulator of fat distribution (Figure 3.24).

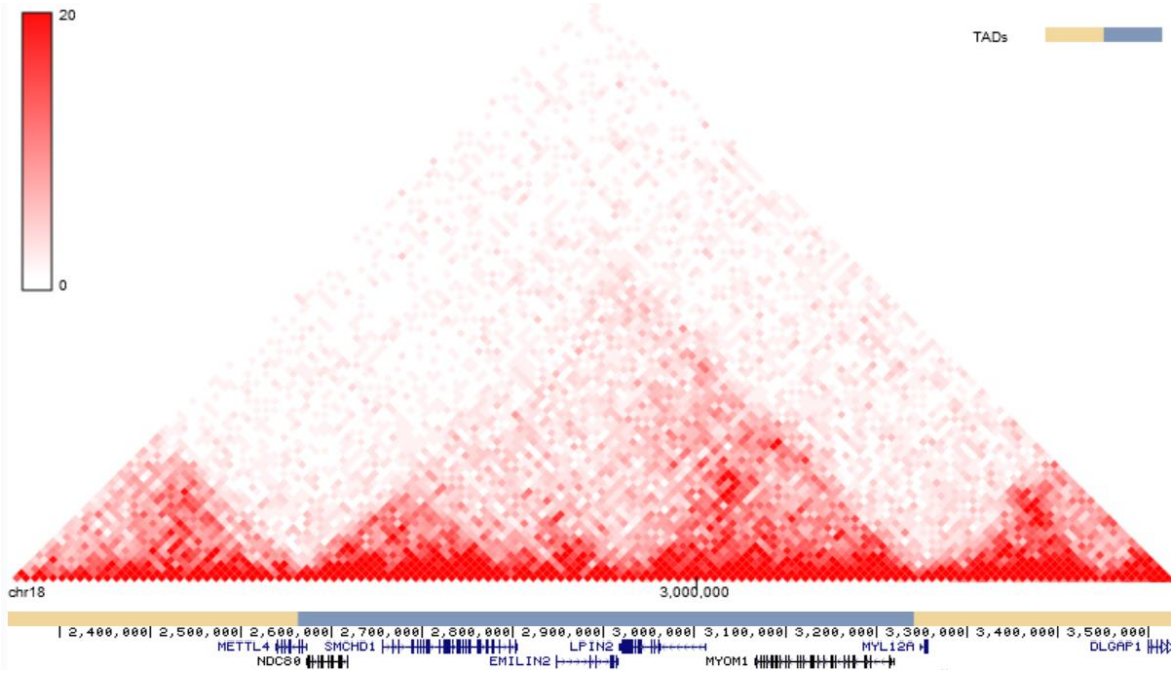

Figure 3.23 | Hi-C interaction map surrounding the *EMILIN2* locus. 3D Genome Browser (http://promoter.bx.psu.edu/hi-c/) image of the Hi-C interactions in IMR90 fibroblasts shows the Topologically Associated Domain (TAD), containing *EMILIN2* locus, in blue. Apart from *EMILIN2*, the TAD contains several other genes including *SMCHD1* and *LPIN2* (Rao *et al.*, 2014; Y. Wang *et al.*, 2018).

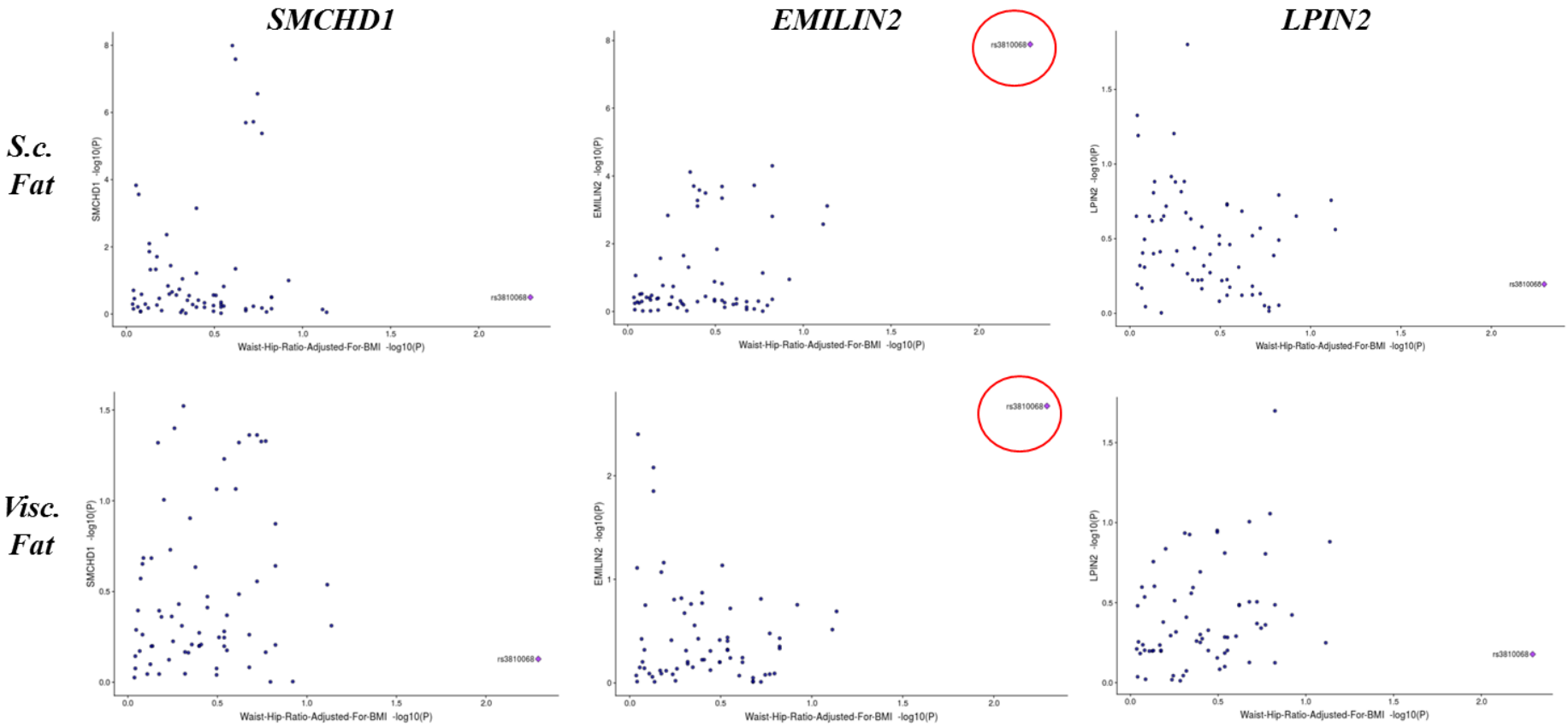

Figure 3.24 | Colocalisation of *SMCHD1*, *EMILIN2* and *LPIN2* expression association in SCAT and VAT with sex-combined WHRadjBMI signal from Shungin et al, 2015. Y-axis shows the p-value for the eQTL association for each SNP, x-axis shows the p-value for the WHRadjBMI associations. Each graph denotes the position of the locus lead SNP rs3810068 and the position of the 3 SNPs in the 1.5kb previously fine-mapped region (Liu *et al.*, 2014). Graphs generated by the LocusCompare online tool (http://locuscompare.com/) (Boxiang Liu, Mike Gloudemans, 2018).

3.4. Discussion

Here I show how high confidence GWAS-association signals in the *C5orf67* and *EMILIN2* loci, selected based on high PPA values and overlap with regulatory elements, act to alter transcription factor binding to DNA in the differentiating hWAT cells. In agreement with this, disease-associated SNPs were previously found to be enriched in enhancer clusters with an effect on DNA-protein binding (Pasquali *et al.*, 2014). In the *VEGFA* locus, the results were very highly variable across technical replicates, indicating that protein binding differences might be subtle and highly sensitive to experimental fluctuations. In the case of the *EMILIN2* locus, I observed a direct effect of rs3810068 on the binding of C/EBPβ, a key transcription factor for early adipocyte differentiation (Tang, Otto and Lane, 2003). This suggests that rs3936510 might affect early adipocyte differentiation programmes downstream of C/EBPβ. Multiple protein-bound DNA bands were affected by the allelic difference in both *EMILIN2* and *C5orf67* loci, indicating that the binding of different, additional and/or co-recruited proteins is affected by the SNPs. In agreement with this, the motifs of about a quarter of the ~1600 human transcription factors remain unknown and also many of the known TF motifs are not occupied by their predicted TFs under physiological conditions (Lambert *et al.*, 2018).

Using luciferase assays, Dr Dumbell and I showed that SNPs in the *C5orf67* and *EMILIN2* loci overlap active regulatory sequences, confirming the annotation derived from the epigenetic profiles. However, no significant differences in luciferase activity between the two alleles were observed in any of the loci. Also, the enhancer activity in the *VEGFA* locus was detected only in half of the luciferase experiments. The poor transfection efficiency (<10%) of the hWAT cell line potentially reduced the sensitivity of the assay to discern the low effect-size GWAS variants and could contribute to this result (Bush and

Moore, 2012). To increase the sensitivity, a more efficient transfection method for adipocytes such as nucleofection could be used (Zaragosi *et al.*, 2007). Alternatively, the motif surrounding the alleles could be multiplied into a concatamer, upstream of the luciferase gene as done previously to study SOX9 DNA binding (Sekiya *et al.*, 2000). Although there is evidence indicating that transfected plasmids might be packaged into histones, many aspects such as biochemical compatibility of specific enhancers and exogenous promoters might be altered in heterologous plasmids (Mladenov and Russev, 2009; Arensbergen, Steensel and Bussemaker, 2014). Furthermore, it is possible that the variants have a functional effect at a specific developmental time-point. Studies in differentiating 3T3-L1 mouse preadipocytes have shown chromatin undergoes extensive remodelling during adipogenesis with the largest number of DNase hypersensitivity sites (DHSs) appearing already 4 hours after the induction of differentiation (Siersbaek *et al.*, 2011). Variants could also affect the preadipocyte pools by affecting enhancer activity further upstream in the mesenchymal stem cells (Q. Chen *et al.*, 2016). Our model of day-4 differentiated hWAT cells thus captures only a limited window of adipogenesis and a functional role of the SNPs in a different developmental time point cannot be fully excluded.

One of the main aims following the GWA studies is the identification of effector genes in each locus. An effective way to predict these is by co-localisation of the GWAS and eQTL signals (Hormozdiari *et al.*, 2016a). Out of the 3 SNPs in this study, rs3810068 in the *EMILIN2* locus is the only one to also harbour an eQTL signal in the GTEx database (GTEx-Consortium, 2013). The T risk allele, which I showed to cause C/EBPβ binding in differentiating hWAT preadipocytes, is significantly associated with lower *EMILIN2* levels only in subcutaneous, but not visceral, adipose tissue, suggesting a potential depot-specific effect. C/EBPß binding is generally associated with transcriptional activation, but

it has also been reported to associate with the transcriptional repressor HDAC1 and can be heavily regulated by post-translational mechanisms (Wiper-Bergeron *et al.*, 2003; Park, Qiang and Farmer, 2004; Tang *et al.*, 2005). The direction of the effect on *EMILIN2* expression may thus depend on the developmental stage of adipocytes and other associatted co-factors. EMILIN2, the elastin microfibril interface-located protein 2, is an extracellular matrix glycoprotein that has been previously shown to promote cell death and angiogenesis, one of the key pathways enriched amongst WHR genes (Mongiat *et al.*, 2007; Shungin *et al.*, 2015; Paulitti *et al.*, 2018). The alternation of *EMILIN2* expression in subcutaneous adipose tissue could regulate adipose size or number by modulating these pathways. This could be tested using cell line knockdown studies or the recently-generated *Emilin2* KO mice from The Jackson Laboratory. These mice show reduced grip strength and several blood phenotypes, whilst data on bodyweight and adiposity remain to be released (Smith *et al.*, 2018). To further study the *EMILIN2*, *VEGFA* and *C5orf67* loci, CRISPR mutagenesis of the candidate SNPs in hWAT cells could be followed by qPCR of genes within the topologically associating domain (TAD). Furthermore, assessing the interactions of the enhancers of interest by 3C-based chromatin-capture methods or fluorescence in situ hybridization (FISH) probes could reveal which promoters are likely to be affected by the enhancer variants (Pan *et al.*, 2018).

One of the greatest challenges of GWAS remains to functionally link risk variants to the phenotypic effects *in vivo*. Previous approaches such as the whole-body deletion of candidate effector genes in mice are not informative with regards to the tissue-specificity of multiple enhancer elements (Laber and Cox, 2017). On the other hand, the multiple developmental origins of adipose depots make identifying a reliable preadipocyte marker for adipose-specific deletions difficult (Sanchez-Gurmaches, Hung and Guertin, 2016; Sebo and Rodeheffer, 2019). None of the 3 regulatory SNPs studied here are conserved in

mice and direct CRISPR SNP-mutagenesis in mice is thus also not a possibility. However, although the non-coding DNA sequence is under low evolutionary constraint between human and mice, regulatory elements may maintain function without strong sequence conservation (Fisher *et al.*, 2006; Wilson *et al.*, 2008; Stergachis *et al.*, 2014). Thus, as demonstrated for two cardiac-specific enhancers, deleting SNP-harboring enhancers can effectively elucidate the effector genes and disease risk mechanisms (Dickel *et al.*, 2016). Other approaches such as humanization of a whole GWAS locus in mice are especially useful for loci with a potential for multiple causal variants.

3.5. Conclusion

This study investigated the functional mechanism of prioritised SNPs associated with WHRadjBMI. I demonstrate that rs3936519 in the *C5orf67* locus and rs3810068 at the *EMILIN2* locus affect the binding of transcription factors to CREs. In the *EMILIN2* locus, I show evidence for the specific effect on C/EBPß binding. Using luciferase assays, Dr Dumbell and I confirm the activity of the overlapping CREs, although the *VEGFA* locus shows highly variable results and no difference is seen between the alleles in any of the loci. Both technical limitations of the reporter assays and the specific spatiotemporal activities of the tested CREs may contribute to this finding. The SNP functionality could be further studied using CRISPR-Cas9 mutagenesis in cell lines. This will build evidence to support regulatory element deletion in mice in order to link our findings with effector genes and fat distribution.

4. Testing the *WARS2* 3'UTR SNP as a functional candidate for waist-hip ratio

4.1. Introduction

The *TBX15-WARS2* locus has been consistently associated with waist-hip ratio (WHR) across multiple meta-analyses and up to four potentially independent associations signals were discovered in the region (Figure 4.1, Table 4.1) (Heid *et al.*, 2010; Shungin *et al.*, 2015; Pulit *et al.*, 2018). In the UK Biobank data, the locus is also further associated with electrical impedance of whole body, leg and arm which are measures used for estimation of body fat and fat-free mass (Figure 4.2) (Canela-Xandri, Rawlik and Tenesa, 2018). Recently, a study in a population of Greenland Inuits has shown that an intergenic region of the *TBX15-WARS2* locus is introgressed from Denisovans and is one of the two loci under positive selection in this population (Racimo *et al.*, 2017). Thus multiple lines of evidence suggest the locus might be a key regulator of body fat distribution and could even provide evolutionary advantages in certain environmental conditions.

The *TBX15-WARS2* WHR-association signal spans ~1Mb and includes genes *TBX15*, *WARS2* and regions downstream of *SPAG17* (Figure 4.1). The transcription factor *TBX15* has been shown to regulate adipocyte differentiation of 3T3-L1 cells and primary preadipocytes, but has also other developmental roles (Singh *et al.*, 2005; Gesta *et al.*, 2011; Gburcik *et al.*, 2012; K. Y. Lee *et al.*, 2015). *TBX15* is differentially expressed across fat depots in both humans and mice, with high expression specifically in the murine subcutaneous inguinal white adipose tissue (iWAT) compared to the visceral gonadal WAT (gWAT) and in human abdominal subcutaneous adipose tissue (ASAT) compared to visceral adipose tissue (VAT) (Tam *et al.*, 2011; Chau *et al.*, 2014; Schleinitz *et al.*, 2014). Within the subcutaneous depots, *Tbx15* marks a glycolytic preadipocyte subpopulation

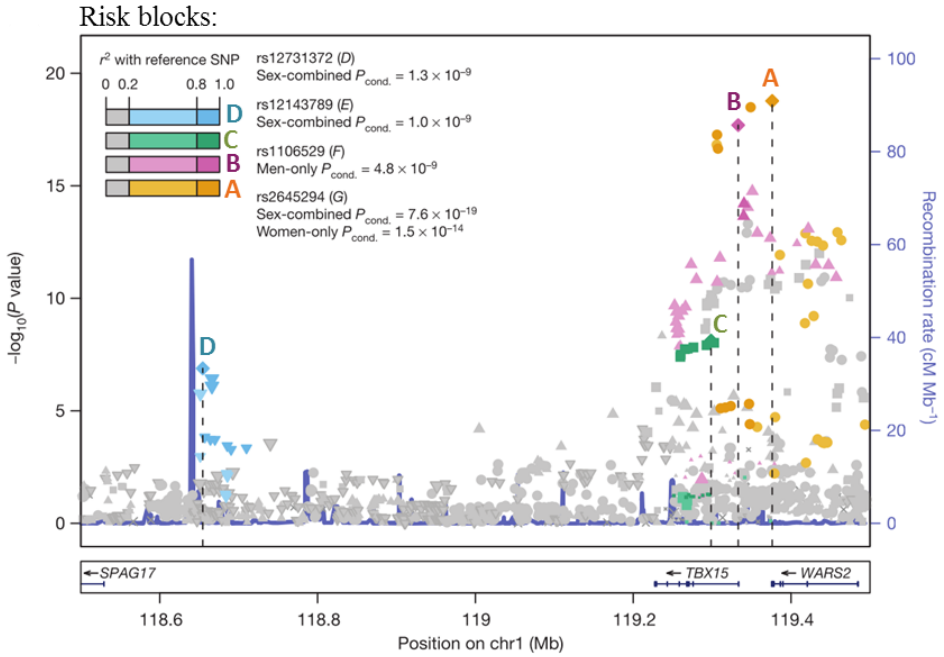

Figure 4.1 | The *TBX15-WARS2* waist-hip ratio locus.
Adapted graph of the *TBX15-WARS2* locus (x axis) against the $-\log_{10}$(P) values of SNP associations with WHRadjBMI (left y-axis) in the sex-combined meta-analysis of European individuals and estimated recombination rates (right y-axis) The different risk blocks are color-coded and the respective lead SNPs shown in the top right corner (Shungin et al., 2015).

(Lee *et al.*, 2017). The expression of both *TBX15* and *WARS2* in subcutaneous adipose tissue was associated with metabolic traits (Civelek, 2018). Although a few studies have linked the *TBX15-WARS2* risk SNPs to *TBX15* expression in adipose, the GTEx database in multiple tissues links the locus predominantly to the expression of *WARS2* (Figure 4.3) (Heid *et al.*, 2010; GTEx-Consortium, 2013; Civelek *et al.*, 2017). WARS2 is a mitochondrial tryptophanyl-tRNA synthetase, recently associated with angiogenesis and brown adipose tissue metabolism (Wang *et al.*, 2016; Pravenec *et al.*, 2017). Our group has previously established a *Wars2*$^{V117L/V117L}$ mutant mouse model that shows a complex phenotype including reduced overall adiposity, browning of white adipose tissue and whitening of brown adipose tissue (Agnew *et al.*, 2018). Importantly, rare variants in another member of the *ARS2* family, *DARS2*, have been associated with waist-hip ratio (Justice *et al.*, 2019). Further waist-hip ratio associations have been discovered in protein

coding genes of the mitochondrial genome (Kraja *et al.*, 2019). These findings together with the established role of mitochondria in adipose differentiation and browning make *WARS2* one potential functional gene in the locus (Wilson-Fritch *et al.*, 2003; Altshuler-Keylin and Kajimura, 2017).

Table 4.1 | The lead SNPs of the *TBX15-WARS2* locus.
NR not reported. r^2 values were based on 1000 Genomes Pilot 1 study. Data from (Shungin et al., 2015).

Risk Block	Lead SNP	Nearby genes	Effect allele	EA freq	β coeff	P	N	Lead SNP in:	LD (r^2) with rs2645294	Distance from rs2645294
A	rs2645294	WARS2	T	0.6	0.031	7.60E-19	209,808	Sex-combined	Same	Same
A	rs2645294	WARS2	T	0.6	0.035	1.50E-14	116,595	Women	Same	Same
B	rs1106529	TBX15	A	0.8	0.034	4.80E-14	93,401	Men	0.43	43kb
C	rs12143789	TBX15	C	0.2	0.026	1.00E-09	209,874	Sex-combined	0.06	77kb
D	rs12731372	SPAG17	C	0.8	0.024	1.30E-09	209,856	Sex-combined	NR	722kb

The existence of four distinct WHR association signals (risk blocks) in the *TBX15-WARS2* locus suggests that it is possible that multiple functional genes and mechanisms are involved. With up to 61 predominantly non-coding SNPs in close LD ($r^2 \geq 0.8$) with the lead SNPs, our collaborators provided us with unbiased approaches to prioritise candidate functional SNPs for testing effects on gene expression. To do this I combined the results of two different computational approaches, the Posterior Probability Analysis (PPA) by Cecilia Lindgren Group (The Big Data Institute, Oxford) and the epigenetic-Phylogenetic Module Complexity Analysis (epi-PMCA) by Melina Claussnitzer group (Broad Institute, USA), and our research group studied each risk block separately. In this study, I focus on Risk block A which shows some of the highest PPA scores and both a physical overlap and an eQTL signal with *WARS2*, the gene previously studied in our lab. I identify rs2645294 in the 3'UTR of *WARS2* as a candidate functional SNP and hypothesise that it influences RNA stability and post-transcriptional regulation of *WARS2*.

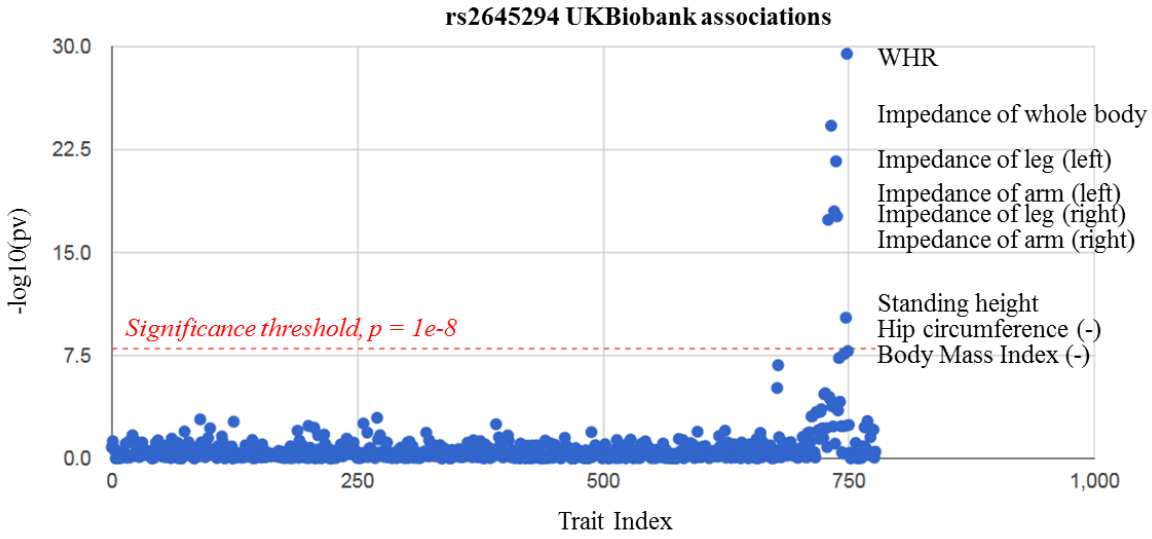

Figure 4.2 | The multiple associations of rs2645294.
Plot from Gene Atlas (http://geneatlas.roslin.ed.ac.uk/) showing the significant associations ($p \leq 1e\text{-}8$) of the lead SNP rs2645294 across the total of 778 traits in the UKBiobank data (Canela-Xandri, Rawlik and Tenesa, 2018).

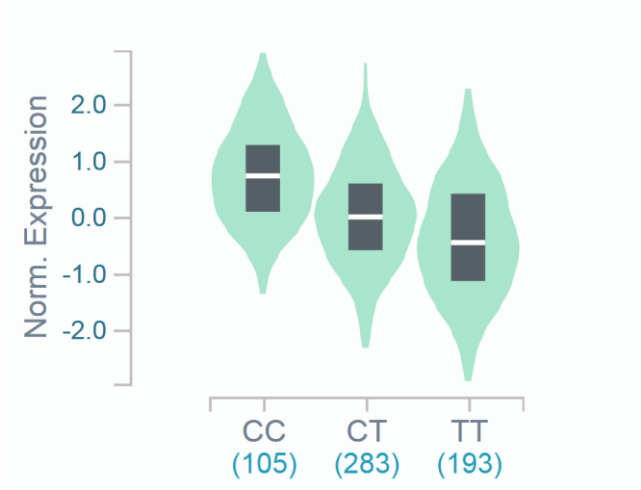

Figure 4.3 | rs2645294 is an eQTL for *WARS2* in subcutaneous adipose tissue.
Violin plot of rank normalised RNA expression data from GTEx individuals with either homozygous reference alleles (C|C), heterozygous (C|T) or homozygous for the alternative alleles (T|T). Significance reached $p = 4.7 \times 10^{-43}$. Similar association is seen in multiple other tissues (GTEx-Consortium, 2013)

4.1.1. Chapter hypothesis

Risk block A alters fat distribution by reducing *WARS2* levels. rs26452954, with the highest PPA score in the block, overlaps the 3'UTR of *WARS2* and is thus likely to regulate *WARS2* post-transcriptionally.

4.1.2. Chapter aims

1. To identify potentially functional SNP/s in the risk block A of the *TBX15*-*WARS2* locus. I combined PPA, epi-PMCA data with human adipose epigenetic tracks and EMSAs to prioritise the most likely functional SNP.

2. To test rs2645294 for an effect on *WARS2* mRNA stability. I performed nascent RNA qPCR, actinomycin D mediated transcription inhibition and 3'UTR luciferase assays to test the effect of rs2645294 on RNA stability.

4.2. Materials and methods

4.2.1. Bioinformatic prioritisation of SNPs

We prioritised SNPs using two different approaches. First, Sara Pulit (Cecilia Lindgren group, Big Data Institute, Oxford, UK) calculated the posterior probability of each SNP in the *TBX15-WARS2* locus, as described previously (Maller *et al.*, 2012). The analysis was performed independently for UK Biobank (UKBB) and The Genetic Investigation of Anthropometric Traits (GIANT) Consortium data in male-only, female-only or sex-combined individuals. All SNPs with PPA scores ≥ 0.2 in any of the sub-groups were chosen for further analysis.

Second, Nasa Sinnott-Armstrong (Melina Claussnitzer group, Broad Institute, Boston, USA) analysed SNPs in close LD ($r^2 \geq 0.8$) with the lead SNPs by the epigenetic-Phylogenetic Module Complexity Analysis (epi-PMCA), which builds on the PMCA, a method that estimates regulatory potential of SNPs by overlap with evolutionary conserved transcription factor (TF) binding sites and TF modules (Claussnitzer *et al.*, 2014). The four core PMCA statistics (number of TFs in TF modules in over half the species, number of TFs in modules in all species, number of TFs in total, and number of modules in total) were calculated for motif cut-offs of both loose (information content >= 5.25) and strict (information content >= 5.75) motif hits. The new epi-PMCA features included the mean effect size result of the sequence-based computational method for prediction of regulatory variation deltaSVM across mesenchymal cell types plus human foetal lung (IMR90) cells. It also included the maximum empirical p-value for deltaSVM across all cell types tested (calculated by randomly permuting the sequence of the reference allele and the 10bp on either side, then replacing the reference allele with the alternative allele in that new permuted context, 10000 times), results of DeepSEA - deep learning–based algorithmic framework predicting chromatin opening and bound TFs inferred from ChIP-Seq

experiments (D. Lee *et al.*, 2015a; Zhou and Troyanskaya, 2015a). Variants are ordered based on the average TFs in Modules (TFiMrestr). 8 SNPs (of the total 61 SNPs) with the highest epi-PMCA ranking were chosen for further analysis.

4.2.2. EMSA

The oligonucleotides were designed, annealed, and the electrophoresis performed as described in Chapter 3. No competing unlabelled oligonucleotides were used in this case. The forward biotinylated sequences are shown in Table 4.2.

Table 4.2 | EMSA oligonucleotides for SNPs of Risk Block A in the *TBX15-WARS2* locus.

SNP	Forward oligonucleotides
rs2645294_C	AACATCATCAGTCGTTCCAACACCCACCTTCAAAATCAGAA
rs2645294_T	AACATCATCAGTCGTTCCAATACCCACCTTCAAAATCAGAA
rs10923724_C	CTTTCTGGAGCTGGCAATCCCATCCCAAATTAAGACTCTAA
rs10923724_T	CTTTCTGGAGCTGGCAATCCTATCCCAAATTAAGACTCTAA
rs6428789_A	GGCGAAGCCCCGACGCCCAGAGGGCGCTTGGGCCCAGCACA
rs6428789_C	GGCGAAGCCCCGACGCCCAGCGGGCGCTTGGGCCCAGCACA

4.2.3. Allele-specific qPCR

The relative expression of the two rs2645294 alleles in hWAT cells was assessed using a TaqMAN SNP Genotyping Assay (Assay ID: C_15913675_20), which contains VIC or FAM labelled allele-specific probes, following the standard TaqMAN Assay protocol. The ratio was determined using fold change on the Comparative C^T Method ($\Delta\Delta C^T$ Method) as described in Chapter 2.

4.2.4. Transcription inhibition

hWAT cells were plated at 120K/well (Scepter™ 2.0 Cell Counter, gating: 11μm - 24 μm) in 6-well plates to reach 60% confluence next day. After 24 hours, cells were treated either with Actinomycin D (Sigma Aldrich, final concentration: 2μg/ml) or corresponding

volume of DMSO for 0, 4, 8, 12 and 24 hours. At each time-point, cells were lysed and frozen in TRIzol (Thermo Fisher). RNA was extracted and reverse transcribed as described in Chapter 2. Expression levels were assessed using the *WARS2* genotyping probe (above) and *MYC* TaqMAN probe (Hs00153408_m1). House-keeping genes were assessed using Double-dye Hydrolysis geNorm probes (PrimerDesign) for beta actin (*ACTB*), glyceraldehyde-3-phosphate dehydrogenase (*GAPDH*), and 18S rRNA (*18S*). Transcript half-life was determined using $t^{1/2}$= ln(2)/-slope, where the slope was calculated from a plot of the log(2) relative expression (*WARS2* or *MYC* transcript normalised to *ACTB* using the Comparative C^T Method ($\Delta\Delta C^T$ Method).

4.2.5. Bioinformatic analysis of *WARS2* 3'UTR

To extract the *WARS2* 3'UTR sequence, I used the ENST00000369426.9 transcript which has the longest (2144bp) 3'UTR sequence of all the *WARS2* isoforms annotated in GENCODE v24. I analysed this sequence using RegRNA 2.0 (Chang *et al.*, 2013). To test the effect of rs2645294 on RNA-binding protein (RBP), miRNA binding and RNA structure I scanned the 100bp surrounding sequence using AtTRACT, Transterm, TargetScan and RNA structure online tools (Jacobs *et al.*, 2000; Reuter and Mathews, 2010; Agarwal *et al.*, 2015; Giudice *et al.*, 2016).

4.2.6. Nascent RNA isolation & validation

Total RNA was isolated from hWAT cells, reverse-transcribed using the SuperScript III Reverse Transcriptase (Thermo Fisher) and PolyA- and PolyA+ mRNA isolated using the PolyATtract® mRNA Isolation Systems (Promega). To ensure improved clearance of polyadenylated mRNA, the PolyA- fraction was passed through a fresh column for a second time. *WARS2* allelic levels were assessed by allele-specific qPCR described above. The method was validated by enrichment of spliced over unspliced *WARS2* in the polyA+ mRNA fraction, assessed by specifically designed qPCR primers (LGC Biosearch)

targeted to regions between exons 2 and 3 of *WARS2*, as listed in Table 4.3 and depicted in Figure 4.15A**.**

Table 4.3 | qPCR primers to distinguish spliced and unspliced *WARS2* mRNA.

Wars2_Universal_Probe	CTGCTGTTCTTCTTGCCTGTGGCA
Wars2_Univ_Forward	GCAGAGCATCCTGGACATGA
Wars2_mRNA_Rev (Spliced)	TTGTGTGTGTTCAGACACCTGAG
Wars2_genomic_Rev (Unspliced)	TCTCAGTTCTAATCTGAGAAGCTGAC

4.2.7. 3'UTR luciferase assays

The 3'UTR of *WARS2* was amplified from hWAT cell genomic DNA using Q5® High-Fidelity DNA Polymerase (NEB, M0491) and cloned using SalI-HF and XhoI downstream of the luciferase gene in the pmirGLO Dual-Luciferase miRNA Target Expression Vector (Promega). The 3'UTR sequence was chosen from ENST00000235521.4, the *WARS2* transcript with the longest annotated 3'UTR in GENCODE v24. The insertion was confirmed by sequencing and restriction enzyme digest. The plasmids were then mutated to generate the alternative alleles using the Q5® Site-Directed Mutagenesis Kit (NEB, E0554S) and the inserts sequenced to ensure no additional mutations were present. The primers used are listed in Table 4.4. The plasmids were transfected and luciferase expression analysed as described in Chapter 3.

Table 4.4 | Cloning primers used for *WARS2* 3'UTR assays.

Cloning Primers	
W2_3UTR_FW	cgcctCgAGCATCCATGAAGAAGGTAAAATCC
W2_3UTR_RV	gcgCgtcgAcTTGGCTTGATAGATCTACCTTTAGTTT
Region amplified (hg19):	chr1:119573839-119575984
Size:	2146bp
Mutagenesis Primers	
W2_rs264_GtoA_FW	GAAGGTGGGTaTTGGAACGAC
W2_rs264_GtoA_FW	AAAATCAGAATGTTTAGAGTCTAAAAAAC

4.3. Results

4.3.1. Prioritising potentially functional SNPs

The *TBX15-WARS2* locus contains potentially four independent associations with WHRadjBMI, thus likely affecting gene expression through multiple mechanisms (Shungin *et al.*, 2015). To determine the candidate functional SNPs, SNPs in close LD ($r^2 \geq 0.8$) with the lead SNPs in each of the four risk blocks were used (Figure 4.4). This list contained a total of 61 SNPs stretching between *WARS2, TBX15* and *SPAG17*. Except for rs10494217 in Risk block C, all SNPs were non-coding. To prioritise SNPs that are likely to affect gene expression, we employed two different bioinformatic approaches.

First, Nasa A S Armstrong in Melina Claussnitzer group performed epi-PMCA to rank the 61 SNPs based on likelihood of affecting gene expression **(**Figure 4.4**)**. This method is based on the PMCA, previously used to prioritise BMI-associated SNPs in the *FTO* locus (Claussnitzer *et al.*, 2014), as described in 4.2.1. We pursued the eight highest ranked SNPs in the list. Second, Sara Pulit performed PPA to reveal likely causative WHRadjBMI-associations in the combined UK Biobank and GIANT data (Maller *et al.*, 2012). We pursued SNPs with a PPA score ≥ 0.2. According to these criteria, three SNPs were shortlisted for further analysis in Risk block A (Table 4.5).

The three shortlisted SNPs in risk block A were then assessed for possibility of altering the activity of cis-regulatory elements (CREs) by altering TF binding and thus affecting gene expression. All three SNPs were relatively low on the epi-PMCA ranking with rs10923724 being the highest at a rank of 21 (Figure 4.4). Furthermore, when overlayed with human white adipocyte cell (hWAT) ATAC-Seq data, previously generated in our lab, none of the three SNPs overlapped open chromatin in preadipocytes or at any stage of adipose differentiation (Figure 4.5). I tested the three SNPs using an electrophoretic mobility shift assay (EMSA) with nuclear protein from day 4-differentiated hWAT cells and found no

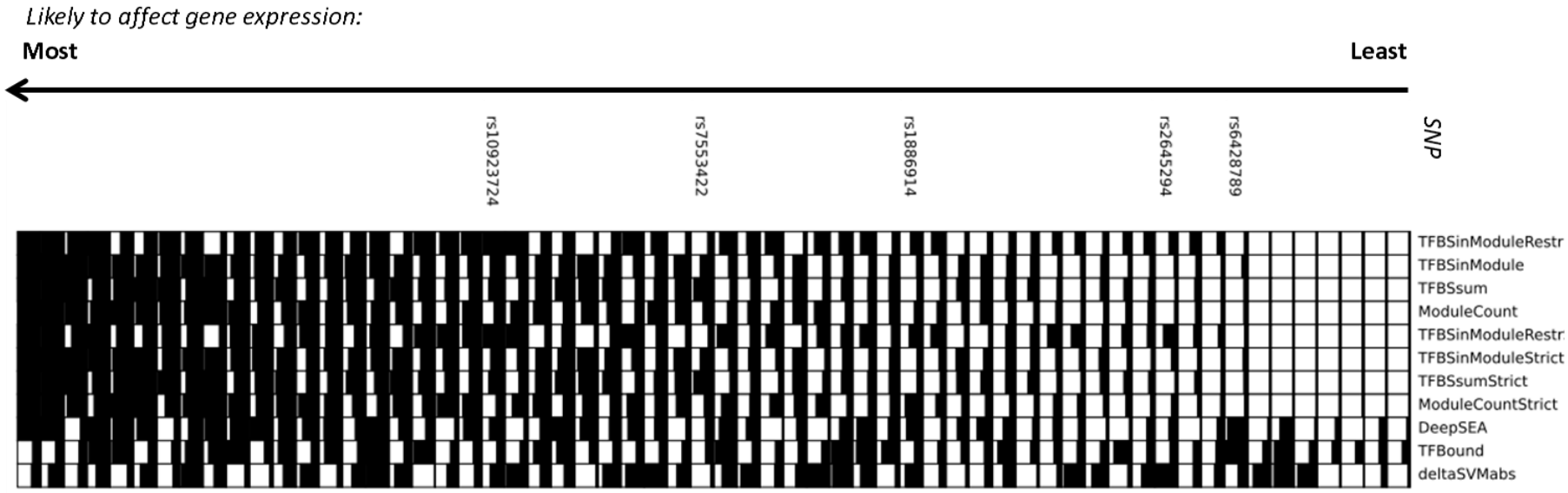

Figure 4.4 | Epigenetic Phylogenetic Module Complexity Analysis (epi-PMCA) to identify potentially functional SNPs in the *TBX15-WARS2* locus. Only Risk Block A (lead SNP: rs2645294) SNPs are annotated. The prioritisation features were the number of TF modules conserved in over half the species (TFBSinModuleRestr) or all the species (TFBSinModule), the number of TFBS in total (TFBSSum) and the number of TF modules in total (ModuleCount). The scores were calculated for both loose (first 4 columns) and strict (columns 5-8) motif cut-offs. Other features included deltaSVM effect size, DeepSEA values and bound TFs inferred from ChIP-Seq data. Variants are ordered based on the average TFs in Modules. Analysis performed by Nasa A S Armstrong.

effect of these SNPs on protein binding (Figure 4.6 & Figure 4.7). In summary, I found no evidence for an effect of the three prioritised SNPs on CRE activity or protein binding.

I searched for alternative mechanisms of gene regulation in the risk block. As shown in Table 4.5, the highest ranking SNP in the PPA analysis is rs2645294 with a PPA score of 0.6 in females of the GIANT Consortium. As shown in Figure 4.5, this SNP overlaps a 3' untranslated region (3'UTR) of the *WARS2* gene. Since SNPs of Risk Blocks A-C, including rs2645294, are also eQTLs for *WARS2*, I hypothesised that rs2645294 affects *WARS2* RNA stability leading to reduced *WARS2* levels and is thus at least partially responsible for the WHRadjBMI association signal of Risk Block A.

Table 4.5 | Risk Block A SNP prioritisation.
For risk block A, 3 SNPs passed the criteria with a PPA score ≥ 0.2 from either GIANT or UK BioBank datasets. PPA performed by Dr Sara Pulit.

Risk Block	SNP	epi-PMCA Rank	PPA score					
			UKBioBank			GIANT		
			All	*Female*	*Male*	*All*	*Female*	*Male*
A	*rs2645294*	50	0.05	0.00	0.01	**0.33**	**0.60**	0.01
	rs10923724	21	**0.53**	0.00	0.07	**0.29**	0.16	0.01
	rs6428789	53	**0.27**	0.00	0.05	N/A	N/A	N/A

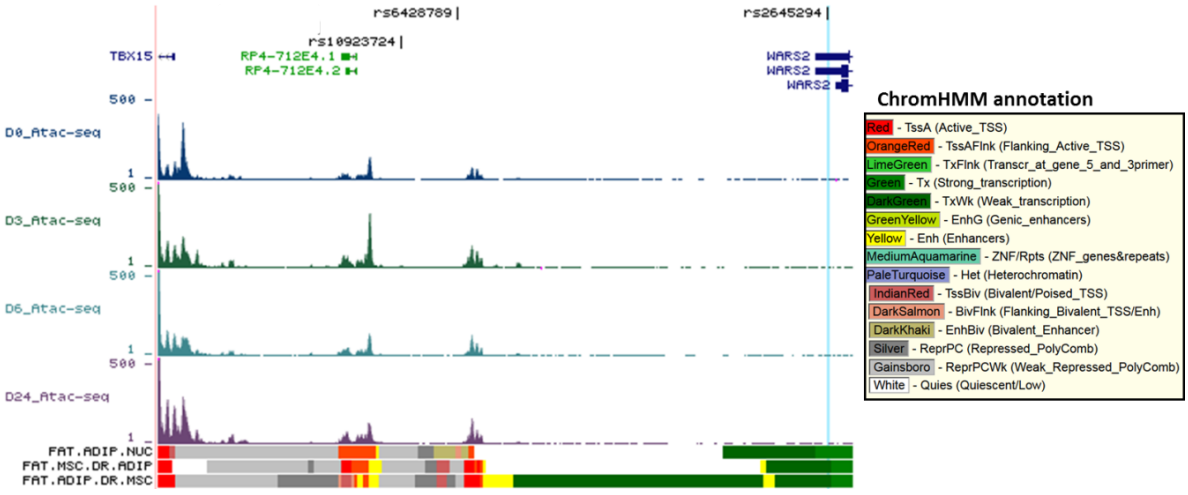

Figure 4.5 | Risk Block A SNPs do not overlap open chromatin in hWAT cells. Overlap of the 3 short-listed SNPs in Risk Block A and their overlap with the ATAC-Seq signal of differentiating hWAT preadipocytes (Day 0, Day 3, Day 6, Day 24) and the primary state ChromHMM annotation from Adipose Nuclei (FAT.ADIP.NUC), Mesenchymal Stem Cell Derived Adipocyte Cultured Cells (FAT.MSC.DR.ADIP) and Adipose Derived Mesenchymal Stem Cell Cultured Cells (FAT.ADIP.DR.MSC) (Kundaje et al., 2015). Region, GRCh37/hg19, chr1:119,531,043-119,576,244. Visualised using the UCSC genome browser.

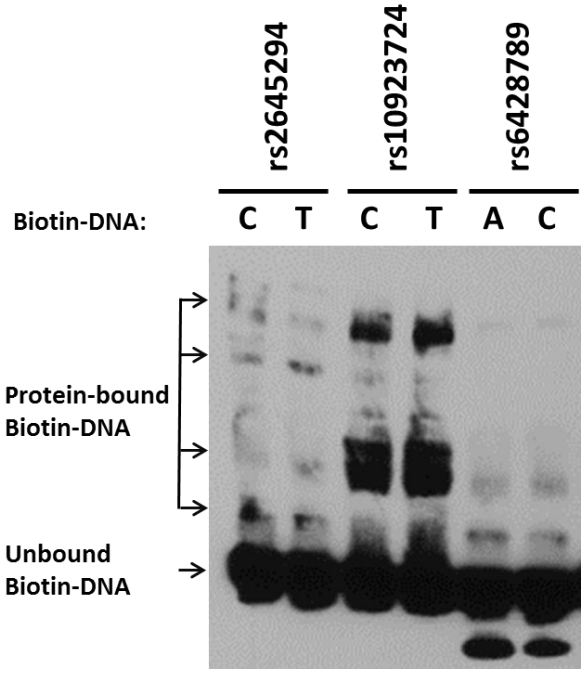

Figure 4.6 | Prioritised Risk Block A SNPs do not affect protein binding in differentiating hWAT cells. 38bp biotin-labelled DNA probes surrounding the 3 SNPs with either alleles were incubated with nuclear protein from day 4 differentiated hWAT cells and resolved on a 6% DNA-retardation gel. No reproducible difference was observed in the protein bound bands between the alleles. The blot was repeated 4 times.

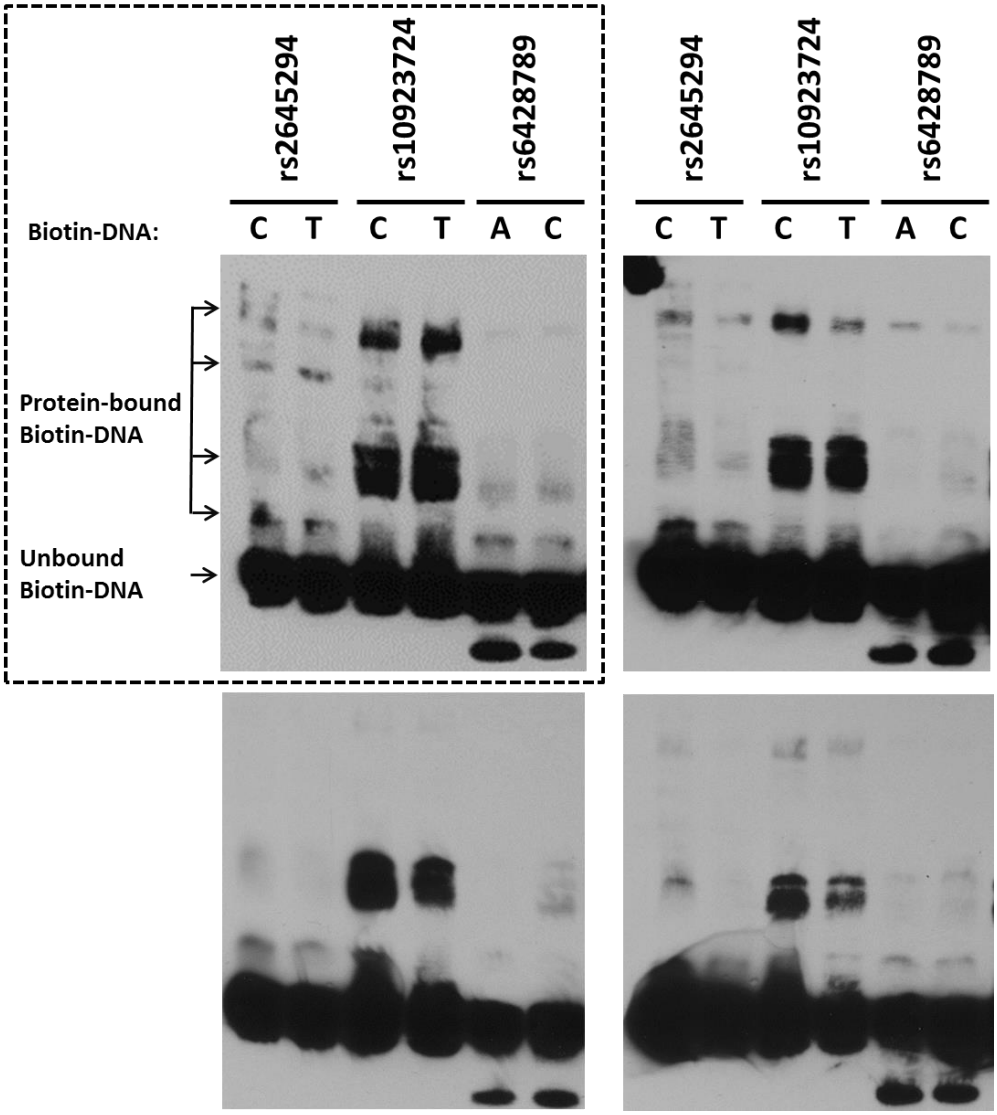

Figure 4.7 | Risk Block A EMSA replicates. There was no reproducible difference observed between the replicates in none of the Risk Block A SNPs. Representative image is marked with dotted line.

4.3.2. Bioinformatic analysis of *WARS2* 3'UTR RNA regulatory elements

3'UTR elements are greatly expanded in humans compared to simpler organisms suggesting an important regulatory role (Mayr, 2016). They can alter gene expression through recruiting miRNAs, non-coding RNA or RNA-binding proteins (RBPs) that either stabilise or destabilise the mRNA (Matoulkova *et al.*, 2012). rs2645295 in the 3'UTR of *WARS2* could be altering a RBP or a miRNA binding motif for proteins and thus affecting RNA stability. I used multiple online tools to test these possibilities.

First, I used RegRNA 2.0 to scan the 2144bp 3'UTR of *WARS2* for functional elements including splicing sites, splicing regulators, polyadenylation sites, structural sequences and miRNA binding sites. There was no overlap of rs2645294 with any of these regulatory elements, but the SNP was found to be in a close proximity to an Intron Splicing Enhancer (ISE) (Figure 4.8). The SNP slightly changed the stability of the stem-loop containing the ISE, but the ISE itself and its accessibility were not predicted to be affected **(**Figure 4.9). The lack of overlap with miRNA binding sites was confirmed by TargetScan and Transterm, but Transterm revealed that two miRNAs could potentially bind in the close proximity of the SNP (Figure 4.10) (Jacobs *et al.*, 2000; Agarwal *et al.*, 2015). To discover which RBP RNA binding motifs were changed due to rs2645294, I used "*A daTabase of RNA binding protein and AssoCiated moTifs*" (AtTRACT), the most comprehensive database to date with information on 370 RBPs and 1583 RBP consensus binding motifs (Giudice *et al.*, 2016). The G allele introduced additional RNA binding sites for UGBP Elav-Like Family Member 1-4 (CELF1-4), Eukaryotic translation initiation factor 4B (EIF4B) and Fused in Sarcoma/Translocated in Sarcoma (FUS) (Table 4.6). In summary, rs2645294 could directly affect RBP binding and thus alter *WARS2* RNA stability. Alternatively, a change in RNA structure due to the SNP could indirectly change accessibility of surrounding RBP or miRNA binding motifs.

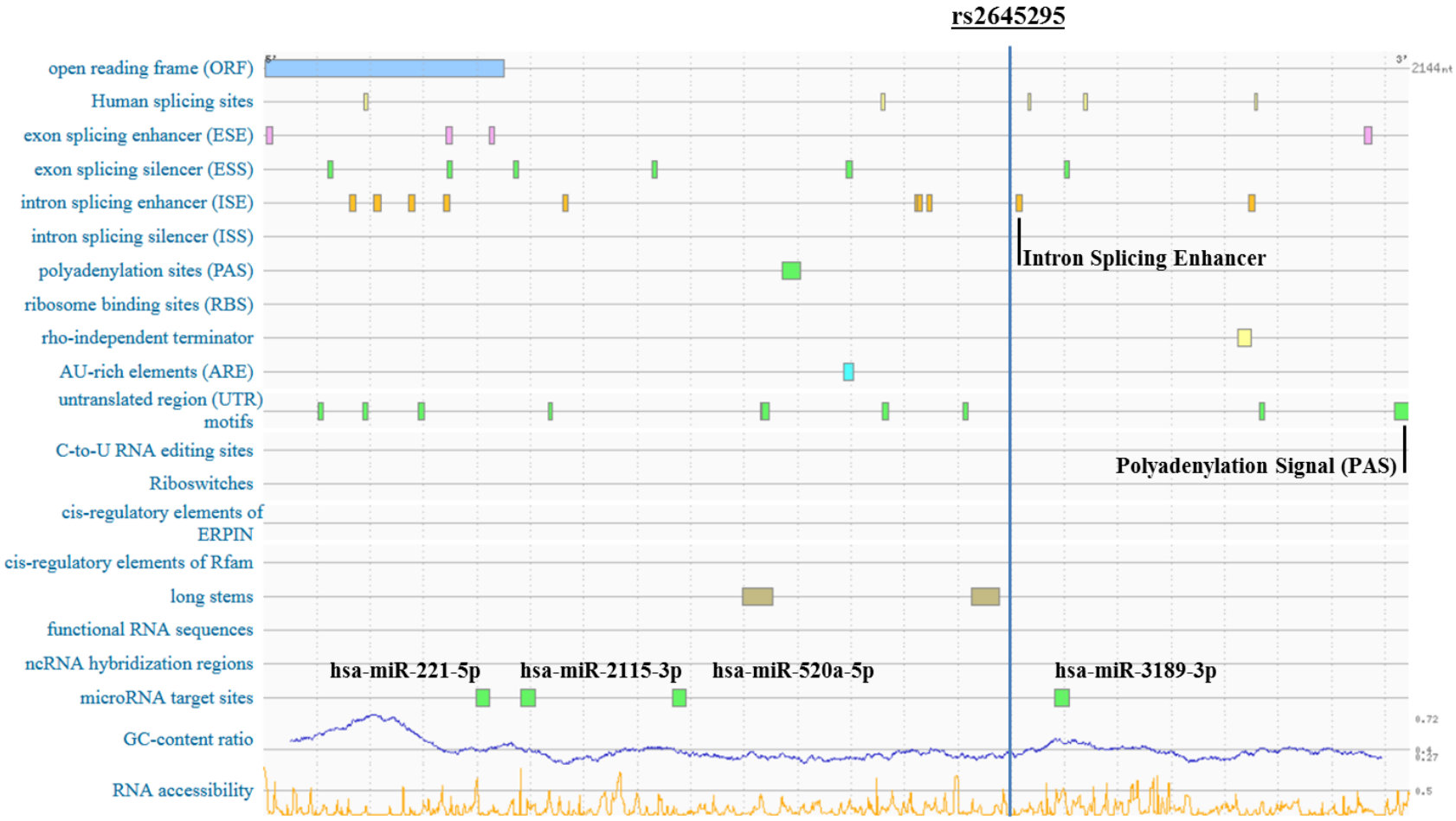

Figure 4.8 | RegRNA 2.0 analysis of *WARS2* 3'UTR. rs2645294 does not directly overlay any known regulatory regions, but is found in a close proximity of an Intron Splicing Enhancer. This diagram shows the annotation for the G allele, the annotation for the A allele was identical except for minor changes in GC-content and RNA accessibility (bottom 2 features).

To study the effect of rs2645294 on RNA structure, I compared several algorithms of the RNA Structure Web server (Reuter and Mathews, 2010). A major change in the stem loop architecture due to the A allele was predicted by Fold and ProbKnot (Figure 4.11**).** On the other hand, MaxExpect predicted RNA structures that were almost identical for the two alleles. Thus it is possible that rs2645294 alters RNA structure, but the specific effects are variable between the prediction methods used.

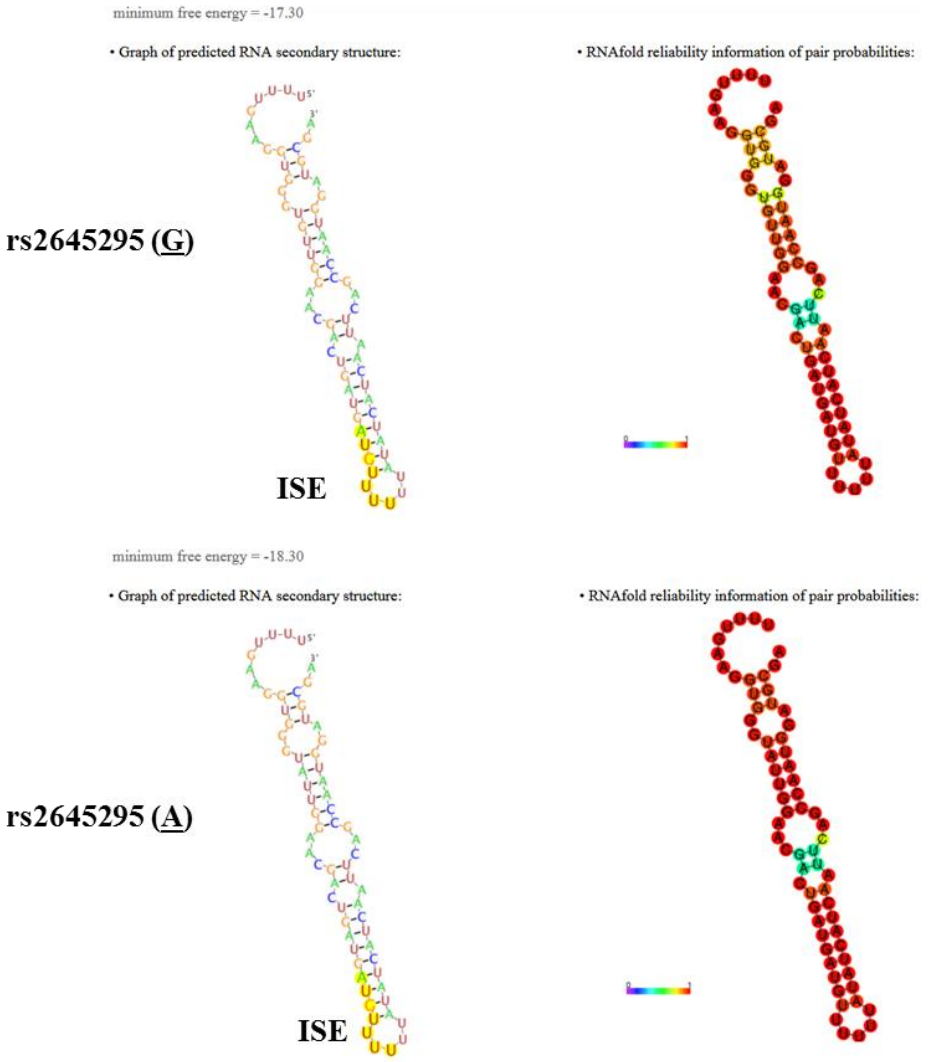

Figure 4.9 | Detailed view of the Intron Splicing Enhancer (ISE) from Figure 4.8. The A allele of rs2645294 results in an RNA structure with a slightly greater stability (lower free energy), but the overall structure and accessibility of the ISE is unchanged. Generated using RegRNA v2.0 (Chang *et al.*, 2013).

In summary, the *WARS2* 3'UTR SNP does not directly overlap a miRNA binding sequence, but may directly affect RBP binding leading to a change RNA stability. The SNP could also affect RNA structure and thus indirectly affect RBPs and miRNAs binding at surrounding sites.

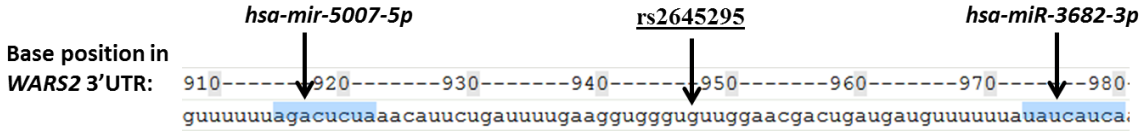

Figure 4.10 | Transterm scan of the proximal region of rs2645294 for miRNA binding sites. No miRNA binding sites directly overlap rs2645294, but 2 miRNAs could bind in its proximity.

Table 4.6 | The new binding motifs introduced by the G allele of rs2645294. The 100bp surrounding rs2645294 with either alleles were scanned using AtTRACT (https://attract.cnic.es/) and compared. 6 novel motifs were introduced by the G allele.

Protein	Gene ID	Motif	Experiment
CELF1	**ENSG00000149187**	UGUU	X-ray diffraction
CELF2	**ENSG00000048740**	UGUU	X-ray diffraction
CELF2	**ENSG00000048740**	UGUUG	SELEX
CELF4	**ENSG00000101489**	GGUGUUG	RNAcompete
EIF4B	**ENSG00000063046**	GUUGGAA	SELEX
FUS	**ENSG00000089280**	GGGUGU	SELEX. SDS-PAGE, EMSA, UV crossli competition and immunoprecipitation assays

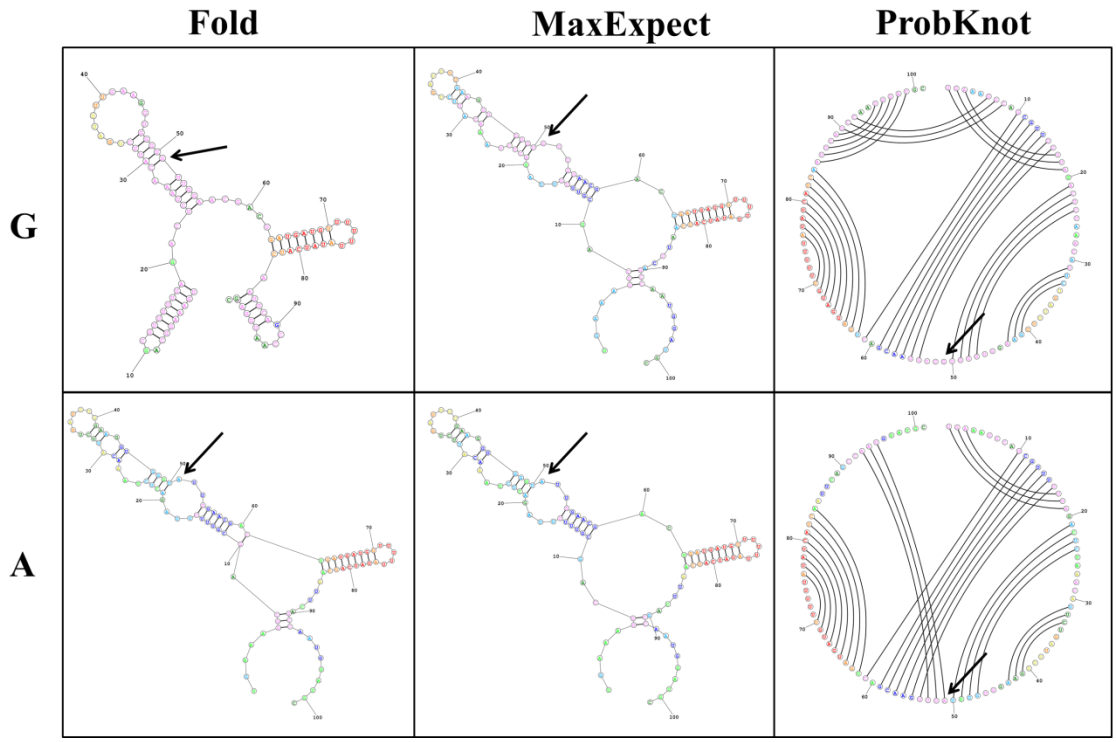

Figure 4.11 | The effect of rs2645294 on RNA structure prediction varies between methods. Comparison of results of the 3 algorithms available at the RNA Structure server (Reuter and Mathews, 2010). 100bp sequence surrounding the SNP was used.

4.3.3. rs2645294-heterozygous hWAT cells show allele-specific expression (ASE) of *WARS2* but no difference in RNA degradation between the alleles

I found that hWAT cells are heterozygous for the rs2645294 and thus used TaqMAN allele-specific genotyping probes to track the levels of the two alleles relative to each other (Figure 4.12A, B). I found that the T risk allele (annotation: T in DNA, A in RNA) is expressed >2 fold lower than the C allele (annotation: C in DNA, G in RNA) (P<0.0001) in these cells which agrees with the direction in the GTEx database (Figure 4.12C, Figure 4.3).

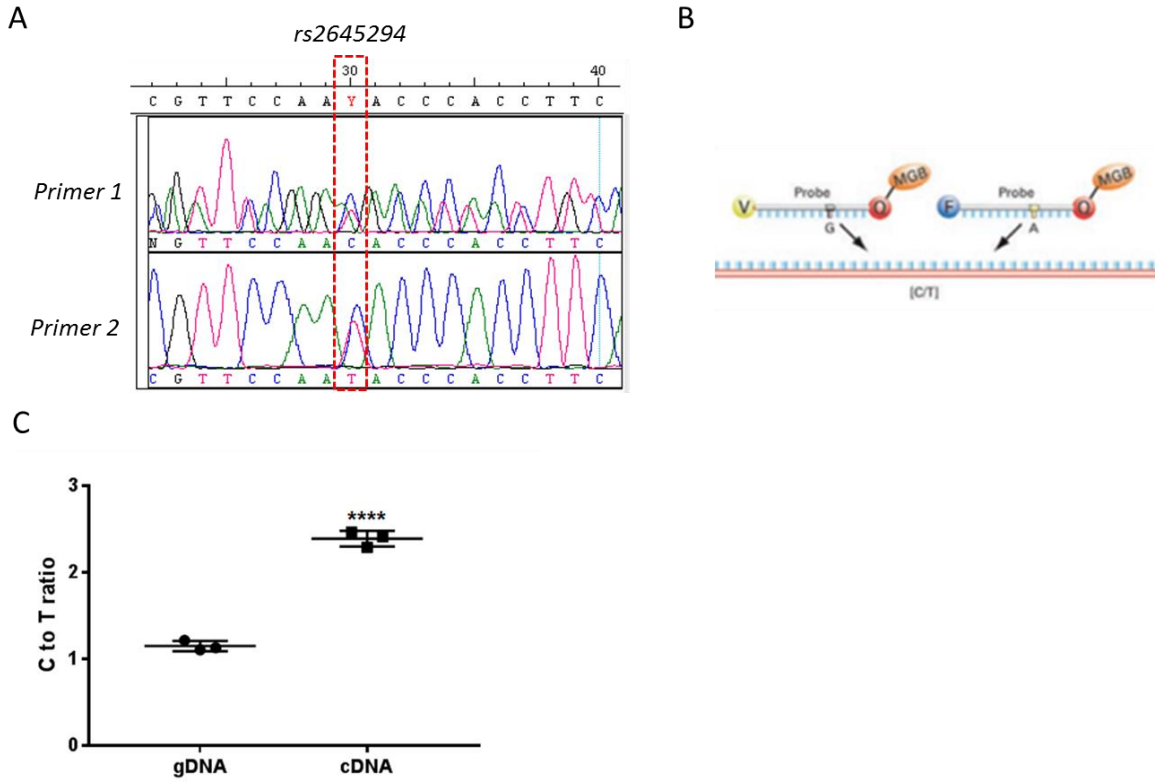

Figure 4.12 | hWAT cells are heterozygous for rs2645294 and show allele-specific expression of *WARS2*.
Sanger sequencing of rs2645294 revealed two peaks, C and T, with both forward and reverse primers (A). Next, both gDNA and cDNA from hWAT cells were analysed using allele-specific TaqMAN genotyping probes (B). The C allele is expressed >2 fold higher than the T (WHRadjBMI-increasing) allele in the cDNA (C). Comparison is by unpaired t-test, **** for $p < 0.0001$.

In order to compare the RNA stability of the two *WARS2* alleles I then used Actinomycin D (ActD), an RNA polymerase inhibitor, to inhibit transcription in hWAT cells. The concentration to inhibit the class II RNA polymerase gene was reported to be >1μg/ml, but concentrations of 5μg/ml and 10μg/ml were also used previously (Sharova *et al.*, 2009; Bensaude, 2011; Russell *et al.*, 2018). To optimise the assay, I thus tested the effect of two ActD concentrations, 2μg/ml and 10μg/ml, on cell morphology and levels of rs2645294 and *MYC* cDNA after 0h, 4h, 8h, 24, 48h, 72h of treatment. Already at 24 hours, wells treated with either 2 μg/ml and 10μg/ml, showed cell detachment and cell death in a bright field image (Figure 4.13A). I thus discarded further time-points and assessed only the range between 0-24 hours by qPCR. *MYC* gene expression previously showed a short half-life and indeed was rapidly reduced already after 4 hours with both ActD concentrations (Figure 4.13D) (Sharova *et al.*, 2009). Similarly, degradation of both T and C alleles of rs2645294 did not differ between the two ActD concentrations (Figure 4.13B,C). Importantly, the levels of multiple housekeeping genes were relatively stable during ActD (2 μg/ml) treatment and the assay could thus distinguish between the half-lives of different RNAs (Figure 4.13E). I thus used the lower concentration of ActD, 2μg/ml, in all future experiments.

I performed three independent replicates of ActD inhibition in hWAT cells for 0-24 hours. The half-life of *WARS2* RNA was 6.3 hours, but no differences between the degradation rate of the two alleles were observed (linear regression of $\log_2$(C) vs $\log_2$(T), P=0.6550) suggesting that rs2645294 does not impact RNA stability of the *WARS2* transcript (Figure 4.14A,B).

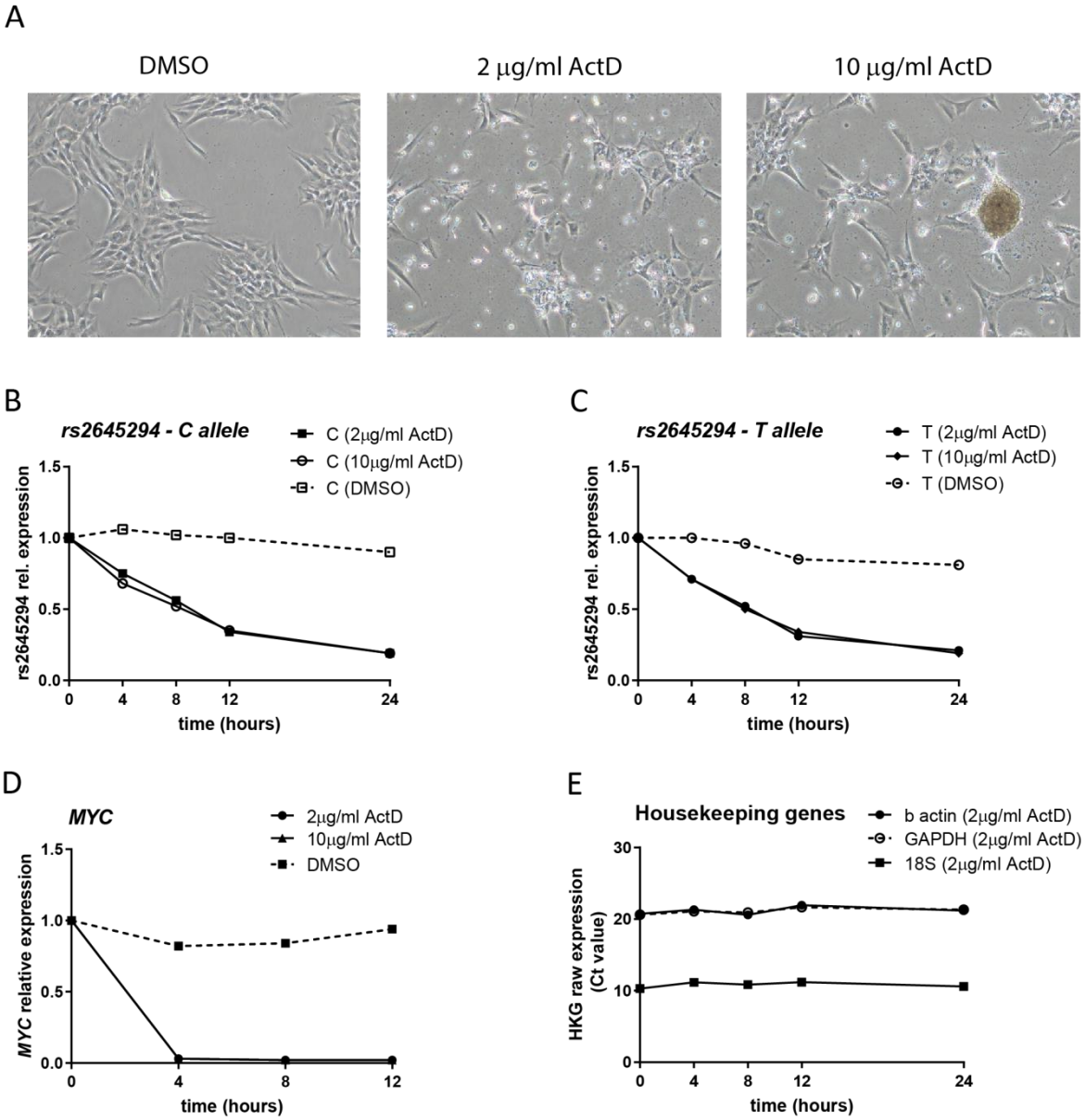

Figure 4.13 | Optimising dose of Actinomycin D in hWAT cells. The effect of two ActD concentrations, 2μg/ml and 10μg/ml, on cell morphology and levels of rs2645294 and *MYC* cDNA after 0h, 4h, 8h, 24, 48h, 72h of treatment was tested in a single experiment. Already after 24 hours, bright-field images revealed marked cell detachment with both ActD concentrations compared to the DMSO control (A). No apparent differences due to the Act D concentration were found for the rs2645294-C allele (B), T-allele (C) or MYC (D) degradation between 0 and 24 hours. Raw Ct values of housekeeping genes were stable during ActD (2μg/ml) treatment. Data for B, C and D were normalised to β-actin.

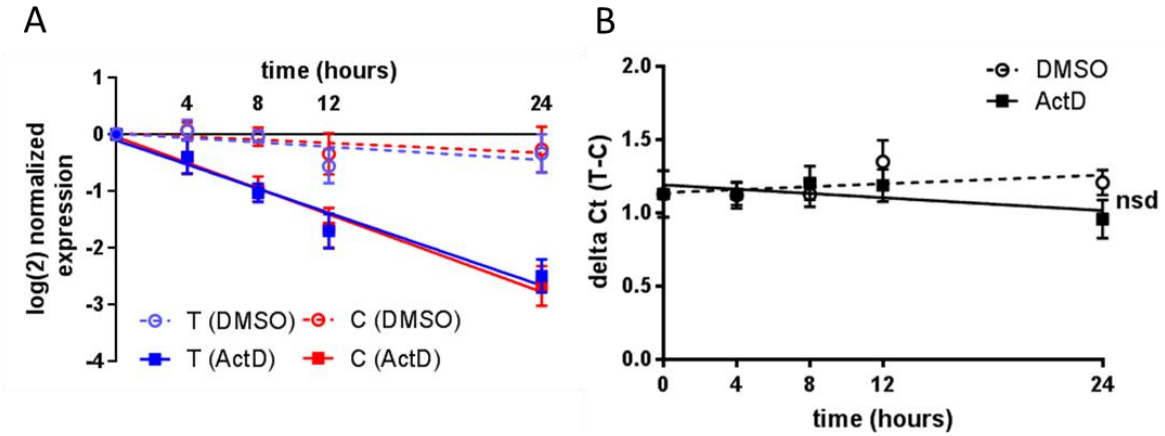

Figure 4.14 | Actinomycin D inhibition in hWAT cells. hWAT cells were treated with Actinomycin D (ActD, 2µg/ml) or DMSO (control) for 0-24 hours and allele-specific qPCR was used to assess differences in allele-specific RNA stability of *WARS2*. All data were normalised to the highly stable β-actin and are shown as mean ± SD. The slopes of T and C alleles upon actinomycin treatment were not significantly different. Assessed by linear regression. Half-life was calculated as ln(2)/-slope. $t^{1/2}$ = 6.3 hours. Three independent experiments (A). Different representation of the data in E showing the difference between the Ct values of the two alleles throughout time (B).

4.3.4. Allele-specific expression is present at both the mature and nascent RNA level in hWAT cells

To test the potential post-transcriptional origin of the ASE seen in hWAT cells, I hypothesised that if the ASE indeed arises post-transcriptionally, it should not be present at nascent RNA level and only appear after RNA processing at the mature RNA level (Figure 4.15A,C). It was previously shown that polyA- can be used as a nascent mRNA fraction (Hosseini *et al.*, 2013). I thus separated RNA from undifferentiated subconfluent hWAT preadipocytes into polyA+ and polyA- RNA. First, I used exon and intron-specific primers to confirm that this method enriched ~3-fold for mature spliced *WARS2* RNA in the polyA+ fraction compared to total RNA and polyA- RNA ($P<0.0001$ for both comparisons) (Figure 4.15B). Interestingly, no reduction in the spliced:unspliced *WARS2* ratio was observed in the polyA- fraction. I then used the rs2645294 allele-specific probes to assess ASE in the different fractions. The mean ΔC_T between C and T alleles in total RNA, poly A+ and polyA- RNA was -1.16, -1.29 and -1.45, without any statistically significant difference ($P=0.1143$) (Figure 4.15D, E). Thus, rather than the expected decrease in C:T ratio, I actually observed a trend for increased ASE (C:T ratio) in the polyA- fraction compared to total RNA (Figure 4.15E). This result suggests that the observed ASE in hWAT cells is not caused by a post-transcriptional mechanism and might instead have a transcriptional origin.

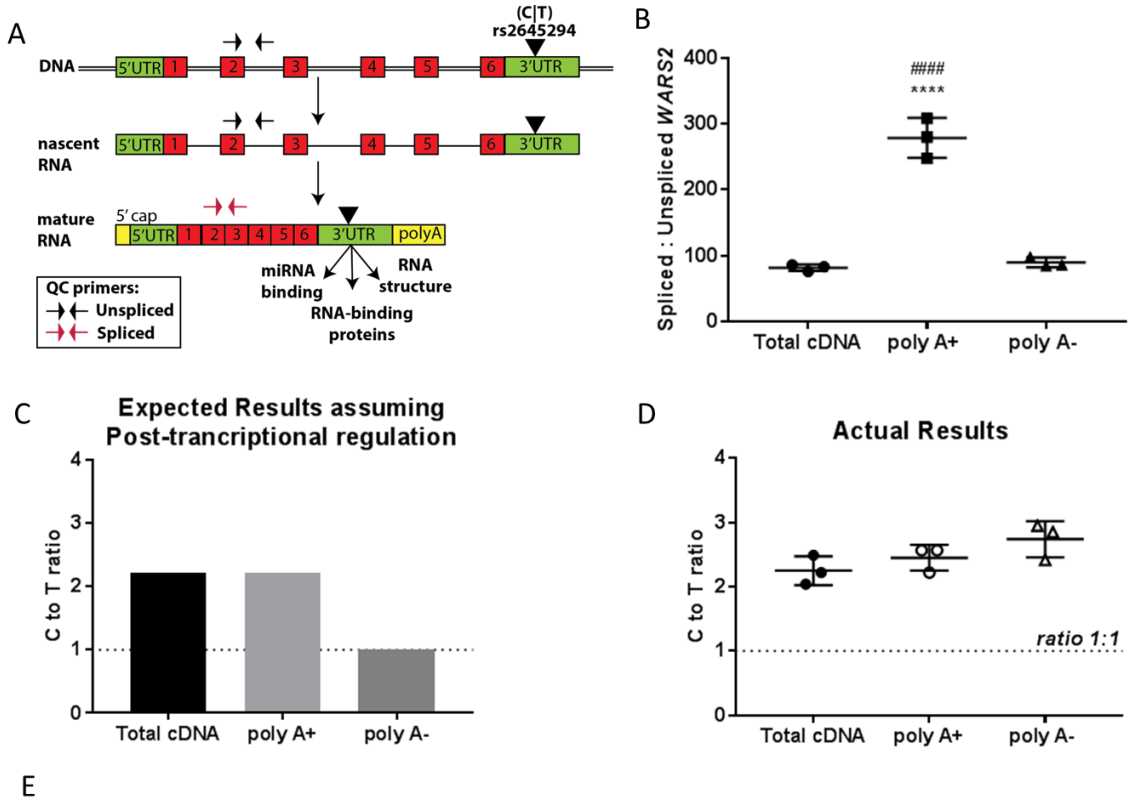

E

Ct ± SD	Total RNA (1000ng)	poly A+ (10ng)	poly A- (1000ng)
T	24.27 ± 0.27	28.19 ± 0.27	27.19 ± 0.48
C	23.11 ± 0.15	26.9 ± 0.17	25.74 ± 0.36
ΔCt	-1.16	-1.29	-1.45
Fold change	2.24	2.45	2.73

Figure 4.15 | ASE is present both at the mature and nascent RNA level in hWAT cells. Diagram illustrating putative RNA processing of the *WARS2* transcript. Primers for both the Spliced and Unspliced *WARS2* transcripts were designed and their binding sites shown (A). RNA from hWAT cells was separated into polyA+ and polyA- fractions and assessed by qPCR. The ratio of Spliced:Unspliced *WARS2* was used to assess the quality of nascent and mature RNA separation. The polyA+ fraction showed a clear enrichment of the mature *WARS2* RNA. (B) Assuming ASE is driven by post-transcriptional mechanism, a lower C:T ratio should be seen in the poly A- fraction compared to the polyA+ fraction (C). The results show there is no statistically significant difference between any of the RNA fractions (D). Raw Ct values used to calculate the C:T ratio in D are also shown (E). Comparison is by one-way ANOVA. **** for Total cDNA vs poly A+, $p \leq 0.0001$; #### for polyA- vs poly A+, $p \leq 0.0001$.

4.3.5. rs2645294 does not alter levels of a luciferase-3'UTR reporter

To test the effect of rs2645294 on protein levels, I cloned the 3'UTR of *WARS2* downstream of the luciferase gene in the pMIR-GLO vector and observed the effect of mutagenizing rs2645294 on reporter expression in transfected cells (Figure 4.16A). Since rs2645294 is associated with reduced *WARS2* levels in multiple human tissues, I transfected both day 4-differentiated hWAT cells and HEK293T cells. The *WARS2* 3'UTR caused a ~3-fold reduction in reporter signal compared to the empty vector both in hWAT cells (C vs empty: P=0.0056, T vs empty: P=0.0007) and HEK293T cells (C vs empty: P=0.0194, T vs empty: P=0.0001). No difference between the alleles was observed in either cell line (Figure 4.16B, C). In summary, rs2645294 does not affect luciferase expression and there is no evidence for it regulating WARS2 protein or RNA levels.

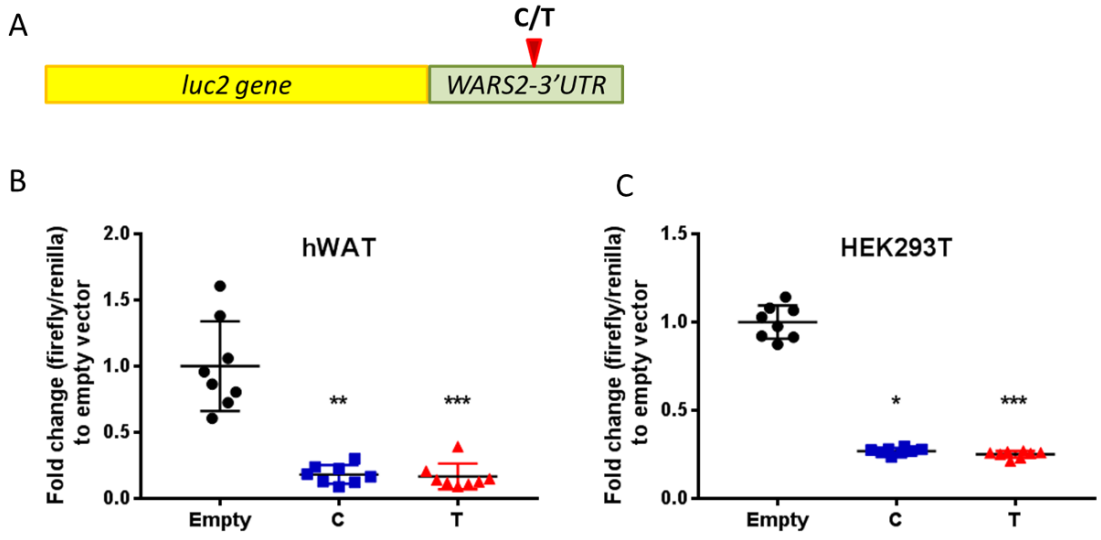

Figure 4.16 | rs2645294 has no effect on expression of the luciferase fused to the 3'UTR of *WARS2*. The 2144bp 3'UTR sequence encompassing the rs2645294 SNP was cloned 3'of the luciferase gene in the pMIR-GLO vector (A). The vectors with either SNP (C or T) were then transfected into day 4-differentiated hWAT cells (B) or HEK293T cells (C) for 24hours (B). Data plotted as replicates with mean ± SD. Comparisons are by Kruskal–Wallis test. *P < 0.05 vs empty, **P < 0.01 vs empty, ***P<0.001 vs empty.

4.4. Discussion

Here I have shown how bioinformatic prioritisation using PPA and epi-PMCA was used for one of the four WHR-association risk blocks in the *TBX15-WARS2* locus to identify a putative functional SNP rs2645294 in the 3'UTR of *WARS2*. I tested its effect on *WARS2* RNA stability.

Using multiple online databases, I report that rs2645294 is not predicted to affect miRNA binding, but the G allele, associated with higher *WARS2* levels, introduces new binding motifs for six RBPs - CELF1-4, EIF4B and FUS. Binding of some of these RBPs could lead to increased stability and levels of *WARS2* (Mayr, 2017). For example, the CELF family was shown to affect alternative splicing, C to U RNA editing, deadenylation, mRNA decay, and translation of multiple transcripts (Dasgupta and Ladd, 2012). rs2645294 could also affect RBP, miRNA binding or splicing indirectly by affecting RNA structure, although only some algorithms predict a major change in the stem-loop structure.

Using a combination of three different methods, I showed that rs2645294 does not affect RNA stability. Actinomycin D inhibition was previously used to detect a stabilising effect of a schizophrenia-linked variant on *Kalirin* (*KALRN)* mRNA (Russell *et al.*, 2018). Using the same method, I determined the half-life of *WARS2* to be 6.3 hours, similar to the 7.2 hours reported for *Wars2* in a transcriptome-wide study of mouse embryonic stem cells (Sharova *et al.*, 2009). No difference in degradation of the two *WARS2* alleles was detected after Actinomycin D inhibition showing that the ASE in hWAT cells is not due to an allelic difference in RNA stability. However, it has been shown that transcription and RNA degradation are tightly linked and the effects of transcription inhibition are thus buffered by consequential downregulation of mRNA decay (Haimovich *et al.*, 2013; Sun *et al.*, 2013). Indeed, when transcription is inhibited using less invasive gene-specific methods,

the median RNA half-life is shorter than reported by actinomycin D inhibition (Sharova *et al.*, 2009; Baudrimont *et al.*, 2017). To support our results, other less-invasive methods such as pulse-chase with 4-thio-uridine (4SU) could be used to demonstrate transcriptional regulation in the genesis of hWAT ASE (Lugowski, Nicholson and Rissland, 2018).

To distinguish post-transcriptional regulation, I assessed the allelic expression at the level of nascent RNA. Previously, the polyA- fraction was used to estimate the nascent RNA population (Hosseini *et al.*, 2013). I found no difference in ASE of *WARS2* between the polyA+ and polyA- fractions, further suggesting a transcriptional origin of the ASE. Although, I did see an enrichment of spliced:unspliced *WARS2* in the polyA+ fraction, interestingly no reduction of the ratio compared to the total RNA was observed in the polyA- fraction. This could be explained by the co-transcriptional nature of splicing (Bentley, 2014). Since our qPCR probes for unspliced *WARS2* targeted intron 2 and exon 2 boundary, it is possible that the majority of these early introns were already spliced before polyadenylation.

Finally, in both the actinomycin experiment and nascent RNA qPCR, other SNPs differing between the two *WARS2* alleles could have counteracted the putative effect of rs2645294 on RNA stability. Thus to isolate the effect of the single SNP, I cloned the 3'UTR of *WARS2* in a luciferase vector and found no differences between the expression of the two alleles. To prevent potential artefacts such as the effect of the luciferase gene on the 3'UTR structure, ideally, rs2645294-directed mutagenesis of endogenous *WARS2* in hWAT cells would be performed in the future. To conclude, although each method had its limitations, none of the three different methods show any evidence for rs2645294 affecting RNA stability.

The effect of the risk block A on *WARS2* levels is probably regulated through a transcriptional mechanism. My initial assessment of the low PPA ranks and no overlap with open chromatin in this risk block suggested that this is unlikely to be the case. Although, some post-GWAS methods use overlap of a SNP with open chromatin in the tissue of interest a pre-requisite for downstream study, in other studies enhancer marks such as H3K27ac suffice to mark potential enhancer variants (Schwessinger *et al.*, 2017; Iotchkova *et al.*, 2019). It is thus possible that other SNPs in the risk block could alter gene expression through transcriptional regulation. For example, rs6428789 which overlaps a putative bivalent enhancer in adipose nuclei, or rs10923724, with a high UK Biobank PPA and the highest epi-PMCA rank amongst the risk block A SNPs, could explain the *WARS2* eQTL and WHRadjBMI association. This model is also supported by the fact that in some tissues, risk block A SNPs are linked to reduced levels of *RP11-418J17.1*, an antisense transcript originating from the *WARS2* promoter (GTEx-Consortium, 2013). Indeed, long distance regulation of the promoter would be expected to affect the expression of both transcripts.

4.5. Conclusion

Risk block A SNPs in the *TBX15-WARS2* locus are associated with increased WHRadjBMI levels and reduced *WARS2* levels in multiple tissues. Low epi-PMCA ranks, poor overlap with open chromatin in hWAT cells and no difference in EMSA experiments suggested *WARS2* might be regulated post-transcriptionally. I thus tested rs2645294 in 3'UTR of *WARS2*, the highest scoring SNP in the GIANT female PPA, for an effect on RNA stability. Using three independent methods assessing RNA degradation, expression in nascent RNA and the effect of the SNP on reporter expression I have shown that rs2645294 does not affect RNA stability. The effect of Risk block A on the surrounding

genes and adipose biology is thus likely to be regulated transcriptionally - through the other SNPs in close LD.

5. Testing *Wars2* as a candidate gene for browning and fat distribution regulation

5.1. Introduction

Mitochondria are essential organelles for ATP generation through oxidative phosphorylation and the Krebs cycle, but are also crucial for other metabolic pathways such as fatty acid (FA) β-oxidation, ketogenesis, gluconeogenesis and the urea cycle (Gorman Grainne S, Radelfahr and Klopstock, 2016). They are also involved in other important cellular functions such as non-shivering thermogenesis, amino acid metabolism, calcium homeostasis and apoptosis (Nunnari and Suomalainen, 2012; Bartelt and Heeren, 2014).

Much of the mitochondrial proteome (~ 1500 proteins) is encoded by the nuclear genome and is transported to mitochondria (Calvo and Mootha, 2010). However, 13 genes encoding components of the mitochondrial electron transport chain (ETC) remain transcribed and translated directly in the mitochondria (Schmidt, Pfanner and Meisinger, 2010). Mitochondrial amino-acyl tRNA synthesases (mt-aaRSs) catalyse the activation and aminoacylation of mitochondrial tRNAs with their cognate amino acids and are thus essential for mitochondrial translation (Ibba and Söll, 2000). Unsurprisingly, global homozygous deletions in mt-aaRS are lethal (http://mousephenotype.org/) (Dickinson *et al.*, 2016). Despite the ubiquitous (except in erythrocytes) presence of mitochondria and the common role of mt-aaRSs, human hypomorphic mutations in these genes cause highly varied and tissue-specific phenotypes (Konovalova and Tyynismaa, 2013).

WARS2 gene encodes a mitochondrial tryptophanyl tRNA synthetase. The first patients with mutations in *WARS2* were reported in 2017 and like for other mt-aaRs mutations,

demonstrated primarily neurological phenotypes, but other tissues such as the liver were also affected (Burke *et al.*, 2017; Musante *et al.*, 2017; Theisen *et al.*, 2017; Vantroys *et al.*, 2018; Maffezzini *et al.*, 2019; Virdee *et al.*, 2019).

In the general population, the risk haplotype of the *TBX15-WARS2* locus is associated with both increased Waist-Hip Ratio adjusted for BMI (WHRadjBMI) and decreased *WARS2* expression suggesting a potential role of *WARS2* in regulating fat distribution (GTEx-Consortium, 2013; Pulit *et al.*, 2018). Since a rare coding variant in another mt-aaRS gene *DARS2* and variants in other mitochondrial-encoded genes *MT-ATP6* and *MT-ND6* were also associated with altered WHR, it is likely that *WARS2* is a functional gene in the *TBX15-WARS2* locus (Justice *et al.*, 2019; Kraja *et al.*, 2019). Expression of *WARS2* in subcutaneous adipose tissue (SAT) has also been associated with BMI and Matsuda insulin sensitivity index and studies in spontaneously hypertensive rats showed that *Wars2* influences angiogenesis and is important for brown adipose tissue (BAT) function (Wang *et al.*, 2016; Civelek *et al.*, 2017; Pravenec *et al.*, 2017).

A previous study from our group, identified an N-ethyl-N-nitrosourea (ENU)-induced hypomorphic mutation $Wars2^{V117L/V117L}$ in mice that causes defective splicing and results in only 0-30% of the full-length protein remaining across different tissues (Agnew *et al.*, 2018). Twelve-month old $Wars2^{V117L/V117L}$ mice showed mitochondrial complex deficiency in multiple tissues, hypertrophic cardiomyopathy, sensorineural hearing loss and failure to gain fat mass. Importantly, white adipose tissue (WAT) showed upregulation of mitochondria and browning markers whereas the BAT was dysfunctional and showed reduced browning marker expression. Elevated levels of Fibroblast growth factor-21

(FGF21) suggested a mechanism by which at least part of the browning in adipose tissue may be mediated systemically (Fisher *et al.*, 2012).

5.1.1. Chapter hypothesis

I hypothesise that *Wars2* deficiency leads to increased visceral to subcutaneous adipose ratio. This is due to mitochondrial complex deficiencies that cause subsequent depot-specific responses including subcutaneous-specific adipose browning which leads to increased energy consumption and thus weight loss in subcutaneous compared to visceral depots.

5.1.2. Chapter aims

1. To assess the body composition and fat distribution of *Wars2*$^{+/-}$, *Wars2*$^{+/V117L}$ and *Wars2*$^{V117L/V117L}$ on low-fat and high-fat diets.

2. To assess whether ETC complex levels and browning is affected more in subcutaneous than visceral depots using Western Blot, qPCR and mitochondrial DNA content assays in 4 month-old *Wars2*$^{V117L/V117L}$ mice.

3. To assess BAT ETC complex levels and BAT marker gene expression in young 4 month-old mice.

4. To distinguish between adipose-intrinsic and systemic responses using primary adipocyte cultures for Seahorse analysis and assessing the plasma for levels of mitokine that could be contributing to a systemic effect.

5. To evaluate potential mechanisms leading to a failure to gain fat mass by measuring food intake.

5.2. Materials and methods

5.2.1. Body weight and body composition analysis and power calculation

Body weight and composition were analysed both in the *Wars2-KO* and *Wars2-V117L* cohorts. For *Wars2-KO* mice, I used a cohort of 31 female mice, on high-fat diet (HFD) or low-fat diet (LFD), and tested these at 12 months of age. $Wars2^{+/-}$ and $Wars2^{+/+}$ littermate numbers were 7 and 7 for LFD and 8 and 9 for HFD, respectively.

To generate the *Wars2-V117L* cohort, I first performed a power calculation based on previously analysed 6-month (n = 3) and 12-month cohorts (n = 6) which showed a trend for increased gWAT:iWAT ratio in male $Wars2^{V117L/V117L}$ mice (Agnew *et al.*, 2018). Using GraphPad StatMate 2, I calculated that to achieve 80% power to detect the difference, I would need at least n = 5 or n = 10, based on the 6-month and 12-month cohorts, respectively. We thus generated three separate cohorts, together totalling to 186 mice, which allowed us to place both male and females on HFD and LFD whilst still achieving n > 10 for each condition. When combined, Cohort 1 (68 mice) and Cohort 2 (88 mice), shown in this chapter, totalled to n = 9 to 15 for each sex and genotype on LFD/HFD. The final Cohort 3 (30 mice) will be added to the dataset after submission of this work.

5.2.2. Food intake study

A separate cohort of 30 mice was generated to test for differences in food intake. There were 3 cages (6 mice) for each of $Wars2^{+/+}$ (WT), $Wars2^{+/V117L}$ (HET) and $Wars2^{V117L/V117L}$ (HOM) males and 2 cages (4 mice) for each genotype of females. Another similar-sized cohort will be generated to reach statistically testable numbers also for the females.

Technical details on body composition, food intake measurement and statistical analysis are described in the main Materials & Methods in Chapter 2.

5.3. Results

5.3.1. Heterozygous *Wars2*-KO mice show no change in body composition, fat distribution and inactive integrated stress response in the heart

Homozygous *Wars2*$^{V117L/V117L}$ mice previously showed failure to gain fat mass with age (Agnew *et al.*, 2018). Severe *Wars2* reduction in these mice caused a complex phenotype including hypertrophic cardiomyopathy, which is likely to be rare in the general human population as the result of inheritance of WHR susceptibility SNPs. I thus chose to study the *Wars2*$^{+/-}$ heterozygous mice, with *Wars2* levels (50%) in the range predicted for the risk-allele carriers in the human population (66%-33%) (Table 5.1). I used Echo-MRI to assess the bodyweights and body composition of 12-month old females and found that diet (HFD or LFD) significantly affected bodyweight ($P < 0.0001$), fat-mass ($P < 0.0001$) and lean mass ($P = 0.0032$) (Figure 5.1). However, I observed no significant effect of genotype on these measures.

Table 5.1 | Comparison of predicted *Wars2* levels in humans and available mouse models.
Based on data from (GTEx-Consortium, 2013; Agnew *et al.*, 2018).

Human rs2645294:	**C|C**	**C|T**	**T|T**
GTEx/ASE-predicted *WARS2 level*	100%	67%	33%

***Wars2* mice:**	**+/+**	**+/-**	**+/V117L**	**V117L/V117L**
Wars2 levels	100%	50%	~50-65%	~0-30%

Since the *TBX15-WARS2* locus shows an association with WHR rather than BMI, we then assessed the weights of different fat depots, dissected as reported previously (de Jong *et al.*, 2015; Shungin *et al.*, 2015) (Figure 5.2). HFD significantly increased the weights of mesenteric WAT (mWAT) ($P < 0.0001$), cardiac WAT (cWAT) ($P < 0.0001$) and reduced the weights of perirenal WAT (prWAT) ($P = 0.0202$) and gonadal WAT (gWAT) ($P = 0.0002$). Interscapular BAT (iBAT) and inguinal WAT (iWAT) did not change due to diet.

No significant difference was detected due to genotype in any of the depots. We then assessed the gWAT:iWAT ratio which was used previously to represent the ratio of visceral to subcutaneous adipose in mice (Gray *et al.*, 2006). The mice showed a reduction in gWAT:iWAT ratio due to HFD (P=0.005), but there was no effect due to the *Wars2*$^{+/-}$ genotype (Figure 5.2G).

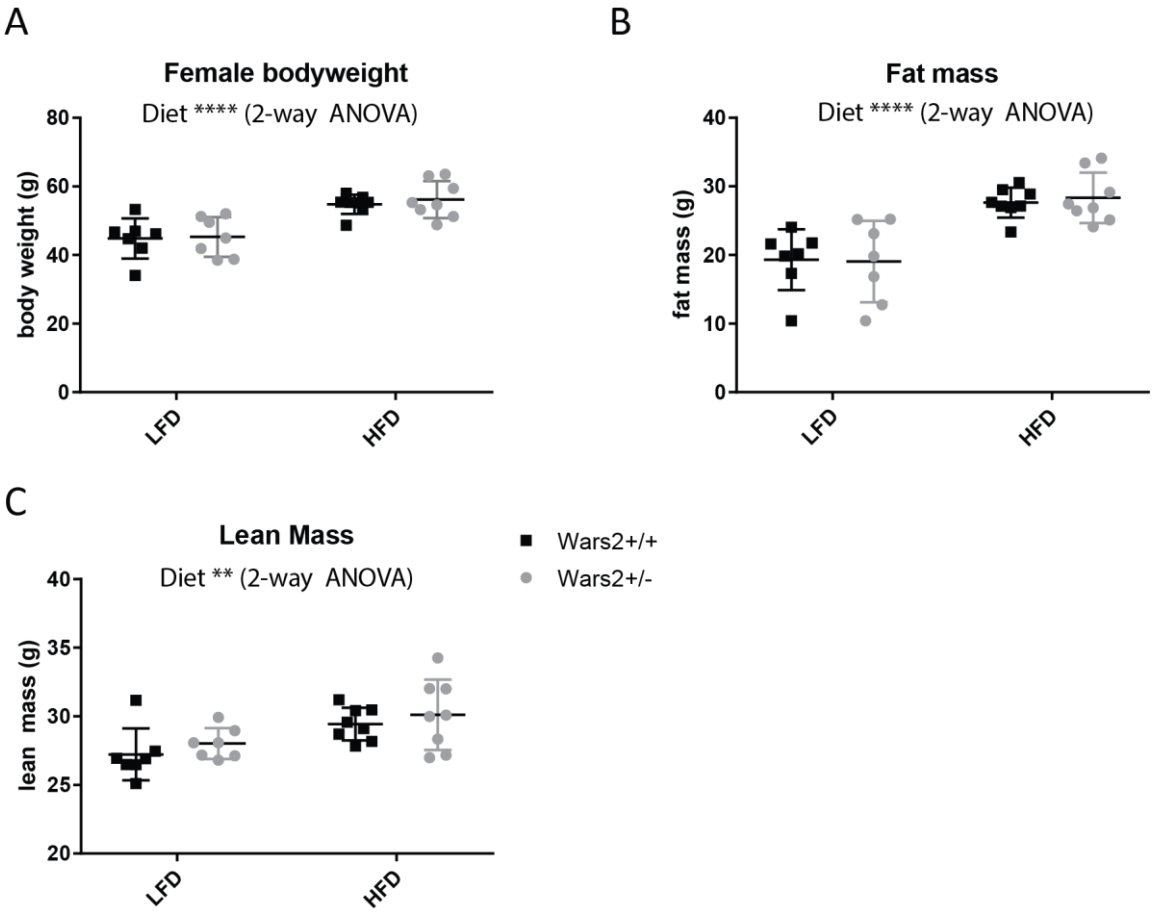

Figure 5.1 | *Wars2*$^{+/-}$ mice show no difference in bodyweight and body composition. 12-month old females either on low fat (LFD) and high fat (HFD) diets were compared for bodyweight (A), fat mass (B) and lean mass (C). *Wars2*$^{+/-}$ and *Wars2*$^{+/+}$ littermate numbers were 7 for LFD and 8 and 9 for HFD, respectively; mean ± SD. Significance was assessed using 2-way ANOVA with multiple comparisons test.

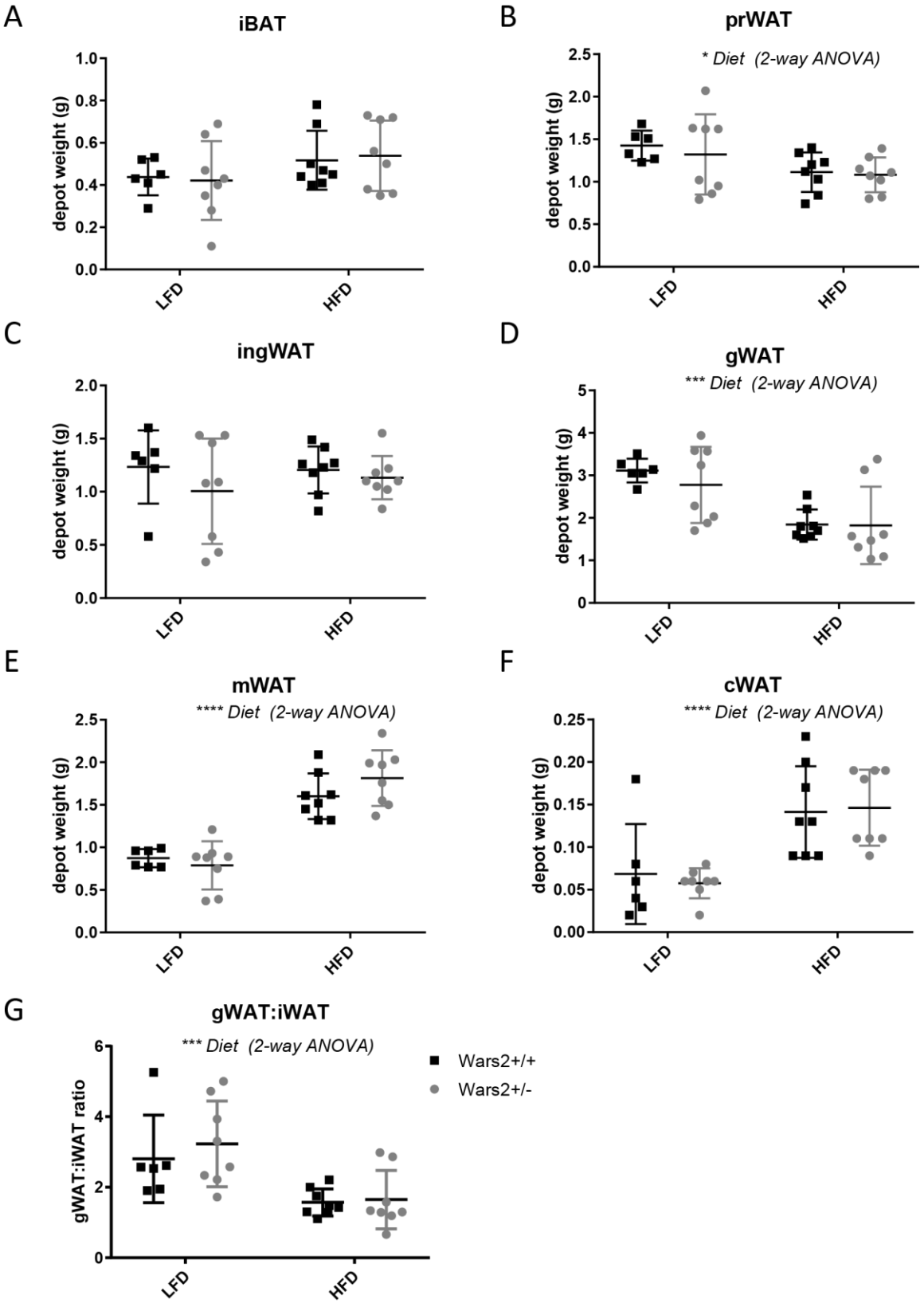

Figure 5.2 | *Wars2*$^{+/-}$ mice show no difference in fat depot weights. 12-month old females either on low fat (LFD) and high fat (HFD) diets were sacrificed and the following fat depots were weighed: interscapular BAT (isBAT), perirenal WAT (prWAT), inguinal WAT (iWAT), gonadal WAT (gWAT), mesenteric WAT (mWAT), cardiac WAT (cWAT). As an indicator of visceral to subcutaneous fat distribution, the gWAT:iWAT

ratio was calculated (G). *Wars2*$^{+/-}$ and *Wars2*$^{+/+}$ littermate numbers were 7 and 7 for LFD and 8 and 9 for HFD, respectively; mean ± SD. gWAT values were not normally distributed and were Y^2 transformed before statistical analysis. All data was analysed using 2-way ANOVA and significant factors due to diet indicated *p < 0.05, **p< 0.01, ***p<0.001. There were no significant differences due to genotype. I dissected and weighed fat depots together with Dr Rebecca Dumbell.

In the homozygous *Wars2*$^{V117L/V117L}$ mice, heart was one of the most severely affected tissues, showing hypertrophic cardiomyopathy, reduction in mitochondrial ETC complex levels and activation of integrated stress response (ISR) through Eukaryotic initiation factor 2 α (eIF2α) phosphorylation (Agnew *et al.*, 2018). To test for a shared heterozygous phenotype, I thus assessed the levels of Complex I-V and the mitochondrial outer membrane marker Voltage-dependent anion-selective channel 1 (VDAC1) in the *Wars2*$^{+/-}$ female hearts, but found no significant difference (Figure 5.3). Similarly, the ratio of P(S51)-eIF2α to eIF2α was not altered in the *Wars2*$^{+/-}$ female hearts (Figure 5.4). In summary, the 12-month old *Wars2*$^{+/-}$ females show no difference in body composition, fat distribution or complex levels and ISR activation in the heart.

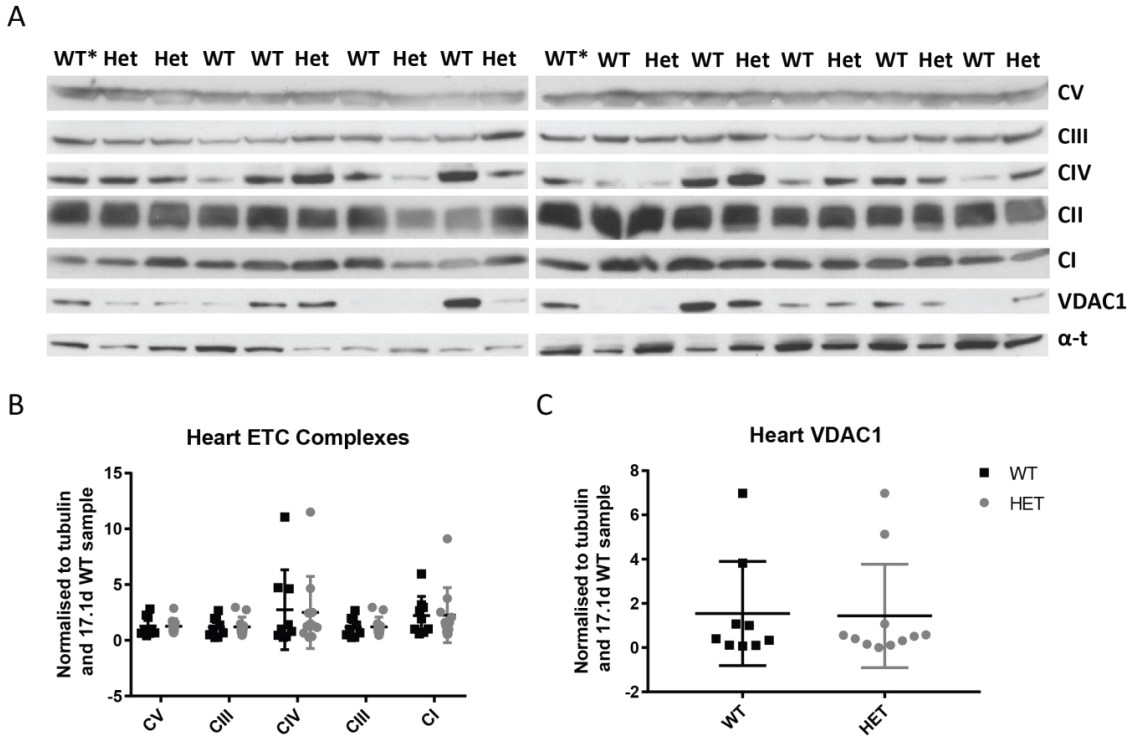

Figure 5.3 | VDAC1 and mitochondrial ETC complex levels are unchanged in the hearts of *Wars2*$^{V117L/V117L}$ mice.
Immunoblot analysis (A) and quantification (B,C) of ATP5A (Complex V), UQCR2 (Complex III), MTCO1 (Complex IV), SDHB (Complex II), NDUFB8 (Complex I) and VDAC1 in the hearts from female months at 12 months of age. *Wars2*$^{+/+}$ and *Wars2*$^{+/-}$ mice numbers were 10 and 10; with one sample from WT mouse 17.1d (*) run on both gels. The bands were normalised to tubulin and the 17.1d (*) sample on respective gels and expressed as mean ± SD. Significance was determined using unpaired t test for CV and CIII and the Mann-Whitney test using CIV, CII, CI and VDAC1.

A

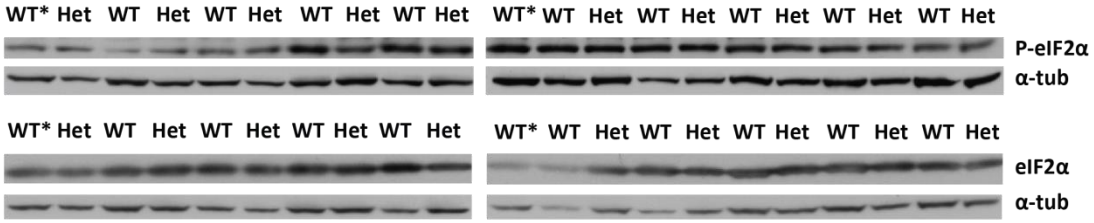

B

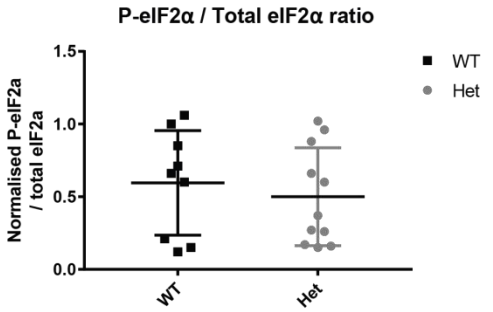

Figure 5.4 | Integrated Stress Response is not activated in in the hearts of *Wars2*$^{V117L/V117L}$ mice.

Immunoblot analysis (A) and quantification (B) of P(S51)-eIF2α and total eIF2α in the hearts from female months at 12 months of age. *Wars2*$^{+/+}$ and *Wars2*$^{+/-}$ mice numbers were 10 and 10; with one sample from WT mouse 17.1d (*) run on both gels. The bands were normalised to tubulin and to the 17.1d (*) sample on respective gels. The ratio of normalised P-eIF2α to total eIF2α was then expressed as mean ± SD. Significance was determined using the Mann-Whitney test.

5.3.2. Homozygous *Wars2*$^{V117L/V117L}$ mice fail to gain fat mass during normal growth and due to high-fat diet

Given the lack of a phenotype in heterozygous KO mice, I next planned to assess fat distribution in the *Wars2*$^{V117L/V117L}$ mice. Data from a small cohort of 6-month old *Wars2*$^{V117L/V117L}$ males showed a trend towards increased gWAT : iWAT ratio (Agnew *et al.*, 2018). I thus generated three new mouse cohorts to further investigate the effect of *Wars2* on fat distribution. For the first time, the mice were placed both on LFD and HFD to investigate whether HFD can alleviate the failure to gain fat mass reported in these mice.

Analysis of the Cohort 1 (67 mice) revealed a clear increase in bodyweight and fat mass due to HFD in both wild-type *Wars2*$^{+/+}$ and heterozygous *Wars2*$^{+/V117L}$ mice (Figure 5.5). Diet first reached significance for effect on bodyweight and fat mass at 10 weeks (P=0.0117) and 8 weeks (P=0.0187) in males and 6 weeks (P=0.0054) and 6 weeks (P=0.0015) in females, respectively. There was no effect of diet on lean mass in either males or females (Figure 5.5E, F). No significant difference between heterozygous mice on LFD or HFD was observed in any of the measures, showing that *Wars2*$^{V117L/V117L}$ mice fail gain fat mass due to HFD feeding.

Next I analysed the results of specific post-hoc comparisons between genotypes on each diet. First statistically significant differences between *Wars2*$^{+/+}$ and *Wars2*$^{V117L/V117L}$ mouse bodyweights of Cohort 1 mice on HFD appear at 8 weeks for males (P=0.0003) and 14 weeks (P=0.0215) for females (Figure 5.5A, B). In the case of LFD, first differences were delayed to 14 weeks in males (P=0.0425) and 24 week in females (P=0.0295). At the level of fat mass, first significant differences between *Wars2*$^{+/+}$ and *Wars2*$^{V117L/V117L}$ mice on HFD appear at 10 weeks for both males and females (P<0.0001, P=0.0200, respectively)

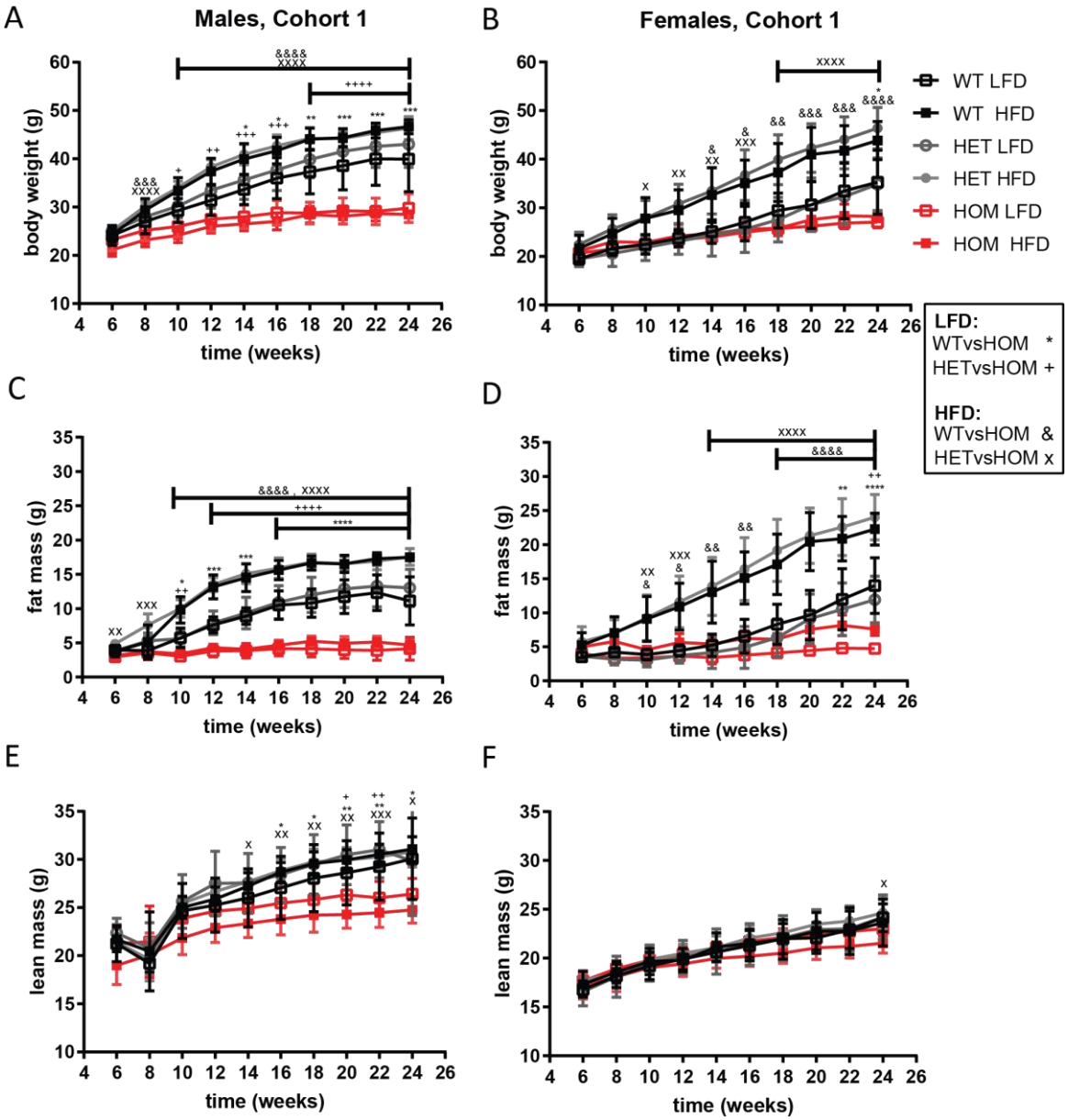

Figure 5.5 | *Wars2*$^{V117L/V117L}$ mice fail to gain fat mass during growth and due to high fat diet feeding.

Male and female cohort 1 mice: body weight (A and B), fat mass (C and D), and lean mass (E and F), respectively. *Wars2*$^{+/+}$ (WT), *Wars2*$^{+/V117L}$ (HET) and *Wars2*$^{V117L/V117L}$ (HOM) littermate numbers were 4, 6, 6 for males on LFD, 4, 6, 6 for males on HFD, 7, 5, 6 for females on LFD and 4, 7, 6 for females on HFD. Significance at specific time points was calculated with 2-way ANOVA with multiple comparison analysis for all groups within each sex. Significance between *Wars2*$^{+/+}$ (WT) and *Wars2*$^{V117L/V117L}$ (HOM) is shown as * $p < 0.05$, ** $p< 0.01$, *** $p<0.001$. Comparisons between other groups are depicted in the same way using the symbols (+, &, x) annotated in the top right corner.

(Figure 5.5C, D). On LFD, differences in fat mass are first seen at 10 weeks in males (P= 0.0173) and only at 22 weeks in females (P=0.0091). Thus in general, differences on HFD appear earlier than on LFD. No difference between *Wars2*$^{+/+}$ and *Wars2*$^{V117L/V117L}$ mice is observed at the level of lean mass on either diet in females, whilst in males this difference first becomes significant at 16 weeks of age for the HFD-fed mice (P=0.0131) (Figure 5.5E, F). For *Wars2*$^{+/V117L}$ mice, significant differences compared to the *Wars2*$^{V117L/V117L}$ mice were observed in bodyweight, fat mass and lean mass (Figure 5.5). Similarly, as for *Wars2*$^{+/+}$ mice comparisons, differences between heterozygous *Wars2*$^{+/V117L}$ mice and *Wars2*$^{V117L/V117L}$ mice were observed first on HFD, suggesting that the HFD potentiates the genotype-dependent differences. Indeed, 2-way ANOVA analysis at 24 weeks revealed the interaction of diet and genotype in male fat mass (P=0.0084) and female bodyweight (P=0.0195) and fat mass (P=0.0019). No significant difference was observed between the wild-type *Wars2*$^{+/+}$ mice and heterozygous *Wars2*$^{+/V117L}$ mice at the level of body weight, fat mass or lean mass at any of the time points.

To confirm these findings, I replicated these findings in Cohort 2 (88 mice) with identical experimental design, but an additional time-point at 4 weeks (Figure 5.6). Similarly to Cohort 1, HFD led to increased bodyweight and fat mass in wild-type and heterozygous mice. In Cohort 2, diet first reached significance for an effect on bodyweight and fat mass at 8 weeks (P=0.0455) and 8 weeks (P=0.0005) in males and at 4 weeks (P=0.0003) and 4 weeks (P<0.0001) in females, respectively. Thus, the onset of the diet effect did not differ more than by 2 weeks between the cohorts. Same as for Cohort 1, diet had no significant effect on lean mass.

Next, I compared the cohorts in terms of the genotype effect. Most importantly, Cohort 2 results confirmed that both male and female *Wars2*$^{V117L/V117L}$ mice fail to gain bodyweight and fat mass in response to HFD. Furthermore, as shown for Cohort 1, comparisons of the

bodyweight and fat mass of the *Wars2*$^{V117L/V11L7}$ mice to the wild-type *Wars2*$^{+/+}$ or heterozygous *Wars2*$^{+/V11L7}$ showed significance earlier in the mice on HFD compared to those on LFD. The particular time-points when significant differences were seen differed only ±2 weeks between males of Cohort 1 and Cohort 2 (Figure 5.5, Figure 5.6). For females, these differences were greater with much earlier detection in Cohort 2. For example, first differences between *Wars2*$^{+/V117L}$ and *Wars2*$^{V117L/V117L}$ female's bodyweights were observed only at 10 weeks for Cohort 1, but already at 6 weeks for Cohort 2 (HFD, P=0.0005). Difference in female lean mass was only detected at 24 weeks in Cohort 1 (HFD, HET vs HOM, P=0.0209), but already at 8 weeks for Cohort 2 (HFD, HET vs HOM, P=0.0197) (Figure 5.6). Another feature specific to Cohort 2 females was the significant increase in bodyweight and fat mass of *Wars2*$^{+/V117L}$ over *Wars2*$^{+/+}$ mice on HFD between 6 weeks (bodyweight, P= 0.0215, fat mass, P=0.0173) to 12 weeks (bodyweight, P= 0.0253, fat mass, P=0.0425).

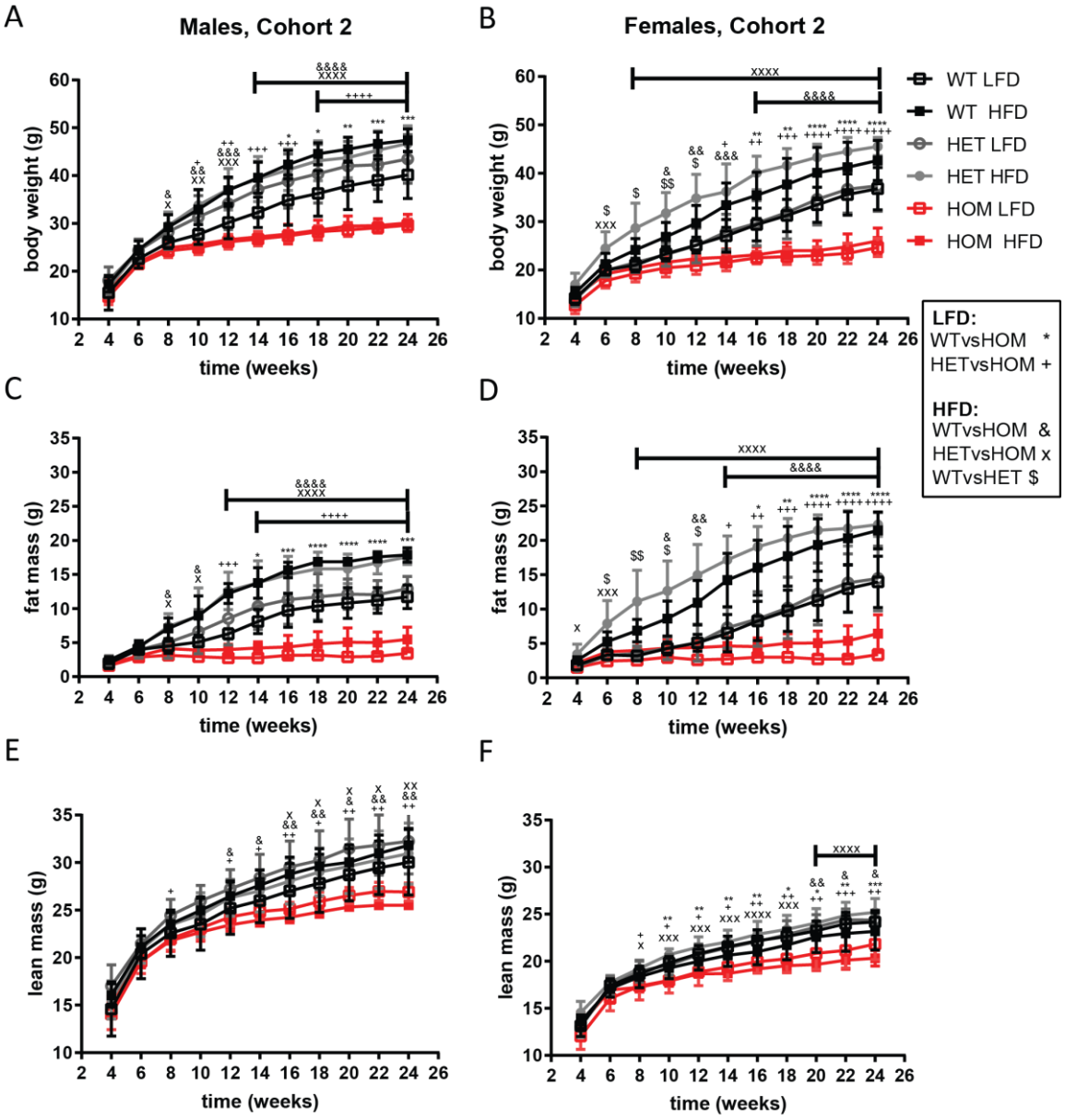

Figure 5.6 | Replication of the study of body composition with Cohort 2. Male and female cohort 1 mice: body weight (A and B), fat mass (C and D), and lean mass (E and F), respectively. *Wars2*$^{+/+}$ (WT), *Wars2*$^{+/V117L}$ (HET) and *Wars2*$^{V117L/V117L}$ (HOM) littermate numbers were 5, 8, 6 for males on LFD, 9, 8, 5, for males on HFD, 8, 9, 8 for females on LFD and 9, 8, 5 for females on HFD. Significance at specific time points was calculated with 2-way ANOVA with multiple comparison analysis for all groups within each sex. Significance between *Wars2*$^{+/+}$ (WT) and *Wars2*$^{V117L/V117L}$ (HOM) is shown as * $p < 0.05$, ** $p< 0.01$, *** $p<0.001$. Comparisons between other groups are depicted in the same way using the symbols (+, &, x, $) annotated in the top right corner.

5.3.3. Multiple fat depots are affected in both *Wars2*$^{+/V117L}$ and *Wars2*$^{V117L/V117L}$ mice

At 6 months, the phenotyping Cohort 1 was sacrificed and different fat depot weights compared in males and females, respectively (Figure 5.7 & Figure 5.8). Diet had a significant effect on male iWAT weight (P<0.0001) and all female depot weights except for cWAT, prBAT and prWAT. Effects of genotype were significant for all fat depots in males and all fat depots in females except for cWAT. All p-values of the 2-way ANOVA analysis and subsequent post-hoc analyses are summarised in Table 5.2**.**

Post-hoc comparisons revealed that in all male depots, except for cWAT, the homozygous *Wars*$^{V117L/V117L}$ mice showed lower fat depot weight compared to either the wild-type or heterozygous mice on at least one of the diets (Figure 5.7). Importantly, male gWAT on HFD was significantly heavier in heterozygous compared to wild-type mice (P=0.0374) (Figure 5.7C, F). A similar non-significant trend was also observed for male prBAT on LFD and male prWAT on HFD (Figure 5.7D). Interestingly, in male *Wars2*$^{V117L/V117L}$ homozygous mice on HFD, gWAT weight was not affected compared to WT (P=0.9803), but iWAT weight reduced dramatically by ~1.6g (P<0.0001) resulting in almost 2-fold increase in gWAT:iWAT ratio (P<0.0001) (Figure 5.9B,D,E). Male iWAT showed a significant interaction between diet and genotype (P=0.0018), supporting the previous finding that unlike wild-type and heterozygous mice, the homozygous *Wars2*$^{V117L/V117L}$ mice are unable to respond to HFD (Figure 5.7E). Thus, weights of brown and white fat depots from male homozygous mice are reduced compared to the wild-type or heterozygous mice, but gWAT appears to be protected in males on HFD and its weight is significantly increased in heterozygous mice.

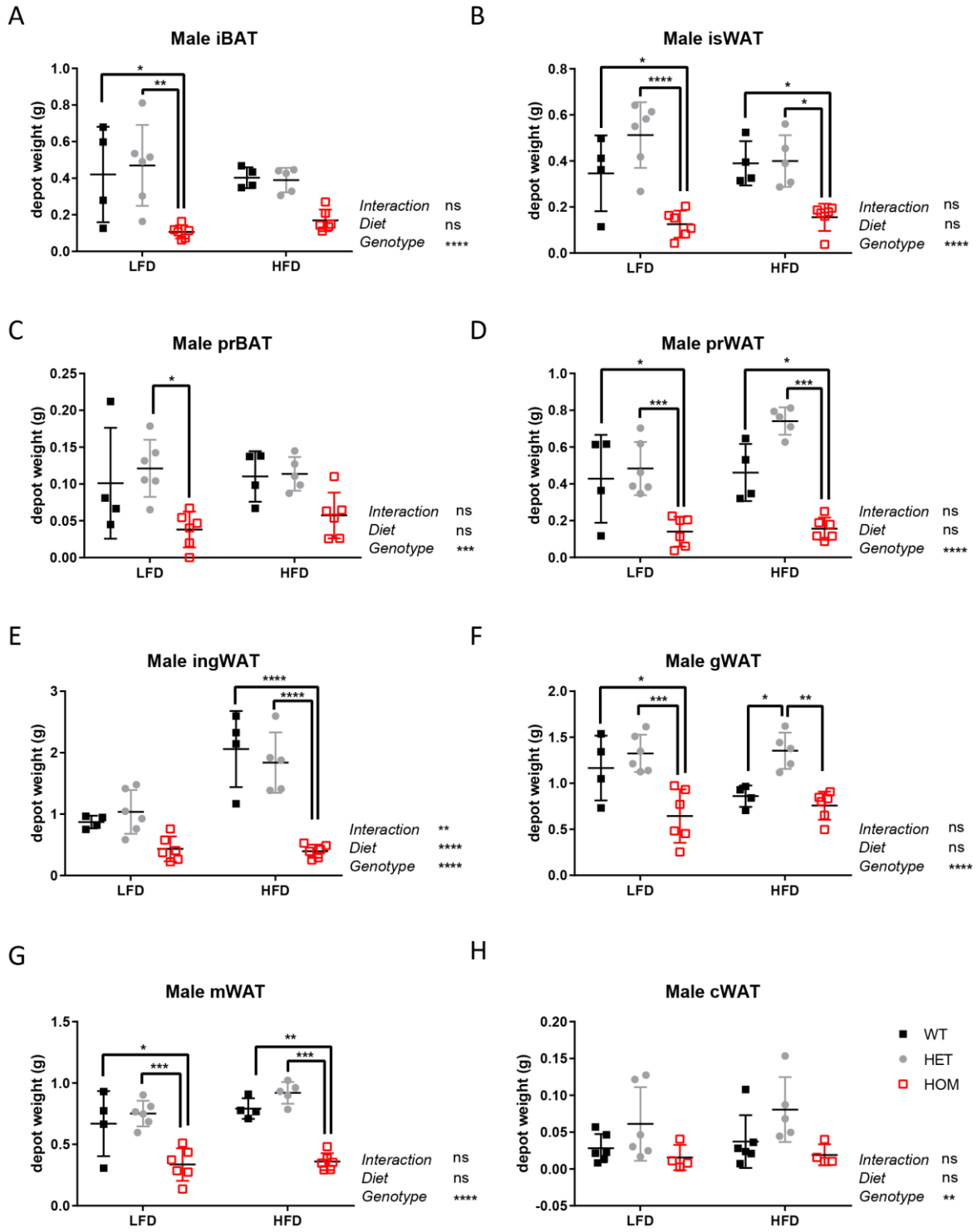

Figure 5.7 | Multiple fat depots are affected in both *Wars2*$^{V117L/V117L}$ and *Wars2*$^{+/V117L}$ males.

6-month old males either on low fat (LFD) and high fat (HFD) diets were sacrificed and the following fat depots were weighed: interscapular BAT (iBAT), interscapular WAT (isWAT), perirenal BAT (prBAT), perirenal WAT (prWAT), inguinal WAT (iWAT), gonadal WAT (gWAT), mesenteric WAT (mWAT), cardiac WAT (cWAT). *Wars2*$^{+/+}$ (WT), *Wars2*$^{+/V117L}$ (HET) and *Wars2*$^{V117L/V117L}$ (HOM) littermate numbers were 4, 6, 6 for males on LFD and 4, 6, 6 for males on HFD, respectively; mean ± SD. To fit a normal

distribution, eWAT, mWAT and prWAT data were transformed by $Log_2(Y)$. Significance was tested using 2-way ANOVA with post-hoc multiple comparison between all the groups. Significant differences due to diet, genotype and interaction are indicated as *p < 0.05, **p< 0.01, ***p<0.001. Significant differences in multiple comparisons of WT, HET and HOM on each diet are depicted too. Performed by Dr Marianne Yonn, Emily File and Lynn Beresford.

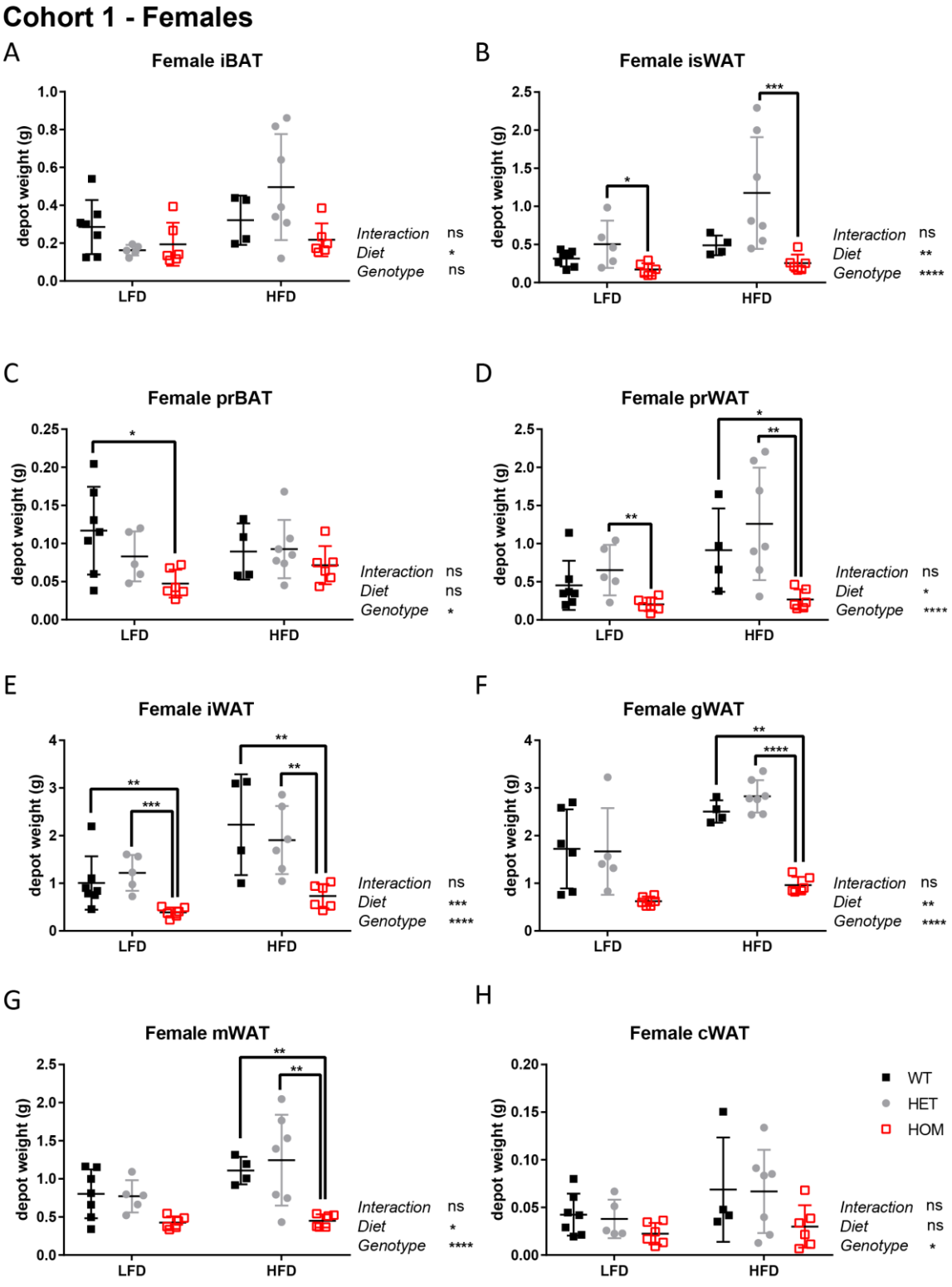

Figure 5.8 | Reduced weight of multiple fat depots in *Wars2*$^{V117L/V117L}$ females.

6-month old females either on low fat (LFD) and high fat (HFD) diets were sacrificed and the following fat depots were weighed: interscapular BAT (iBAT), interscapular WAT (isWAT), perirenal BAT (prBAT), perirenal WAT (prWAT), inguinal WAT (iWAT), gonadal WAT (gWAT), mesenteric WAT (mWAT), cardiac WAT (cWAT). *Wars2*$^{+/+}$ (WT), *Wars2*$^{+/V117L}$ (HET) and *Wars2*$^{V117L/V117L}$ (HOM) littermate numbers were 7, 5, 6 for females on LFD and 4, 7, 6 for females on HFD, respectively; mean ± SD. To fit a normal

distribution, eWAT data was transformed by $(Y)^2$ and $Log_2(Y)$ for all other depots. Significance was tested using 2-way ANOVA with post-hoc multiple comparison between all the groups. Significant differences due to diet, genotype and interaction are indicated as *p < 0.05, **p< 0.01, ***p<0.001. Significant differences in multiple comparisons of WT, HET and HOM on each diet are depicted too. Performed by Dr Marianne Yonn, Emily File and Lynn Beresford.

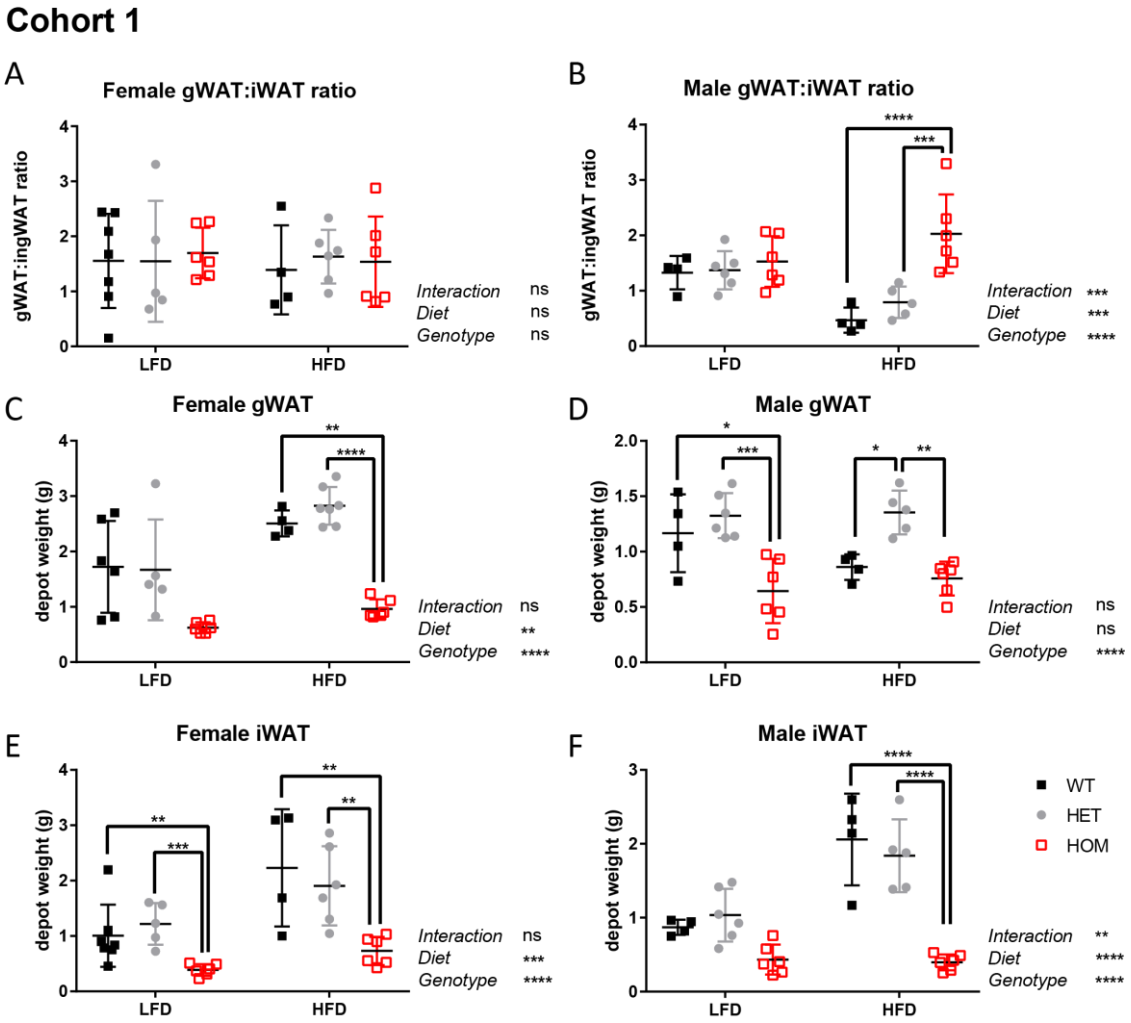

Figure 5.9 | Male-specific increase in gWAT:iWAT ratio in both *Wars2*$^{V117L/V117L}$ and *Wars2*$^{+/V117L}$ mice. gWAT:iWAT ratio was calculated for 6-month old Cohort 1 mice either on low fat (LFD) and high fat (HFD) diets (A, B). To fit a normal distribution, male gWAT:iWAT data was transformed by $Log_2(Y)$. Significance was tested using 2-way ANOVA with post-hoc multiple comparison between all the groups. Significant differences due to diet, genotype and interaction are indicated as *p < 0.05, **p< 0.01, ***p<0.001. Significant differences in multiple comparisons of WT, HET and HOM on each diet are depicted too. The individual gWAT and iWAT weights from Figure 5.7 Figure 5.8 are also shown (C, D, E, F).

In females, weights of all depots except cWAT and iBAT were reduced in homozygous mice compared to either wild-type or heterozygous mice on at least one of the diets (Figure 5.8, Table 5.2). Unlike for males, no significant increase in gWAT weight was observed in heterozygous compared to wild-type mice (P=0.7840) (Figure 5.8B). In females on HFD, both gWAT (P=0.0076) and iWAT (P=0.0040) depots of homozygous *Wars2*$^{V117L/V117L}$ mice were markedly reduced compared to the wild type and thus there was no significant difference in the gWAT:iWAT ratio (P=0.9965) (Figure 5.8A,C,E).

To identify the most robust results, I then compared the fat depot weights of Cohort 1 to those of Cohort 2 (Figure 5.10, Figure 5.11, Figure 5.12). Similarly to Cohort 1, Cohort 2 males showed significant effect of Diet on the weight of iWAT (P<0.0001). In females of Cohort 2, Diet influenced all depot weights except female iBAT (All the p-values are listed in Table 5.2). Thus although, there are some differences between specific depots affected, both cohorts show that Diet has a more wide effect on the fat depots in females compared to males.

Regarding fat distribution, the male-specific increase of gWAT:iWAT ratio in *Wars2*$^{V117L/V117L}$ mice was observed also in Cohort 2 (P=0.0006) (Figure 5.12). Same as in the previous cohort, this was because of the marked reduction in iWAT weight in both male (P<0.0001) and female *Wars2*$^{V117L/V117L}$ mice (P≤0.0002) on both diets and the lack of significant effect on gWAT in *Wars2*$^{V117L/V117L}$ males on HFD (P=0.4935). Uniquely in Cohort 2, *Wars2*$^{+/V117L}$ males on LFD showed significantly reduced gWAT:iWAT ratio compared to *Wars2*$^{+/+}$ mice (P=0.0004). Apart from gWAT, male iBAT and prBAT showed also no significant reduction on HFD consistently between the two cohorts, although a clear trend and non-significant (P=0.0599) reduction was observed for iBAT in Cohort 2 (Figure 5.7A,C Figure 5.10A,C). The lack of effect in homozygous prBAT on HFD was consistent in both cohorts and males and females (Figure 5.8C, Figure 5.11C).

Depot-specific differences were seen between the cohorts but importantly, none of the significant increases in *Wars2*$^{+/V117L}$ male depot-weights were replicated in Cohort 2 (Figure 5.10). Depot weights of all fat depot in *Wars2*$^{V117L/V117L}$ males and females in Cohort 2 are reduced compared to either the wild-type or heterozygous mice on at least one of the diets (Figure 5.10, Figure 5.11). Thus Cohort 2 detects a clear effect also in cWAT, where no difference was observed in the post-hoc comparisons of Cohort 1. A clear genotype influence is observed also in female iBAT, where no effect was observed in Cohort 1 (Figure 5.8A, Figure 5.11A).

In summary, most white and brown depots weights in both male and female homozygous *Wars2*$^{V117L/V117L}$ were reduced compared to the wild-type or heterozygous littermates in at least one of the diets and this was replicated in two independent cohorts. Increases in some fat depot weights of male heterozygous *Wars2*$^{+/V117L}$ mice in Cohort 1 were not replicated in Cohort 2. The consistently observed reduction of iWAT in homozygous mice of both sexes and specific lack of effect on male gWAT on HFD resulted in male and HFD-specific increase in gWAT:iWAT ratio in *Wars2*$^{V117L/V117L}$ mice.

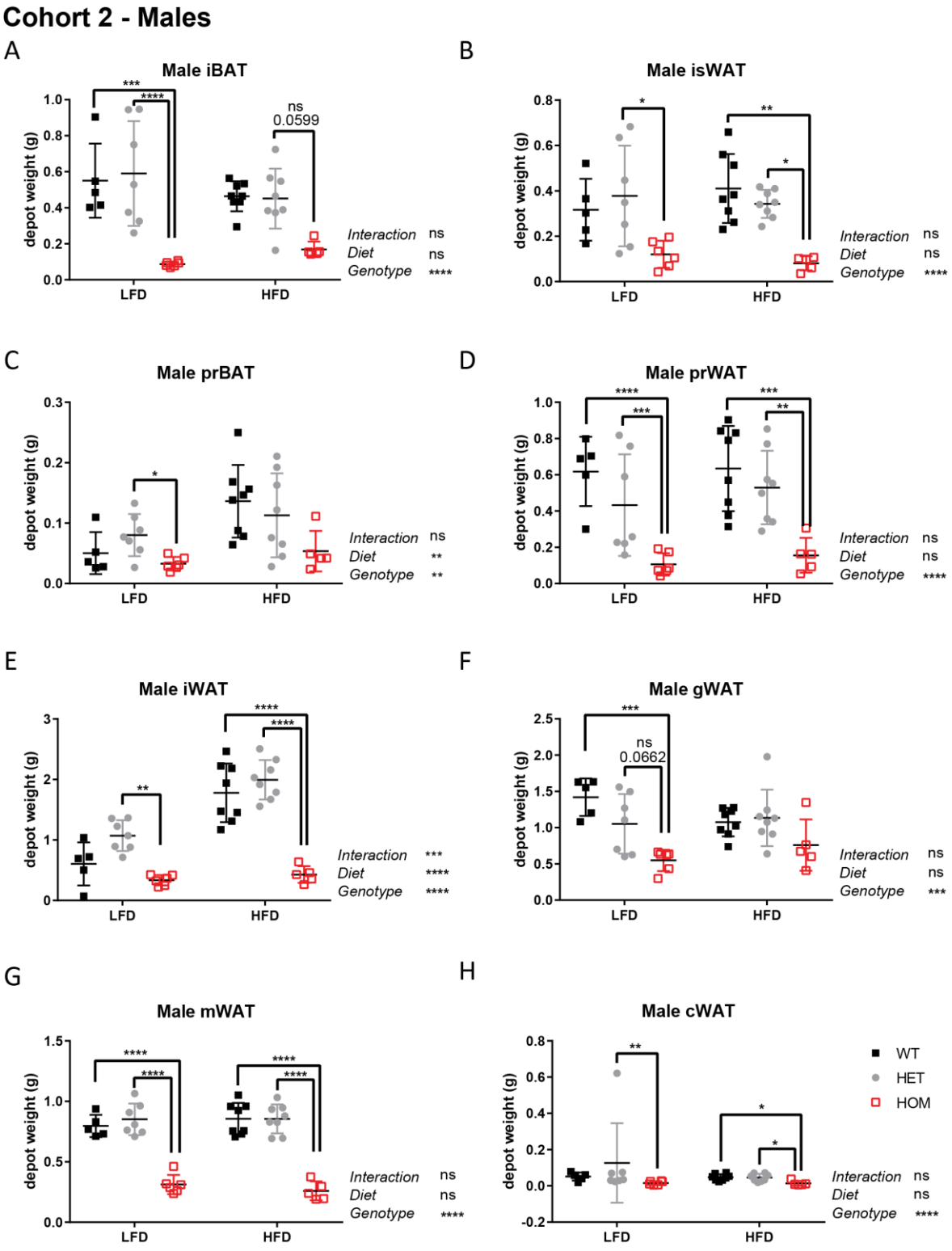

Figure 5.10 | Replication of the study of fat depot weights in Cohort 2 males. 6-month old males either on low fat (LFD) and high fat (HFD) diets were sacrificed and the following fat depots were weighed: interscapular BAT (iBAT), interscapular WAT (isWAT), perirenal BAT (prBAT), perirenal WAT (prWAT), inguinal WAT (iWAT), gonadal WAT (gWAT), mesenteric WAT (mWAT), cardiac WAT (cWAT). *Wars2*$^{+/+}$ (WT), *Wars2*$^{+/V117L}$ (HET) and *Wars2*$^{V117L/V117L}$ (HOM) littermate numbers were 5, 7, 6 for females on LFD and 8, 8, 5 for females on HFD, respectively; mean ± SD. iBAT, isWAT,

gWAT were normally distributed. To fit a normal distribution, iWAT, prWAT and cWAT data were transformed by Log(Y), prBAT by 1/Y and mWAT by exp(Y). Significance was tested using 2-way ANOVA with post-hoc multiple comparison between all the groups. Significant differences due to diet, genotype and interaction are indicated as *$p < 0.05$, **$p< 0.01$, ***$p<0.001$. Significant differences in multiple comparisons of WT, HET and HOM on each diet are depicted too. Performed by Dr Marianne Yonn, Emily File and Lynn Beresford.

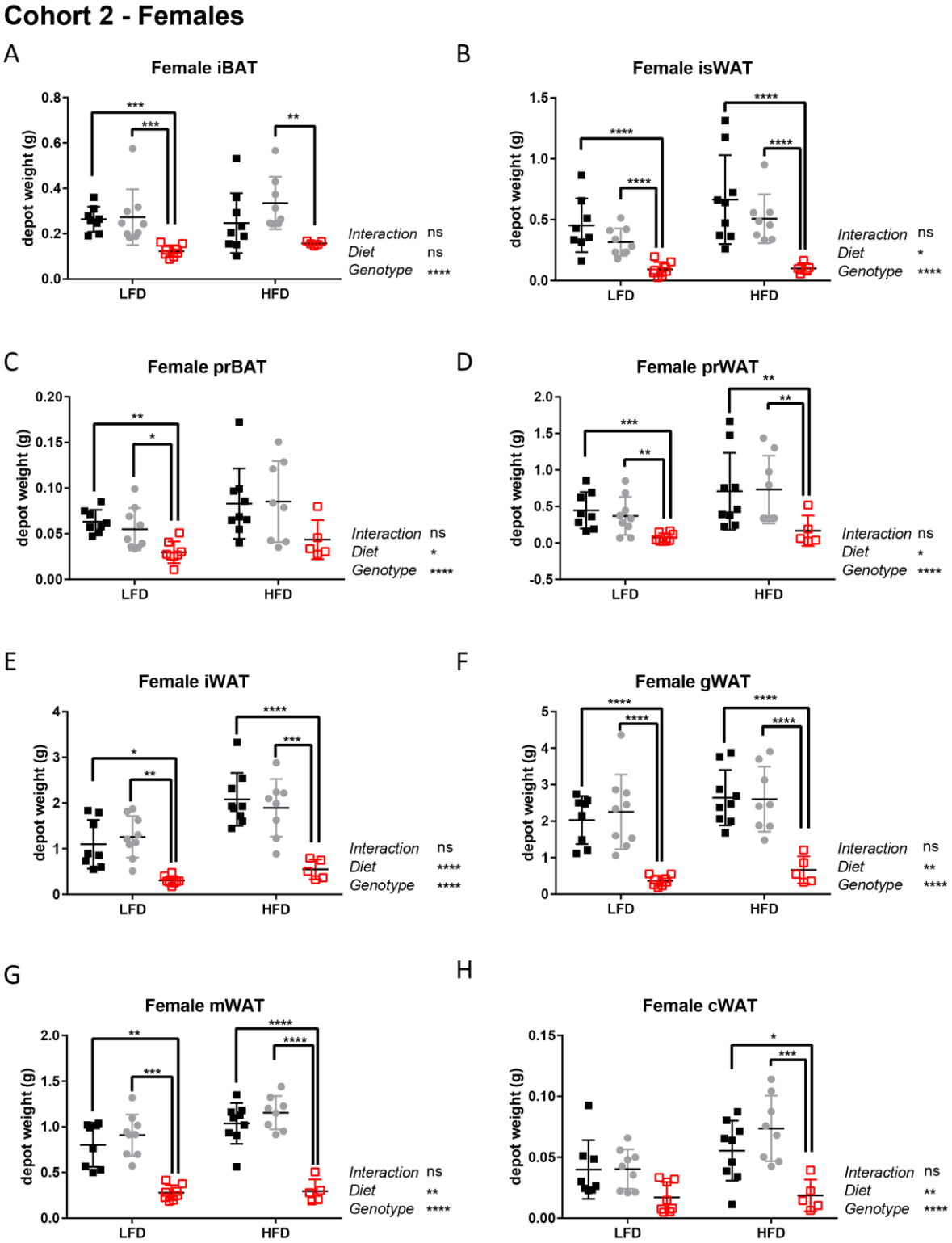

Figure 5.11 | Replication of the study of fat depot weights in Cohort 2 females. 6-month old females either on low fat (LFD) and high fat (HFD) diets were sacrificed and the following fat depots were weighed: interscapular BAT (iBAT), interscapular WAT (isWAT), perirenal BAT (prBAT), perirenal WAT (prWAT), inguinal WAT (iWAT), gonadal WAT (gWAT), mesenteric WAT (mWAT), cardiac WAT (cWAT). *Wars2*$^{+/+}$ (WT), *Wars2*$^{+/V117L}$ (HET) and *Wars2*$^{V117L/V117L}$ (HOM) littermate numbers were 7, 8, 8 for females on LFD and 9, 8, 5 for females on HFD, respectively; mean ± SD. iWAT, gWAT, cWAT data were normally distributed. To fit a normal distribution, iBAT, prBAT, isWAT

and prWAT were transformed by Log(Y) and mWAT data by exp(Y). Significance was tested using 2-way ANOVA with post-hoc multiple comparison between all the groups. Significance was tested using 2-way ANOVA with post-hoc multiple comparison between all the groups. Significant differences due to diet, genotype and interaction are indicated as *p < 0.05, **p< 0.01, ***p<0.001. Significant differences in multiple comparisons of WT, HET and HOM on each diet are depicted too. Performed by Dr Marianne Yonn, Emily File and Lynn Beresford.

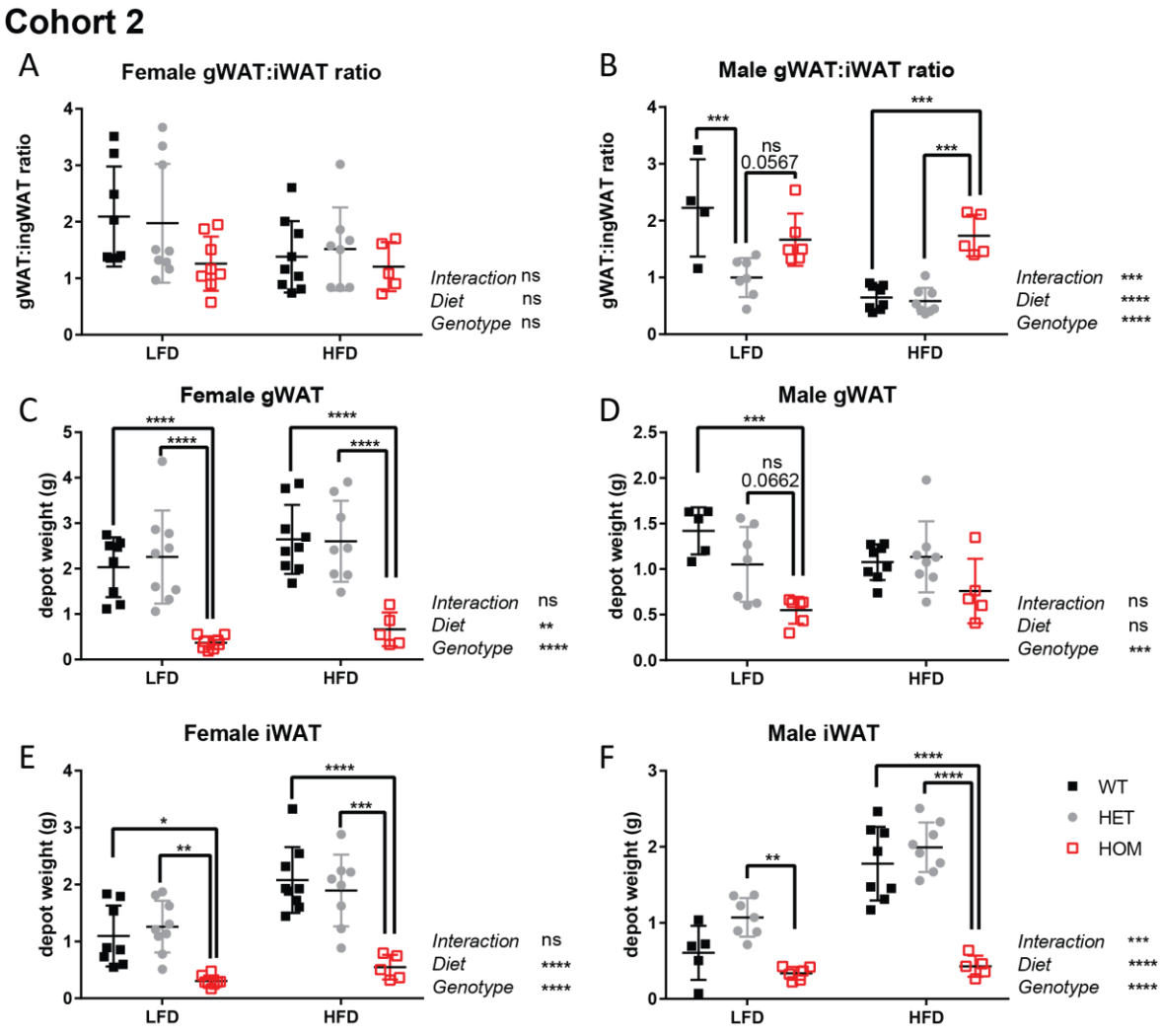

Figure 5.12 | gWAT:iWAT ratio in Cohort 2. gWAT:iWAT ratio was calculated for 6-month old Cohort 2 mice either on low fat (LFD) and high fat (HFD) diets (A, B). To fit a normal distribution, male iWAT data were transformed by Log(Y), all other data were normally distributed. Significance was tested using 2-way ANOVA with post-hoc multiple comparison between all the groups. Significant differences due to diet, genotype and interaction are indicated as *p < 0.05, **p< 0.01, ***p<0.001. Significant differences in multiple comparisons of WT, HET and HOM on each diet are depicted too. The individual gWAT and iWAT weights from Figure 5.10 and Figure 5.11 are also shown (C, D, E, F).

Table 5.2 | P-value summary of 2-way ANOVA analyses of fat depot weight differences between *Wars2*$^{+/+}$, *Wars2*$^{+/V117L}$ and *Wars2*$^{V117L/V117L}$ mice. Shows also results for specified post-hoc analyses. Significant p-values ≤ 0.05 are shown in bold.

Males	iBAT		isWAT		prBAT		prWAT		iWAT		gWAT		mWAT		cWAT		gWAT:iWAT	
Cohort:	1	2	1	2	1	2	1	2	1	2	1	2	1	2	1	2	1	2
Interaction	0.487	0.254	0.2133	0.3753	0.7172	0.1575	0.8321	0.6599	**0.0018**	0.1315	0.1416	0.4888	0.9144	0.5831	0.8661	0.8462	**0.0003**	**0.0001**
Diet	0.8233	0.3874	0.7444	0.8847	0.6306	**0.0057**	0.105	0.1847	**<0.0001**	**<0.0001**	0.5186	**0.0073**	0.0811	0.7561	0.211	0.4609	**0.0006**	**<0.0001**
Genotype	**<0.0001**	**<0.0001**	**<0.0001**	**<0.0001**	**0.0005**	**0.0044**	**<0.0001**	**<0.0001**	**<0.0001**	**<0.0001**	**<0.0001**	**<0.0001**	**<0.0001**	**<0.0001**	**0.0015**	**<0.0001**	**<0.0001**	**<0.0001**
Post-Hoc Analysis																		
LFD:WT vs. LFD:HOM	**0.0301**	**0.001**	**0.0436**	0.1704	0.1621	0.8124	**0.0193**	**0.0002**	0.4039	0.7331	**0.0183**	**0.0008**	**0.0136**	**<0.0001**	0.5744	0.0524	0.9904	0.2856
LFD:WT vs. LFD:HET	>0.9999	>0.9999	0.2067	0.9685	0.965	0.517	0.956	0.9624	0.9761	0.1583	0.8862	0.3558	0.9197	0.9402	0.6791	0.9933	>0.9999	**0.0004**
LFD:HOM vs. LFD:HET	**0.0023**	**<0.0001**	<0.0001	**0.0162**	**0.0125**	0.0343	**0.0007**	**0.0019**	0.0617	**0.003**	**0.0003**	0.0662	**0.0003**	**<0.0001**	0.0629	**0.0062**	0.9953	0.0567
LFD:HOM vs. HFD:HOM	0.9999	0.9998	0.9966	0.9961	0.9547	0.59	0.9573	0.8578	>0.9999	0.9964	0.9549	0.8706	0.9659	0.9971	0.9468	0.9996	0.6873	0.9997
HFD:WT vs. HFD:HOM	0.229	0.0599	**0.0283**	**0.0016**	0.3178	0.1234	**0.0229**	**0.0032**	**<0.0001**	**<0.0001**	0.9803	0.4935	**0.0034**	**<0.0001**	0.9147	**0.0191**	**<0.0001**	**0.0006**
HFD:WT vs. HFD:HET	>0.9999	>0.9999	>0.9999	0.9075	>0.9999	0.9141	0.6459	>0.9999	0.932	0.7551	0.0374	0.9989	0.9702	>0.9999	0.354	>0.9999	0.1579	0.9995
HFD:HOM vs. HFD:HET	0.2219	0.083	**0.0119**	**0.0172**	0.1983	0.5223	**0.0002**	**0.0025**	**<0.0001**	**<0.0001**	0.0028	0.308	**0.0002**	**<0.0001**	0.092	**0.0305**	**0.0008**	**0.0003**

Females	iBAT		isWAT		prBAT		prWAT		iWAT		gWAT		mWAT		cWAT		gWAT:iWAT	
Cohort:	1	2	1	2	1	2	1	2	1	2	1	2	1	2	1	2	1	2
Interaction	0.1169	0.1413	0.5453	0.749	0.2469	0.8057	0.8321	0.7685	0.5754	0.1315	0.0894	0.4888	0.4505	0.1949	0.8607	0.8462	0.9147	0.5175
Diet	**0.017**	0.2597	**0.0019**	**0.0253**	0.4701	**0.0146**	0.105	**0.0252**	**0.0002**	**<0.0001**	**0.0015**	**0.0073**	**0.0364**	**0.0056**	0.186	0.4609	0.7707	0.079
Genotype	0.1586	**<0.0001**	**<0.0001**	**<0.0001**	**0.02**	**<0.0001**	**<0.0001**	**<0.0001**	**<0.0001**	**<0.0001**	**<0.0001**	**<0.0001**	**<0.0001**	**<0.0001**	**0.0233**	**<0.0001**	0.899	0.145
Post-Hoc Analysis																		
LFD:WT vs. LFD:HOM	0.7206	**0.0004**	0.1873	<0.0001	**0.0185**	**0.005**	0.2604	**0.0002**	**0.0062**	**0.0219**	0.1547	**<0.0001**	0.0894	**0.005**	0.5614	0.264	0.9994	0.263
LFD:WT vs. LFD:HET	0.6298	>0.9999	0.7989	0.7906	0.8791	0.9298	0.8468	0.9624	0.8824	0.9814	>0.9999	0.9991	>0.9999	0.9032	0.9998	>0.9999	>0.9999	0.9995
LFD:HOM vs. LFD:HET	>0.9999	**0.0004**	**0.0201**	**<0.0001**	0.301	**0.0471**	**0.0379**	**0.0019**	**0.0009**	**0.0024**	0.2177	**<0.0001**	0.1265	**0.0002**	0.7921	0.2199	0.9995	0.3973
LFD:HOM vs. HFD:HOM	0.9874	0.7105	0.6614	0.9835	0.5382	0.623	0.9676	0.8578	0.1229	0.9469	0.9976	0.1929	0.9999	>0.9999	0.9992	>0.9999	0.9992	>0.9999
HFD:WT vs. HFD:HOM	0.8433	0.448	0.2671	**<0.0001**	0.9761	0.0905	**0.0424**	**0.0032**	**0.004**	**<0.0001**	**0.0076**	**<0.0001**	**0.0073**	**<0.0001**	0.3405	**0.033**	0.9996	0.9983
HFD:WT vs. HFD:HET	0.8983	0.1963	0.1919	0.9625	>0.9999	>0.9999	0.9745	>0.9999	0.9975	0.9676	0.784	>0.9999	>0.9999	0.7326	0.9999	0.4812	0.9965	0.999
HFD:HOM vs. HFD:HET	0.1442	0.0056	**0.0002**	**<0.0001**	0.9197	0.1295	**0.0014**	**0.0025**	**0.0041**	**0.0002**	**<0.0001**	**<0.0001**	**0.0014**	**<0.0001**	0.3125	**0.0005**	>0.9999	0.9779

5.3.4. Defective brown adipose tissue already at 4 months of age

Previously, 12-month old *Wars2*$^{V117L/V117L}$ mice showed a reduction in mitochondrial ETC Complex I, III and IV levels, UCP1 protein levels and reduced browning marker mRNA expression in interscapular BAT (Agnew et al., 2018). To see whether brown adipose is affected at an earlier time-point, I assessed the levels of ETC complexes in mice at 4 months of age on RM3 diet. Both male and female mice showed an almost complete lack of MTCO1 (Complex IV) (males P=0.0007, females P=0.0079) and NDUFB8 (Complex I) (males P=0.0004, females P=0.0079) compared to wild-type mice (Figure 5.13A-D). To assess an effect on mitochondrial mass, I also quantified VDAC1 levels, but found no significant differences. The increase of VDAC in *Wars2*$^{V117L/V117L}$ BAT in males was also not significant (P=0.0539) (Figure 5.13E, F). UCP1 levels were significantly reduced in males (P=0.0258) (Figure 5.14A, B) with a no significant difference in females (P=0.1594) (Figure 5.14C, D).

In agreement with findings in the older mice, mRNA expression of all tested browning markers *cell death-inducing DNA fragmentation factor subunit alpha (DFFA)-like effector a (Cidea), cytochrome c oxidase polypeptide 7A (Cox7a), iodothyronine deiodinase 2 (Dio2), PR domain containing 16 (Prdm16)* and *Ucp1* was reduced in the BAT of 4-month old *Wars2*$^{V117L/V117L}$ mice (Figure 5.15A,B) (p-values and fold changes are listed in Table 5.3). Both male and female BAT showed also reduced expression of the transcription factors *Peroxisome proliferator-activated receptor alpha (Pparα)* and *Peroxisome proliferator-activated receptor gamma (Pparγ)* and a decrease in *β-clotho (Kl)*, which encodes a co-receptor for FGF21. In female BAT, this reduction was accompanied by a ~2-fold increase in *Fgf21* expression (P= 0.0128) (Figure 5.15B). To directly assess mitochondrial content, I used SYBR-Green qPCR to quantify mtDNA (*Mitochondrially encoded NADH:Ubiquinone oxidoreductase core subunit 1* (*mt-Nd1)* gene) and gDNA

(*Glyceraldehyde 3-phosphate dehydrogenase (Gapdh)* gene) and calculate the

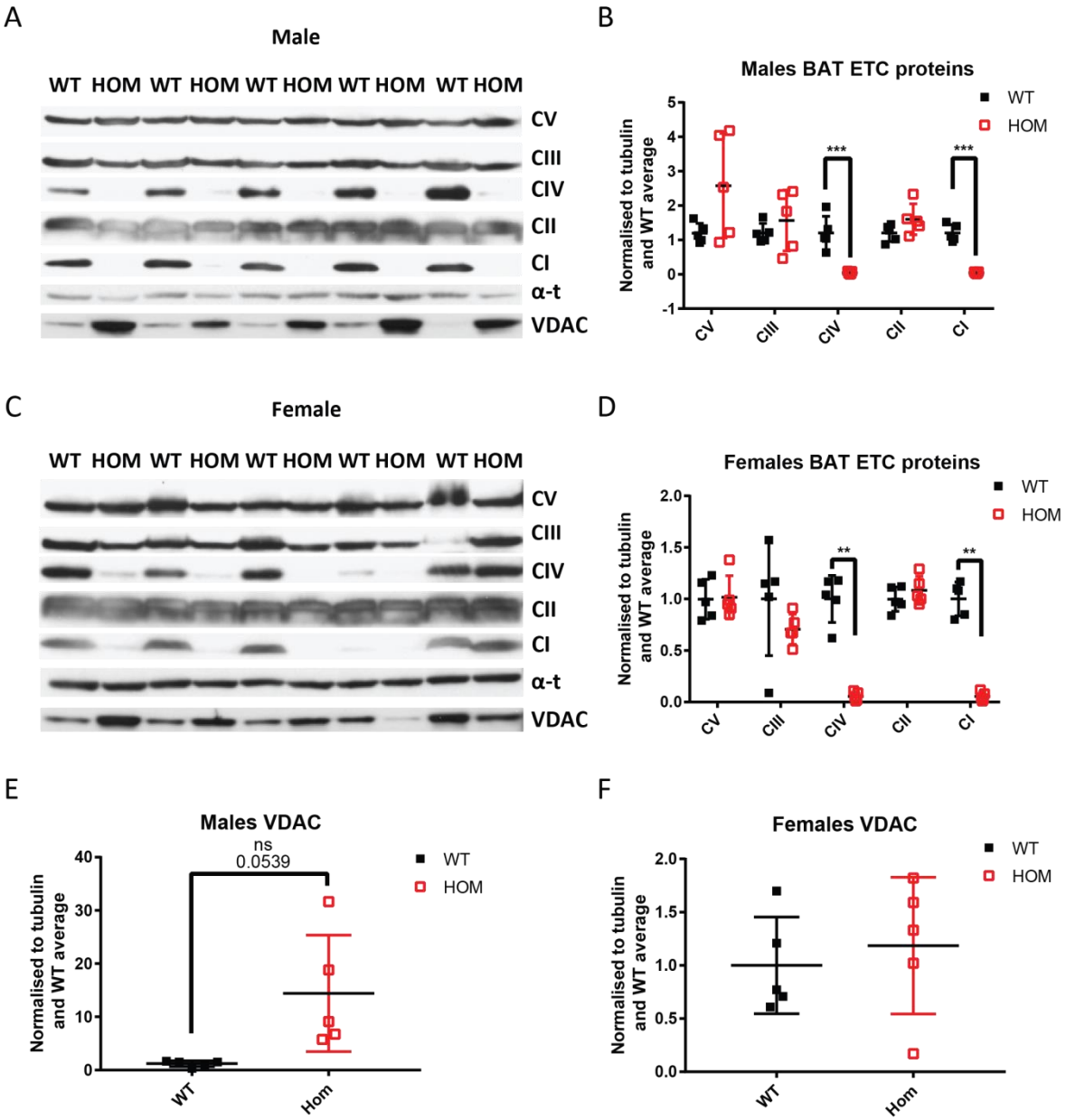

Figure 5.13 | Reduced levels of mitochondrial Complex IV and Complex I in brown adipose of 4 month old *Wars2*$^{V117L/V117L}$ mice.

Immunoblot analysis (A, C) and quantification (B, D, E, F) of ATP5A (Complex V), UQCR2 (Complex III), MTCO1 (Complex IV), SDHB (Complex II), NDUFB8 (Complex I) and VDAC1 in interscapular brown adipose (BAT) from mice at 4 months of age. *Wars2*$^{+/+}$ and *Wars2*$^{V117L/V117L}$ mice numbers were 5 and 5, respectively. The bands were normalised to tubulin and to WT average and shown as mean ± SD. Significance was determined using the Mann Whitney test for male BAT CII, VDAC1 and female BAT CIV, CI or unpaired t test for female BAT CV, CII, VDAC1, or Welch's t test for male CV, CIII, CIV, CI and female CIII. *p < 0.05, **p< 0.01, ***p<0.001.

mtDNA:gDNA ratio in male and female fat BAT (Figure 5.15C). In agreement with the reduced browning marker expression, I found a 10% and 18% decrease in the mtDNA:gDNA ratio in male (P=0.0461) and female BAT (P=0.0002), respectively. In summary, the BAT of *Wars2*$^{V117L/V117L}$ mice is severely affected already at 4 months of age and shows marked ETC complex deficiency, reduced brown fat marker expression and reduced mitochondrial mass.

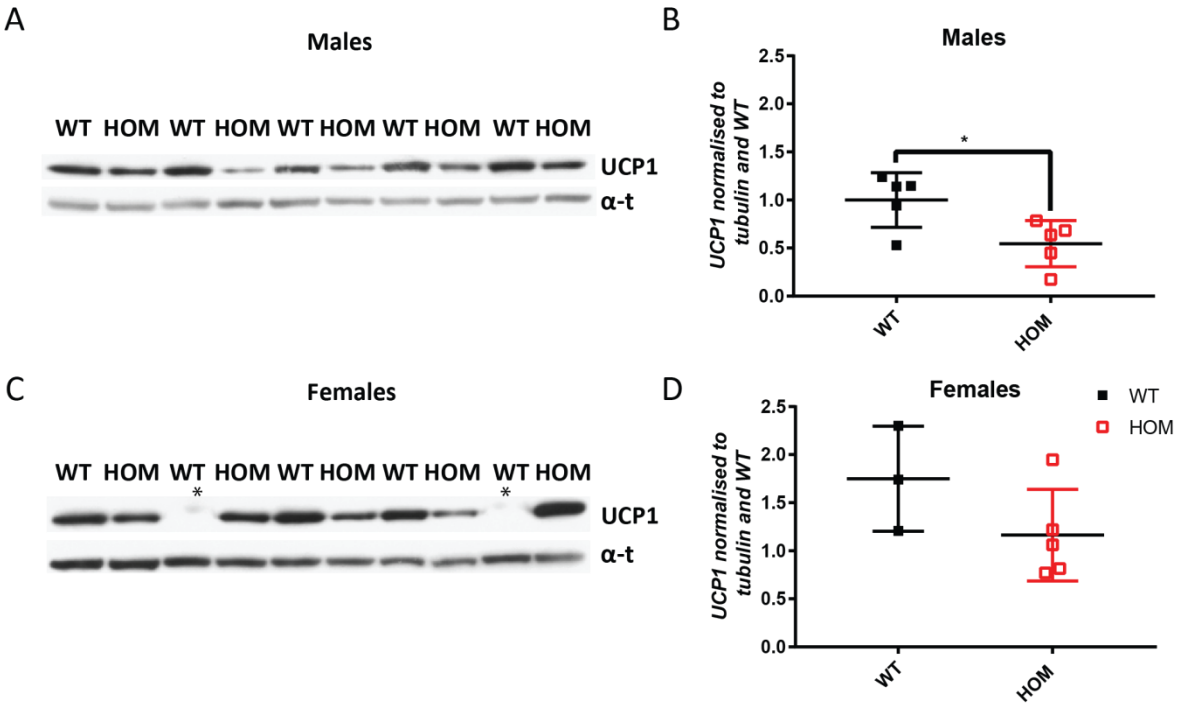

Figure 5.14 | Levels of UCP1 protein are reduced in interscapular BAT of 4 month old *Wars2*$^{V117L/V117L}$ males. Immunoblot analysis (A, C) and quantification (B, D) of UCP1 in interscapular brown adipose (BAT) from mice at 4 months of age. *Wars2*$^{+/+}$ and *Wars2*$^{V117L/V117L}$ mice numbers were 5 and 5, respectively. The bands were normalised to tubulin and to WT average and shown as mean ± SD. Significance was determined using unpaired t test. *p < 0.05. Two female WT samples marked with an asterisk (*) were not included due to smeary bands.

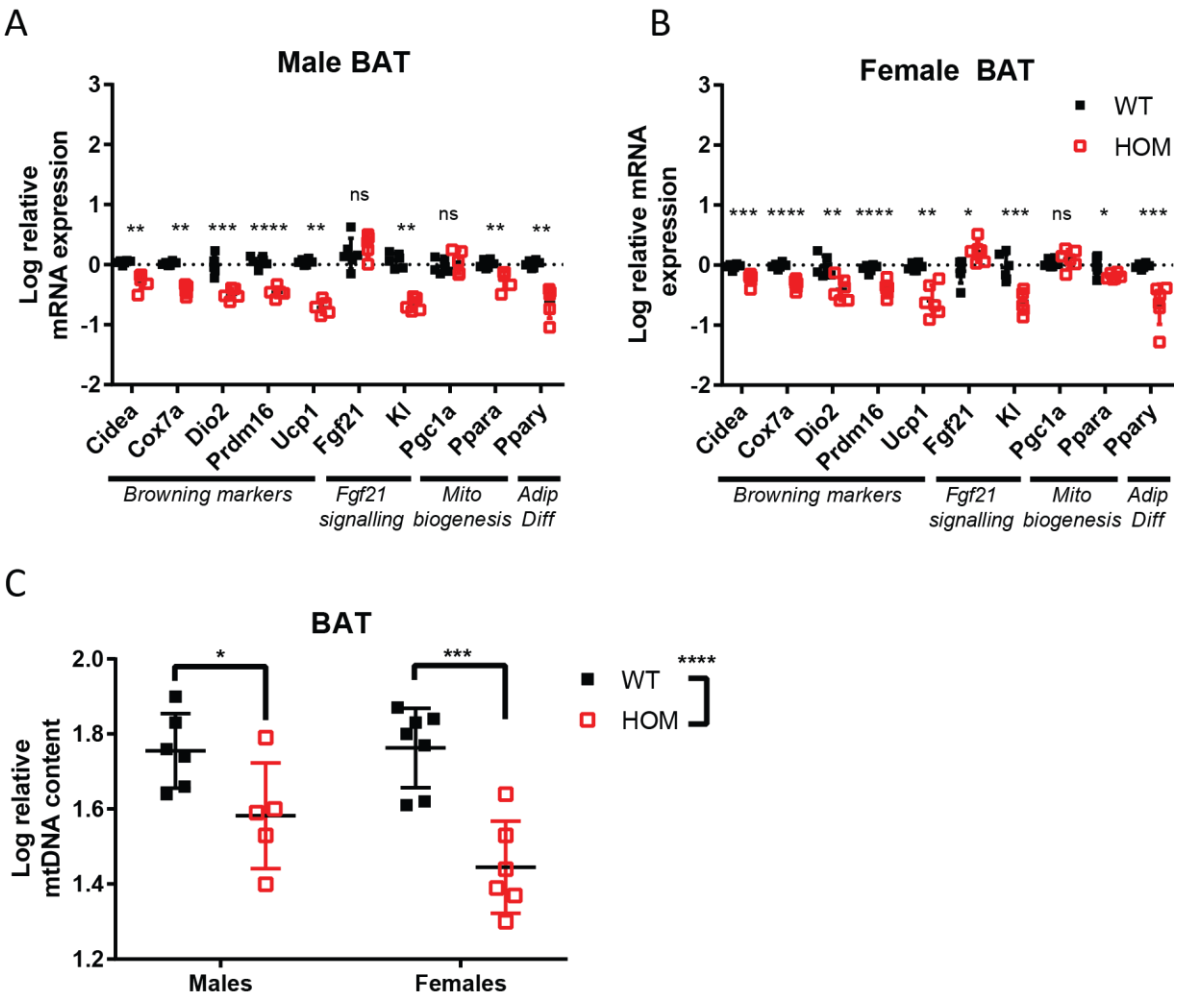

Figure 5.15 | Downregulation of brown fat marker genes and mitochondrial content in the brown fat of *Wars2*$^{V117L/V117L}$ mice. Relative mRNA expression analysis of markers of brown fat genes, FGF21 signalling, mitochondrial biogenesis and adipose differentiation in male and female interscapular BAT (A, B). Data were normalised to the geometric mean of *Canx* and *Ywhaz*. *Wars2*$^{+/+}$ and *Wars2*$^{V117L/V117L}$ mice numbers were 5 and 5 for females and 6 and 5 for males, respectively; mean ± SD. Data were log transformed and analysed using unpaired t test or Mann-Whitney test based on the data distribution. The specific tests used and p-values are listed in Table 5.3. The ratio of mitochondrial DNA to genomic DNA was assessed by qPCR of *mt-Nd1* and *Gapdh* in iWAT and gWAT from the same mice used in A and B (C). Data were log-transformed and compared by 2-way ANOVA followed by post-hoc comparison of genotypes within each depot. *p < 0.05, **p< 0.01, ***p<0.001.

Table 5.3 | Summary of significant differences and respective fold changes in BAT gene markers of the *Wars2*$^{V117L/V117L}$ mouse BAT. Data refers to the results shown in Figure 5.15A, B. Fold change is only shown for significant results with p-values ≤ 0.05.

	Males			Females		
Gene	*Test*	*p-value*	*fold change*	*Test*	*p-value*	*fold change*
Cidea	*Welch's t*	*0.0052*	*0.49*	*Unpaired t*	*0.0004*	*0.63*
Cox7a	*Mann-Whitney*	*0.0043*	*0.36*	*Unpaired t*	*<0.0001*	*0.50*
Dio2	*Unpaired t*	*0.0002*	*0.31*	*Unpaired t*	*0.0040*	*0.42*
Prdm16	*Unpaired t*	*<0.0001*	*0.31*	*Unpaired t*	*<0.0001*	*0.47*
Ucp1	*Mann-Whitney*	*0.0043*	*0.18*	*Welch's t*	*0.0026*	*0.32*
Fgf21	*Unpaired t*	*0.3630*		*Unpaired t*	*0.0128*	*2.11*
Kl	*Mann-Whitney*	*0.0043*	*0.18*	*Unpaired t*	*0.0007*	*0.27*
Pgc1a	*Unpaired t*	*0.4725*		*Unpaired t*	*0.3351*	
Ppara	*Unpaired t*	*0.0047*	*0.56*	*Unpaired t*	*0.0177*	*0.62*
Ppary	*Welch's t*	*0.0048*	*0.26*	*Unpaired t*	*0.0010*	*0.28*

5.3.5. Increased browning in both subcutaneous and visceral white adipose tissue in 4-month old *Wars2*$^{V117L/V117L}$ mice

Previously, 12-month old *Wars2*$^{V117L/V117L}$ mice showed increased Complex I levels and upregulation of mitochondria and browning markers in iWAT (Agnew *et al.*, 2018). I hypothesised that the upregulation of complexes and browning is specific to subcutaneous adipose leading to increased energy expenditure and reduced subcutaneous depot weight. To test this I first assessed the levels of mitochondrial complex proteins in 4-month old males and females (Figure 5.16 & Figure 5.17, respectively). There were no statistically significant differences. Increases in MTCO1 (Complex IV) expression in male iWAT and UQCR2 (Complex III) expression in female gWAT were also not statistically significant (P=0.057 and P=0.056, respectively).

To compare browning in the two fat depots, I first quantified levels of VDAC1 (porin), the outer mitochondrial membrane marker in males and females and found a significant increase in male iWAT (P=0.0020) (Figure 5.18). Uncoupling protein 1 (UCP1), a key mediator of proton leak and non-shivering thermogenesis, was significantly upregulated in male iWAT (P= 0.0437) (Figure 5.20A), but was absent in male gWAT of both genotypes (Figure 5.20B). In females, UCP1 was expressed in both depots, but its levels in the homozygous mice showed a high standard deviation and no statistically significant differences in either of the depots (Figure 5.21).

I then assessed the expression of markers of browning, mitochondrial biogenesis and FGF21 signalling using qPCR (Figure 5.22). In male iWAT, the expression of *Cidea*, *Cox7a*, and *Dio2* were significantly increased by a fold-change of 3, 3 and 9, respectively (P values = 0.0343, 0.0414, 0.0133, respectively) (Figure 5.22A). Male gWAT showed ~1.5-fold increase in mRNA levels of both *Cidea* (P=0.0025) and the master regulator of

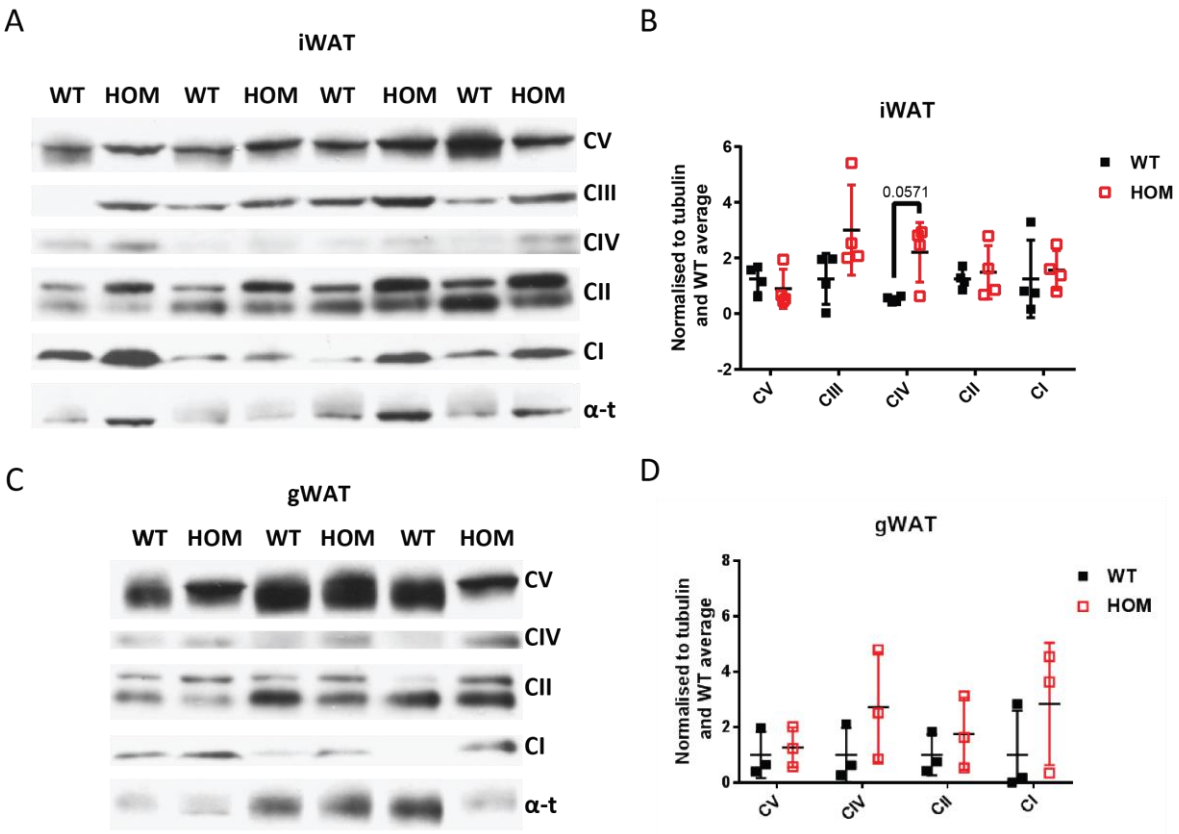

Figure 5.16 | Males - Levels of mitochondrial ETC complexes are unaffected in both iWAT and gWAT of 4-month old *Wars2*$^{V117L/V117L}$ mice.
Immunoblot analysis (A, C) and quantification (B, D) of ATP5A (Complex V), UQCR2 (Complex III), MTCO1 (Complex IV), SDHB (Complex II), NDUFB8 (Complex I) in the iWAT and gWAT from male months at 4 months of age. *Wars2*$^{+/+}$ and *Wars2*$^{V117L/V117L}$ mice numbers were 4 and 4 for iWAT and 3 and 3 for gWAT, respectively. The bands were normalised to tubulin and to WT average and shown as mean ± SD. Significance was determined using the Mann Whitney test for iWAT CIV or unpaired t-test for all other comparisons.

mitochondrial biogenesis *peroxisome proliferator-activated receptor gamma coactivator 1-α* (*Pgc1α)* (P=0.0006) (Figure 5.22B). There was also a small non-significant (P=0.0584) increase in *Dio2* levels. In female iWAT, *Cidea*, *Dio2*, *Pgc1α* were ~3.5-fold increased (P= 0.0122, 0.0130, 0.0026, respectively) and *Pparα* 2.3-fold upregulated (P=0.0179) in the homozygous *Wars2*$^{V117L/V117L}$ mice (Figure 5.22C). The expression of browning genes in female gWAT was highly variable.

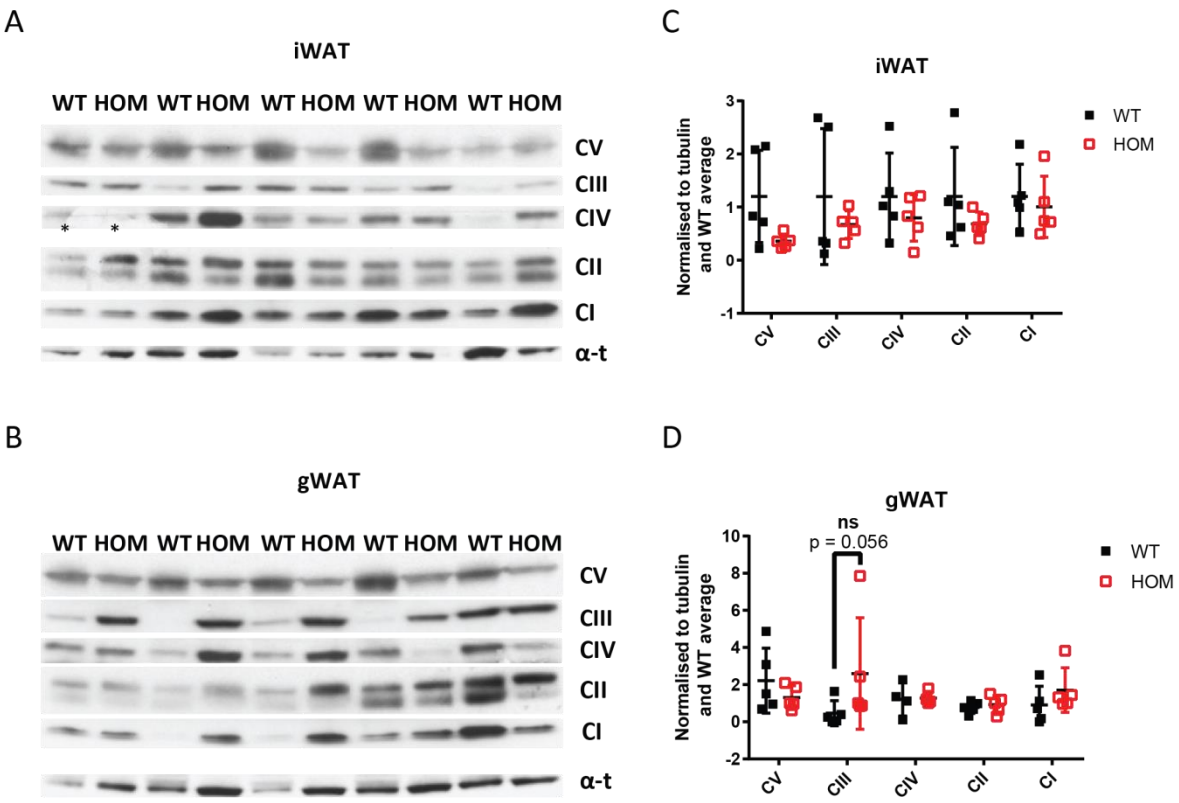

Figure 5.17 | Females - Levels of mitochondrial ETC complex levels are unaffected in both iWAT and gWAT of 4-month old *Wars2*$^{V117L/V117L}$ mice.
Immunoblot analysis (A, C) and quantification (B, D) of ATP5A (Complex V), UQCR2 (Complex III), MTCO1 (Complex IV), SDHB (Complex II), NDUFB8 (Complex I) in the iWAT and gWAT from female months at 4 months of age. *Wars2*$^{+/+}$ and *Wars2*$^{V117L/V117L}$ mice numbers were 5 and 5, respectively. The bands were normalised to tubulin and to WT average and shown as mean ± SD. Significance was determined using the Mann Whitney test for iWAT CIV, CII and gWAT CV, CIII or unpaired t test for iWAT CI, gWAT CIV, CII, CI, or Welch's t test for iWAT CIV, CII.

Pgc1α was the only significantly upregulated gene with a ~3-fold increase (P=0.0176) in the homozygous mice (Figure 5.22D). Next, I observed a significant increase of 45% and 24% in mtDNA:gDNA ratio in male *Wars2*$^{V117L/V117L}$ iWAT (P=0.0002) and gWAT (P=0.0264), respectively (Figure 5.22E). No difference was seen in female mice (Figure 5.22F).

In summary, evidence of increased browning was observed at multiple levels (mRNA, protein, mtDNA) in both iWAT and gWAT depots in *Wars2*$^{V117L/V117L}$ mice. The specific

effects differed between sexes with iWAT generally showing changes of greater magnitude (Table 5.4).

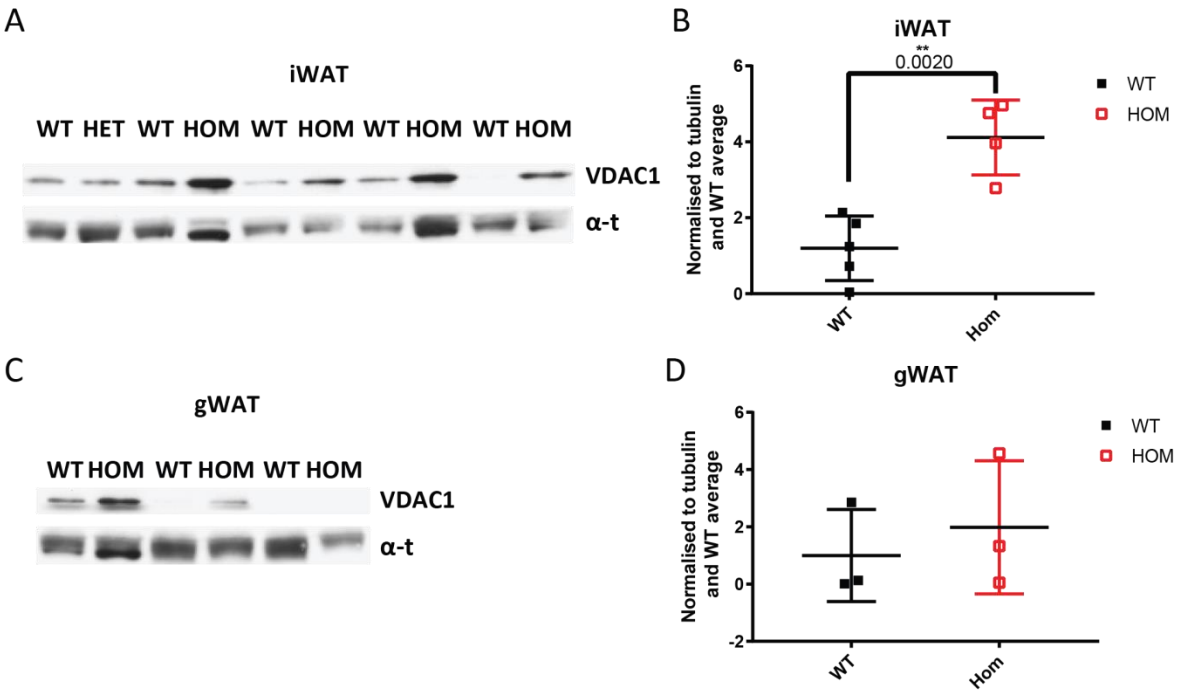

Figure 5.18 | Males – VDAC1 levels are increased in iWAT, but not gWAT of *Wars2*$^{V117L/V117L}$ mice. Immunoblot analysis (A, C) and quantification (B, D) of VDAC1 levels in iWAT and gWAT of male mice at 4 months of age**.** *Wars2*$^{+/+}$ and *Wars2*$^{V117L/V117L}$ mice numbers were 4 and 4 for iWAT and 3 and 3 for gWAT, respectively. The bands were normalised to tubulin and to WT average and shown as mean ± SD. Significance was determined using the unpaired t-test.

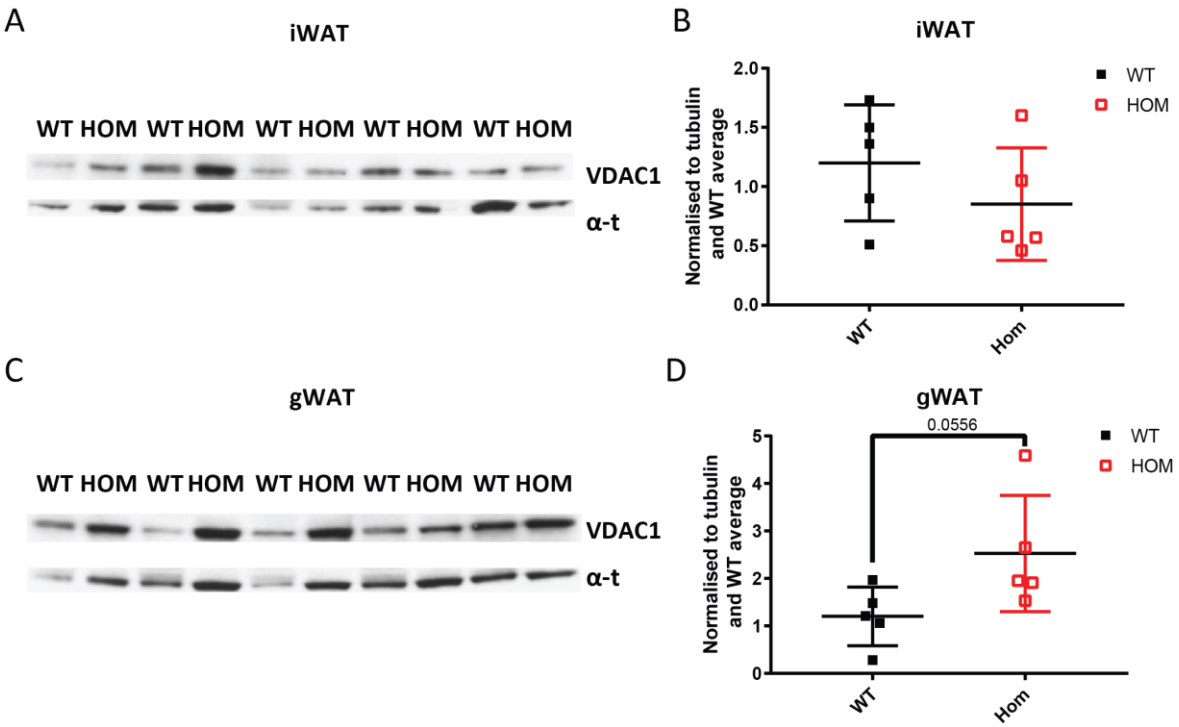

Figure 5.19 | Females – VDAC1 levels are unchanged in iWAT and gWAT of *Wars2*$^{V117L/V117L}$ mice. Immunoblot analysis (A, C) and quantification (B, D) of VDAC1 levels in iWAT and gWAT of female mice at 4 months of age**.** *Wars2*$^{+/+}$ and *Wars2*$^{V117L/V117L}$ mice numbers were 5 and 5, respectively. The bands were normalised to tubulin and to WT average and shown as mean ± SD. Significance was determined using the unpaired t-test for iWAT and Mann-Whitney test for gWAT.

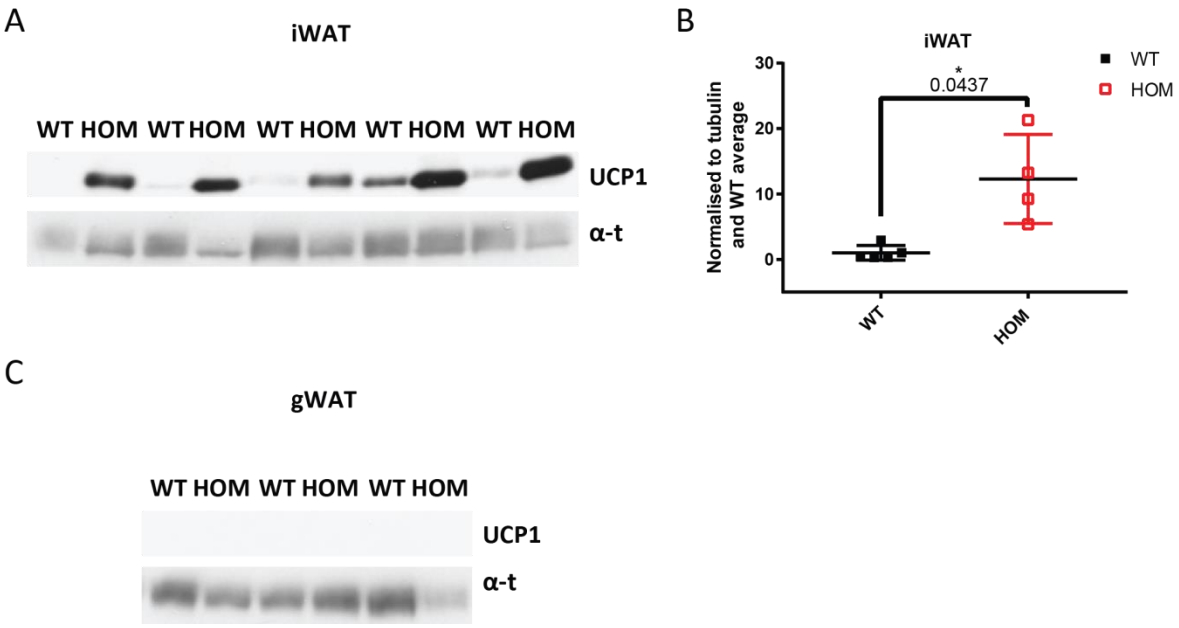

Figure 5.20 | Males - UCP1 levels are elevated in the iWAT of *Wars2*$^{V117L/V117L}$ mice. Immunoblot analysis (A, C) and quantification (B) of UCP1 levels in iWAT and gWAT of male mice at 4 months of age**.** *Wars2*$^{+/+}$ and *Wars2*$^{V117L/V117L}$ mice numbers were 5 and 5 in iWAT and 4 and 4 in gWAT, respectively. The bands were normalised to tubulin and to WT average and shown as mean ± SD. No UCP1 bands were detected in gWAT. Significance was determined using the Welch's t test.

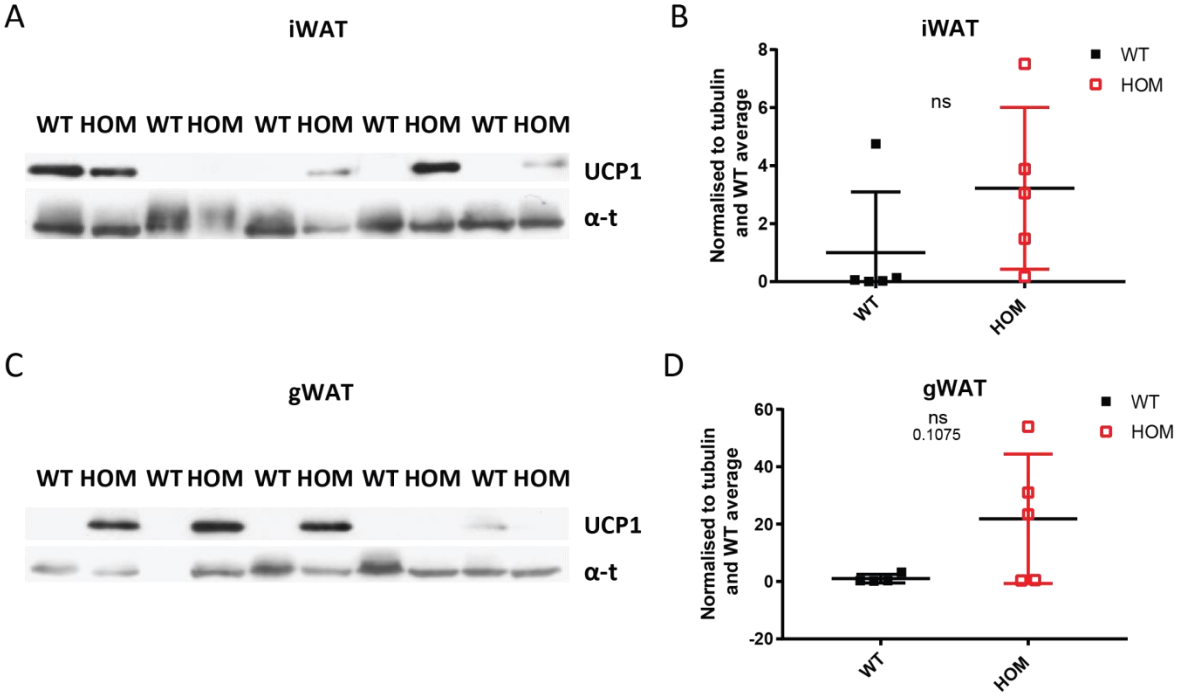

Figure 5.21 | Females - UCP1 levels are not significantly increased in iWAT and gWAT of *Wars2*$^{V117L/V117L}$ mice. Immunoblot analysis (A, C) and quantification (B, D) of UCP1 levels in iWAT and gWAT of female mice at 4 months of age**.** *Wars2*$^{+/+}$ and *Wars2*$^{V117L/V117L}$ mice numbers were 5 and 5 in iWAT, respectively. Bands were normalised to tubulin and WT average, mean ± SD. Significance was determined using the unpaired t test with Welch's correction (gWAT) and unpaired t test (iWAT).

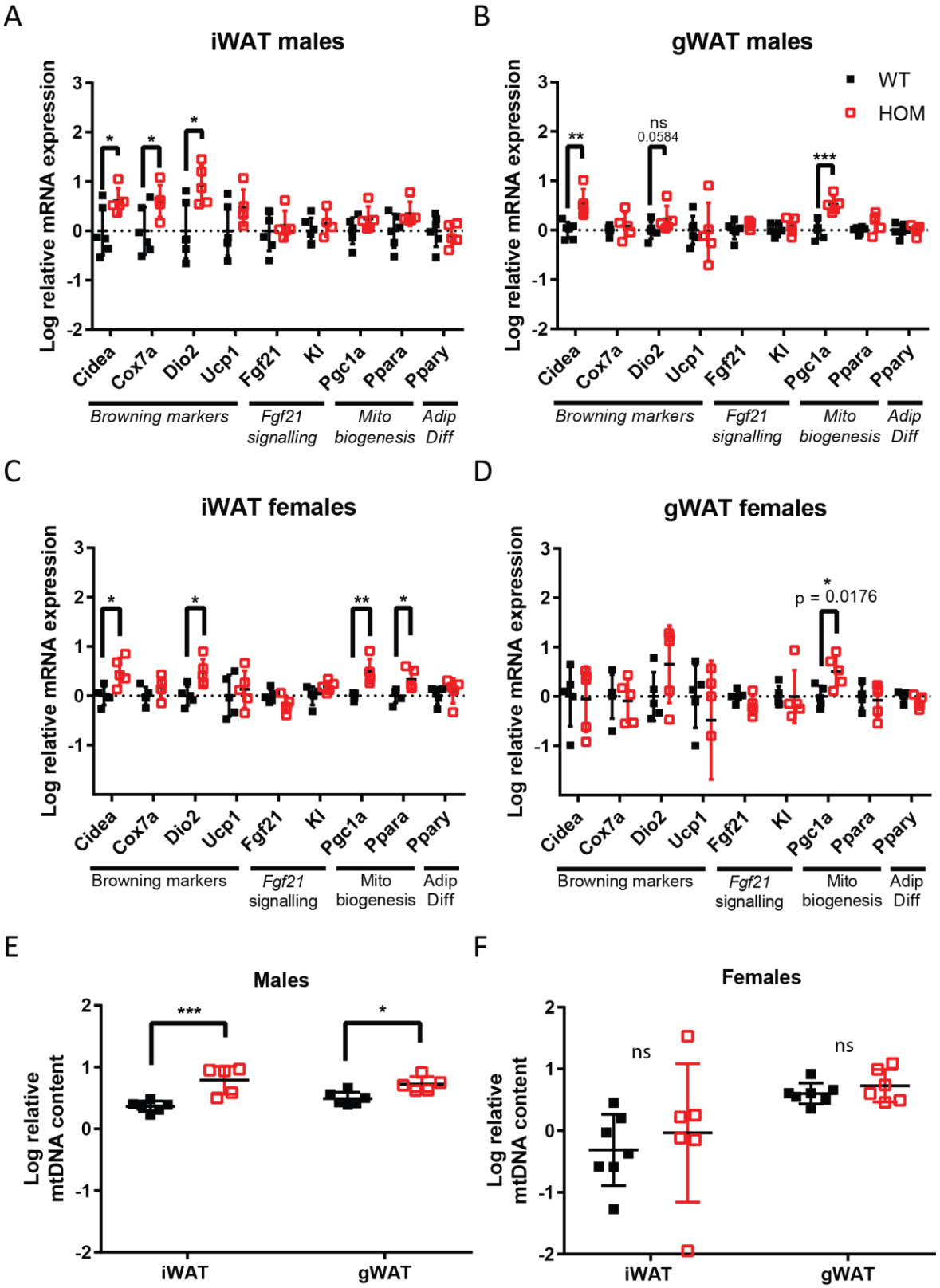

Figure 5.22 | Both iWAT and gWAT depots show browning in 4-month old *Wars2*$^{V117L/V117L}$ mice. Relative mRNA expression analysis of browning, Fgf21 signalling, mitochondrial biogenesis and adipose differentiation markers in male and female iWAT (A, C) and gWAT (B, D). Data were normalised to the geometric mean of *Canx* and *Ywhaz*. *Wars2*$^{+/+}$ and *Wars2*$^{V117L/V117L}$ mice numbers were 5 and 5 for females and 6 and 5 for males, respectively; mean ± SD. Data were log transformed and analysed using

unpaired t test or Mann-Whitney test based on the data distribution. The ratio of mitochondrial DNA to genomic DNA was assessed by qPCR of *mt-Nd1* and *Gapdh* in iWAT and gWAT for males (E) and females (F). *Wars2*$^{+/+}$ and *Wars2*$^{V117L/V117L}$ mice numbers were 5 and 5 for males and 6 and 5 for females, respectively; mean ± SD. Data were log-transformed and compared by 2-way ANOVA followed by post-hoc comparison of genotypes within each depot. *p < 0.05, **p< 0.01, ***p<0.001.

Table 5.4 | Summary showing upregulation of browning markers across gWAT and iWAT in 4-month old *Wars2*$^{V117L/V117L}$ mice. Data from Figure 5.18 to Figure 5.22.

	Males		Females	
Assay:	**iWAT**	**gWAT**	**iWAT**	**gWAT**
Cidea	3-fold	1.5-fold	3-fold	ns
Cox7a	3-fold	ns	3-fold	ns
Dio2	9-fold	ns	ns	ns
Ucp1	ns	ns	ns	ns
Pgc1a	ns	1.5-fold	4-fold	4-fold
Ppara	ns	ns	2-fold	ns
UCP1	12-fold	not detected	ns	ns
VDAC1	4-fold	ns	ns	ns
mtDNA:gDNA	1.45-fold	1.24-fold	ns	ns

5.3.6. Proton leak and mitochondrial respiration are not altered in primary preadipocytes and differentiated adipocytes of the *Wars2*$^{V117L/V117L}$ mice

Next I asked whether the increased browning gene expression and mitochondrial content observed in white adipose of *Wars2*$^{V117L/V117L}$ mice may be due to an adipose-intrinsic effect of *Wars2* deficiency. I isolated the stromal vascular fraction (SVF) and differentiated primary preadipocytes from 6-week old *Wars2*$^{V117L/V117L}$ and *Wars2*$^{+/+}$ mice and tested for increased proton leak by measuring the oxygen consumption rate (OCR) using the Seahorse XF96 Analyser. Bright-field images showed that only male iWAT preadipocytes differentiated successfully (Figure 5.23A). Male gWAT preadipocytes differentiated to a lesser extent and female iWAT and gWAT preadipocytes showed almost no lipid-filled cells suggesting that their OCR profiles are mainly representative of preadipocyte rather than adipocyte metabolism (Figure 5.23A). No significant differences in OCR were detected for cells from these undifferentiated cells (Figure 5.23B, C, D). The increase in OCR and ECAR in male differentiated male iWAT preadipocytes from *Wars2*$^{V117L/V117L}$ mice was not significant (Figure 5.24A, Figure 5.24B), and the curves became identical to wild type mice after baseline normalisation (Figure 5.24C, D). Analysis of the individual parameters derived from the OCR profiles showed upregulated non-mitochondrial metabolism (P=0.0380) in *Wars2*$^{V117L/V117L}$ differentiated adipocytes, but no significant increase in proton leak (Figure 5.24E). Based on these findings, browning seen in the *Wars2*$^{V117L/V117L}$ WAT tissues is thus unlikely to result from the intrinsic effect of *Wars2* deficiency in adipocytes.

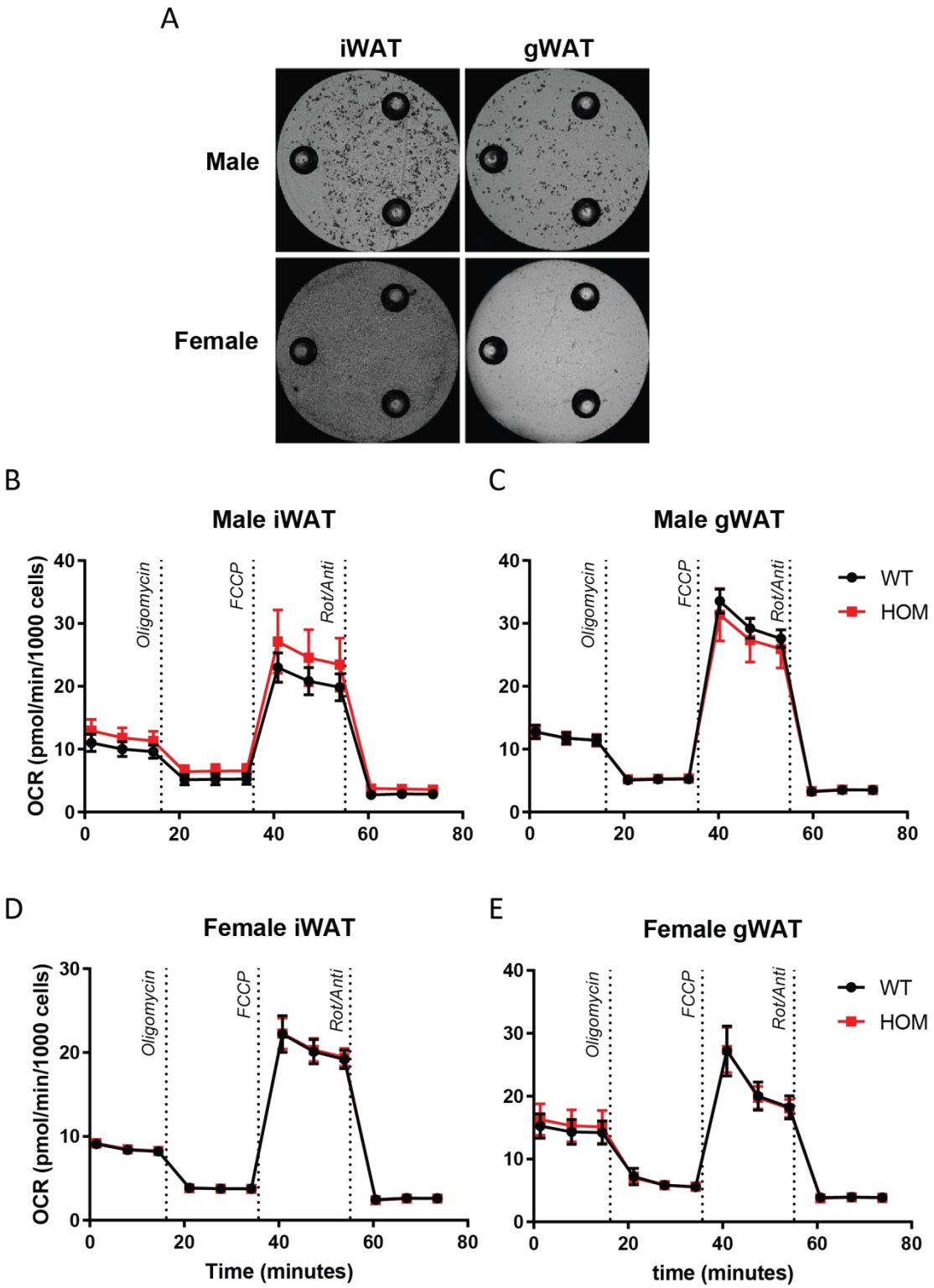

Figure 5.23 | Primary SVF cells from the *Wars2*$^{V117L/V117L}$ mice differentiated into white adipocytes show no major differences in mitochondrial respiration. 1° SVF cells from iWAT and gWAT of *Wars2*$^{+/+}$ and *Wars2*$^{V117L/V117L}$ were isolated, cultured and differentiated for 9 days. Oxygen consumption rate (OCR) was then measured using Seahorse XFe96 Analyser. *Wars2*$^{+/+}$ and *Wars2*$^{V117L/V117L}$ mice numbers were 6 and 6, respectively. Light microscopy imaging (A) revealed the dark lipid-filled cells and showed differentiation was only effective in male iWAT, less so in male gWAT and almost absent in female cells.

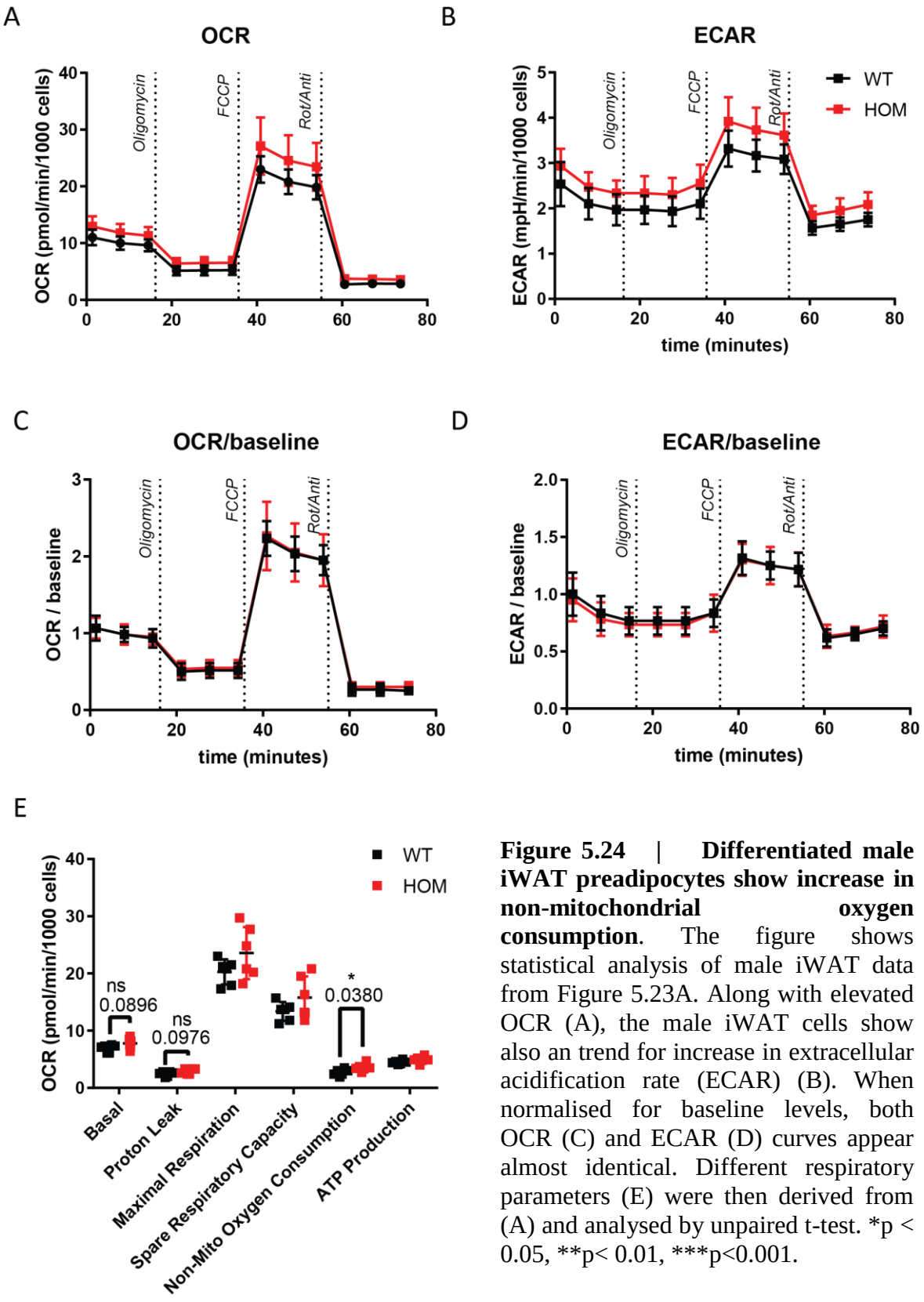

Figure 5.24 | Differentiated male iWAT preadipocytes show increase in non-mitochondrial oxygen consumption. The figure shows statistical analysis of male iWAT data from Figure 5.23A. Along with elevated OCR (A), the male iWAT cells show also an trend for increase in extracellular acidification rate (ECAR) (B). When normalised for baseline levels, both OCR (C) and ECAR (D) curves appear almost identical. Different respiratory parameters (E) were then derived from (A) and analysed by unpaired t-test. *p < 0.05, **p< 0.01, ***p<0.001.

5.3.7. FGF21 and GDF15 are elevated in *Wars2*$^{V117L/V117L}$ plasma

Previously, Fibroblast frowth factor-21 (FGF21) was found to be elevated in 12-month and 4-month old fasted *Wars2*$^{V117L/V117L}$ mice. FGF21 is a secreted peptide and marker of mitochondrial stress that could be mediating the browning of white adipose seen in these mice (Fisher *et al.*, 2012). Another mitokine, a diffusible factor released in response to mitochondrial stress, Growht/Differentiation Factor-15 (GDF15), has been shown to supress food intake and mediate taste aversion suggesting that its release could contribute to reduced fat mass in *Wars2*$^{V117L/V117L}$ mice (Patel *et al.*, 2019). To test these hypotheses, I used ELISA to quantify the levels of FGF21 and GDF15 in the plasma of 4-month old unfasted mice. Both mitokines showed a significant effect of genotype (Figure 5.25A, B). Post-hoc multiple comparison analysis revealed significantly increased FGF21 levels only in female mice, with a 86% increase (P= 0.0364) (Figure 5.25A). GDF15 was significantly increased in both sexes, with a 112% (P= 0.0014) increase in males and 158% increase (P= 0.0001) in females (Figure 5.25B).

To assess which tissue could be responsible for the rise in plasma FGF21 and GDF15, I performed qPCR analysis across multiple female tissues to quantify the expression of *Fgf21*, *Gdf15* and Activating transcription factor 4 (*Atf4)*, the transcription factor involved in the integrated stress response (ISR) that can induce the expression of both of the mitokines (Patel *et al.*, 2019). *Fgf21* expression was 62-fold (P=0.0012), 1.4-fold (P=0.0055), 2.4-fold (P=0.0157) and 1.6-elevated (P=0.0447) in the heart, BAT, muscle and kidney of *Wars2*$^{V117L/V117L}$ mice (Figure 5.26A). *Gdf15* was elevated 3.6-fold (P<0.0001) and 5.8-fold (P=0.0003) in the heart and BAT, respectively. In gWAT, *Gdf15* expression was ~2-fold reduced (P=0.0273) (Figure 5.26B). Interestingly, *Atf4* was unaffected in all the tissues except gWAT where a ~20-fold increase (P=0.0079) in expression was observed (Figure 5.26C). In summary, GDF15 and FGF21 were elevated

in the plasma of unfasted *Wars2*$^{V117L/V117L}$ mice and expression of *Fgf21* and *Gdf15* genes is elevated in tissues including heart and BAT.

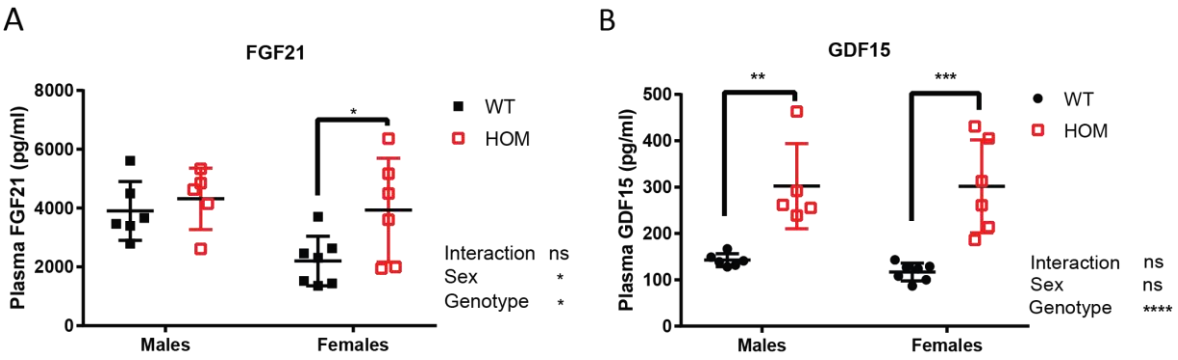

Figure 5.25 | Mitokines FGF21 and GDF15 are elevated in 4-month old *Wars2*$^{V117L/V117L}$ plasma. *Wars2*$^{+/+}$ and *Wars2*$^{V117L/V117L}$ mice numbers were 6 and 5 for males, 7 and 6 for females, respectively. Analysis by 2-way ANOVA followed by post-hoc comparison of genotypes within each sex. *p < 0.05, **p< 0.01, ***p<0.001. The GDF15 ELISA was performed by the lab of S 'O'Rahilly at the Institute of Metabolic Science, Cambridge, UK.

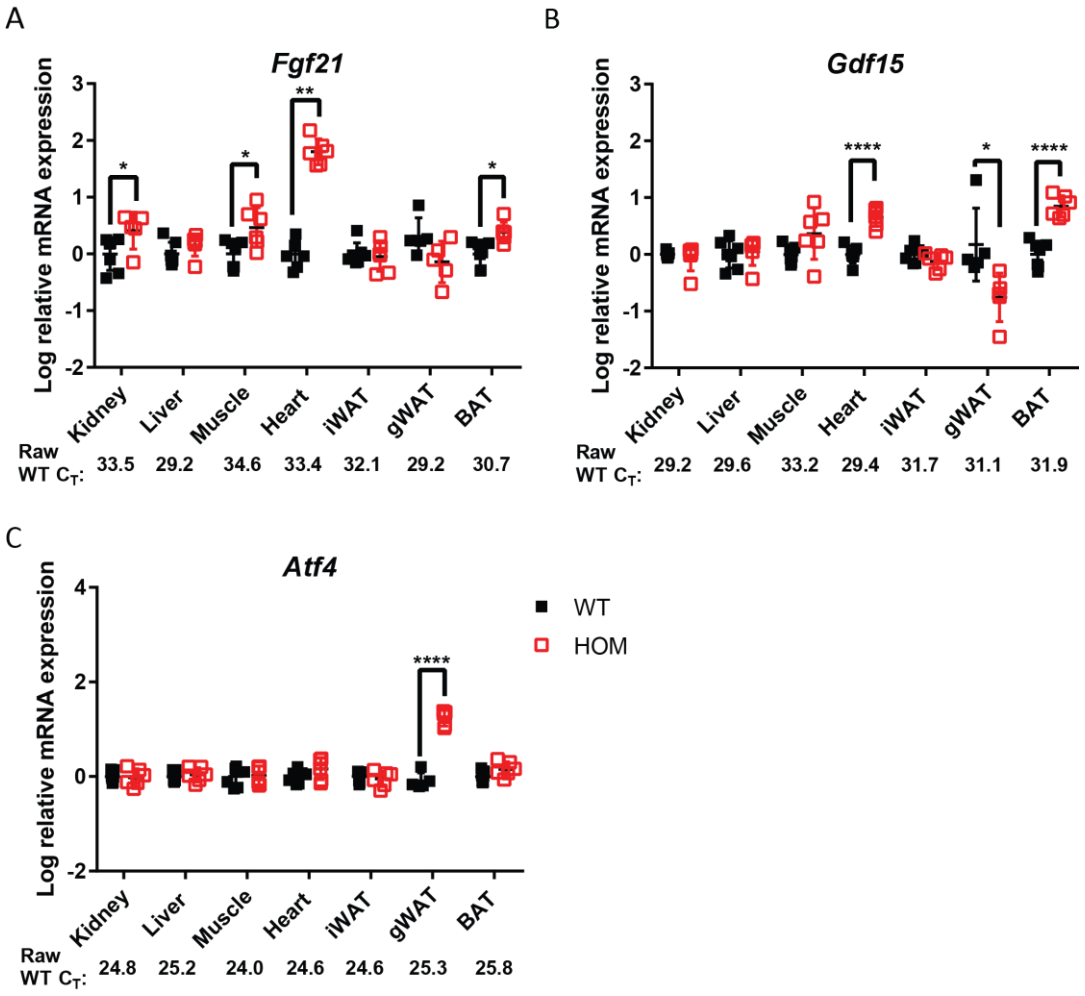

Figure 5.26 | *Fgf21* and *Gdf15* expression are altered in multiple tissues. Log relative mRNA expression of *Fgf21* (A), *Gdf1*5 (B), *Atf4* (C) in multiple tissues from female *Wars2*$^{V117L/V117L}$ mice. *Wars2*$^{+/+}$ and *Wars2*$^{V117L/V117L}$ mice numbers were 5 and 5 for gWAT and 7 and 6 for all other tissues, respectively; mean ± SD. Data were log transformed and analysed using unpaired t test or Mann-Whitney test based on the data distribution. *p < 0.05, **p< 0.01, ***p<0.001. For comparison of expression between tissues, the average of raw *Wars2*$^{+/+}$ C_T values are shown beneath the graphs.

5.3.8. Food Intake is reduced in *Wars2*$^{V117L/V117L}$ male mice

GDF15 was previously reported as an inducer of taste aversion and a suppressor of food intake (Mullican *et al.*, 2017). I thus set up an independent cohort of mice pair-housed by genotype to test for an effect on food intake. Male *Wars2*$^{V117L/V117L}$ mice showed reduced food intake compared to *Wars2*$^{+/+}$ males from 7 weeks onwards (Figure 5.27A). The homozygous mice ate from 18% less at 7 weeks (P=0.0075) to 27% less at 14 weeks (P=0.0018). This effect was attenuated, but still present after normalisation to lean mass (Figure 5.27C). At 7 weeks the mice ate 10% less/g of lean mass (P=0.0291) to 18.4% less/g of lean mass at 14 weeks (P=0.0034). Low number of female cages (n = 2) did not allow for a valid statistical analysis, but based on the initial data, there seems to be no difference in total or normalised food intake, comparable to that seen in males (Figure 5.27B, D).

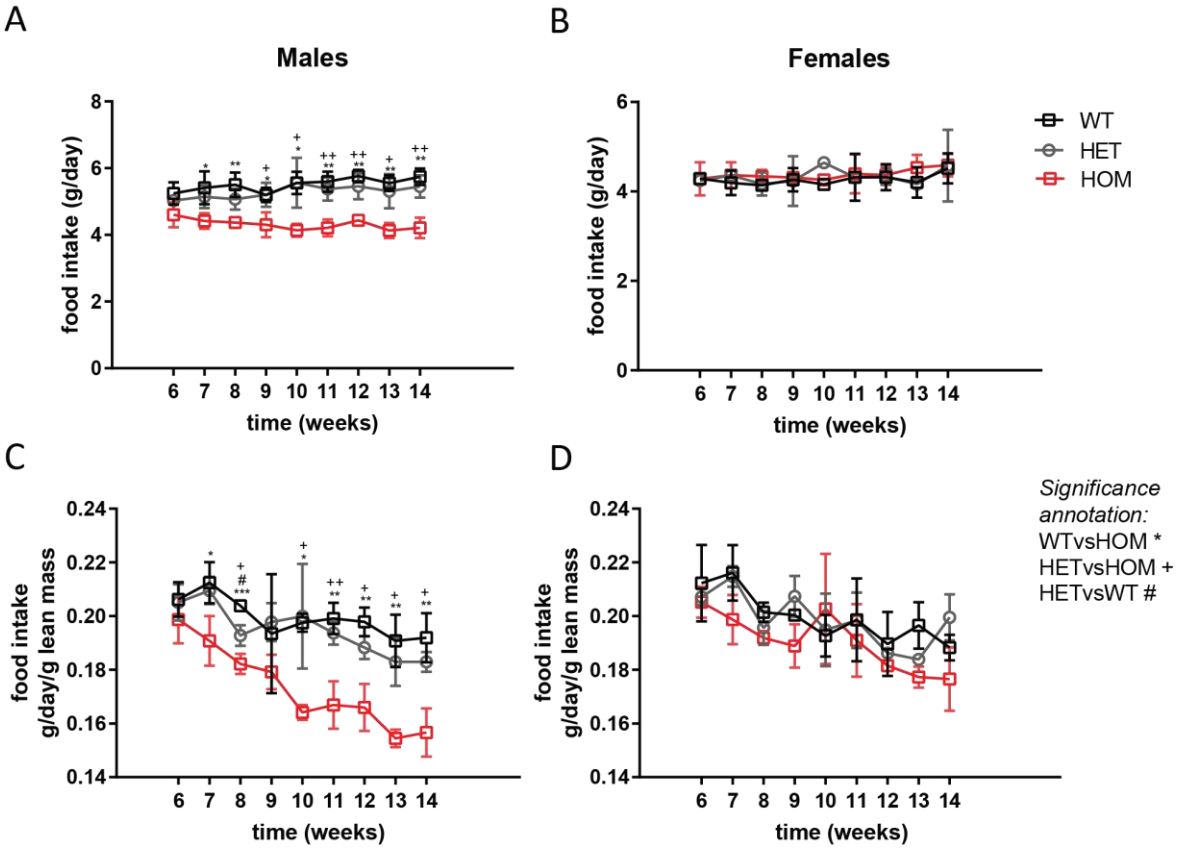

Figure 5.27 | Food intake is reduced in *Wars2*$^{V117L/V117L}$ males. 4-week old mice were administered the RM3 diet, pair-housed by genotype and food consumption was weighed until 14-weeks of age. There were 3 cages (6 mice) for each of *Wars2*$^{+/+}$ (WT), *Wars2*$^{+/V117L}$ (HET) and *Wars2*$^{V117L/V117L}$ (HOM) males and 2 cages (4 mice) for each genotype of females. Shown is raw food intake and food intake normalised to lean weight in males (A, C) and females (B, D), mean ± SD. All male data was normally distributed and significance at specific time points was calculated with 1-way ANOVA with multiple comparisons. Significance between *Wars2*$^{+/+}$ (WT) and *Wars2*$^{V117L/V117L}$ (HOM) is shown as * $p < 0.05$, ** $p< 0.01$, *** $p<0.001$. Comparisons between the other groups are depicted in the same way using the symbols (+, #) annotated in the top right corner. Female n number (n = 2) was too low for statistical comparison.

5.4. Discussion

GWA studies revealed that, unlike for BMI, expression of genes in WHRadjBMI-associated loci is specifically enriched in adipose and adipocyte cell lines (Shungin *et al.*, 2015). Recently, SNPs in 24 loci with nuclear-encoded mitochondrial genes, including *WARS2*, were found to be associated with WHR (Justice *et al.*, 2019). Such association was found also for mitochondrial-encoded genes *MT-ATP6* and *MT-ND6* and coding variants in *DARS2* suggesting that mitochondria and mitochondrial aminoacyl synthesases could modulate fat distribution (Kraja *et al.*, 2019). Other evidence comes from human mutations in mitofusin 2 (MFN2) and mitochondrial lysyl tRNA (LysRS) which cause multiple symmetrical lipomatosis (MSL), a disease characterised by massive increase in upper body adipose tissue (Chong *et al.*, 2003; Rocha *et al.*, 2017).

In two separate cohorts, I show that *Wars2*$^{V117L/V117L}$ mice fail to gain fat mass during normal growth and HFD and also show a male and HFD-specific upregulation of gWAT:iWAT ratio. This ratio was used previously to approximate visceral to subcutaneous fat distribution, but indeed does not equate to a whole-body representation of fat distribution (Gray *et al.*, 2006). In line with the effect in iWAT, the weights of the other subcutaneous WAT depot prWAT were also consistently reduced in both males and females with either diet. To confirm my findings, also additional subcutaneous fat measures such as dermal skin fat thickness will be assessed (Hew *et al.*, 2016). Regarding visceral tissues, male and female cWAT of Cohort 1 were also resistant to fat mass loss due to the homozygous mutation, but this was not replicated in Cohort 2. The weight of the other major visceral depot – mesenteric WAT, was clearly reduced in both sexes with both diets in the *Wars2*$^{V117L/V117L}$ mice. Thus although I clearly demonstrate an increased effect on gWAT:iWAT ratio, not all visceral depots show the same trend as gWAT. Ideally,

small animal X-ray computed tomography (CT) system would be used to accurately quantify the volumes of multiple different fat depots in a longitudinal study (Sasser *et al.*, 2012). The male-specific effect on gWAT:iWAT ratio seen in *Wars2*$^{V117L/V117L}$ mice could explain the lack of phenotype in heterozygous *Wars2*$^{+/-}$ females and is in line with sexual dimorphism which is an established feature of fat distribution (Pulit, Karaderi and Lindgren, 2017). In line with these findings, the *TBX15-WARS2* locus contains shared WHRadjBMI-associations between sexes, but there is also an independent male-specific signal (Risk Block B) (Shungin *et al.*, 2015).

Previously, iBAT was shown to be one of the most severely affected tissues in the 6-month old *Wars2*$^{V117L/V117L}$ mice (Agnew *et al.*, 2018). Indeed, male iBAT on LFD showed the same effect in both cohorts. Interestingly when on HFD, male iBAT and prBAT and female prBAT showed consistent protection from weight loss, similarly to gWAT. Given that I performed post-hoc comparisons between all tested groups (15 comparisons in total), the statistical power was reduced in favour of avoiding false positives, and may explain our inability to detect significance for these apparent differences. However, data of female prBAT in both cohorts suggests that gWAT may not be the only depot which may be affected to a lesser extent.

In high-energy demanding tissues such as the brain, muscle and BAT, defects in mitochondrial translation and mtAARs often result in ETC complex deficiency and severe pathology (Elo *et al.*, 2012; Cassandrini *et al.*, 2013). In line with this, heart and BAT showed upregulation of the mitokines *Fgf21* and *Gdf15* expression, markers of mitochondrial disease. Furthermore, reduction of ETC Complex I and IV subunit proteins and reduced browning marker RNA expression was observed in the *Wars2*$^{V117L/V117L}$ BAT.

This is in line with previous findings of severely affected ETC Complex levels in the hearts and BAT of 6-month old *Wars2*$^{V117L/V117L}$ mice (Agnew *et al.*, 2018).

I hypothesised that the increased gWAT:iWAT ratio observed in *Wars2*$^{V117L/V117L}$ mice arises by subcutaneous-specific browning of WAT. Indeed, altering the browning capacity of WAT, such as by adipose-specific deletion of *Prdm16*, was shown to modulate WAT energy expenditure in a depot-specific way and also alter fat distribution (Cohen *et al.*, 2014). Interestingly, both iWAT and gWAT of the 4 month old *Wars2*$^{V117L/V117L}$ mice showed increases in browning gene expression and mitochondrial content. There was no change in ETC Complex levels in these tissues. A defect in ETC function could be compensated for by increased mitochondrial content observed in these tissues. In line with this, activating the AMPK/PGC1α axis by PGC1α overexpression or increasing the activity of Sirtuin 1 (SIRT1) was able to increase COX levels and correct some of the pathologies in mouse models of mitochondrial disease (Viscomi *et al.*, 2011; Cerutti *et al.*, 2014). WAT browning markers in *Wars2*$^{V117L/V117L}$ mice were upregulated to a greater extent in iWAT than gWAT, especially since no UCP1 was detected in male gWAT of any genotype. Indeed, this could contribute to the protection of *Wars2*$^{V117L/V117L}$ gWAT against the loss of fat mass on HFD and the sex-specific nature of this effect. It remains to be seen why this effect is not reproduced on LFD. HFD has been previously shown to induce browning and could thus potentiate any depot-specific differences in browning susceptibility (García-Ruiz *et al.*, 2015). In agreement with my findings, previous research showed that gWAT, compared to iWAT, has low browning marker expression and very low browning capacity (de Jong *et al.*, 2015; Zuriaga *et al.*, 2017). Whether browning is truly the main mechanism of the fat distribution effect in *Wars2*$^{V117L/V117L}$ could be resolved by housing the mice at thermoneutrality (~30°C) and repeating the fat depot weight analysis. It also remains to be seen how relevant this finding is to humans where

visceral fat was shown to be generally more prone to browning than subcutaneous fat (Giordano, Frontini and Cinti, 2016; Zuriaga *et al.*, 2017).

Analysis of OCR in differentiated male primary iWAT preadipocytes did not reveal any changes in proton leak or maximal mitochondrial respiration, suggesting the browning response seen in *Wars2*$^{V117L/V117L}$ WAT is probably due to the increase in FGF21 levels (Fisher *et al.*, 2012). FGF21 treatment was previously shown to induce browning in mice, but the amounts were delivered in supraphysiological concentrations, thus it remains to be seen whether a ~2-fold increase in FGF21 levels would be sufficient to elicit a browning response (Samms *et al.*, 2015; Véniant *et al.*, 2015). Furthermore, all mice were kept at standard temperatures of 22°C (below 28°C thermoneutrality) and a prolonged treatment of the primary cells with an inducer of browning such as isoprotrenolol would thus be needed to confirm that there is no adipose-intrinsic effect of *Wars2* deficiency on browning (Miller *et al.*, 2015).

Elevated levels of GDF15 and markedly reduced food intake in *Wars2*$^{V117L/V117L}$ male mice suggest that at least some of the reduction in fat mass and bodyweight may be due to reduced food intake. GDF15 is known to supress food intake by acting on the area postrema and nucleus of the solitary tract in the hindbrain where its receptor GDNF family receptor α–like (GFRAL) is expressed (Mullican *et al.*, 2017). To confirm the effect of GDF15 on GRAFL, phosphorylation of the downstream cascade proteins Rearranged during transfection tyrosine kinase (RET), Protein kinase B (PKB), Extracellular signal-regulated kinase (ERK) and Phospholipase C-γ1 (PLC-γ1) should be assessed in the hindbrain (Mullican *et al.*, 2017). Although lacking statistical power (n=2), no trend for reduction of food intake was observed in *Wars2*$^{V117L/V117L}$ females. If this result is

confirmed, this will suggest other mechanisms for reduction of bodyweight and fat mass must exist, since body composition of females is affected to a similar extent as that of males. Reduced energy expenditure due to ETC complex deficiency of the main energy-consuming tissues such as the heart, BAT and brain could be one such mechanism.

5.5. Conclusion

In this study, I used mouse models to investigate the role of *Wars2* as a modulator of fat mass, fat distribution and adipose tissue browning. I showed that the hypomorphic *Wars2*$^{V117L/V117L}$ mice failed to gain fat mass during normal growth and HFD and that this may be in part due to reduced food intake. A male-specific and HFD-specific increase in the gWAT:iWAT ratio was observed in heterozygous *Wars2*$^{+/V117L}$ mice, primarily through the resistance of gWAT to the loss of fat mass observed in other white fat depots. This difference could be in part caused by the increase in browning, which I have shown to be more pronounced in the subcutaneous depot, especially by male-specific upregulation of UCP1 in iWAT and not gWAT of 4 month-old *Wars2*$^{V117L/V117L}$. The lack of increase in mitochondrial respiration and proton leak in differentiated primary preadipocytes from male *Wars2*$^{V117L/V117L}$ iWAT mice suggested that WAT browning may be due a systemic effect mediated by other tissues. Indeed, BAT showed severe ETC complex deficiency and along with other tissues, such as the heart, an increase in the expression of mitokines *Fgf21* and *Gdf15*. These mitokines were significantly elevated in the plasma and may thus mediate the increase in WAT browning and the reduced food intake.

6. General discussion

6.1. Summary

This thesis aimed to expand our understanding of the genetic mechanisms underlying the variance in fat distribution by deciphering four WHRadjBMI GWAS loci.

In *EMILIN2*, *C5orf67* and *VEGFA* loci, a single SNP could explain the majority of the association in the PPA. EMSAs and luciferase assays were used to study functional effects of the SNPs in hWAT differentiating adipocytes. I provide evidence of promoter and enhancer activities in the regions surrounding the SNPs in *EMILIN2* and *C5orf67* loci, respectively. Using EMSAs, I show that SNPs in these loci altered protein binding and that the T WHR-increasing allele of rs3810069 creates a functional C/EBPβ binding site in the *EMILIN2* promoter. Luciferase assays showed no differences between the activities of the different alleles.

The *TBX15*-*WARS2* locus harbours four risk association signals with WHRadjBMI and eQTLs for both *WARS2* and *TBX15*. In this work, I set to test whether Risk Block A mediates the WHRadjBMI signal by reducing *WARS2* levels. Using PPA and epi-PMCA, three SNPs were prioritised for further functional analysis. I show no overlap of these SNPs with open chromatin in adipocytes and no effect on DNA-protein binding in EMSA. I thus test rs2645294, the lead SNP in the 3'UTR of *WARS2*, for an effect on RNA stability. I show that hWAT cells are heterozygous for rs2645294 and show allelic imbalance at the RNA level. Luciferase assays, nascent RNA qPCR and actinomycin-mediated transcription inhibition do not show any evidence of rs2645294 influence on RNA stability. This suggests that allelic imbalance is mediated transcriptionally, likely through another SNP in the locus.

To independently test the effect of *WARS2* on fat distribution, I assessed the weights of different fat depots in *Wars2*$^{+/-}$, *Wars2*$^{+/V117L}$ and *Wars2*$^{V117L/V117L}$ mice. No reproducible phenotype was observed in the heterozygous mice, but weights of multiple white and brown adipose depots were reduced in the *Wars2*$^{V117L/V117L}$ mice, with a male-specific increase in gWAT:iWAT ratio on HFD. qPCR and Western Blots of both male and female *Wars2*$^{V117L/V117L}$ mice at 4 months of age revealed browning marker and ETC complex deficiencies in BAT. WAT showed upregulation of browning marker expression, UCP1 protein and mtDNA, especially in iWAT. No increases in proton leak were observed in primary adipocyte cultures, suggesting browning of WAT might be due to systemic effects. Indeed, FGF21 and GDF15 were elevated in the plasma of these mice, most likely due to the observed increased expression in the heart and BAT. Subsequent experiments discovered a significant reduction of food intake in the *Wars2*$^{V117L/V117L}$ male mice.

6.2. GWAS functional follow-up: Statistical and Functional approaches

PPA effectively identified the most likely causal SNP in the *EMILIN2*, *C5orf67* and *VEGFA* loci with over 0.95 posterior probability scores. Although validation in a cell line or mouse model is required to confirm the effect on gene expression, rs3810068 and rs3936510 showed a clear effect on protein binding. PPA was previously used on 380 distinct T2D association signals, identifying 51 signals where the most strongly associated variant accounted for >80% PPA and 18 signals with a single variant in the >99% PPA credible set (Mahajan *et al.*, 2018). In the Risk Block A of the *TBX15*-*WARS2* locus, PPA values were lower (maximum 0.6 for rs2645294 in females of GIANT dataset) and markedly different between UKBB and GIANT datasets and between sexes. This could be attributed in part to the sexual dimorphism of fat distribution genetics and also to the different population structures within the two human datasets (Pulit et al., 2017). Although the major participants in both UKBB and GIANT are of European Ancestry, a large part of

the GIANT dataset is composed of studies in citizens of Finland, Sweden and the United States, rather than just of United Kingdom as in the UKBB (Sudlow *et al.*, 2015; G. B. Chen *et al.*, 2016). The other possibility is that the complexity of this locus of four association signals, with Risk Block A and B showing moderate correlation (LD, r^2 = 0.43), reduces the accuracy of the PPA estimates (Shungin *et al.*, 2015). Statistical approaches by themselves may thus be limited to decipher only a portion of GWAS loci with either single causal SNPs or simpler LD structures (Schaid, Chen and Larson, 2018).

Multiple tools have been developed that can predict non-coding SNP functionality based on a combination of large amounts of functional genomic data such as evolutionary conservation, TF binding sites, TF or histone ChIP-Seq peaks or DNase-Seq peaks (e.g., DeepSEA, Eigen, Sasquatch), segment annotations (chromHMM, Segway) or sequence-based models (deltaSVM) (D. Lee *et al.*, 2015b; Zhou and Troyanskaya, 2015b; Ionita-Laza *et al.*, 2016; Ernst and Kellis, 2017; Schwessinger *et al.*, 2017; Chan *et al.*, 2018). Epi-PMCA, used in this study, integrates some of these models and identifies strong functional candidates in Risk Blocks B, C and D (not shown in this work). The low epi-PMCA ranking of Risk Block A SNPs suggested an alternative mechanism of SNP action, but no evidence for altered RNA stability was discovered in Chapter 4. Due to the low amount of "known" functional GWAS variants, different GWAS prioritisation methods cannot be easily compared and benchmarked. Recently, a study by Kircher et al. used error-prone PCR to mutate almost every base in 20 disease-associated regulatory elements and tested these in massively parallel reporter assay (MPRA) in relevant cell lines (Kircher *et al.*, 2019). The effects of the mutations were then compared to predictions made between some of the above-mentioned predictive tools. In support of the epi-PMCA methodology, conservation across species was one of the strongest predictors of SNP effect overall. However, no single tool, including phastCons, performed consistently-well

across most of the 20 different elements. This is in line with the proposed key role of the non-coding genome in shaping and fine-tuning gene expression during evolution and might suggest recent evolution in some of the low-scoring loci or presence of yet undescribed mechanisms of gene expression regulation (King and Wilson, 1975; Berthelot *et al.*, 2018). Very exciting research, such as by Farley et al, is aiming to decipher the "grammar" of the non-coding genome (Farley *et al.*, 2015). The integration of newly discovered concepts, such as the need for suboptimal TF binding affinities and distances for enhancer specificity in development, are likely to generate better predictive models of SNP functionality.

6.3. Functional SNP/s in Risk Block A

Effect of rs2645294 on RNA stability was not detected either in luciferase assays, nascent RNA qPCR or after transcription inhibition in hWAT cells. Although each method has its limitations (described in Chapter 4), the agreement of three different methods provides strong evidence that Risk Block A does not mediate its effect through altering RNA stability of *WARS2*. The effect on *WARS2* expression is most likely to be mediated transcriptionally.

None of the 3 SNPs short-listed in our initial analysis showed a reproducible effect on protein binding in the EMSAs, but it is possible that they act at a different developmental time-point, such as in preadipocytes or mature adipocytes. Whilst the EMSA experiments were carried out in day 4-differentiated hWAT cells, the human *WARS2* eQTL data originate from mature adipose tissue which contain multiple cell types, including one of the largest precursor fractions of any tissue (Tchkonia *et al.*, 2013). For example, the specific binding difference of rs3810068 in the *EMILIN2* locus was only observed at Day 4, but not at Day 0 or Day 21 of hWAT differentiation (Figure 7.2). Further EMSA

experiments or mutagenesis of the 3 prioritised Risk Block A SNPs in hWAT cells at other time-points could thus identify the functional SNP and also the effector genes.

Is it possible that different SNPs or genes other than *WARS2* are mediating the WHRadjBMI signal in the Risk Block A? Indeed, GWAS loci may often associate with expression of multiple genes of which only some may be causal (Hormozdiari *et al.*, 2016b). Although reaching lower significance values than *WARS2*, Risk Block A is also associated with *TBX15* expression in VAT and SAT and this eQTL also highly correlates with WHRadjBMI (Figure 7.1). Thus both *TBX15* and *WARS2* could be regulated by Risk Block A SNPs to alter WHR. Interestingly, the SNPs that form the peak of the *TBX15* SAT eQTL and WHRadjBMI correlation, rs984222, rs984225 and rs10923712, all fall into the previously specified 1.5kb fine-mapped region in intron 1 of *TBX15* (Liu *et al.*, 2014). However, in the PPA of the GIANT dataset, these SNPs scored relatively low – 0.14, 0.2 and 0.2, respectively, suggesting that they are unlikely to be the mediators of the WHRadjBMI signal.

In a recent study, CRISPR-mediated activation of *Sim1* and *Mc4r* promoters and enhancers prevented monogenic obesity in mice and demonstrated a therapeutic potential for targeting regulatory elements (Matharu *et al.*, 2019). However, identifying individual functional SNPs to define the functional genes in a locus may not always be necessary. Especially for complex multi-signal GWAS loci, systematic KD testing of all genes in a locus or TAD might be a useful complementary approach. For example, in the hypertension-associated *AGTRAP-PLOD1* locus, systematically mutating genes of the locus in mice showed that 5 out of 6 genes affected blood pressure and renal phenotypes (Flister *et al.*, 2013). In line with this notion, our research group independently generated and studied several mouse models of *Wars2* (this work) and *Tbx15* (unpublished).

6.4 Browning as a mechanism for altered fat mass and distribution

Previous work of our group has shown that *Wars2*$^{V117L/V117L}$ mice fail to gain fat mass during growth on the RM3 diet and show signs of WAT browning (Agnew *et al.*, 2018). Here, I have shown that similar effect on fat mass is observed also on LFD and HFD, suggesting that dietary fat is unable to rescue this phenotype. By assessing fat depot weights, I have shown that this reduction in fat mass is seen in almost all white and brown depots of *Wars2*$^{V117L/V117L}$ mice with the only exception being gWAT which is protected from fat loss leading to increased gWAT:iWAT ratios in males on a HFD.

What is the reason for the protection of male gWAT on HFD and fat loss in the other depots? I hypothesised that depot-specific differences in browning and subsequently energy expenditure are responsible. Indeed, gWAT was previously reported to be less susceptible to browning and in agreement, my results showed smaller increases in browning marker mRNA expression and mtDNA levels in gWAT compared to iWAT (Vitali *et al.*, 2012). Furthermore, gWAT of neither *Wars2*$^{+/+}$ nor *Wars2*$^{V117L/177L}$ males expressed UCP1 which could explain the male-specific protection of gWAT mass. A previous study in C57BL/6J mice, showed that whereas both female gWAT and iWAT respond to β3-adrenergic receptor agonist CL316,243 (CL) by browning, in males, only iWAT is responsive whilst gWAT fails to upregulate UCP1 (Kim *et al.*, 2016). These differences were at least in part due to higher sympathetic innervation in female gWAT and could be attenuated by inducing ovarian failure (Kim *et al.*, 2016). Although conflicting findings exist, HFD was shown to upregulate browning markers such as *Cidea* in multiple WAT depots and also iBAT (García-Ruiz *et al.*, 2015; Hu *et al.*, 2018). HFD could thus accentuate any depot-specific differences in browning potential and led to the increased gWAT:iWAT ratio seen in HFD-fed males. Given its anatomical location, it is interesting to speculate that reduced browning potential of male gWAT is genetically

encoded to specifically protect the highly temperature-sensitive spermatozoa and process of spermatogenesis (Yaeram, Setchell and Maddocks, 2006). This could be facilitated through the different developmental origins of male and female gWAT progenitors in the embryonic mesoderm (Sanchez-Gurmaches and Guertin, 2014; Sebo and Rodeheffer, 2019). In summary, I show depot and sex-specific differences in fat mass and browning. However, these findings alone do not prove a causal relation.

To test this, I showed that adipocytes differentiated from primary SVF cells of *Wars2*$^{V117L/V117L}$ iWAT do not show any differences in proton leak. This could be due to the lack of cold or β-adrenergic stimulus, but also due to the lack of systemic determinants present *in vivo*. Indeed my previous results show that FGF21 is upregulated in the *Wars2*$^{V117L/V117L}$ mice, especially by the heart and BAT (Agnew *et al.*, 2018). Since FGF21 is known to upregulate *Pgc1α*, mediator of mitochondrial biogenesis, it is likely that it contributes to the browning of iWAT (Fisher *et al.*, 2012). FGF21 was also upregulated in the heart-specific *Dars2*-KO mice, which also showed reduced fat mass confirming that mt-aaRS mutations can affect fat mass indirectly (Dogan *et al.*, 2014).

Could browning alter fat distribution and fat depot weight also directly? And how relevant is this to humans? In mice, mature adipocyte-specific overexpression of *Prdm16*, a key transcription factor regulating BAT development and browning, increased energy expenditure, glucose tolerance and limited diet-induced weight gain (Seale *et al.*, 2011). On the other hand, mature adipose-specific KO of *Prdm16* prevented browning of iWAT and led to increase in the weight of iWAT, but not gWAT (Cohen *et al.*, 2014). This shows that, at least in mice, alteration of browning can impact fat distribution. In humans, cold-induced BAT activation is associated with increased rate of lipolysis, FFA oxidation, FFA cycling and improved adipose insulin sensitivity (Hanssen *et al.*, 2015; Chondronikola *et al.*, 2016). A few studies have also assessed the correlation between BAT activity and

WAT distribution, but a causative link is currently missing (Yoneshiro *et al.*, 2011; Brendle *et al.*, 2018). The most recent study of FDG-PET/CT scans from 4852 patients identified a stronger inverse correlation of BAT activity with VAT area, than SCAT area, but the strength of this association differs with age and sex (Brendle *et al.*, 2018). Furthermore, suppression of browning was one of the proposed mechanisms that could contribute to obesity in the strongest BMI-associated *FTO* locus (Claussnitzer *et al.*, 2015). However, rs1421085 in this locus was not associated with WHR after adjustment for BMI (Pulit *et al.*, 2018). Importantly, humans do not have a depot directly comparable to gWAT (the depot that showed unique effects in the *Prdm16*-KO and my *Wars2*$^{V117L/V117L}$ mice) (Chusyd *et al.*, 2016). Instead, the mesenteric WAT (mWAT) appears to be a more comparable visceral depot between mice and humans (Tchkonia *et al.*, 2013). Although I did not assess browning in mWAT, its weight was reduced in both male and female *Wars2*$^{V117L/V117L}$ mice on HFD, suggesting that the protection from fat loss in *Wars2*$^{V117L/V117L}$ mice was unique to gWAT. In humans, the depots most susceptible to browning were found to be in periaortic regions, but visceral depots such as the omental fat were also shown to upregulate browning marker expression in pheochromocytoma patients (Frontini *et al.*, 2013; Giordano, Frontini and Cinti, 2016). On the other hand, human GSAT showed very limited browning capacity, which seems to contrast the browning capacity of murine subcutaneous iWAT, observed in this work and previous studies (Zuriaga *et al.*, 2017). This could be resolved by a recent study which showed that in physiologically "humanised" mice, housed at thermoneutrality (~30°C) and with access to calorie-rich (high-fat, high-sugar) diet, iWAT was resistant to browning (de Jong *et al.*, 2019). This agrees with the lack of effect on proton leak in the *Wars2*$^{V117L/V117L}$ primary adipocytes cultured under standard conditions at 37°C. Thus, although I detect upregulated browning in iWAT of *Wars*$^{V117L/V117L}$ mice, this is likely to be caused by upregulated

FGF21 signalling and it is not clear whether similar effects would occur in the GSAT of humans, who mostly live at thermoneutrality.

The study of "humanised" mice further showed that it was the classical murine interscapular BAT that was capable of browning and most closely resembled human interscapular BAT, in terms of gene expression and histology (de Jong *et al.*, 2019). In *Wars2*$^{V177L/V117L}$ mice, BAT showed severe ETC complex deficiencies, reduction of mtDNA, UCP1 protein and browning marker mRNA expression. However, since the BAT of these mice is already activated due to cold exposure, it would be interesting to test whether the *Wars2*$^{V117L/V117L}$ mutation in the less metabolically-demanding physiologically "humanised" condition could instead upregulate BAT activity. This could increase energy expenditure by BAT and indirectly affect WAT weight, by upregulating lipolysis and reduction of FA storage (Vegiopoulos, Rohm and Herzig, 2017). Ideally, the causative effect of BAT activity on fat distribution could be tested also in humans by long-term cold-exposure and correlating FDG-PET/CT scan with the rate of change in the volumes of different WAT depots.

6.5. *Wars2*$^{V117L/V117L}$ mice in the light of lipodystrophy and cachexia

Apart from browning of WAT, *Wars2*$^{V117L/V117L}$ mice previously showed reduced overall energy expenditure per gram of lean weight, an effect most likely due to ETC complex deficiencies in other tissues such as the heart, skeletal muscle and BAT (Agnew *et al.*, 2018). It was thus unclear why *Wars2*$^{V117L/V117L}$ mice failed to gain fat mass, even on a HFD. Such marked effects on adipose tissue are frequently observed in cachexia and lipodystrophies which may help with explaining the *Wars2*$^{V117L/V117L}$ phenotype (Vegiopoulos, Rohm and Herzig, 2017).

Lipodystrophies, such as congenital generalised lipodystrophy, often arise as a result of intrinsic defects in adipose, and in effect, fat is often stored ectopically contributing to elevated plasma TGs and insulin resistance (Patni and Garg, 2015). Unlike lipodsytrophic mouse models, such as the *Plin1*$^{-/-}$ mouse, *Wars2*$^{V117L/V117L}$ mice do not show insulin resistance and in fact show improved glucose tolerance and reduced TG levels (Agnew *et al.*, 2018). Furthermore, I do not find a significant reduction in mitochondrial ETC complex levels in iWAT and gWAT of 4 month old mice. Together, these findings suggest that the primary cause of fat loss is not adipose tissue dysfunction.

Cachexia is a pathological wasting condition defined by loss of fat mass and muscle that cannot be reversed by nutrition. It is commonly observed in patients with conditions such as cancer, chronic obstructive pulmonary disorder (COPD) or congestive heart failure (Morley, Thomas and Wilson, 2006). Similarly to *Wars2*$^{V117L/V117L}$ mice, fat loss in cachetic patients precedes loss of lean mass (Fouladiun *et al.*, 2005). Further in line with the above conclusion for *Wars2*$^{V117L/V171L}$ mice, fat loss in cachexia is not caused by an adipose-intrinsic mechanism, but instead through upregulation of cytokines, such as IL-6 and TNFα and reduced food intake (Oliff *et al.*, 1987; Baltgalvis *et al.*, 2008; Solheim *et al.*, 2014). Indeed, the *Wars2*$^{V117L/V11L}$ mice show elevated levels of the appetite-suppressor hormone GDF15 and reduced food intake in males from as early as 7 weeks of age. GDF15 is also upregulated in some cancers and it could be contributing to the reduced food intake in cachexia patients (O'Rahilly, 2017). In support of this, antibody targeting of GDF15 in mouse models with tumour xenografts rescued normal levels of food intake and fat mass (Johnen *et al.*, 2007). Thus, it would be interesting to test GDF15 levels also in the *Dars2*-KO model and observe whether its antibody targeting could rescue some of the phenotypes observed in both the *Dars2* and *Wars2* models. Since GDF15 was found to be

elevated in the serum of patients with mitochondrial disease, there could be a general link between mitochondrial diseases and cachexia mechanisms (Yatsuga *et al.*, 2015). However, in *Wars2*$^{V117L/V11L}$ females (n=2), where similar fat loss as in males is observed, food intake does not seem to be affected. This suggests there may still be other mechanisms explaining the failure to gain fat mass.

A key marker of cachexia is upregulation of lipolysis and its key enzymes ATGL and HSL in WAT which directly contribute to fat mass loss due to cancer (Das *et al.*, 2011). Surprisingly, lipogenesis has also been found to be upregulated in cachexia, most likely through increased *Cidea* levels which leads to degradation of AMP-activated protein kinase (AMPK), a canonical inhibitor of Acetyl-CoA carboxylase 1 (ACC1) & Hormone-sensitive lipase (HSL) (Garton and Yeaman, 1990; Sullivan *et al.*, 1994; Rohm *et al.*, 2016). Since *Cidea* was upregulated also in the iWAT and gWAT of *Wars2*$^{V117L/V117L}$ mice, it is possible that substrate cycling due to simultaneous activation of lipolysis and lipogenesis could directly contribute to the fat mass loss. Phosphorylation of AMPK, ACC and ATGL should thus be tested to confirm this hypothesis. Furthermore, it will be interesting to see whether the fat loss-resistant gWAT of males on HFD differs in its lipolytic-lipogenic balance.

6.6. Proposed mechanism for the *Wars2*$^{V117L/V117L}$ mice

In summary, I propose a model where severe ETC complex deficiencies in heart, muscle and BAT in the *Wars2*$^{V117L/V117L}$ mice lead to reduced energy expenditure and stress signalling via *Fgf21* and *Gdf15* expression (Figure 6.1). Whilst reduced energy expenditure and GDF15 contribute to reduced food intake and fat mass loss, FGF21 activates browning in WAT, especially iWAT. It is likely that the depot-specific browning susceptibility of iWAT, as opposed to gWAT, contributes to the increased gWAT:iWAT

ratio. This difference might be further pronounced in males, which lack UCP1 in gWAT, and on HFD. Other mechanisms, such as altered lipolysis and lipogenesis rates between the depots, could contribute to the protection of gWAT in the face of reduction of almost all other depots.

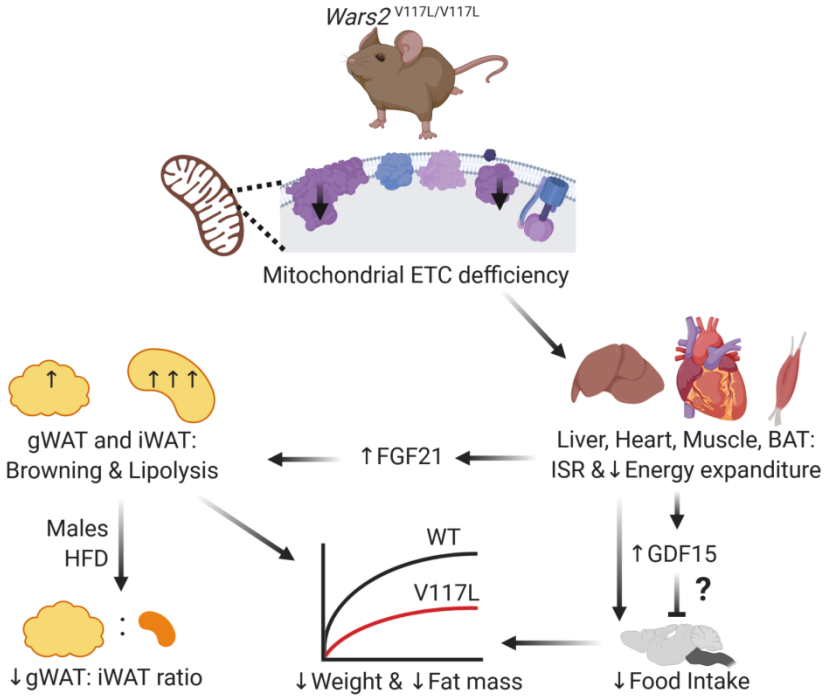

Figure 6.1 | The proposed mechanism for reduced fat mass and altered fat distribution in *Wars2*$^{V117L/V117L}$ mice. The mutation primarily affects high-energy demanding tissues such as the heart and BAT, which present complex deficiencies and secrete mitokines GDF15 and FGF21. Reduced energy expenditure and increased GDF15 levels from these tissues could contribute to reduced food intake and loss of fat mass. Systemic FGF21 signalling likely contributes to the browning of WAT and depot-specific differences in this process are likely to be accentuated in males and by HFD, leading to elevated gWAT:iWAT ratio. Created with BioRender.

6.7. No phenotype observed in heterozygous *Wars2*$^{+/V117L}$ and *Wars2*$^{+/-}$ mice

Allele-specific expression (ASE) in Risk Block A, indicated that on average carriers of the C|T and T|T genotypes for rs2645294 have ~66% and ~33% of C|C *WARS2* expression, respectively (Table 7.1) (Mele *et al.*, 2015). The phenotype of a *Wars2*$^{V117L/V117L}$ mouse with only 0-30% (depending on the tissue) of WT WARS2 protein expression is thus likely to be more extreme than in the human situation. For this reason, I also tested the heterozygous *Wars2*$^{+/V117L}$ and *Wars2*$^{+/-}$ mice for effects on body composition and weight of different fat depots, but found no differences. This agrees with the consensus that mt-aaRS genes do not cause a pathology in the heterozygous state (Sissler, Gonzalez-Serrano and Westhof, 2017).

Does this mean that *WARS2* is not the functional gene in the *TBX15-WARS2* locus? There are at least two possible explanations. First, indeed, *WARS2* is not a functional gene in the locus. If only severe *WARS2* reduction (>50% reduction) could affect adipose, that would likely be in parallel with a severe effect on the heart and BAT, as seen in the *Wars2*$^{V117L/V117L}$ mice. However, this locus is not associated with cardiovascular traits in humans.

The second possibility is that *WARS2* is the functional gene, but my study of fat-depot weights in the heterozygous mice might have been too imprecise, either due to technical or biological variation, to detect the small effect on fat distribution. Indeed, most common SNPs discovered in GWAS studies have minor effects on traits and gene expression in general (Shungin *et al.*, 2015; Kircher *et al.*, 2019). Furthermore, a recent review showed that the majority of missing heritability of complex traits observed in GWAS studies can be explained by signals that did not reach significance with small effect sizes interspaced throughout the genome. Thus although several "core" highly interconnected genes have major effects on a trait, alternations in most genes have small indirect effects (Boyle, Li

and Pritchard, 2017). It remains to be seen whether *TBX15-WARS2* locus lies at the core of a key network regulating fat distribution. Identifying more functional genes across other WHRadjBMI loci, by integration of experimental, statistical and systems biology approaches is likely to reveal answers to this question (Barroso and McCarthy, 2019). Meanwhile a larger animal cohort or more precise method such as animal CT scan might allow detection of more subtle differences in the heterozygous mice (Sasser *et al.*, 2012).

6.8. Conclusion

In this work, I provide evidence for molecular effect of rs3810068 and rs3936510 on protein binding in differentiating human adipocytes. Since these SNPs explain the majority of the signals in their respective GWAS loci, this study paves the way for CRISPR editing in human cell lines and implication of novel genes such as *EMILIN2* as regulators of fat distribution. In Risk Block A of the *TBX15-WARS2*, I identified 3 potentially functional SNPs and I disproved one of them as a regulator of RNA stability. This suggests the WHRadjBMI signal is likely to act through transcriptional regulation by affecting either *WARS2* or *TBX15* expression. The enhancer SNP rs10923274 with the best epi-PMCA score and a relatively high PPA score in both UKBB and GIANT datasets is the next most likely functional candidate in the locus.

Independently, I tested *Wars2* as regulator of WHRadjBMI in the *TBX15-WARS2* locus. Whilst heterozygous $Wars2^{+/V117L}$ and $Wars2^{+/-}$ mice showed no effect on body composition and fat depot weights, I demonstrate that the hypomorphic $Wars2^{V117L/V117L}$ mouse fails to gain fat mass, despite administration of HFD, and shows male and HFD-specific upregulation of gWAT:iWAT ratio. I tested the hypothesis that browning might contribute to these depot-specific differences and confirm browning of WAT, especially in the iWAT. Since primary adipocyte cultures do not show a difference in proton leak and the plasma of $Wars2^{V117L/V117L}$ mice shows elevated levels of the browning-inducing

FGF21 and appetite-suppressing GDF15, it is likely that the effect on adipose is indirect, through signalling from the ETC-deficient and severely affected heart and BAT. Indeed, for the first time in this mouse model, I demonstrate downregulated food intake which could be a major contributor to the fat mass loss. It remains to be seen how relevant are these findings to humans who live at thermoneutrality and are unlikely to experience such severe reduction of *WARS2* levels as *Wars2*$^{V117L/V117L}$ mice. Studying these mice under thermoneutrality and testing the effects on interscapular BAT might reveal mechanisms closer to the human situation.

On a different note, if future works confirms the key role for GDF15 in mediating some of the cachexia-like phenotype in the *Wars2*$^{V117L/V117L}$, it will be interesting to see whether interference with GDF15 would alleviate some of the symptoms observed in these mice, *Dars2*-KO mice and also human mt-aaRS patients.

7. Appendix

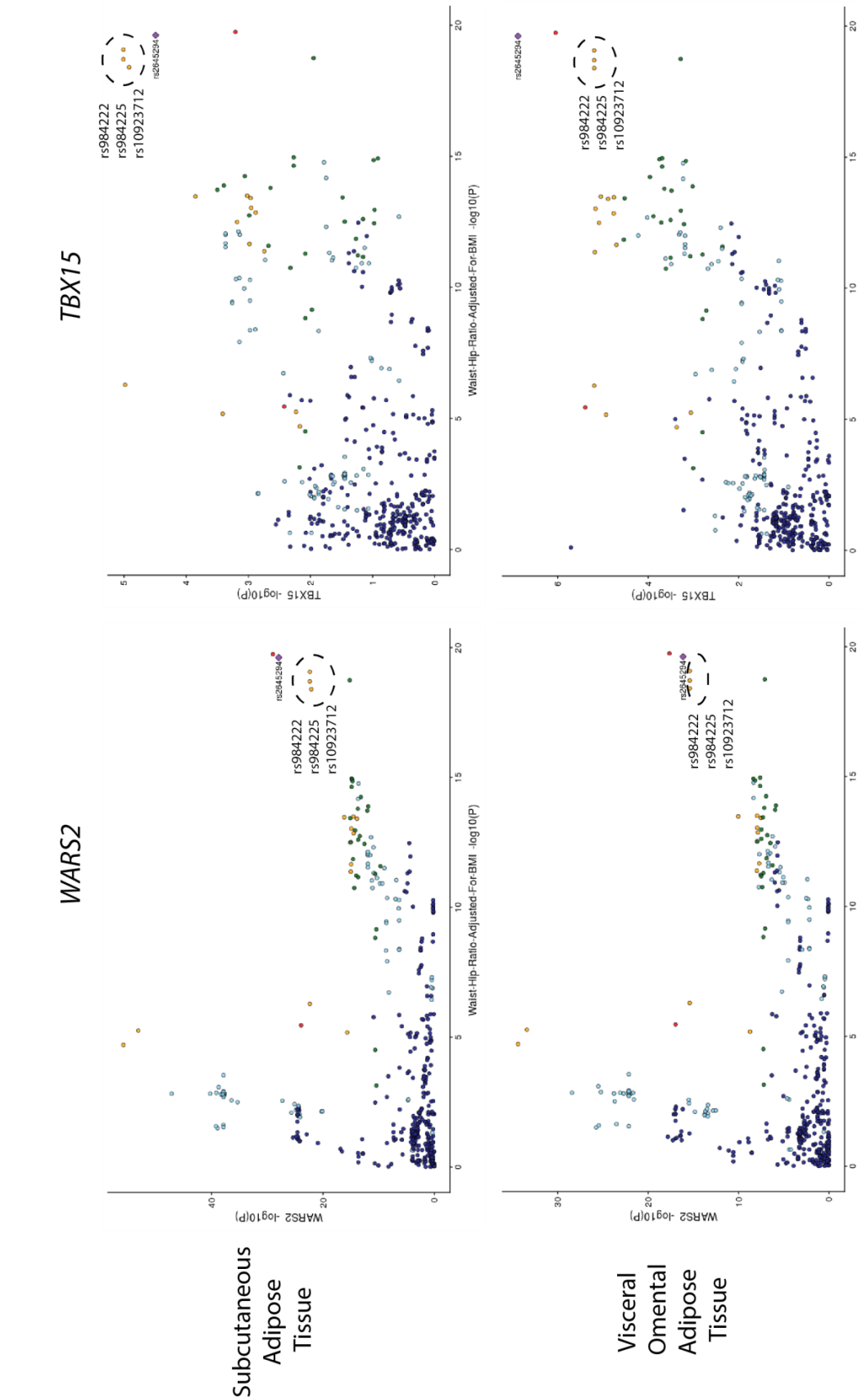

Figure 7.1 | Colocalisation of *TBX15* and *WARS2* levels in SCAT and VAT with sex-combined WHRadjBMI signal from Shungin et al, 2015. Y-axis shows the p-value for the eQTL association for each SNP, x-axis shows the p-value for the WHRadjBMI associations. Each graph denotes the position of the Risk Block A lead SNP rs2645294 and the position of the 3 SNPs in the 1.5kb previously fine-mapped region (Liu *et al.*, 2014). Graphs generated by the LocusCompare online tool (http://locuscompare.com/) (Boxiang Liu, Mike Gloudemans, 2018).

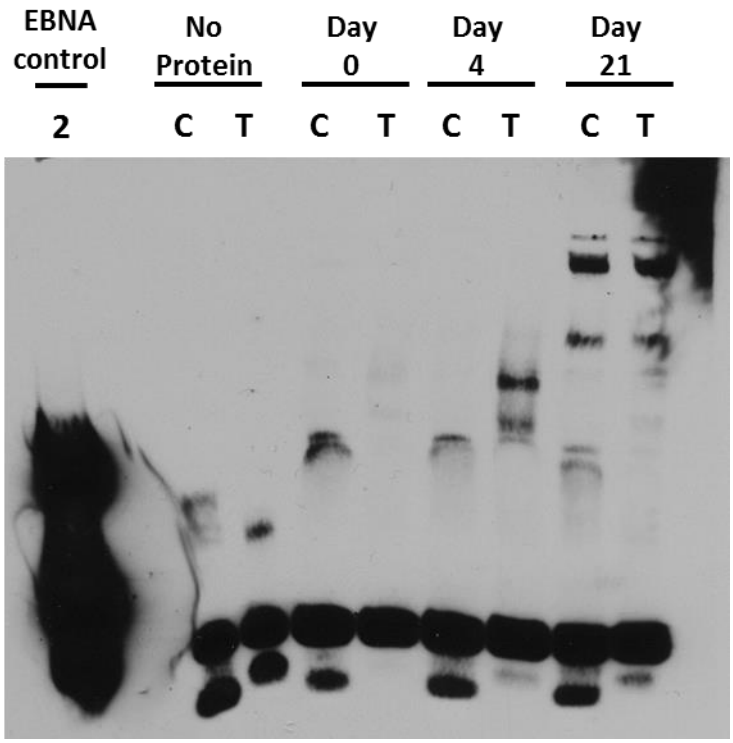

Figure 7.2 | rs3810068 EMSA at different time-point of hWAT differentiation. 38bp biotinylated DNA probes surrounding rs3810068 with either the T or C allele were incubated with nuclear protein from hWAT cells differentiated for 0, 4 and 21 days or with no protein. Differences in binding differed at different differentiation time-points. The first lane is a control sample from the kit which incubates the control sequence with Epstein–Barr virus nuclear antigen 1 (EBNA) protein.

Table 7.1 | Allele-specific expression (ASE) data for rs2645294 from the GTEx dataset. Showing the 5 tissues where ASE reached statistical significance. Listed are the scores for the strength of the signal, median fold change, minimum and maximum ASE across the samples and other descriptive statistics (GTEx-Consortium, 2013). Data was obtained via the UCSC browser (Kent *et al.*, 2002).

ASE: rs2645294	Colon - Sigmoid	Brain - Anterior cingulate cortex	Brain - Cortex	Cervix - Endocervix	Spleen
Score*	540	500	500	540	500
Allelic imbalance (0-.5) median	0.27	0.25	0.25	0.27	0.25
Median fold change	0.37	0.33	0.33	0.37	0.33
RNA-seq reads overlapping this position	10	9	10	22	8
Sample count	28	9	9	1	11
Donor count	28	9	9	1	11
Minimum ASE	0	0.13	0.14	0.27	0
Q1 ASE	0.14	0.14	0.2	0.27	0.13
Q3 ASE	0.39	0.38	0.3	0.27	0.31
Maximum ASE	0.5	0.39	0.39	0.27	0.5
ASE standard deviation	0.138	0.102	0.08	0	0.143

8. References

Abel, E. D. *et al.* (2001) 'Adipose-selective targeting of the GLUT4 gene impairs insulin action in muscle and liver.', *Nature*. England, 409(6821), pp. 729–733. doi: 10.1038/35055575.

Abraham, T. M. *et al.* (2015) 'Association between visceral and subcutaneous adipose depots and incident cardiovascular disease risk factors.', *Circulation*. United States, 132(17), pp. 1639–1647. doi: 10.1161/CIRCULATIONAHA.114.015000.

Afshin, A. *et al.* (2017) 'Health Effects of Overweight and Obesity in 195 Countries over 25 Years.', *The New England journal of medicine*. United States, 377(1), pp. 13–27. doi: 10.1056/NEJMoa1614362.

Agarwal, V. *et al.* (2015) 'Predicting effective microRNA target sites in mammalian mRNAs.', *eLife*. England, 4. doi: 10.7554/eLife.05005.

Agnew, T. *et al.* (2018) 'A Wars2 Mutant Mouse Model Displays OXPHOS Deficiencies and Activation of Tissue-Specific Stress Response Pathways.', *Cell reports*. United States, 25(12), pp. 3315-3328.e6. doi: 10.1016/j.celrep.2018.11.080.

Akinci, B., Meral, R. and Oral, E. A. (2018) 'Phenotypic and Genetic Characteristics of Lipodystrophy: Pathophysiology, Metabolic Abnormalities, and Comorbidities', *Current Diabetes Reports*, 18(12), p. 143. doi: 10.1007/s11892-018-1099-9.

Altshuler-Keylin, S. and Kajimura, S. (2017) 'Mitochondrial homeostasis in adipose tissue remodeling', *Science Signaling*, 10(468), pp. 1–11. doi: 10.1126/scisignal.aai9248.

Arensbergen, J. Van, Steensel, B. Van and Bussemaker, H. J. (2014) 'In search of the determinants of enhancer – promoter interaction specificity', *Trends in Cell Biology*. Elsevier Ltd, 24(11), pp. 695–702. doi: 10.1016/j.tcb.2014.07.004.

Arita, Y. *et al.* (1999) 'Paradoxical decrease of an adipose-specific protein, adiponectin, in obesity.', *Biochemical and biophysical research communications*. United States, 257(1), pp. 79–83. doi: 10.1006/bbrc.1999.0255.

Arnaldi, G. *et al.* (2010) 'Pathophysiology of dyslipidemia in Cushing's syndrome', *Neuroendocrinology*, 92(SUPPL. 1), pp. 86–90. doi: 10.1159/000314213.

Arner, P. *et al.* (1990) 'Beta-adrenoceptor expression in human fat cells from different regions.', *The Journal of clinical investigation*. United States, 86(5), pp. 1595–1600. doi: 10.1172/JCI114880.

Arner, P. *et al.* (1991) 'Expression of lipoprotein lipase in different human subcutaneous adipose tissue regions.', *Journal of lipid research*. United States, 32(3), pp. 423–429.

Astrup, A. *et al.* (1985) 'Enhanced thermogenic responsiveness during chronic ephedrine treatment in man.', *The American journal of clinical nutrition*. United States, 42(1), pp. 83–94. doi: 10.1093/ajcn/42.1.83.

Atit, R. *et al.* (2006) 'Beta-catenin activation is necessary and sufficient to specify the dorsal dermal fate in the mouse.', *Developmental biology*. United States, 296(1), pp. 164–176. doi: 10.1016/j.ydbio.2006.04.449.

Aulchenko, Y. S. *et al.* (2007) 'LPIN2 is associated with type 2 diabetes, glucose metabolism, and body composition', *Diabetes*, 56(12), pp. 3020–3026. doi: 10.2337/db07-0338.

Bachman, E. S. *et al.* (2002) 'betaAR signaling required for diet-induced thermogenesis and obesity resistance.', *Science (New York, N.Y.)*. United States, 297(5582), pp. 843–845. doi: 10.1126/science.1073160.

Baltgalvis, K. A. *et al.* (2008) 'Interleukin-6 and cachexia in ApcMin/+ mice.', *American journal of physiology. Regulatory, integrative and comparative physiology*. United States, 294(2), pp. R393-401. doi: 10.1152/ajpregu.00716.2007.

Barbatelli, G. *et al.* (2010) 'The emergence of cold-induced brown adipocytes in mouse white fat depots is determined predominantly by white to brown adipocyte transdifferentiation.', *American journal of physiology. Endocrinology and metabolism*. United States, 298(6), pp. E1244-53. doi: 10.1152/ajpendo.00600.2009.

Barroso, I. and McCarthy, M. I. (2019) 'The Genetic Basis of Metabolic Disease', *Cell*. Elsevier, 177(1), pp. 146–161. doi: 10.1016/j.cell.2019.02.024.

Bartelt, A. and Heeren, J. (2014) 'Adipose tissue browning and metabolic health', *Nat Rev Endocrinol*. 2013/10/23, 10(1), pp. 24–36. doi: 10.1038/nrendo.2013.204.

Baudrimont, A. *et al.* (2017) 'Multiplexed gene control reveals rapid mRNA turnover', *Science Advances*, 3(7). doi: 10.1126/sciadv.1700006.

Bensaude, O. (2011) 'Inhibiting eukaryotic transcription: Which compound to choose? How to evaluate its activity?', *Transcription*, 2(3), pp. 103–108. doi: 10.4161/trns.2.3.16172.

Bentley, D. L. (2014) 'Coupling mRNA processing with transcription in time and space', *Nature Reviews Genetics*. Nature Publishing Group, 15(3), pp. 163–175. doi: 10.1038/nrg3662.

Berthelot, C. *et al.* (2018) 'Complexity and conservation of regulatory landscapes underlie evolutionary resilience of mammalian gene expression.', *Nature ecology & evolution*. England, 2(1), pp. 152–163. doi: 10.1038/s41559-017-0377-2.

Billon, N. *et al.* (2007) 'The generation of adipocytes by the neural crest', *Development*, 134(12), pp. 2283–2292. doi: 10.1242/dev.002642.

Bond, G. L. *et al.* (2004) 'A single nucleotide polymorphism in the MDM2 promoter attenuates the p53 tumor suppressor pathway and accelerates tumor formation in humans.', *Cell*. United States, 119(5), pp. 591–602. doi: 10.1016/j.cell.2004.11.022.

Boxiang Liu, Mike Gloudemans, S. M. (2018) 'LocusCompare: A Tool to Visualize Pairs of Association'. Available at: http://locuscompare.com/.

Boyle, E. A., Li, Y. I. and Pritchard, J. K. (2017) 'An Expanded View of Complex Traits: From Polygenic to Omnigenic.', *Cell*. United States, 169(7), pp. 1177–1186. doi: 10.1016/j.cell.2017.05.038.

Brendle, C. *et al.* (2018) 'Correlation of Brown Adipose Tissue with Other Body Fat Compartments and Patient Characteristics: A Retrospective Analysis in a Large Patient

Cohort Using PET/CT', *Academic Radiology*. Elsevier Inc., 25(1), pp. 102–110. doi: 10.1016/j.acra.2017.09.007.

Brown, K. F. *et al.* (2018) 'The fraction of cancer attributable to modifiable risk factors in England, Wales, Scotland, Northern Ireland, and the United Kingdom in 2015.', *British journal of cancer*. England, 118(8), pp. 1130–1141. doi: 10.1038/s41416-018-0029-6.

Buckley, M. *et al.* (2016) 'Enhancer scanning to locate regulatory regions in genomic loci', *Nat Protoc*. 2015/12/15, 11(1), pp. 46–60. doi: 10.1038/nprot.2015.136.

Bugge, A., Dib, L. and Collins, S. (2014) *Measuring respiratory activity of adipocytes and adipose tissues in real time*. 1st edn, *Methods in Enzymology*. 1st edn. Elsevier Inc. doi: 10.1016/B978-0-12-800280-3.00013-X.

Burke, E. A. *et al.* (2017) 'Biallelic Mutations in Mitochondrial Tryptophanyl-tRNA Synthetase Cause Levodopa-Rresponsive Infantile-Onset Parkinsonism.', *Clinical genetics*. Denmark. doi: 10.1111/cge.13172.

Bush, W. S. and Moore, J. H. (2012) 'Chapter 11: Genome-wide association studies', *PLoS computational biology*. Public Library of Science, 8(12), pp. e1002822–e1002822. doi: 10.1371/journal.pcbi.1002822.

Calo, E. and Wysocka, J. (2013) 'Modification of Enhancer Chromatin: What, How, and Why?', *Molecular Cell*. Elsevier Inc., pp. 825–837. doi: 10.1016/j.molcel.2013.01.038.

Calvo, S. E. and Mootha, V. K. (2010) 'The Mitochondrial Proteome and Human Disease', *Annual Review of Genomics and Human Genetics*. Annual Reviews, 11(1), pp. 25–44. doi: 10.1146/annurev-genom-082509-141720.

Cancer Research UK (2019) 'Obese people outnumber smokers two to one'. Available at: https://www.cancerresearchuk.org/about-us/cancer-news/press-release/2019-07-03-obese-people-outnumber-smokers-two-to-one.

Candille, S. I. *et al.* (2004) 'Dorsoventral patterning of the mouse coat by Tbx15', *PLoS Biology*, 2(1). doi: 10.1371/journal.pbio.0020003.

Canela-Xandri, O., Rawlik, K. and Tenesa, A. (2018) 'An atlas of genetic associations in UK Biobank', *Nature Genetics*. Springer US, 50(11), pp. 1593–1599. doi: 10.1038/s41588-018-0248-z.

Cannon, B. and Nedergaard, J. (2004) 'Brown adipose tissue: function and physiological significance.', *Physiological reviews*. United States, 84(1), pp. 277–359. doi: 10.1152/physrev.00015.2003.

Canoy, D. (2008) 'Distribution of body fat and risk of coronary heart disease in men and women', *Curr Opin Cardiol*. 2008/10/03, 23(6), pp. 591–598. doi: 10.1097/HCO.0b013e328313133a.

Caserta, F. *et al.* (2001) 'Fat depot origin affects fatty acid handling in cultured rat and human preadipocytes', *American Journal of Physiology - Endocrinology and Metabolism*, 280(2 43-2), pp. 238–247. doi: 10.1152/ajpendo.2001.280.2.e238.

Cassandrini, D. *et al.* (2013) 'Pontocerebellar hypoplasia type 6 caused by mutations in RARS2: definition of the clinical spectrum and molecular findings in five patients.',

Journal of inherited metabolic disease. United States, 36(1), pp. 43–53. doi: 10.1007/s10545-012-9487-9.

Castan, I. *et al.* (1994) 'Antilipolytic effects of alpha 2-adrenergic agonists, neuropeptide Y, adenosine, and PGE1 in mammal adipocytes', *American Journal of Physiology-Regulatory, Integrative and Comparative Physiology*. American Physiological Society, 266(4), pp. R1141–R1147. doi: 10.1152/ajpregu.1994.266.4.R1141.

Cerutti, R. *et al.* (2014) 'NAD(+)-dependent activation of Sirt1 corrects the phenotype in a mouse model of mitochondrial disease.', *Cell metabolism*. United States, 19(6), pp. 1042–1049. doi: 10.1016/j.cmet.2014.04.001.

Chan, R. C. W. *et al.* (2018) 'Segway 2.0: Gaussian mixture models and minibatch training.', *Bioinformatics (Oxford, England)*. England, 34(4), pp. 669–671. doi: 10.1093/bioinformatics/btx603.

Chang, T. H. *et al.* (2013) 'An enhanced computational platform for investigating the roles of regulatory RNA and for identifying functional RNA motifs', *BMC Bioinformatics*. BioMed Central Ltd, 14(Suppl 2), p. S4. doi: 10.1186/1471-2105-14-S2-S4.

Chau, Y. Y. *et al.* (2014) 'Visceral and subcutaneous fat have different origins and evidence supports a mesothelial source', *Nature Cell Biology*, 16(4), pp. 367–375. doi: 10.1038/ncb2922.

Chen, G. B. *et al.* (2016) 'Across-cohort QC analyses of GWAS summary statistics from complex traits', *European Journal of Human Genetics*, 25(1), pp. 137–146. doi: 10.1038/ejhg.2016.106.

Chen, Q. *et al.* (2016) 'Fate decision of mesenchymal stem cells: Adipocytes or osteoblasts?', *Cell Death and Differentiation*, 23(7), pp. 1128–1139. doi: 10.1038/cdd.2015.168.

Chi, J. *et al.* (2018) 'Three-Dimensional Adipose Tissue Imaging Reveals Regional Variation in Beige Fat Biogenesis and PRDM16-Dependent Sympathetic Neurite Density', *Cell Metabolism*, 27(1), pp. 226-236.e3. doi: 10.1016/j.cmet.2017.12.011.

Chimnaronk, S. *et al.* (2005) 'Dual-mode recognition of noncanonical tRNAs(Ser) by seryl-tRNA synthetase in mammalian mitochondria.', *The EMBO journal*. England, 24(19), pp. 3369–3379. doi: 10.1038/sj.emboj.7600811.

Chondronikola, M. *et al.* (2016) 'Brown Adipose Tissue Activation Is Linked to Distinct Systemic Effects on Lipid Metabolism in Humans', *Cell Metabolism*, 23(6), pp. 1200–1206. doi: 10.1016/j.cmet.2016.04.029.

Chong, P. S. T. *et al.* (2003) 'Multiple Symmetric Lipomatosis (Madelung's Disease) Caused by the MERRF (A8344G) Mutation: A Report of Two Cases and Review of the Literature.', *Journal of clinical neuromuscular disease*. United States, 5(1), pp. 1–7.

Chrétien, D. *et al.* (2018) 'Mitochondria are physiologically maintained at close to 50 °C', *PLOS Biology*. Public Library of Science, 16(1), p. e2003992. Available at: https://doi.org/10.1371/journal.pbio.2003992.

Chu, A. Y. *et al.* (2017) 'Multiethnic genome-wide meta-analysis of ectopic fat depots identifies loci associated with adipocyte development and differentiation', *Nature*

Genetics, 49(1), pp. 125–130. doi: 10.1038/ng.3738.

Church, C. D., Berry, R. and Rodeheffer, M. S. (2014) 'Isolation and study of adipocyte precursors.', *Methods in enzymology*. United States, 537, pp. 31–46. doi: 10.1016/B978-0-12-411619-1.00003-3.

Chusyd, D. E. *et al.* (2016) 'Relationships between Rodent White Adipose Fat Pads and Human White Adipose Fat Depots.', *Frontiers in nutrition*. Switzerland, 3, p. 10. doi: 10.3389/fnut.2016.00010.

Cinti, S. (2005) 'The adipose organ.', *Prostaglandins, leukotrienes, and essential fatty acids*. Scotland, 73(1), pp. 9–15. doi: 10.1016/j.plefa.2005.04.010.

Civelek, M. *et al.* (2017) 'Genetic Regulation of Adipose Gene Expression and Cardio-Metabolic Traits', *American Journal of Human Genetics*, 100(3), pp. 428–443. doi: 10.1016/j.ajhg.2017.01.027.

Claussnitzer, M. *et al.* (2014) 'Leveraging cross-species transcription factor binding site patterns: from diabetes risk loci to disease mechanisms', *Cell*. 2014/01/21, 156(1–2), pp. 343–358. doi: 10.1016/j.cell.2013.10.058.

Claussnitzer, M. *et al.* (2015) 'FTO Obesity Variant Circuitry and Adipocyte Browning in Humans', *N Engl J Med*. 2015/08/20, 373(10), pp. 895–907. doi: 10.1056/NEJMoa1502214.

Cohen, P. *et al.* (2014) 'Ablation of PRDM16 and beige adipose causes metabolic dysfunction and a subcutaneous to visceral fat switch', *Cell*, 156(1–2), pp. 304–316. doi: 10.1016/j.cell.2013.12.021.

Colditz, G. A. *et al.* (1995) 'Weight gain as a risk factor for clinical diabetes mellitus in women.', *Annals of internal medicine*. United States, 122(7), pp. 481–486. doi: 10.7326/0003-4819-122-7-199504010-00001.

Cousin, B. *et al.* (1992) 'Occurrence of brown adipocytes in rat white adipose tissue: molecular and morphological characterization.', *Journal of cell science*. England, 103 (Pt 4, pp. 931–942.

Curry, G. A. (1959) 'Genetical and Developmental Studies on Droopy-eared Mice', *Journal of Embryology and Experimental Morphology*, 7(1), pp. 39 LP – 65. Available at: http://dev.biologists.org/content/7/1/39.abstract.

Cypess, A. M. *et al.* (2015) 'Activation of human brown adipose tissue by a beta3-adrenergic receptor agonist.', *Cell metabolism*. United States, 21(1), pp. 33–38. doi: 10.1016/j.cmet.2014.12.009.

Dahlman, I. *et al.* (2016) 'Numerous Genes in Loci Associated With Body Fat Distribution Are Linked to Adipose Function', *Diabetes*. 2016/01/23, 65(2), pp. 433–437. doi: 10.2337/db15-0828.

Das, S. K. *et al.* (2011) 'Adipose triglyceride lipase contributes to cancer-associated cachexia.', *Science (New York, N.Y.)*. United States, 333(6039), pp. 233–238. doi: 10.1126/science.1198973.

Dasgupta, T. and Ladd, A. N. (2012) 'The importance of CELF control: molecular and

biological roles of the CUG-BP, Elav-like family of RNA-binding proteins', *Wiley interdisciplinary reviews. RNA*. 2011/08/17, 3(1), pp. 104–121. doi: 10.1002/wrna.107.

Denny, J. C. *et al.* (2013) 'Systematic comparison of phenome-wide association study of electronic medical record data and genome-wide association study data', *Nature Biotechnology*. Nature Publishing Group, a division of Macmillan Publishers Limited. All Rights Reserved., 31, p. 1102. Available at: https://doi.org/10.1038/nbt.2749.

Despang, A. *et al.* (2019) 'Functional dissection of TADs reveals non-essential and instructive roles in regulating gene expression', *bioRxiv*, p. 566562. doi: 10.1101/566562.

Dickel, D. E. *et al.* (2016) 'Genome-wide compendium and functional assessment of in vivo heart enhancers', *Nat Commun*. 2016/10/06, 7, p. 12923. doi: 10.1038/ncomms12923.

Dickinson, M. E. *et al.* (2016) 'High-throughput discovery of novel developmental phenotypes', *Nature*. Macmillan Publishers Limited, part of Springer Nature. All rights reserved., 537, p. 508. Available at: https://doi.org/10.1038/nature19356.

Dikoglu, E. *et al.* (2013) 'Homozygosity for a novel truncating mutation confirms TBX15 deficiency as the cause of Cousin syndrome', *Am J Med Genet A*. 2013/09/17, 161A(12), pp. 3161–3165. doi: 10.1002/ajmg.a.36173.

Ding, H. *et al.* (2016) 'Fasting induces a subcutaneous-to-visceral fat switch mediated by microRNA-149-3p and suppression of PRDM16', *Nature Communications*. Nature Publishing Group, 7(May), pp. 1–17. doi: 10.1038/ncomms11533.

Dixon, J. R. *et al.* (2012) 'Topological domains in mammalian genomes identified by analysis of chromatin interactions.', *Nature*. England, 485(7398), pp. 376–380. doi: 10.1038/nature11082.

Dobbs, R. *et al.* (2014) 'Overcoming obesity: an initial economic analysis: McKinsey Global Institute, 2014.' Available at: https://www.mckinsey.com/~/media/McKinsey/Business %0AFunctions/Economic Studies TEMP/Our Insights/%0AHow the world could better fight obesity/%0AMGI_Overcoming_obesity_Full_report.ashx.

Dogan, S. A. *et al.* (2014) 'Tissue-specific loss of DARS2 activates stress responses independently of respiratory chain deficiency in the heart.', *Cell metabolism*. United States, 19(3), pp. 458–469. doi: 10.1016/j.cmet.2014.02.004.

van Dongen, J. *et al.* (2013) 'Heritability of metabolic syndrome traits in a large population-based sample', *Journal of Lipid Research* , 54(10), pp. 2914–2923. doi: 10.1194/jlr.P041673.

Dulloo, A. G. *et al.* (2010) 'Body composition phenotypes in pathways to obesity and the metabolic syndrome.', *International journal of obesity (2005)*. England, 34 Suppl 2, pp. S4-17. doi: 10.1038/ijo.2010.234.

Elo, J. M. *et al.* (2012) 'Mitochondrial phenylalanyl-tRNA synthetase mutations underlie fatal infantile Alpers encephalopathy.', *Human molecular genetics*. England, 21(20), pp. 4521–4529. doi: 10.1093/hmg/dds294.

Ernst, J. *et al.* (2011) 'Mapping and analysis of chromatin state dynamics in nine human cell types', *Nature*. Nature Publishing Group, a division of Macmillan Publishers Limited.

All Rights Reserved., 473, p. 43. Available at: https://doi.org/10.1038/nature09906.

Ernst, J. and Kellis, M. (2012) 'ChromHMM: automating chromatin-state discovery and characterization', *Nature Methods*. Nature Publishing Group, a division of Macmillan Publishers Limited. All Rights Reserved., 9, p. 215. Available at: https://doi.org/10.1038/nmeth.1906.

Ernst, J. and Kellis, M. (2017) 'Chromatin-state discovery and genome annotation with ChromHMM.', *Nature protocols*. England, 12(12), pp. 2478–2492. doi: 10.1038/nprot.2017.124.

Fabbrini, E. *et al.* (2010) 'Surgical removal of omental fat does not improve insulin sensitivity and cardiovascular risk factors in obese adults.', *Gastroenterology*. United States, 139(2), pp. 448–455. doi: 10.1053/j.gastro.2010.04.056.

Fain, J. N. *et al.* (2004) 'Comparison of the release of adipokines by adipose tissue, adipose tissue matrix, and adipocytes from visceral and subcutaneous abdominal adipose tissues of obese humans.', *Endocrinology*. United States, 145(5), pp. 2273–2282. doi: 10.1210/en.2003-1336.

Farin, H. F. *et al.* (2007) 'Transcriptional repression by the T-box proteins Tbx18 and Tbx15 depends on Groucho corepressors', *J Biol Chem*. 2007/06/23, 282(35), pp. 25748–25759. doi: 10.1074/jbc.M703724200.

Farley, E. K. *et al.* (2015) 'Suboptimization of developmental enhancers', *Science*. United States, 350(6258), pp. 325–328. doi: 10.1126/science.aac6948.

Fedorenko, A., Lishko, P. V and Kirichok, Y. (2012) 'Mechanism of fatty-acid-dependent UCP1 uncoupling in brown fat mitochondria', *Cell*. 2012/10/16, 151(2), pp. 400–413. doi: 10.1016/j.cell.2012.09.010.

Feldmann, H. M. *et al.* (2009) 'UCP1 ablation induces obesity and abolishes diet-induced thermogenesis in mice exempt from thermal stress by living at thermoneutrality.', *Cell metabolism*. United States, 9(2), pp. 203–209. doi: 10.1016/j.cmet.2008.12.014.

Fisher, F. F. *et al.* (2012) 'FGF21 regulates PGC-1α and browning of white adipose tissues in adaptive thermogenesis', *Genes and Development*, 26(3), pp. 271–281. doi: 10.1101/gad.177857.111.

Fisher, F. M. *et al.* (2002) 'Differences in adiponectin protein expression: effect of fat depots and type 2 diabetic status.', *Hormone and metabolic research = Hormon- und Stoffwechselforschung = Hormones et metabolisme*. Germany, 34(11–12), pp. 650–654. doi: 10.1055/s-2002-38246.

Fisher, S. *et al.* (2006) 'Conservation of RET regulatory function from human to zebrafish without sequence similarity.', *Science (New York, N.Y.)*. United States, 312(5771), pp. 276–279. doi: 10.1126/science.1124070.

Flemming, W. (1871) 'Ueber Bildung und Rückbildung der Fettzelle im Bindegewebe, und Bemerkungen über die Structur des Letzteren', *Archiv für mikroskopische Anatomie*, 7(1), pp. 32–80. doi: 10.1007/BF02956045.

Flister, M. J. *et al.* (2013) 'Identifying multiple causative genes at a single GWAS locus', *Genome Research*, 23(12), pp. 1996–2002. doi: 10.1101/gr.160283.113.

Fontana, L. *et al.* (2007) 'Visceral fat adipokine secretion is associated with systemic inflammation in obese humans.', *Diabetes*. United States, 56(4), pp. 1010–1013. doi: 10.2337/db06-1656.

Fornes, O. *et al.* (2019) 'JASPAR 2020: update of the open-access database of transcription factor binding profiles', *Nucleic acids research*. England, p. gkz1001. doi: 10.1093/nar/gkz1001.

Fouladiun, M. *et al.* (2005) 'Body composition and time course changes in regional distribution of fat and lean tissue in unselected cancer patients on palliative care--correlations with food intake, metabolism, exercise capacity, and hormones.', *Cancer*. United States, 103(10), pp. 2189–2198. doi: 10.1002/cncr.21013.

Fox, C. S. *et al.* (2007) 'Abdominal visceral and subcutaneous adipose tissue compartments: association with metabolic risk factors in the Framingham Heart Study.', *Circulation*. United States, 116(1), pp. 39–48. doi: 10.1161/CIRCULATIONAHA.106.675355.

Fox, C. S. *et al.* (2012) 'Genome-wide association of pericardial fat identifies a unique locus for ectopic fat.', *PLoS genetics*. United States, 8(5), p. e1002705. doi: 10.1371/journal.pgen.1002705.

Frontini, A. *et al.* (2013) 'White-to-brown transdifferentiation of omental adipocytes in patients affected by pheochromocytoma.', *Biochimica et biophysica acta*. Netherlands, 1831(5), pp. 950–959. doi: 10.1016/j.bbalip.2013.02.005.

Frontini, A. and Cinti, S. (2010) 'Distribution and development of brown adipocytes in the murine and human adipose organ.', *Cell metabolism*. United States, 11(4), pp. 253–256. doi: 10.1016/j.cmet.2010.03.004.

Fu, X. D. and Ares, M. (2014) 'Context-dependent control of alternative splicing by RNA-binding proteins', *Nature Reviews Genetics*. Nature Publishing Group, 15(10), pp. 689–701. doi: 10.1038/nrg3778.

Gabriely, I. *et al.* (2002) 'Removal of visceral fat prevents insulin resistance and glucose intolerance of aging: an adipokine-mediated process?', *Diabetes*. United States, 51(10), pp. 2951–2958. doi: 10.2337/diabetes.51.10.2951.

Gallagher, D. *et al.* (2005) 'Adipose tissue in muscle: a novel depot similar in size to visceral adipose tissue.', *The American journal of clinical nutrition*. United States, 81(4), pp. 903–910. doi: 10.1093/ajcn/81.4.903.

García-Ruiz, E. *et al.* (2015) 'The intake of high-fat diets induces the acquisition of brown adipocyte gene expression features in white adipose tissue', *International Journal of Obesity*, 39(11), pp. 1619–1629. doi: 10.1038/ijo.2015.112.

Garg, A. *et al.* (1992) 'Peculiar distribution of adipose tissue in patients with congenital generalized lipodystrophy.', *The Journal of clinical endocrinology and metabolism*. United States, 75(2), pp. 358–361. doi: 10.1210/jcem.75.2.1639935.

Garg, A. (2004) 'Acquired and inherited lipodystrophies.', *The New England journal of medicine*. United States, 350(12), pp. 1220–1234. doi: 10.1056/NEJMra025261.

Garg, A., Peshock, R. M. and Fleckenstein, J. L. (1999) 'Adipose tissue distribution

pattern in patients with familial partial lipodystrophy (Dunnigan variety).', *The Journal of clinical endocrinology and metabolism*. United States, 84(1), pp. 170–174. doi: 10.1210/jcem.84.1.5383.

Garton, A. J. and Yeaman, S. J. (1990) 'Identification and role of the basal phosphorylation site on hormone-sensitive lipase.', *European journal of biochemistry*. England, 191(1), pp. 245–250. doi: 10.1111/j.1432-1033.1990.tb19116.x.

Gburcik, V. *et al.* (2012) 'An essential role for Tbx15 in the differentiation of brown and "brite" but not white adipocytes', *American Journal of Physiology-Endocrinology and Metabolism*, 303(8), pp. E1053–E1060. doi: 10.1152/ajpendo.00104.2012.

Gesta, S. *et al.* (2006) 'Evidence for a role of developmental genes in the origin of obesity and body fat distribution', *Proc Natl Acad Sci U S A*. 2006/04/18, 103(17), pp. 6676–6681. doi: 10.1073/pnas.0601752103.

Gesta, S. *et al.* (2011) 'Mesodermal developmental gene Tbx15 impairs adipocyte differentiation and mitochondrial respiration', *Proc Natl Acad Sci U S A*. 2011/02/02, 108(7), pp. 2771–2776. doi: 10.1073/pnas.1019704108.

Giordano, A., Frontini, A. and Cinti, S. (2016) 'Convertible visceral fat as a therapeutic target to curb obesity.', *Nature reviews. Drug discovery*. England, 15(6), pp. 405–424. doi: 10.1038/nrd.2016.31.

Giudice, G. *et al.* (2016) 'ATtRACT-a database of RNA-binding proteins and associated motifs.', *Database : the journal of biological databases and curation*. England, 2016. doi: 10.1093/database/baw035.

Gjedsted, J. *et al.* (2007) 'Effects of a 3-day fast on regional lipid and glucose metabolism in human skeletal muscle and adipose tissue.', *Acta physiologica (Oxford, England)*. England, 191(3), pp. 205–216. doi: 10.1111/j.1748-1716.2007.01740.x.

Goduti, D. J. and Smith, E. F. (2012) 'Analyses of functional domains within the PF6 protein of the central apparatus reveal a role for PF6 sub-complex members in regulating flagellar beat frequency.', *Cytoskeleton (Hoboken, N.J.)*. United States, 69(3), pp. 179–194. doi: 10.1002/cm.21010.

Goodpaster, B. H. *et al.* (1999) 'Effects of weight loss on regional fat distribution and insulin sensitivity in obesity.', *Diabetes*. United States, 48(4), pp. 839–847. doi: 10.2337/diabetes.48.4.839.

Gorman Grainne S, Radelfahr, F. and Klopstock, T. (2016) 'Mitochondrial diseases', *Nature Reviews*. Macmillan Publishers Limited, 2(1), pp. 1–21. doi: 10.1007/s00115-018-0666-2.

Gotz, A. *et al.* (2011) 'Exome sequencing identifies mitochondrial alanyl-tRNA synthetase mutations in infantile mitochondrial cardiomyopathy.', *American journal of human genetics*. United States, 88(5), pp. 635–642. doi: 10.1016/j.ajhg.2011.04.006.

Grandl, G. *et al.* (2016) 'Depot specific differences in the adipogenic potential of precursors are mediated by collagenous extracellular matrix and Flotillin 2 dependent signaling.', *Molecular metabolism*. Germany, 5(10), pp. 937–947. doi: 10.1016/j.molmet.2016.07.008.

Gray, S. L. *et al.* (2006) 'Leptin Deficiency Unmasks the Deleterious Effects of Function (P465L PPAR) in Mice', *Diabetes*, 55(October), pp. 2669–2677. doi: 10.2337/db06-0389.

Grinspoon, S. and Carr, A. (2005) 'Cardiovascular risk and body-fat abnormalities in HIV-infected adults.', *The New England journal of medicine*. United States, 352(1), pp. 48–62. doi: 10.1056/NEJMra041811.

Grove, K. L. *et al.* (2010) 'A microarray analysis of sexual dimorphism of adipose tissues in high-fat-diet-induced obese mice.', *International journal of obesity (2005)*. England, 34(6), pp. 989–1000. doi: 10.1038/ijo.2010.12.

GTEx-Consortium (2013) 'The Genotype-Tissue Expression (GTEx) project', *Nat Genet*. 2013/05/30, 45(6), pp. 580–585. doi: 10.1038/ng.2653.

Guo, Z. *et al.* (1999) 'Regional postprandial fatty acid metabolism in different obesity phenotypes.', *Diabetes*. United States, 48(8), pp. 1586–1592. doi: 10.2337/diabetes.48.8.1586.

Gupta, R. K. *et al.* (2012) 'Zfp423 Expression Identifies Committed Preadipocytes and Localizes to Adipose Endothelial and Perivascular Cells', *Cell Metabolism*, 15(2), pp. 230–239. doi: https://doi.org/10.1016/j.cmet.2012.01.010.

Habicht, J.-P. (2008) 'Malnutrition kills directly, not indirectly.', *Lancet (London, England)*. England, pp. 1749–50; author reply 1750. doi: 10.1016/S0140-6736(08)60755-2.

Haimovich, G. *et al.* (2013) 'Gene expression is circular: factors for mRNA degradation also foster mRNA synthesis.', *Cell*. United States, 153(5), pp. 1000–1011. doi: 10.1016/j.cell.2013.05.012.

Hait, T. A. *et al.* (2018) 'FOCS: a novel method for analyzing enhancer and gene activity patterns infers an extensive enhancer-promoter map.', *Genome biology*. England, 19(1), p. 56. doi: 10.1186/s13059-018-1432-2.

Hanssen, M. J. W. *et al.* (2015) 'Short-term cold acclimation improves insulin sensitivity in patients with type 2 diabetes mellitus.', *Nature medicine*. United States, 21(8), pp. 863–865. doi: 10.1038/nm.3891.

Heid, I. M. *et al.* (2010) 'Meta-analysis identifies 13 new loci associated with waist-hip ratio and reveals sexual dimorphism in the genetic basis of fat distribution', *Nat Genet*. 2010/10/12, 42(11), pp. 949–960. doi: 10.1038/ng.685.

Herrera, M. F. *et al.* (2010) 'Potential additional effect of omentectomy on metabolic syndrome, acute-phase reactants, and inflammatory mediators in grade III obese patients undergoing laparoscopic Roux-en-Y gastric bypass: a randomized trial.', *Diabetes care*. United States, 33(7), pp. 1413–1418. doi: 10.2337/dc09-1833.

Hew, J. *et al.* (2016) 'The Effects of Dietary Macronutrient Balance on Skin Structure in Aging Male and Female Mice.', *PloS one*. United States, 11(11), p. e0166175. doi: 10.1371/journal.pone.0166175.

Hormozdiari, F. *et al.* (2016a) 'Colocalization of GWAS and eQTL Signals Detects Target Genes', *American Journal of Human Genetics*, 99(6), pp. 1245–1260. doi:

10.1016/j.ajhg.2016.10.003.

Hormozdiari, F. *et al.* (2016b) 'Colocalization of GWAS and eQTL Signals Detects Target Genes', *American Journal of Human Genetics*, 99(6), pp. 1245–1260. doi: 10.1016/j.ajhg.2016.10.003.

Horowitz, J. F. and Klein, S. (2000) 'Whole body and abdominal lipolytic sensitivity to epinephrine is suppressed in upper body obese women.', *American journal of physiology. Endocrinology and metabolism*. United States, 278(6), pp. E1144-52. doi: 10.1152/ajpendo.2000.278.6.E1144.

Hosseini, M. *et al.* (2013) 'Causes and Consequences of Chromatin Variation between Inbred Mice', *PLOS Genetics*. Public Library of Science, 9(6), p. e1003570. Available at: https://doi.org/10.1371/journal.pgen.1003570.

Hu, S. *et al.* (2018) 'Dietary Fat, but Not Protein or Carbohydrate, Regulates Energy Intake and Causes Adiposity in Mice.', *Cell metabolism*. United States, 28(3), pp. 415-431.e4. doi: 10.1016/j.cmet.2018.06.010.

Ibba, M. and Söll, D. (2000) 'Aminoacyl-tRNA Synthesis', *Annual Review of Biochemistry*. Annual Reviews, 69(1), pp. 617–650. doi: 10.1146/annurev.biochem.69.1.617.

Ibrahim, M. M. (2010) 'Subcutaneous and visceral adipose tissue: Structural and functional differences', *Obesity Reviews*, 11(1), pp. 11–18. doi: 10.1111/j.1467-789X.2009.00623.x.

Ikeda, K. *et al.* (2017) 'UCP1-independent signaling involving SERCA2b- mediated calcium cycling regulates beige fat thermogenesis and systemic glucose homeostasis', *Nature Publishing Group*. Nature Publishing Group, 23(12). doi: 10.1038/nm.4429.

Inoue, F. *et al.* (2017) 'A systematic comparison reveals substantial differences in chromosomal versus episomal encoding of enhancer activity', *Genome Research*, 27(1), pp. 38–52. doi: 10.1101/gr.212092.116.

Ionita-Laza, I. *et al.* (2016) 'A spectral approach integrating functional genomic annotations for coding and noncoding variants.', *Nature genetics*. United States, 48(2), pp. 214–220. doi: 10.1038/ng.3477.

Iotchkova, V. *et al.* (2019) 'GARFIELD classifies disease-relevant genomic features through integration of functional annotations with association signals', *Nature Genetics 2019*. Springer US, 51(February), p. 1. doi: 10.1038/s41588-018-0322-6.

Jacobs, G. H. *et al.* (2000) 'Transterm: a database of messenger RNA components and signals', *Nucleic acids research*. Oxford University Press, 28(1), pp. 293–295. Available at: https://www.ncbi.nlm.nih.gov/pubmed/10592251.

Jensen, M. D. *et al.* (1999) 'Regional leptin kinetics in humans.', *The American journal of clinical nutrition*. United States, 69(1), pp. 18–21. doi: 10.1093/ajcn/69.1.18.

Jensen, M. D. *et al.* (2003) 'Regional uptake of meal fatty acids in humans', *American Journal of Physiology-Endocrinology and Metabolism*, 285(6), pp. E1282–E1288. doi: 10.1152/ajpendo.00220.2003.

Johnen, H. *et al.* (2007) ‘Tumor-induced anorexia and weight loss are mediated by the TGF-beta superfamily cytokine MIC-1.’, *Nature medicine*. United States, 13(11), pp. 1333–1340. doi: 10.1038/nm1677.

de Jong, J. M. A. *et al.* (2015) ‘A stringent validation of mouse adipose tissue identity markers.’, *American journal of physiology. Endocrinology and metabolism*. United States, 308(12), pp. E1085-105. doi: 10.1152/ajpendo.00023.2015.

de Jong, J. M. A. *et al.* (2019) ‘Human brown adipose tissue is phenocopied by classical brown adipose tissue in physiologically humanized mice’, *Nature Metabolism*. doi: 10.1038/s42255-019-0101-4.

Justice, A. E. *et al.* (2019) ‘Protein-coding variants implicate novel genes related to lipid homeostasis contributing to body-fat distribution’, *Nature Genetics*, 18. doi: 10.1038/s41588-018-0334-2.

Kaess, B. M. *et al.* (2012) ‘The ratio of visceral to subcutaneous fat, a metric of body fat distribution, is a unique correlate of cardiometabolic risk.’, *Diabetologia*. Germany, 55(10), pp. 2622–2630. doi: 10.1007/s00125-012-2639-5.

Kazak, L. *et al.* (2015) ‘A creatine-driven substrate cycle enhances energy expenditure and thermogenesis in beige fat.’, *Cell*. United States, 163(3), pp. 643–655. doi: 10.1016/j.cell.2015.09.035.

Kazarian, E. *et al.* (2018) ‘SPAG17 is required for male germ cell differentiation and fertility’, *International Journal of Molecular Sciences*, 19(4). doi: 10.3390/ijms19041252.

Kent, W. J. *et al.* (2002) ‘The human genome browser at UCSC’, *Genome Res*. 2002/06/05, 12(6), pp. 996–1006. doi: 10.1101/gr.229102. Article published online before print in May 2002.

Kim, J. J. *et al.* (2010) ‘Identification of 15 loci influencing height in a Korean population’, *J Hum Genet*. 2009/11/07, 55(1), pp. 27–31. doi: 10.1038/jhg.2009.116.

Kim, S. N. *et al.* (2016) ‘Sex differences in sympathetic innervation and browning of white adipose tissue of mice’, *Biology of Sex Differences*. Biology of Sex Differences, 7(1), pp. 1–13. doi: 10.1186/s13293-016-0121-7.

King, M. C. and Wilson, A. C. (1975) ‘Evolution at two levels in humans and chimpanzees.’, *Science (New York, N.Y.)*. United States, 188(4184), pp. 107–116. doi: 10.1126/science.1090005.

Kircher, M. *et al.* (2019) ‘Saturation mutagenesis of twenty disease-associated regulatory elements at single base-pair resolution’, *Nature Communications*. Springer US, 10(1), p. 3583. doi: 10.1038/s41467-019-11526-w.

Klopfenstein, B. J. *et al.* (2012) ‘Comparison of 3 T MRI and CT for the measurement of visceral and subcutaneous adipose tissue in humans’, *The British journal of radiology*. The British Institute of Radiology., 85(1018), pp. e826–e830. doi: 10.1259/bjr/57987644.

Kloting, N. *et al.* (2010) ‘Insulin-sensitive obesity.’, *American journal of physiology. Endocrinology and metabolism*. United States, 299(3), pp. E506-15. doi: 10.1152/ajpendo.00586.2009.

Konovalova, S. and Tyynismaa, H. (2013) ‘Mitochondrial aminoacyl-tRNA synthetases in human disease’, *Molecular Genetics and Metabolism*. Elsevier Inc., 108(4), pp. 206–211. doi: 10.1016/j.ymgme.2013.01.010.

Kovacova, Z. *et al.* (2012) ‘The impact of obesity on secretion of adiponectin multimeric isoforms differs in visceral and subcutaneous adipose tissue’, *International Journal of Obesity*. Nature Publishing Group, 36(10), pp. 1360–1365. doi: 10.1038/ijo.2011.223.

Kraja, A. T. *et al.* (2019) ‘Associations of Mitochondrial and Nuclear Mitochondrial Variants and Genes with Seven Metabolic Traits’, *The American Journal of Human Genetics*, 104, pp. 1–27. doi: 10.1016/j.ajhg.2018.12.001.

Kuk, J. L. *et al.* (2009) ‘Age-related changes in total and regional fat distribution’, *Ageing Research Reviews*, 8(4), pp. 339–348. doi: https://doi.org/10.1016/j.arr.2009.06.001.

Kumar, S. *et al.* (2017) ‘TimeTree: A Resource for Timelines, Timetrees, and Divergence Times’, *Molecular biology and evolution*, 34(7), pp. 1812–1819. doi: 10.1093/molbev/msx116.

Kundaje, A. *et al.* (2015) ‘Integrative analysis of 111 reference human epigenomes’, *Nature*. 2015/02/20, 518(7539), pp. 317–330. doi: 10.1038/nature14248.

Laber, S. and Cox, R. D. (2017) ‘Mouse models of human GWAS hits for obesity and diabetes in the post genomic era: Time for reevaluation’, *Frontiers in Endocrinology*, pp. 1–5. doi: 10.3389/fendo.2017.00011.

Lambert, S. A. *et al.* (2018) ‘The Human Transcription Factors’, *Cell*. Elsevier Inc., 172(4), pp. 650–665. doi: 10.1016/j.cell.2018.01.029.

Laurencikiene, J. *et al.* (2011) ‘Regulation of lipolysis in small and large fat cells of the same subject.’, *The Journal of clinical endocrinology and metabolism*. United States, 96(12), pp. E2045-9. doi: 10.1210/jc.2011-1702.

Lausch, E. *et al.* (2008) ‘TBX15 mutations cause craniofacial dysmorphism, hypoplasia of scapula and pelvis, and short stature in Cousin syndrome.’, *American journal of human genetics*. United States, 83(5), pp. 649–655. doi: 10.1016/j.ajhg.2008.10.011.

Lee, D. *et al.* (2015a) ‘A method to predict the impact of regulatory variants from DNA sequence’, *Nat Genet*. Nature Publishing Group, a division of Macmillan Publishers Limited. All Rights Reserved., 47(8), pp. 955–961. Available at: http://dx.doi.org/10.1038/ng.3331.

Lee, D. *et al.* (2015b) ‘A method to predict the impact of regulatory variants from DNA sequence’, *Nature Genetics*. Nature Publishing Group, a division of Macmillan Publishers Limited. All Rights Reserved., 47, p. 955. Available at: https://doi.org/10.1038/ng.3331.

Lee, K. Y. *et al.* (2013) ‘Shox2 is a molecular determinant of depot-specific adipocyte function.’, *Proceedings of the National Academy of Sciences of the United States of America*. United States, 110(28), pp. 11409–11414. doi: 10.1073/pnas.1310331110.

Lee, K. Y. *et al.* (2015) ‘Tbx15 controls skeletal muscle fibre-type determination and muscle metabolism’, *Nat Commun*. 2015/08/25, 6, p. 8054. doi: 10.1038/ncomms9054.

Lee, K. Y. *et al.* (2017) ‘Tbx15 Defines a Glycolytic Subpopulation and White Adipocyte

Heterogeneity.', *Diabetes*. United States, 66(11), pp. 2822–2829. doi: 10.2337/db17-0218.

Lee, P., Swarbrick, M. M. and Ho, K. K. Y. (2013) 'Brown Adipose Tissue in Adult Humans: A Metabolic Renaissance', *Endocrine Reviews*, 34(3), pp. 413–438. doi: 10.1210/er.2012-1081.

Lee, S. Y. and Gallagher, D. (2008) 'Assessment methods in human body composition.', *Current opinion in clinical nutrition and metabolic care*. England, 11(5), pp. 566–572. doi: 10.1097/MCO.0b013e32830b5f23.

Lee, Y.-H. *et al.* (2015) 'Cellular origins of cold-induced brown adipocytes in adult mice.', *FASEB journal : official publication of the Federation of American Societies for Experimental Biology*. United States, 29(1), pp. 286–299. doi: 10.1096/fj.14-263038.

Lee, Y. *et al.* (2004) 'Hyperleptinemia prevents lipotoxic cardiomyopathy in acyl CoA synthase transgenic mice.', *Proceedings of the National Academy of Sciences of the United States of America*. United States, 101(37), pp. 13624–13629. doi: 10.1073/pnas.0405499101.

Lepper, C. and Fan, C.-M. (2010) 'Inducible lineage tracing of Pax7-descendant cells reveals embryonic origin of adult satellite cells.', *Genesis (New York, N.Y. : 2000)*. United States, 48(7), pp. 424–436. doi: 10.1002/dvg.20630.

Li, Y. *et al.* (2018) 'Secretin-Activated Brown Fat Mediates Prandial Thermogenesis to Induce Satiation.', *Cell*. United States, 175(6), pp. 1561-1574.e12. doi: 10.1016/j.cell.2018.10.016.

Liu, C. T. *et al.* (2014) 'Multi-ethnic fine-mapping of 14 central adiposity loci', *Hum Mol Genet*. 2014/04/25, 23(17), pp. 4738–4744. doi: 10.1093/hmg/ddu183.

Locke, A. E. *et al.* (2015) 'Genetic studies of body mass index yield new insights for obesity biology', *Nature*. 2015/02/13, 518(7538), pp. 197–206. doi: 10.1038/nature14177.

Lott, M. T. *et al.* (2013) 'mtDNA Variation and Analysis Using Mitomap and Mitomaster.', *Current protocols in bioinformatics*. United States, 44, pp. 1.23.1-26. doi: 10.1002/0471250953.bi0123s44.

Lovejoy, J. C. *et al.* (2008) 'Increased visceral fat and decreased energy expenditure during the menopausal transition.', *International journal of obesity (2005)*. England, 32(6), pp. 949–958. doi: 10.1038/ijo.2008.25.

Lu, Y.-P. *et al.* (2012) 'Surgical removal of the parametrial fat pads stimulates apoptosis and inhibits UVB-induced carcinogenesis in mice fed a high-fat diet.', *Proceedings of the National Academy of Sciences of the United States of America*. United States, 109(23), pp. 9065–9070. doi: 10.1073/pnas.1205810109.

Lugowski, A., Nicholson, B. and Rissland, O. S. (2018) 'Determining mRNA half-lives on a transcriptome-wide scale', *Methods*. The Authors, 137, pp. 90–98. doi: 10.1016/j.ymeth.2017.12.006.

Luppino, F. S. *et al.* (2010) 'Overweight, obesity, and depression: a systematic review and meta-analysis of longitudinal studies.', *Archives of general psychiatry*. United States, 67(3), pp. 220–229. doi: 10.1001/archgenpsychiatry.2010.2.

Macotela, Y. *et al.* (2012) 'Intrinsic differences in adipocyte precursor cells from different white fat depots', *Diabetes*, 61(7), pp. 1691–1699. doi: 10.2337/db11-1753.

Maffezzini, C. *et al.* (2019) 'Mutations in the mitochondrial tryptophanyl-tRNA synthetase cause growth retardation and progressive leukoencephalopathy.', *Molecular genetics & genomic medicine*. United States, 7(6), p. e654. doi: 10.1002/mgg3.654.

Mahajan, A. *et al.* (2018) 'Fine-mapping type 2 diabetes loci to single-variant resolution using high-density imputation and islet-specific epigenome maps', *Nature Genetics*, 50(11), pp. 1505–1513. doi: 10.1038/s41588-018-0241-6.

Van Maldergem, L. *et al.* (2002) 'Genotype-phenotype relationships in Berardinelli-Seip congenital lipodystrophy.', *Journal of medical genetics*. England, 39(10), pp. 722–733. doi: 10.1136/jmg.39.10.722.

Malicki, J. J. and Johnson, C. A. (2017) 'The Cilium: Cellular Antenna and Central Processing Unit', *Trends in Cell Biology*. Elsevier, 27(2), pp. 126–140. doi: 10.1016/j.tcb.2016.08.002.

Maller, J. B. *et al.* (2012) 'Bayesian refinement of association signals for 14 loci in 3 common diseases', *Nat Genet*. 2012/10/30, 44(12), pp. 1294–1301. doi: 10.1038/ng.2435.

Mao, J. *et al.* (2009) 'aP2-Cre-mediated inactivation of acetyl-CoA carboxylase 1 causes growth retardation and reduced lipid accumulation in adipose tissues.', *Proceedings of the National Academy of Sciences of the United States of America*. United States, 106(41), pp. 17576–17581. doi: 10.1073/pnas.0909055106.

Marzola, P. *et al.* (2016) 'Preclinical in vivo imaging for fat tissue identification, quantification, and functional characterization', *Frontiers in Pharmacology*, 7(SEP), pp. 1–14. doi: 10.3389/fphar.2016.00336.

Mason, C., Craig, C. L. and Katzmarzyk, P. T. (2008) 'Influence of central and extremity circumferences on all-cause mortality in men and women', *Obesity (Silver Spring)*. 2008/10/18, 16(12), pp. 2690–2695. doi: 10.1038/oby.2008.438.

Matesanz, F. *et al.* (2015) 'A functional variant that affects exon-skipping and protein expression of SP140 as genetic mechanism predisposing to multiple sclerosis.', *Human molecular genetics*. England, 24(19), pp. 5619–5627. doi: 10.1093/hmg/ddv256.

Matharu, N. *et al.* (2019) 'CRISPR-mediated activation of a promoter or enhancer rescues obesity caused by haploinsufficiency.', *Science (New York, N.Y.)*. United States, 363(6424). doi: 10.1126/science.aau0629.

Matoulkova, E. *et al.* (2012) 'The role of the 3′ untranslated region in post-transcriptional regulation of protein expression in mammalian cells', *RNA Biology*, 9(5), pp. 563–576. doi: 10.4161/rna.20231.

De Matteis, R. *et al.* (2013) 'Exercise as a new physiological stimulus for brown adipose tissue activity.', *Nutrition, metabolism, and cardiovascular diseases : NMCD*. Netherlands, 23(6), pp. 582–590. doi: 10.1016/j.numecd.2012.01.013.

Maurano, Matthew T *et al.* (2012) 'Systematic localization of common disease-associated variation in regulatory DNA.', *Science*, 337(September), pp. 1190–1195. doi: 10.1126/science.1222794.

Maurano, M T *et al.* (2012) 'Systematic localization of common disease-associated variation in regulatory DNA', *Science*. 2012/09/08, 337(6099), pp. 1190–1195. doi: 10.1126/science.1222794.

Maurovich-Horvat, P. *et al.* (2007) 'Comparison of anthropometric, area- and volume-based assessment of abdominal subcutaneous and visceral adipose tissue volumes using multi-detector computed tomography.', *International journal of obesity (2005)*. England, 31(3), pp. 500–506. doi: 10.1038/sj.ijo.0803454.

Mayr, C. (2016) 'Evolution and Biological Roles of Alternative 3'UTRs.', *Trends in cell biology*. England, 26(3), pp. 227–237. doi: 10.1016/j.tcb.2015.10.012.

Mayr, C. (2017) 'Regulation by 3'-Untranslated Regions', *Annual Review of Genetics, Vol 51*, 51, pp. 171–194. doi: 10.1146/annurev-genet-120116-024704.

McDuffie, J. R. *et al.* (2004) 'Effects of exogenous leptin on satiety and satiation in patients with lipodystrophy and leptin insufficiency.', *The Journal of clinical endocrinology and metabolism*. United States, 89(9), pp. 4258–4263. doi: 10.1210/jc.2003-031868.

Medina-Rivera, A. *et al.* (2018) 'Widespread Enhancer Activity from Core Promoters.', *Trends in biochemical sciences*. England, 43(6), pp. 452–468. doi: 10.1016/j.tibs.2018.03.004.

Meek, S. E., Nair, K. S. and Jensen, M. D. (1999) 'Insulin regulation of regional free fatty acid metabolism.', *Diabetes*. United States, 48(1), pp. 10–14. doi: 10.2337/diabetes.48.1.10.

Mele, M. *et al.* (2015) 'Human genomics. The human transcriptome across tissues and individuals.', *Science (New York, N.Y.)*. United States, 348(6235), pp. 660–665. doi: 10.1126/science.aaa0355.

Meyer, C. W. *et al.* (2010) 'Adaptive thermogenesis and thermal conductance in wild-type and UCP1-KO mice.', *American journal of physiology. Regulatory, integrative and comparative physiology*. United States, 299(5), pp. R1396-406. doi: 10.1152/ajpregu.00021.2009.

Miettinen, S., Sarkanen, J. R. and Ashammakhi, N. (2008) 'Adipose Tissue and Adipocyte Differentiation: Molecular and Cellular Aspects and Tissue Engineering Applications', *Topics in Tissue Engineering*, 4, pp. 1–26.

Miller, C. N. *et al.* (2015) 'Isoproterenol Increases Uncoupling, Glycolysis, and Markers of Beiging in Mature 3T3-L1 Adipocytes', *PloS one*. Public Library of Science, 10(9), pp. e0138344–e0138344. doi: 10.1371/journal.pone.0138344.

Mills, G. W. *et al.* (2004) 'Heritability estimates for beta cell function and features of the insulin resistance syndrome in UK families with an increased susceptibility to type 2 diabetes', *Diabetologia*. 2004/08/10, 47(4), pp. 732–738. doi: 10.1007/s00125-004-1338-2.

Misra, A., Peethambaram, A. and Garg, A. (2004) 'Clinical features and metabolic and autoimmune derangements in acquired partial lipodystrophy: report of 35 cases and review of the literature.', *Medicine*. United States, 83(1), pp. 18–34. doi:

10.1097/01.md.0000111061.69212.59.

Mladenov, E. and Russev, G. (2009) ‘Organization of Plasmid DNA into Nucleosome-Like Structures after Transfection in Eukaryotic Cells’, *Biotechnology & Biotechnological Equipment*. Taylor & Francis, 23(1), pp. 1044–1047. doi: 10.1080/13102818.2009.10817609.

Mongiat, M. *et al.* (2007) ‘Regulation of the Extrinsic Apoptotic Pathway by the Extracellular Matrix Glycoprotein EMILIN2’, *Molecular and Cellular Biology*, 27(20), pp. 7176–7187. doi: 10.1128/MCB.00696-07.

Mori, Y. *et al.* (1999) ‘Effect of troglitazone on body fat distribution in type 2 diabetic patients.’, *Diabetes care*. United States, 22(6), pp. 908–912. doi: 10.2337/diacare.22.6.908.

Morley, J. E., Thomas, D. R. and Wilson, M.-M. G. (2006) ‘Cachexia: pathophysiology and clinical relevance.’, *The American journal of clinical nutrition*. United States, 83(4), pp. 735–743. doi: 10.1093/ajcn/83.4.735.

Moulinier, L. *et al.* (2017) ‘MiSynPat: An integrated knowledge base linking clinical, genetic, and structural data for disease-causing mutations in human mitochondrial aminoacyl-tRNA synthetases.’, *Human mutation*. United States, 38(10), pp. 1316–1324. doi: 10.1002/humu.23277.

Mullican, S. E. *et al.* (2017) ‘GFRAL is the receptor for GDF15 and the ligand promotes weight loss in mice and nonhuman primates.’, *Nature medicine*. United States, 23(10), pp. 1150–1157. doi: 10.1038/nm.4392.

Murano, I. *et al.* (2009) ‘Noradrenergic parenchymal nerve fiber branching after cold acclimatisation correlates with brown adipocyte density in mouse adipose organ.’, *Journal of anatomy*. England, 214(1), pp. 171–178. doi: 10.1111/j.1469-7580.2008.01001.x.

Musante, L. *et al.* (2017) ‘Mutations of the aminoacyl-tRNA-synthetases SARS and WARS2 are implicated in the etiology of autosomal recessive intellectual disability.’, *Human mutation*. United States, 38(6), pp. 621–636. doi: 10.1002/humu.23205.

Must, A. *et al.* (1999) ‘The disease burden associated with overweight and obesity.’, *JAMA*. United States, 282(16), pp. 1523–1529. doi: 10.1001/jama.282.16.1523.

Muzumdar, M. D. *et al.* (2007) ‘A global double-fluorescent Cre reporter mouse.’, *Genesis (New York, N.Y. : 2000)*. United States, 45(9), pp. 593–605. doi: 10.1002/dvg.20335.

Naiche, L. A. *et al.* (2005) ‘T-box genes in vertebrate development.’, *Annual review of genetics*. United States, 39, pp. 219–239. doi: 10.1146/annurev.genet.39.073003.105925.

Nedergaard, J., Bengtsson, T. and Cannon, B. (2007) ‘Unexpected evidence for active brown adipose tissue in adult humans.’, *American journal of physiology. Endocrinology and metabolism*. United States, 293(2), pp. E444-52. doi: 10.1152/ajpendo.00691.2006.

Nelson, D. L. and Cox, M. (2005) ‘17 Fatty Acid Catabolism’, in *Lehninger Principles of Biochemistry, 4th Edition*.

Nicholls, D. G. (2006) ‘The physiological regulation of uncoupling proteins.’, *Biochimica et biophysica acta*. Netherlands, 1757(5–6), pp. 459–466. doi:

10.1016/j.bbabio.2006.02.005.

Nicolae, D. L. *et al.* (2010) 'Trait-associated SNPs are more likely to be eQTLs: annotation to enhance discovery from GWAS.', *PLoS genetics*. United States, 6(4), p. e1000888. doi: 10.1371/journal.pgen.1000888.

Nunnari, J. and Suomalainen, A. (2012) 'Mitochondria: In sickness and in health', *Cell*. Elsevier Inc., 148(6), pp. 1145–1159. doi: 10.1016/j.cell.2012.02.035.

O'Rahilly, S. (2017) 'GDF15—From Biomarker to Allostatic Hormone', *Cell Metabolism*. Elsevier Inc., pp. 807–808. doi: 10.1016/j.cmet.2017.10.017.

Oliff, A. *et al.* (1987) 'Tumors secreting human TNF/cachectin induce cachexia in mice.', *Cell*. United States, 50(4), pp. 555–563. doi: 10.1016/0092-8674(87)90028-6.

Ouellet, V. *et al.* (2011) 'Outdoor temperature, age, sex, body mass index, and diabetic status determine the prevalence, mass, and glucose-uptake activity of 18F-FDG-detected BAT in humans.', *The Journal of clinical endocrinology and metabolism*. United States, 96(1), pp. 192–199. doi: 10.1210/jc.2010-0989.

Pan, D. Z. *et al.* (2018) 'Integration of human adipocyte chromosomal interactions with adipose gene expression prioritizes obesity-related genes from GWAS', *Nature Communications*. Springer US, 9(1). doi: 10.1038/s41467-018-03554-9.

Park, B.-H., Qiang, L. and Farmer, S. R. (2004) 'Phosphorylation of C/EBPbeta at a consensus extracellular signal-regulated kinase/glycogen synthase kinase 3 site is required for the induction of adiponectin gene expression during the differentiation of mouse fibroblasts into adipocytes.', *Molecular and cellular biology*. United States, 24(19), pp. 8671–8680. doi: 10.1128/MCB.24.19.8671-8680.2004.

Park, J. *et al.* (2017) 'VEGF-A - Expressing adipose tissue shows rapid beiging and enhanced survival after transplantation and confers IL-4-independent metabolic improvements', *Diabetes*, 66(6), pp. 1479–1490. doi: 10.2337/db16-1081.

Park, K.-G. *et al.* (2004) 'Relationship between serum adiponectin and leptin concentrations and body fat distribution.', *Diabetes research and clinical practice*. Ireland, 63(2), pp. 135–142.

Pasquali, L. *et al.* (2014) 'Pancreatic islet enhancer clusters enriched in type 2 diabetes risk-associated variants', 46(2). doi: 10.1038/ng.2870.

Patel, S. *et al.* (2019) 'GDF15 Provides an Endocrine Signal of Nutritional Stress in Mice and Humans', *Cell Metabolism*, 29(3), pp. 707-718.e8. doi: https://doi.org/10.1016/j.cmet.2018.12.016.

Patni, N. and Garg, A. (2015) 'Congenital generalized lipodystrophies--new insights into metabolic dysfunction.', *Nature reviews. Endocrinology*. England, 11(9), pp. 522–534. doi: 10.1038/nrendo.2015.123.

Paulitti, A. *et al.* (2018) 'The ablation of the matricellular protein EMILIN2 causes defective vascularization due to impaired EGFR-dependent IL-8 production affecting tumor growth', *Oncogene*. Springer US, 37(25), pp. 3399–3414. doi: 10.1038/s41388-017-0107-x.

Peters, J. M. *et al.* (1998) ‘Localization of the gene for familial partial lipodystrophy (Dunnigan variety) to chromosome 1q21-22.’, *Nature genetics*. United States, 18(3), pp. 292–295. doi: 10.1038/ng0398-292.

Peters, S. A. E., Bots, S. H. and Woodward, M. (2018) ‘Sex Differences in the Association Between Measures of General and Central Adiposity and the Risk of Myocardial Infarction: Results From the UK Biobank.’, *Journal of the American Heart Association*. England, 7(5). doi: 10.1161/JAHA.117.008507.

Petruzzelli, M. *et al.* (2014) ‘A switch from white to brown fat increases energy expenditure in cancer-associated cachexia.’, *Cell metabolism*. United States, 20(3), pp. 433–447. doi: 10.1016/j.cmet.2014.06.011.

Potter, P. K. *et al.* (2016) ‘Novel gene function revealed by mouse mutagenesis screens for models of age-related disease’, *Nature Communications*. The Author(s), 7, p. 12444. Available at: https://doi.org/10.1038/ncomms12444.

Pouliot, M. C. *et al.* (1991) ‘Regional variation in adipose tissue lipoprotein lipase activity: association with plasma high density lipoprotein levels.’, *European journal of clinical investigation*. England, 21(4), pp. 398–405.

Pravenec, M. *et al.* (2017) ‘Mutant Wars2 gene in spontaneously hypertensive rats impairs brown adipose tissue function and predisposes to visceral obesity.’, *Physiological research*. Czech Republic, 66(6), pp. 917–924.

Pulit, S. L. *et al.* (2018) ‘Meta-analysis of genome-wide association studies for body fat distribution in 694,649 individuals of European ancestry.’, *Human molecular genetics*. England. doi: 10.1093/hmg/ddy327.

Pulit, S. L., Karaderi, T. and Lindgren, C. M. (2017) ‘Sexual dimorphisms in genetic loci linked to body fat distribution’, *Bioscience Reports*, 37(1), p. BSR20160184. doi: 10.1042/BSR20160184.

Raajendiran, A. *et al.* (2019) ‘Identification of Metabolically Distinct Adipocyte Progenitor Cells in Human Adipose Tissues’, *Cell Reports*. Elsevier, 27(5), pp. 1528-1540.e7. doi: 10.1016/j.celrep.2019.04.010.

Rabani, M. *et al.* (2017) ‘A Massively Parallel Reporter Assay of 3’ UTR Sequences Identifies In Vivo Rules for mRNA Degradation.’, *Molecular cell*. United States, 68(6), pp. 1083-1094.e5. doi: 10.1016/j.molcel.2017.11.014.

Racimo, F. *et al.* (2017) ‘Archaic adaptive introgression in TBX15/WARS2’, *Molecular Biology and Evolution*, 34(3), pp. 509–524. doi: 10.1093/molbev/msw283.

Rakotoarivelo, V. *et al.* (2018) ‘Inflammatory Cytokine Profiles in Visceral and Subcutaneous Adipose Tissues of Obese Patients Undergoing Bariatric Surgery Reveal Lack of Correlation With Obesity or Diabetes’, *EBioMedicine*, 30, pp. 237–247. doi: https://doi.org/10.1016/j.ebiom.2018.03.004.

Ramirez, M. E. *et al.* (1997) ‘Evidence for sex steroid inhibition of lipoprotein lipase in men: comparison of abdominal and femoral adipose tissue.’, *Metabolism: clinical and experimental*. United States, 46(2), pp. 179–185.

Rao, S. S. P. *et al.* (2014) ‘A 3D map of the human genome at kilobase resolution reveals

principles of chromatin looping.', *Cell*. United States, 159(7), pp. 1665–1680. doi: 10.1016/j.cell.2014.11.021.

Rasmussen, M. S. *et al.* (2006) 'Adiponectin receptors in human adipose tissue: effects of obesity, weight loss, and fat depots.', *Obesity (Silver Spring, Md.)*. United States, 14(1), pp. 28–35. doi: 10.1038/oby.2006.5.

Reaven, G. M. (1993) 'Role of insulin resistance in human disease (syndrome X): an expanded definition.', *Annual review of medicine*. United States, 44, pp. 121–131. doi: 10.1146/annurev.me.44.020193.001005.

Reuter, J. S. and Mathews, D. H. (2010) 'RNAstructure: software for RNA secondary structure prediction and analysis.', *BMC bioinformatics*. England, 11, p. 129. doi: 10.1186/1471-2105-11-129.

Riley, L. G. *et al.* (2010) 'Mutation of the mitochondrial tyrosyl-tRNA synthetase gene, YARS2, causes myopathy, lactic acidosis, and sideroblastic anemia--MLASA syndrome.', *American journal of human genetics*. United States, 87(1), pp. 52–59. doi: 10.1016/j.ajhg.2010.06.001.

Ritter, A. *et al.* (2018) 'Primary Cilia Are Dysfunctional in Obese Adipose-Derived Mesenchymal Stem Cells.', *Stem cell reports*. United States, 10(2), pp. 583–599. doi: 10.1016/j.stemcr.2017.12.022.

Roca-Rivada, A. *et al.* (2015) 'CILAIR-Based Secretome Analysis of Obese Visceral and Subcutaneous Adipose Tissues Reveals Distinctive ECM Remodeling and Inflammation Mediators.', *Scientific reports*. England, 5, p. 12214. doi: 10.1038/srep12214.

Rocha, N. *et al.* (2017) 'Human biallelic MFN2 mutations induce mitochondrial dysfunction, upper body adipose hyperplasia, and suppression of leptin expression.', *eLife*. England, 6. doi: 10.7554/eLife.23813.

Rohm, M. *et al.* (2016) 'An AMP-activated protein kinase-stabilizing peptide ameliorates adipose tissue wasting in cancer cachexia in mice.', *Nature medicine*. United States, 22(10), pp. 1120–1130. doi: 10.1038/nm.4171.

Romere, C. *et al.* (2016) 'Asprosin, a Fasting-Induced Glucogenic Protein Hormone', *Cell*. Elsevier, 165(3), pp. 566–579. doi: 10.1016/j.cell.2016.02.063.

Romero-Corral, A. *et al.* (2008) 'Accuracy of body mass index in diagnosing obesity in the adult general population.', *International journal of obesity (2005)*. England, 32(6), pp. 959–966. doi: 10.1038/ijo.2008.11.

Rose, K. M. *et al.* (1998) 'Genetic and behavioral determinants of waist-hip ratio and waist circumference in women twins', *Obes Res*. 1998/12/09, 6(6), pp. 383–392.

Rosen, E. D. and MacDougald, O. A. (2006) 'Adipocyte differentiation from the inside out', *Nature Reviews Molecular Cell Biology*, 7(12), pp. 885–896. doi: 10.1038/nrm2066.

Rosenquist, K. J. *et al.* (2013) 'Visceral and subcutaneous fat quality and cardiometabolic risk.', *JACC. Cardiovascular imaging*. United States, 6(7), pp. 762–771. doi: 10.1016/j.jcmg.2012.11.021.

Rosenquist, K. J. *et al.* (2015) 'Fat quality and incident cardiovascular disease, all-cause

mortality, and cancer mortality.', *The Journal of clinical endocrinology and metabolism*. United States, 100(1), pp. 227–234. doi: 10.1210/jc.2013-4296.

Rothwell, N. J. and Stock, M. J. (1983) 'Luxuskonsumption, diet-induced thermogenesis and brown fat: the case in favour.', *Clinical science (London, England : 1979)*. England, 64(1), pp. 19–23.

Rothwell, N. J. and Stock, M. J. (1997) 'A role for brown adipose tissue in diet-induced thermogenesis.', *Obesity research*. United States, 5(6), pp. 650–656.

Rowland, L. A. *et al.* (2015) 'Uncoupling Protein 1 and Sarcolipin Are Required to Maintain Optimal Thermogenesis, and Loss of Both Systems Compromises Survival of Mice under Cold Stress', *The Journal of biological chemistry*. 2015/03/30. American Society for Biochemistry and Molecular Biology, 290(19), pp. 12282–12289. doi: 10.1074/jbc.M115.637603.

Russell, T. A. *et al.* (2018) 'A Schizophrenia-Linked KALRN Coding Variant Alters Neuron Morphology, Protein Function, and Transcript Stability.', *Biological psychiatry*. United States, 83(6), pp. 499–508. doi: 10.1016/j.biopsych.2017.10.024.

Ryden, A. and Torgerson, J. S. (2006) 'The Swedish Obese Subjects Study--what has been accomplished to date?', *Surgery for obesity and related diseases : official journal of the American Society for Bariatric Surgery*. United States, 2(5), pp. 549–560. doi: 10.1016/j.soard.2006.07.006.

Saito, M. *et al.* (2009) 'High incidence of metabolically active brown adipose tissue in healthy adult humans: effects of cold exposure and adiposity.', *Diabetes*. United States, 58(7), pp. 1526–1531. doi: 10.2337/db09-0530.

Samms, R. J. *et al.* (2015) 'Discrete Aspects of FGF21 In Vivo Pharmacology Do Not Require UCP1', *Cell Reports*. The Authors, 11(7), pp. 991–999. doi: 10.1016/j.celrep.2015.04.046.

Sanchez-Gurmaches, J. and Guertin, D. A. (2014) 'Adipocytes arise from multiple lineages that are heterogeneously and dynamically distributed.', *Nature communications*. England, 5, p. 4099. doi: 10.1038/ncomms5099.

Sanchez-Gurmaches, J., Hsiao, W.-Y. and Guertin, D. A. (2015) 'Highly selective in vivo labeling of subcutaneous white adipocyte precursors with Prx1-Cre.', *Stem cell reports*. United States, 4(4), pp. 541–550. doi: 10.1016/j.stemcr.2015.02.008.

Sanchez-Gurmaches, J., Hung, C. M. and Guertin, D. A. (2016) 'Emerging Complexities in Adipocyte Origins and Identity', *Trends Cell Biol*. 2016/02/15. doi: 10.1016/j.tcb.2016.01.004.

Sasarman, F. *et al.* (2012) 'A novel mutation in YARS2 causes myopathy with lactic acidosis and sideroblastic anemia.', *Human mutation*. United States, 33(8), pp. 1201–1206. doi: 10.1002/humu.22098.

Sasser, T. A. *et al.* (2012) 'Segmentation and measurement of fat volumes in murine obesity models using X-ray computed tomography', *Journal of visualized experiments : JoVE*. MyJove Corporation, (62), pp. e3680–e3680. doi: 10.3791/3680.

Savage, D. B. *et al.* (2003) 'Human metabolic syndrome resulting from dominant-negative

mutations in the nuclear receptor peroxisome proliferator-activated receptor-gamma.', *Diabetes*. United States, 52(4), pp. 910–917. doi: 10.2337/diabetes.52.4.910.

Schaid, D. J., Chen, W. and Larson, N. B. (2018) 'From genome-wide associations to candidate causal variants by statistical fine-mapping', *Nature Reviews Genetics*. Springer US, 19(8), pp. 491–504. doi: 10.1038/s41576-018-0016-z.

Schaub, M. A. *et al.* (2012) 'Linking disease associations with regulatory information in the human genome', *Genome Res.* 2012/09/08, 22(9), pp. 1748–1759. doi: 10.1101/gr.136127.111.

Scheper, G. C. *et al.* (2007) 'Mitochondrial aspartyl-tRNA synthetase deficiency causes leukoencephalopathy with brain stem and spinal cord involvement and lactate elevation.', *Nature genetics*. United States, 39(4), pp. 534–539. doi: 10.1038/ng2013.

Schleinitz, D. *et al.* (2014) 'Fat depot-specific mRNA expression of novel loci associated with waist-hip ratio', *Int J Obes (Lond)*. 2013/05/15, 38(1), pp. 120–125. doi: 10.1038/ijo.2013.56.

Schlitt, J. M. and Schulz, L. C. (2012) 'The source of leptin, but not leptin depletion in response to food restriction, changes during early pregnancy in mice', *Endocrine*. 2011/11/01, 41(2), pp. 227–235. doi: 10.1007/s12020-011-9548-0.

Schmidt, H. H. *et al.* (2001) 'Dyslipemia in familial partial lipodystrophy caused by an R482W mutation in the LMNA gene.', *The Journal of clinical endocrinology and metabolism*. United States, 86(5), pp. 2289–2295. doi: 10.1210/jcem.86.5.7500.

Schmidt, O., Pfanner, N. and Meisinger, C. (2010) 'Mitochondrial protein import: from proteomics to functional mechanisms.', *Nature reviews. Molecular cell biology*. England, 11(9), pp. 655–667. doi: 10.1038/nrm2959.

Schwessinger, R. *et al.* (2017) 'Sasquatch: Predicting the impact of regulatory SNPs on transcription factor binding from cell- and tissue-specific DNase footprints', *Genome Research*, 27(10), pp. 1730–1742. doi: 10.1101/gr.220202.117.

Seale, P. *et al.* (2008) 'PRDM16 controls a brown fat/skeletal muscle switch', *Nature*, 454(7207), pp. 961–967. doi: 10.1038/nature07182.

Seale, P. *et al.* (2011) 'Prdm16 determines the thermogenic program of subcutaneous white adipose tissue in mice', *The Journal of clinical investigation*. 2010/12/01. American Society for Clinical Investigation, 121(1), pp. 96–105. doi: 10.1172/JCI44271.

Sebo, Z. L. *et al.* (2018) 'A mesodermal fate map for adipose tissue', *Development (Cambridge)*, 145(17), pp. 1–11. doi: 10.1242/dev.166801.

Sebo, Z. L. and Rodeheffer, M. S. (2019) 'Assembling the adipose organ: Adipocyte lineage segregation and adipogenesis in vivo', *Development (Cambridge)*, 146(7). doi: 10.1242/dev.172098.

Sekiya, I. *et al.* (2000) 'SOX9 enhances aggrecan gene promoter/enhancer activity and is up-regulated by retinoic acid in a cartilage-derived cell line, TC6.', *The Journal of biological chemistry*. United States, 275(15), pp. 10738–10744.

Sharova, L. V *et al.* (2009) 'Database of mRNA Half-Life of 19977 Genes Obtained by

DNA Microarray Analysis of Pluripotent and Differentiating Mouse Embryonic Stem Cells Supplementary data', *DNA research*, 16(1), p. S1. doi: 10.1093/dnares/dsn030.

Sheeba, C. J. and Logan, M. P. O. (2017) 'The Roles of T-Box Genes in Vertebrate Limb Development.', *Current topics in developmental biology*. United States, 122, pp. 355–381. doi: 10.1016/bs.ctdb.2016.08.009.

Shungin, D. *et al.* (2015) 'New genetic loci link adipose and insulin biology to body fat distribution', *Nature*. 2015/02/13, 518(7538), pp. 187–196. doi: 10.1038/nature14132.

Sidebottom, A. C., Brown, J. E. and Jacobs, D. R. J. (2001) 'Pregnancy-related changes in body fat.', *European journal of obstetrics, gynecology, and reproductive biology*. Ireland, 94(2), pp. 216–223.

Sidossis, L. S. *et al.* (2015) 'Browning of Subcutaneous White Adipose Tissue in Humans after Severe Adrenergic Stress.', *Cell metabolism*. United States, 22(2), pp. 219–227. doi: 10.1016/j.cmet.2015.06.022.

Siersbaek, R. *et al.* (2011) 'Extensive chromatin remodelling and establishment of transcription factor "hotspots" during early adipogenesis', *Embo j*. 2011/03/24, 30(8), pp. 1459–1472. doi: 10.1038/emboj.2011.65.

Siersbaek, R. *et al.* (2014) 'Molecular architecture of transcription factor hotspots in early adipogenesis', *Cell Rep*. 2014/05/27, 7(5), pp. 1434–1442. doi: 10.1016/j.celrep.2014.04.043.

Siersbæk, R. *et al.* (2017) 'Dynamic Rewiring of Promoter-Anchored Chromatin Loops during Adipocyte Differentiation', *Molecular Cell*. Elsevier Inc., 66(3), pp. 420-435.e5. doi: 10.1016/j.molcel.2017.04.010.

Silina, K. *et al.* (2011) 'Sperm-associated antigens as targets for cancer immunotherapy: expression pattern and humoral immune response in cancer patients.', *Journal of immunotherapy (Hagerstown, Md. : 1997)*. United States, 34(1), pp. 28–44. doi: 10.1097/CJI.0b013e3181fb64fa.

Singh, M. K. *et al.* (2005) 'The T-box transcription factor Tbx15 is required for skeletal development', *Mech Dev*. 2005/01/18, 122(2), pp. 131–144. doi: 10.1016/j.mod.2004.10.011.

Sissler, M., Gonzalez-Serrano, L. E. and Westhof, E. (2017) 'Recent Advances in Mitochondarial Aminoacyl-tRNA Synthetases and Disease.', *Trends in molecular medicine*. England, 23(8), pp. 693–708. doi: 10.1016/j.molmed.2017.06.002.

Sluse, F. E. *et al.* (2006) 'Mitochondrial UCPs: new insights into regulation and impact.', *Biochimica et biophysica acta*. Netherlands, 1757(5–6), pp. 480–485. doi: 10.1016/j.bbabio.2006.02.004.

Smith, C. L. *et al.* (2018) 'Mouse Genome Database (MGD)-2018: knowledgebase for the laboratory mouse.', *Nucleic acids research*. England, 46(D1), pp. D836–D842. doi: 10.1093/nar/gkx1006.

Snijder, M. B. *et al.* (2003) 'Associations of hip and thigh circumferences independent of waist circumference with the incidence of type 2 diabetes: the Hoorn Study', *Am J Clin Nutr*. 2003/04/30, 77(5), pp. 1192–1197.

Snijder, M. B. *et al.* (2004) 'Trunk fat and leg fat have independent and opposite associations with fasting and postload glucose levels: the Hoorn study', *Diabetes Care*. 2004/01/30, 27(2), pp. 372–377.

Solheim, T. S. *et al.* (2014) 'Weight loss, appetite loss and food intake in cancer patients with cancer cachexia: three peas in a pod? - analysis from a multicenter cross sectional study.', *Acta oncologica (Stockholm, Sweden)*. England, 53(4), pp. 539–546. doi: 10.3109/0284186X.2013.823239.

Spalding, K. L. *et al.* (2008) 'Dynamics of fat cell turnover in humans', *Nature*, 453(7196), pp. 783–787. doi: 10.1038/nature06902.

Stergachis, A. B. *et al.* (2014) 'Conservation of trans-acting circuitry during mammalian regulatory evolution', *Nature*. Nature Publishing Group, 515(7527), pp. 365–370. doi: 10.1038/nature13972.

Student, A. K., Hsu, R. Y. and Lane, M. D. (1980) 'Induction of fatty acid synthetase synthesis in differentiating 3T3-L1 preadipocytes.', *The Journal of biological chemistry*. United States, 255(10), pp. 4745–4750.

Sudlow, C. *et al.* (2015) 'UK biobank: an open access resource for identifying the causes of a wide range of complex diseases of middle and old age.', *PLoS medicine*. United States, 12(3), p. e1001779. doi: 10.1371/journal.pmed.1001779.

Sullivan, J. E. *et al.* (1994) 'Inhibition of lipolysis and lipogenesis in isolated rat adipocytes with AICAR, a cell-permeable activator of AMP-activated protein kinase.', *FEBS letters*. England, 353(1), pp. 33–36. doi: 10.1016/0014-5793(94)01006-4.

Sun, K., Kusminski, C. M. and Scherer, P. E. (2011) 'Adipose tissue remodeling and obesity.', *The Journal of clinical investigation*. United States, 121(6), pp. 2094–2101. doi: 10.1172/JCI45887.

Sun, M. *et al.* (2013) 'Global analysis of eukaryotic mRNA degradation reveals Xrn1-dependent buffering of transcript levels.', *Molecular cell*. United States, 52(1), pp. 52–62. doi: 10.1016/j.molcel.2013.09.010.

Sun, W. *et al.* (2019) 'Tbx15 is required for adipocyte browning induced by adrenergic signaling pathway', *Molecular Metabolism*. Elsevier GmbH, (xxxx). doi: 10.1016/j.molmet.2019.07.004.

Swinburn, B. A. *et al.* (2019) 'The Global Syndemic of Obesity, Undernutrition, and Climate Change: The Lancet Commission report', *The Lancet*, 393(10173), pp. 791–846. doi: https://doi.org/10.1016/S0140-6736(18)32822-8.

Tam, C. S. *et al.* (2011) 'An early inflammatory gene profile in visceral adipose tissue in children', *Int J Pediatr Obes*. 2011/05/26, 6(2–2), pp. e360-3. doi: 10.3109/17477166.2011.575152.

Tan, G. D. *et al.* (2004) 'Upper and lower body adipose tissue function: a direct comparison of fat mobilization in humans.', *Obesity research*. United States, 12(1), pp. 114–118. doi: 10.1038/oby.2004.15.

Tang, H. N. *et al.* (2017) 'Plasticity of adipose tissue in response to fasting and refeeding in male mice', *Nutrition and Metabolism*. Nutrition & Metabolism, 14(1), pp. 1–14. doi:

10.1186/s12986-016-0159-x.

Tang, Q.-Q. *et al.* (2005) 'Sequential phosphorylation of CCAAT enhancer-binding protein beta by MAPK and glycogen synthase kinase 3beta is required for adipogenesis.', *Proceedings of the National Academy of Sciences of the United States of America*. United States, 102(28), pp. 9766–9771. doi: 10.1073/pnas.0503891102.

Tang, Q.-Q., Otto, T. C. and Lane, M. D. (2003) 'CCAAT/enhancer-binding protein beta is required for mitotic clonal expansion during adipogenesis.', *Proceedings of the National Academy of Sciences of the United States of America*. United States, 100(3), pp. 850–855. doi: 10.1073/pnas.0337434100.

Tang, W. *et al.* (2008) 'White fat progenitor cells reside in the adipose vasculature.', *Science (New York, N.Y.)*. United States, 322(5901), pp. 583–586. doi: 10.1126/science.1156232.

Tchkonia, T. *et al.* (2002) 'Fat depot origin affects adipogenesis in primary cultured and cloned human preadipocytes.', *American journal of physiology. Regulatory, integrative and comparative physiology*. United States, 282(5), pp. R1286-96. doi: 10.1152/ajpregu.00653.2001.

Tchkonia, T. *et al.* (2005) 'Abundance of two human preadipocyte subtypes with distinct capacities for replication, adipogenesis, and apoptosis varies among fat depots.', *American journal of physiology. Endocrinology and metabolism*. United States, 288(1), pp. E267-77. doi: 10.1152/ajpendo.00265.2004.

Tchkonia, T. *et al.* (2006) 'Fat depot-specific characteristics are retained in strains derived from single human preadipocytes.', *Diabetes*. United States, 55(9), pp. 2571–2578. doi: 10.2337/db06-0540.

Tchkonia, T. *et al.* (2007) 'Identification of depot-specific human fat cell progenitors through distinct expression profiles and developmental gene patterns', *American Journal of Physiology-Endocrinology and Metabolism*, 292(1), pp. E298–E307. doi: 10.1152/ajpendo.00202.2006.

Tchkonia, T. *et al.* (2013) 'Mechanisms and metabolic implications of regional differences among fat depots', *Cell Metabolism*. Elsevier Inc., 17(5), pp. 644–656. doi: 10.1016/j.cmet.2013.03.008.

Tchoukalova, Y. D. *et al.* (2010) 'Regional differences in cellular mechanisms of adipose tissue gain with overfeeding', *Proceedings of the National Academy of Sciences*, 107(42), pp. 18226 LP – 18231. doi: 10.1073/pnas.1005259107.

Tenesa, A. and Haley, C. S. (2013) 'The heritability of human disease: estimation, uses and abuses', *Nature Reviews Genetics*. Nature Publishing Group, a division of Macmillan Publishers Limited. All Rights Reserved., 14, p. 139. Available at: https://doi.org/10.1038/nrg3377.

Teves, M. E. *et al.* (2013) 'Sperm-associated antigen-17 gene is essential for motile cilia function and neonatal survival.', *American journal of respiratory cell and molecular biology*. United States, 48(6), pp. 765–772. doi: 10.1165/rcmb.2012-0362OC.

Teves, M. E. *et al.* (2015) 'Spag17 deficiency results in skeletal malformations and bone

abnormalities', *PLoS One*. 2015/05/29, 10(5), p. e0125936. doi: 10.1371/journal.pone.0125936.

Theisen, B. E. *et al.* (2017) 'Deficiency of WARS2, encoding mitochondrial tryptophanyl tRNA synthetase, causes severe infantile onset leukoencephalopathy.', *American journal of medical genetics. Part A*. United States, 173(9), pp. 2505–2510. doi: 10.1002/ajmg.a.38339.

ThermoFisher (2009) 'Anneal complementary pairs of oligonucleotides'. Available at: http://tools.thermofisher.com/content/sfs/brochures/TR0045-Anneal-oligos.pdf.

Timmons, J. A. *et al.* (2007) 'Myogenic gene expression signature establishes that brown and white adipocytes originate from distinct cell lineages.', *Proceedings of the National Academy of Sciences of the United States of America*. United States, 104(11), pp. 4401–4406. doi: 10.1073/pnas.0610615104.

Tran, T. T. *et al.* (2008) 'Beneficial Effects of Subcutaneous Fat Transplantation on Metabolism', *Cell Metabolism*, 7(5), pp. 410–420. doi: 10.1016/j.cmet.2008.04.004.

Trayhurn, P. *et al.* (1995) 'Effects of fasting and refeeding on ob gene expression in white adipose tissue of lean and obese (ob/ob) mice', *FEBS Letters*, 368(3), pp. 488–490. doi: https://doi.org/10.1016/0014-5793(95)00719-P.

Unger, R. H. and Scherer, P. E. (2010) 'Gluttony, sloth and the metabolic syndrome: a roadmap to lipotoxicity.', *Trends in endocrinology and metabolism: TEM*. United States, 21(6), pp. 345–352. doi: 10.1016/j.tem.2010.01.009.

Vague, J. (1956) 'The degree of masculine differentiation of obesities: a factor determining predisposition to diabetes, atherosclerosis, gout, and uric calculous disease.', *The American journal of clinical nutrition*. United States, 4(1), pp. 20–34. doi: 10.1093/ajcn/4.1.20.

Valet, P. *et al.* (2000) 'Expression of human alpha 2-adrenergic receptors in adipose tissue of beta 3-adrenergic receptor-deficient mice promotes diet-induced obesity.', *The Journal of biological chemistry*. United States, 275(44), pp. 34797–34802. doi: 10.1074/jbc.M005210200.

Vantroys, E. *et al.* (2018) 'Severe hepatopathy and neurological deterioration after start of valproate treatment in a 6-year-old child with mitochondrial tryptophanyl-tRNA synthetase deficiency.', *Orphanet journal of rare diseases*. England, 13(1), p. 80. doi: 10.1186/s13023-018-0822-6.

Vegiopoulos, A., Rohm, M. and Herzig, S. (2017) 'Adipose tissue: between the extremes', *The EMBO Journal*, 36(14), pp. 1999–2017. doi: 10.15252/embj.201696206.

Véniant, M. M. *et al.* (2015) 'Pharmacologic Effects of FGF21 Are Independent of the "Browning" of White Adipose Tissue', *Cell Metabolism*, 21(5), pp. 731–738. doi: 10.1016/j.cmet.2015.04.019.

Vijgen, G. H. E. J. *et al.* (2011) 'Brown adipose tissue in morbidly obese subjects.', *PloS one*. United States, 6(2), p. e17247. doi: 10.1371/journal.pone.0017247.

Virdee, M. *et al.* (2019) 'Expanding the Phenotype: Neurodevelopmental Disorder, Mitochondrial, With Abnormal Movements and Lactic Acidosis, With or Without Seizures

(NEMMLAS) due to WARS2 Biallelic Variants, Encoding Mitochondrial Tryptophanyl-tRNA Synthase.', *Journal of child neurology*. United States, p. 883073819854604. doi: 10.1177/0883073819854604.

Virtanen, K. A. *et al.* (2009) 'Functional brown adipose tissue in healthy adults.', *The New England journal of medicine*. United States, 360(15), pp. 1518–1525. doi: 10.1056/NEJMoa0808949.

Virtue, S. and Vidal-Puig, A. (2010) 'Adipose tissue expandability, lipotoxicity and the Metabolic Syndrome--an allostatic perspective.', *Biochimica et biophysica acta*. Netherlands, 1801(3), pp. 338–349. doi: 10.1016/j.bbalip.2009.12.006.

Viscomi, C. *et al.* (2011) 'In vivo correction of COX deficiency by activation of the AMPK/PGC-1alpha axis.', *Cell metabolism*. United States, 14(1), pp. 80–90. doi: 10.1016/j.cmet.2011.04.011.

Vitali, A. *et al.* (2012) 'The adipose organ of obesity-prone C57BL/6J mice is composed of mixed white and brown adipocytes.', *Journal of lipid research*. United States, 53(4), pp. 619–629. doi: 10.1194/jlr.M018846.

van Vliet-Ostaptchouk, J. V *et al.* (2014) 'The prevalence of metabolic syndrome and metabolically healthy obesity in Europe: a collaborative analysis of ten large cohort studies.', *BMC endocrine disorders*. England, 14, p. 9. doi: 10.1186/1472-6823-14-9.

Wahrenberg, H., Lonnqvist, F. and Arner, P. (1989) 'Mechanisms underlying regional differences in lipolysis in human adipose tissue.', *The Journal of clinical investigation*. United States, 84(2), pp. 458–467. doi: 10.1172/JCI114187.

Wang, M. *et al.* (2016) 'Wars2 is a determinant of angiogenesis', *Nat Commun*. 2016/07/09, 7, p. 12061. doi: 10.1038/ncomms12061.

Wang, X. *et al.* (2018) 'High-resolution genome-wide functional dissection of transcriptional regulatory regions and nucleotides in human.', *Nature communications*. England, 9(1), p. 5380. doi: 10.1038/s41467-018-07746-1.

Wang, Y. *et al.* (2005) 'Comparison of abdominal adiposity and overall obesity in predicting risk of type 2 diabetes among men', *Am J Clin Nutr*. 2005/03/10, 81(3), pp. 555–563.

Wang, Y. *et al.* (2018) 'The 3D Genome Browser: a web-based browser for visualizing 3D genome organization and long-range chromatin interactions', *Genome Biology*, 19(1), p. 151. doi: 10.1186/s13059-018-1519-9.

Ward, L. D. and Kellis, M. (2012) 'Interpreting noncoding genetic variation in complex traits and human disease', *Nature Biotechnology*. Nature Publishing Group, 30(11), pp. 1095–1106. doi: 10.1038/nbt.2422.

WHO (2011) *Waist circumference and waist–hip ratio Report of a WHO expert consultation, Geneva, 8-11 December 2008*. Geneva.

Wiest, R. *et al.* (2010) 'Splanchnic concentrations and postprandial release of visceral adipokines', *Metabolism*, 59(5), pp. 664–670. doi: https://doi.org/10.1016/j.metabol.2009.09.011.

Wilson-Fritch, L. *et al.* (2003) 'Mitochondrial biogenesis and remodeling during adipogenesis and in response to the insulin sensitizer rosiglitazone', *Mol Cell Biol*. 2003/01/17, 23(3), pp. 1085–1094.

Wilson, M. D. *et al.* (2008) 'Species-specific transcription in mice carrying human chromosome 21', *Science*. 2008/09/13, 322(5900), pp. 434–438. doi: 10.1126/science.1160930.

Wiper-Bergeron, N. *et al.* (2003) 'Stimulation of preadipocyte differentiation by steroid through targeting of an HDAC1 complex.', *The EMBO journal*. England, 22(9), pp. 2135–2145. doi: 10.1093/emboj/cdg218.

Xavier Pi-Sunyer, M. (2009) 'The Medical Risks of Obesity', *Postgraduate medicine*, 121(6), pp. 21–33. doi: 10.3810/pgm.2009.11.2074.The.

Xu, X. *et al.* (2018) 'A familial study of twins with severe asthenozoospermia identified a homozygous SPAG17 mutation by whole-exome sequencing.', *Clinical genetics*. Denmark, 93(2), pp. 345–349. doi: 10.1111/cge.13059.

Xue, R. *et al.* (2015) 'Clonal analyses and gene profiling identify genetic biomarkers of the thermogenic potential of human brown and white preadipocytes', *Nat Med*. 2015/06/16, 21(7), pp. 760–768. doi: 10.1038/nm.3881.

Yaeram, J., Setchell, B. P. and Maddocks, S. (2006) 'Effect of heat stress on the fertility of male mice in vivo and in vitro.', *Reproduction, fertility, and development*. Australia, 18(6), pp. 647–653.

Yatsuga, S. *et al.* (2015) 'Growth differentiation factor 15 as a useful biomarker for mitochondrial disorders.', *Annals of neurology*. United States, 78(5), pp. 814–823. doi: 10.1002/ana.24506.

Yengo, L. *et al.* (2018) 'Meta-analysis of genome-wide association studies for height and body mass index in ~700 000 individuals of European ancestry', *Human Molecular Genetics*, 27(20), pp. 3641–3649. doi: 10.1093/hmg/ddy271.

Yoneshiro, T. *et al.* (2011) 'Age-related decrease in cold-activated brown adipose tissue and accumulation of body fat in healthy humans', *Obesity*. Nature Publishing Group, 19(9), pp. 1755–1760. doi: 10.1038/oby.2011.125.

Yusuf, S. *et al.* (2005) 'Obesity and the risk of myocardial infarction in 27,000 participants from 52 countries: a case-control study', *Lancet*. 2005/11/08, 366(9497), pp. 1640–1649. doi: 10.1016/s0140-6736(05)67663-5.

Zahorska-Markiewicz, B. *et al.* (2000) 'Serum concentrations of TNF-alpha and soluble TNF-alpha receptors in obesity.', *International journal of obesity and related metabolic disorders : journal of the International Association for the Study of Obesity*. England, 24(11), pp. 1392–1395.

Zaragosi, L.-E. *et al.* (2007) 'Nucleofection is a valuable transfection method for transient and stable transgene expression in adipose tissue-derived stem cells.', *Stem cells (Dayton, Ohio)*. United States, 25(3), pp. 790–797. doi: 10.1634/stemcells.2006-0235.

Zhang, H.-M. *et al.* (2009) 'Macrophage infiltrates with high levels of Toll-like receptor 4 expression in white adipose tissues of male Chinese.', *Nutrition, metabolism, and*

cardiovascular diseases : NMCD. Netherlands, 19(10), pp. 736–743. doi: 10.1016/j.numecd.2008.12.016.

Zhou, J. and Troyanskaya, O. G. (2015a) 'Predicting effects of noncoding variants with deep learning-based sequence model', *Nat Meth*. Nature Publishing Group, a division of Macmillan Publishers Limited. All Rights Reserved., 12(10), pp. 931–934. Available at: http://dx.doi.org/10.1038/nmeth.3547.

Zhou, J. and Troyanskaya, O. G. (2015b) 'Predicting effects of noncoding variants with deep learning–based sequence model', *Nature Methods*. Nature Publishing Group, a division of Macmillan Publishers Limited. All Rights Reserved., 12, p. 931. Available at: https://doi.org/10.1038/nmeth.3547.

Zhou, Y. P. and Grill, V. E. (1994) 'Long-term exposure of rat pancreatic islets to fatty acids inhibits glucose-induced insulin secretion and biosynthesis through a glucose fatty acid cycle', *The Journal of clinical investigation*, 93(2), pp. 870–876. doi: 10.1172/JCI117042.

Zuriaga, M. A. *et al.* (2017) 'Humans and Mice Display Opposing Patterns of "Browning" Gene Expression in Visceral and Subcutaneous White Adipose Tissue Depots', *Frontiers in Cardiovascular Medicine*, 4(May), pp. 1–5. doi: 10.3389/fcvm.2017.00027.